A CHEMICAL BIOLOGY APPROACH TO UNDERSTANDING CELLULAR MANGANESE HOMEOSTASIS IN THE BRAIN

By

Kyle Jeffrey Horning

Dissertation

Submitted to the Faculty of the

Graduate School of Vanderbilt University

in partial fulfillment of the requirements

for the degree of

DOCTOR OF PHILOSOPHY

in

Neuroscience

May 14th, 2021

Nashville, Tennessee

Approved by:

Ariel Deutch, Ph.D. (Chair)

Ethan Lippmann, Ph.D.

Eric Skaar, Ph.D.

C. David Weaver, Ph.D.

Aaron B. Bowman, Ph.D.

ACKNOWLEDGEMENTS

First and foremost, I would like to thank my PI and mentor, Dr. Aaron B. Bowman. His endless patience and confidence in me are the primary reason why I've made it so far in graduate school to defend my thesis. I'd also like to thank my Bowman lab mates, who were like family to me for so many years. Thank you, Miles Bryan, Piyush Joshi, Rachana Nitin, Terry Jo Bichell, Grace Tipps, Anna Pfalzer, Diana Neely, and Patti Ward. You all have kept me (mostly) sane. I'd also like to thank the undergrads that have helped me with the workload: Jessica Jimenez, Taylor Duncan, and Bianca Gardner. Thank you to current post-doc and Bowman lab member Rekha Balachandran, who oversaw the ICP-MS data that solidified the MESMER manuscript. Thank you to David Weaver, who guided the calcium flow experiments that also helped form the MESMER manuscript. Thank you to the former Bowman graduate, Dr. Kevin K. Kumar, whose project I inherited. I'm grateful for your mentorship and the solid foundation of data to build upon.

I also need to acknowledge collaborators: From Micki Aschner's lab: Samuel Caito and Tanara Perez, who I have coauthored papers with, and Micki himself. Thank you to Lillian Johnson Juttukonda and Eric Skaar for your interest in our "921" project, despite how frustrating it was. Thank you to Debbie Mi, Paige Vinson, and the rest of the HTS Core for all their help regarding the VICTR grant. Thank you to the Gary Sulikowski lab for answering all of our questions and synthesizing so many of our molecules.

Thank you to the rest of my thesis committee for your insights, support, and understanding. I'd like to thank to Vanderbilt Neuroscience Graduate Program for having me, and a special thank you to the Biomedical Informatics Department who took me in with open arms to keep me at Vanderbilt. Thank you to my T32 Toxicology funding for their support over

the years. Lastly, thank you to my family and friends who dealt with me throughout my time in graduate school. I couldn't have done it without you.

TABLE OF CONTENTS

LIST OF TABLES

Table Page

LIST OF FIGURES

A version of the following chapter, including text and figures, have previously been published in The Annual Review of Nutrition, 2015. 35:71–108, as “Manganese is Essential for Neuronal Health”. 10.1146/annurev-nutr-071714-034419

CHAPTER I

MANGANESE IS ESSENTIAL FOR NEURONAL HEALTH

INTRODUCTION

Manganese (Mn) is an essential metal that is critical for human health. It is the fifth most abundant metal and twelfth most abundant element overall on earth. Mn is found in a variety of ores, oxides, carbonates and silicates. Erosion naturally distributes Mn into air, soil and waterways, ultimately entering into our food supply. Legumes, rice, nuts and whole grains contain the highest Mn levels, while Mn is also found in seafood, seeds, chocolate, tea, leafy green vegetables, spices, and some fruits such as pineapple and acai [1]. Mn is also present in nutritional supplements and vitamins commonly taken on a daily basis. Due to the numerous sources of Mn in food, sufficient Mn levels are easily attained. This is important as Mn is involved in several important physiological processes, including development, reproduction, immune function, energy metabolism and antioxidant defenses.

While the major source of Mn exposure is dietary, occupational exposures to Mn can produce toxic sequelae. Mn is used in a wide range of industrial processes and commercial products, including steel and stainless-steel production and formation of aluminum alloys. Mn is also incorporated into fungicides, such as maneb and mancozeb. Proper levels of Mn are necessary for life, but excessive levels of Mn may result in a neurotoxic condition known as “manganism.” This condition resembles Parkinson’s disease (PD), sharing similar cognitive, motor, and emotional deficits [2, 3]. However, it is well recognized that manganism and PD are distinct from

one another and have differing etiologies. (See subsection below "*Mn excess in neurological disease*"). Mn exposure has not been linked with cancer or damage to heart, kidney, liver, skin, blood, or stomach. The nervous system is the primary target for excessive Mn.

Mn toxicity may also arise from certain medical conditions. Mn is present in significant concentrations in both total parenteral nutrition (TPN) and infant and neonatal formulas. These solutions contain many trace elements necessary for life support, but may allow for the accumulation of high levels of Mn when given for prolonged periods of time [4-6]. This may be harmful for the development of the child, especially the central nervous system (CNS) which has a long period of development before reaching maturity. Individuals suffering from liver failure or hepatic encephalopathy can develop Mn toxicity, as Mn is excreted in the bile [7]. Finally, iron (Fe) deficiency, one of the most common nutritional deficiencies in the world, can result in Mn toxicity. As Fe and Mn compete for similar transport proteins, decreased Fe levels leads to an accumulation of Mn to toxic levels over time [8, 9].

It is therefore apparent that Mn levels in the body be properly maintained. This is achieved through mechanisms for absorption, distribution, storage and excretion of the metal. In this review we discuss the importance on Mn for physiological functions, sources of exposure, toxicity, cellular and subcellular transport, Mn-responsive pathways, and the impact of Mn on neuronal health.

MANGANESE IS AN ESSENTIAL METAL

Essentiality

Mn is an essential metal for the human diet as it is required for proper immune function, regulation of blood sugar and cellular energy, reproduction, digestion, bone growth, blood

coagulation and hemostasis, and defense against reactive oxygen species (ROS). The beneficial effects of Mn are due to the incorporation of the metal into metalloproteins. The functions carried out by Mn metalloproteins include oxidoreductases, transferases, hydrolases, lyases, isomerases, and ligases. Additionally, Mn is incorporated into arginase, glutamine synthetase, phosphoenolpyruvate decarboxylase, pyruvate carboxylase, and Mn superoxide dismutase enzymes. Tissue contents in mammals are in the range of 0.3-2.9 μg Mn/g wet tissue weight [10], making Mn one of the most common metals found in tissues. More commonly, Mn levels in humans are reported either as g Mn consumed per day or blood concentration of Mn, as these measures are the least invasive to assess. There is no formal recommended dietary allowance (RDA) for Mn, however the US National Research Council (NRC) has established an estimated safe and adequate dietary intake of 2–5 mg/day for adults [11]. The Institute of Medicine's Dietary Reference Intakes (DRI) for Mn cites approximately 2 mg/day as adequate intake for adults, and 1.2-1.5 mg/day for children. The DRI also lists 9-11 mg/day as the upper tolerable limit likely to pose no risk of adverse effects for adults, and 2-6 mg/day Mn for children, varying with age [12].

Deficiency

Due to the numerous dietary sources of Mn, Mn deficiency is exceptionally rare, and has not been reported in the literature under non-experimental settings. Under experimental settings, studies regarding insufficient dietary Mn are also rare and tend to be small in scale. In animal models, deficient Mn have resulted in impaired growth, poor bone formation and skeletal defects, and altered lipid and carbohydrate metabolism [13, 14]. A study of nearly 600 schoolchildren in Spain found that girls that were below the recommended adequate intake level of Mn had higher levels of insulin and insulin resistance scores, compared to girls that were at or above the adequate

intake values (13). Five of seven college-aged men experimentally placed on Mn-depleted diets developed a transient skin rash on their torsos and had decreased serum cholesterol levels [15]. Blood calcium, phosphorus, and alkaline phosphatase levels were also elevated in the men on a Mn deficient diet. This may indicate increased bone remodeling as seen in animal studies, though this has not been observed in a controlled clinical study. Lastly, a very small study of ten women split into four groups found that women on a lower dietary manganese supplement had increased mood and pain symptoms during their premenstrual phase, despite increasing calcium intake which tended to lessen menstrual phase symptoms [16]. Due to the ultra-rare occurrence of Mn-deficiency, efforts to clearly and effectively define the physiological and biochemical consequences of a Mn-deficiency are very limited and rely heavily on case studies.

Biological Sources of Mn

Diet and water. The average American diet allows for intake of Mn to be between 0.9-10 mg Mn/kg/day, with an average around 5 mg Mn/kg. Whole grains (wheat germ, oats, and bran), rice and nuts (hazelnuts, almonds, and pecans) contain the highest levels of Mn (30 mg Mn/kg). Chocolate, tea, mussels, clams, legumes, fruit, leafy vegetables (spinach), seeds (flax, sesame, pumpkin, sunflower and pine nuts) and spices (chili powder, cloves and saffron) are also rich in Mn. Dietary supplements and vitamins are another source of Mn, some of which contain up to 20 mg Mn. Mn is taken as a supplement for a variety of conditions, including osteoarthritis and osteoporosis [17-19]. The concentration of Mn in drinking water varies by location, ranging between 1 and 100 µg/l. The US Environmental Protection Agency (EPA) has set 50 µg/l as the maximum allowable Mn concentration in drinking water.

Milk and infant formulas. Milk is an important source of Mn for infants. Human milk contains around 3–10 µg Mn/l, which is sufficient to prevent Mn deficiency. Commercial infant formulas contain significantly higher levels of Mn, with cow's milk-based formulas containing 30-50 µg Mn/l and soy-based formulas containing 200–300 µg Mn/l [20]. Similarly, a study investigating infant solid foods found levels of Mn over 100-fold higher than cow's milk [21]. Very little is known about infant absorption of Mn, however there is no evidence that the high Mn content of infant foods are associated with Mn toxicity. Adults are able to absorb 8% of the Mn from human milk, but only 2% from cow's milk, and <1% from soy-based formulas [22]. It is unknown whether infants absorb Mn similarly as adults. Interestingly, in a study examining serum levels of Mn in infants fed either human milk (4.1 µg Mn/l) or infant formula (303 µg Mn/l), there was no significant difference in serum Mn levels [23]. This suggests that the homeostatic mechanisms required for proper Mn levels are in place and functioning in neonates.

Airborne exposure. Mn is used for multiple industrial purposes, including steel and stainless-steel production, formation of aluminum alloys, purification of oxygen and chlorine, and also as a component of fungicides. Many of the individuals exposed to Mn in the occupational setting inhale Mn as a result of creating fine dusts from welding or smelting [24, 25]. Unlike ingested Mn, inhaled Mn does not pass through the liver, but can be directly transported into the brain by olfactory or trigeminal presynaptic nerve ending transport [26, 27]. In the brain Mn disrupts dopamine, serotonin, and glutamine signaling [28, 29] and can lead to the development of manganism [2, 3]. Inhaled Mn additionally can cause cough, acute bronchitis, and decreased lung function [30]. This however is due to lung irritation and inflammation that may be produced from inhaling any metal

dusts and is not specific to Mn [30].

Environmentally, Mn can be deposited for inhalation by humans from automobile exhaust. Methylcyclopentadienyl Mn tricarbonyl (MMT) is an anti-knock additive in nonleaded gasoline, which contains roughly 24.4% Mn by weight. The combustion of MMT in the automobile engine emits 15% of the Mn in MTT as Mn phosphate and/or sulfate particles, with a mass mean aerodynamic diameter of 0.5–1.0 μm [31]. Studies performed in Canada, where MTT had been used for 10 years prior to the sampling, found average total atmospheric concentrations of Mn in Montreal from 27 to 50 ng Mn/m^3 and 21.5 ng Mn/m^3 in Toronto [32, 33], which were similar to the typical urban ambient air 33 ng Mn/m^3 [1]. Similar results were also reported from experiments conducted in Indianapolis [34]. While the contribution of MMT combustion to environmental exposure to Mn appears to be minimal, the impact of long-term exposure to low levels of MMT combustion products requires further investigation.

Parenteral exposure. The risk of Mn toxicity deriving from TPN is well documented, and has recently been reviewed [35]. Although Mn is supplemented in TPN to prevent depletion of endogenous Mn stores, there have been no cases reported of Mn deficiency (no changes in blood Mn observed) in patients receiving TPN without Mn supplementation [36]. Mn content varies in TPN administered, with a range of 0.18 μmol/d (0.01 mg/d) to 40 μmol/d (2.2 mg/d) [35]. Part of this variability is due to Mn also being a contaminant of TPN solutions. With such a range of TPN Mn content in use, toxicity to Mn has been observed in adults receiving >500 μg/d and in pediatric patients receiving >40 μg/kg/d [35]. Additionally, duration of TPN treatment is associated with increased blood and brain concentrations of Mn [4-6]. Current guidelines recommend monitoring patients for Mn toxicity if they receive TPN longer than 30 days. Long term TPN can lead to the

development of biliary stasis or obstructive jaundice [37-39], which can lead to increased Mn levels due to the importance of bile in the elimination of Mn. Additionally, patients that receive TPN may already have an increased risk for Mn toxicity. Infirm neonates receiving TPN are extremely vulnerable as young individuals absorb more Mn and excrete fewer stools [10, 40, 41]. Patients with compromised liver function also need to be monitored for Mn toxicity when receiving TPN.

MANGANESE ABSORPTION, TRANSPORT IN BLOOD AND EXCRETION

Absorption

Adult humans absorb around 3-5% of ingested Mn. Radiolabeled ^{54}Mn uptake studies show differential uptake of Mn based on gender; for a meal containing 1 mg Mn adult males absorb 1.35 ± 0.51% while adult females absorb 3.55 ± 2.11% [42, 43]. Ingested Mn is readily absorbed in the intestine; however molecular mechanisms of Mn uptake are not well characterized. Studies using the Caco-2 intestinal cell line describe a biphasic uptake process, where Mn transport achieves a steady-state condition after a brief period of equilibration between intracellular and extracellular components [44]. It is thought that Mn can enter cells either through passive diffusion or active transport via the divalent metal transporter 1 (DMT1) [45, 46]. The existence of an active transport mechanism was initially identified from *in vivo* studies using rat intestinal perfusions that showed intestinal Mn uptake was saturable and likely involved a high affinity, low capacity active transport mechanism [47]. DMT1 is a membrane-associated transport protein that uses the proton gradient across the cell membrane to translocate several divalent metals into the cell, including Mn, Fe, and Cu [46]. Both Fe and Mn are first-row transition metals with similar atomic masses, radii, and

electron structure allowing for shared transport mechanisms. Therefore, altered Fe concentrations have been shown to influence the amount of Mn absorbed [48, 49]. Additionally, studies using rat brush border membrane vesicles have also defined lactoferrin receptor-mediated uptake of Mn [50]. Other dietary components alter Mn absorption, such as phytates, ascorbic acid, and polyphenols [51, 52].

The absorption of Mn is governed by many factors. The GI tract responds to dietary Mn levels to regulate Mn uptake. High Mn intake, either through dietary or environmental exposure, causes the GI tract to absorb less Mn while the liver increases metabolism and biliary and pancreatic excretion increases [42, 53, 54]. Age is a significant determinant of Mn absorption. Younger individuals absorb and retain higher levels of Mn than adults [40, 41], most likely because their requirements for Mn are much higher than for adults. This is especially true for infants. TPN used in the treatment of severely ill or premature infants is usually supplemented with a trace element solution that contains small amounts of Mn. However, unlike the absorption of Mn from milk which must traverse the GI tract, the intravenous exposure to Mn-supplemented TPN solutions bypasses GI tract absorption. Consequently, nearly 100% of Mn is available for absorption, which can lead to toxic conditions

Transport in blood

The mechanism by which Mn enters the blood stream upon exiting the GI tract is poorly understood, however it is known that distribution to tissues by plasma is quick. The estimated half-life for Mn to leave plasma is 1 min [55]. Mn distribution from plasma to the liver (30% of total Mn), kidney (5%), pancreas (5%), colon (1%), urinary system (0.2%), bone (0.5%), brain (0.1%), erythrocytes (0.02%), and the remaining 58.18% to the remaining soft tissues [55]. The liver,

pancreas, bone, kidney and brain retain Mn more than other tissues and have the highest Mn concentrations in the body [10]. This is likely due to the essential nature of Mn in energy production and the high-energy demands of these tissues.

Mn speciation is important in how Mn is bound and transported in the blood [56, 57]. Mn can exist in 11 different oxidation states; the most commonly ingested forms include Mn^{2+} and Mn^{3+}. Mn^{2+} is the most predominant form found in the human body, although it is unknown the exact percentage of the total Mn pool consists of Mn^{3+} out of the total Mn pool [58]. Mn^{3+} is highly reactive and will undergo disproportionation to Mn^{2+} and Mn^{4+} unless stabilized in a complex with a ligand [57]. Interestingly, Mn^{2+} can be oxidized in the blood to Mn^{3+} by ceruloplasmin [59]. Mn^{2+} is bound by several species in the blood for transport and distribution. These include albumin (84% of total Mn^{2+}), hexahydrated ion (6%), bicarbonate (6%), citrate (2%), and transferrin (Tf) (1%) [60, 61]. Albumin is the major protein bound to Mn^{2+} [62, 63], with a K_D of 0.63×10^{-4} M^{-1}. Tf is a circulating Fe-binding protein that has affinity for Mn in both the Mn^{2+} and Mn^{3+} states [64]. Tf mediated transport of Mn^{3+} allows for delivery of Mn^{3+} to neuronal tissues similarly as with Fe^{3+}Tf transport, though Mn^{3+}Tf transport is noticeably slower and occurs to a lesser degree than other Mn transport processes [65].

Biliary excretion

Turnover of the ingested Mn is rapid, showing a mean retention of 10 days after ingestion [22]. In the liver, excess Mn is conjugated to bile and passed to the intestine for fecal excretion [42, 66]. Small amounts of bile-Mn conjugates are reabsorbed in enterohepatic circulation [66]. Trace amounts of Mn can also be detected in urine, sweat, and breast milk [42, 67].

MANGANESE DISTRIBUTION AND CONCENTRATIONS IN THE CENTRAL NERVOUS SYSTEM

Transport across the blood-brain barrier

Mn can cross the blood-brain barrier (BBB); however, the mechanisms of influx and efflux of Mn across the BBB are not yet clearly understood. Several carrier proteins may actively or passively facilitate Mn influx across the BBB, although their identities are uncertain. A major route of Mn ion influx across the BBB may be mediated by Transferrin (Tf), the iron-carrying plasma protein [68]. Mn citrate, in addition to Mn ion and the Mn-Tf complex, crosses the BBB, most likely via carrier-mediated transport [69]. Store operated calcium channels have also been implicated in brain Mn influx [70]. The role of divalent metal transporter 1 (DMT1) has been debated, but studies of Mn uptake in the rat model do not support the hypothesis that DMT1 plays a primary role in Mn transport across the BBB [71]. Studies using an *in vitro* model of the blood brain barrier suggest that Mn is actively transported across the BBB via a process that depends on time, temperature, and pH [72]. In human brain microvascular endothelial cells, inhibition of iron accumulation by Mn points to the expression of a Mn-sensitive divalent cation transporter at the plasma membrane of BBB capillary endothelial cells [73]. It is unlikely that Mn flux across the BBB can be attributed to one transport system; rather, studies suggest that this process occurs through a number of coinciding mechanisms [74]. A recent study suggests that the blood-CSF barrier, rather than the blood-brain barrier, may in fact be the chief interface for Mn uptake in the brain [75]. Even less is known about Mn efflux across the blood-CSF; however, evidence points to diffusion as the major mechanism of Mn efflux [76]. Recent studies suggest that Mn may alter the permeability of the BBB, contributing to its own toxic effect and that of other cytotoxins [77, 78].

Distribution in the CNS

Mn levels in the human brain have been found to be highest in the putamen, caudate nucleus, and globus pallidus and lowest in the pons and medulla. Human Mn brain levels, especially in the putamen, globus pallidus, and middle temporal gyrus, were found to positively correlate with age. Additionally, significantly increased Mn levels were observed in a Parkinson's diseased brain, particularly in the putamen, along with decreased Mn levels in the superior and middle temporal gyrus and globus pallidus [79]. In Wilson's disease murine brain and post-mortem human brain tissue taken from patients with Alzheimer's disease (AD) and dementia with Lewy bodies, Mn levels were not found to be significantly altered [80, 81]. Magnetic resonance and x-ray fluorescence have indicated significant accumulation of Mn in the hippocampus, brain stem and midbrain, basal ganglia, and thalamus as well as the choroid plexus and olfactory bulbs following subchronic Mn exposure [82-84]. On the sub-cellular level, Mn has long been thought to accumulate primarily in brain mitochondria, from which it has been shown to efflux very slowly [85, 86]; however, in more recent investigations of intracellular distribution, Mn has been shown to accumulate mainly in the nuclei of cultured choroidal epithelial and brain endothelium cells and in the nuclei and cytoplasm of cultured dopaminergic (DAergic) neuronal cells upon exposure [87]. Furthermore, in neurons and astrocytes of the striatum and globus pallidus, Mn levels were found to be lowest in the mitochondria compared to the cytoplasm, where levels were intermediate, and the heterochromatin and nucleolus, where the highest levels were found. However, in the same study, after chronic Mn treatment the rate of Mn increase was higher in the mitochondria of these cells than in the nuclei, with astrocytes sequestering more Mn than neurons [88]. Sub-cellular distribution of Mn has yet to be indisputably characterized.

Mn speciation and oxidation state may play an important role in its uptake and distribution

in the central nervous system, as Mn-citrate has been shown to predominate in the CSF, and Mn^{3+} exposures have been shown to result in higher concentrations of Mn in the brain than Mn^{2+} exposures [89, 90]. Indeed, recently the subcellular distribution and speciation of Mn within PC12 cells, an immortalized cell line with neural crest origins treated with various Mn compounds, was examined [91]. Differential toxicities and subcellular distributions were observed depending on the chemical form of Mn exposed to the cells. PC12 cells exposed to Mn_2O_3 demonstrated normal Mn^{3+} particles within the cytoplasm with little toxicity, presumably due to its insolubility. For cells treated with $MnCl_2$, $MnSO_4$, and other organic compounds, Mn^{2+} was observed mainly in the Golgi apparatus [91]. Mode of Mn delivery to the brain may mediate patterns of accumulation, as evidenced by the differential distribution across brain regions of injected Mn versus Mn released from peripheral tissues such as the liver [92]. An investigation of low-level Mn exposure via drinking water showed significant levels of Mn deposited in several brain regions including the olfactory bulb, cortex, striatum, globus pallidus, and hippocampus [93].

The normal, physiological concentration of Mn in the human brain is estimated to be 5.32–14.03 ng Mn/mg protein (20.0–52.8 μM Mn), while 15.96–42.09ng Mn/mg protein (60.1–158.4 μM Mn) is the estimated pathophysiological threshold [94]. A variety of factors may affect Mn accumulation and distribution, thereby altering Mn homeostasis and toxicity. In a study of chromium (VI) stress, a two-fold increase in brain Mn levels accompanied increased Cr concentrations [95]. Metabolic stress may alter Mn distribution in tissues, as suggested by a recent study which found decreased levels of Mn in the brain stem and frontal lobe after strenuous exercise relative to control conditions and moderate exercise [96]. Dietary iron levels may have an impact on levels of Mn accumulation in the brain [97]. Ceruloplasmin, a plasma protein involved in the oxidation and mobilization of iron, may also affect the distribution of Mn in brain tissues

[59]. These studies point to related mechanisms of Mn and Fe homeostasis. 3-D elemental bio-imaging, which has revealed elevated levels of Mn in the anterior pretectal nucleus, deep mesencephalic nucleus and medial geniculate nucleus in a Parkinson's disease model, also showed a high concentration of Mn in the region of the needle track where brain tissue was lesioned by injection of the neurotoxin 6-hydroxydopamine, suggesting that trauma may also lead to alterations in Mn distribution [98].

Type of Mn transporter	Name	Localization	Function	Primary metal of transport
Uptake	DMT1	Plasma membrane	Transports divalent metal cations (Co^{2+}, Fe^{2+}, Mn^{2+}, Ni^{2+}, Pb^{2+}, and Zn^{2+}) across cell membrane using proton gradient	Fe
Uptake	Transferrin	Plasma membrane	Transports Fe and Mn across plasma membrane by endocytosis via transferrin receptor	Fe
Uptake	Ceruloplasmin	Plasma membrane	Oxidizes and mobilizes Fe	Fe
Uptake	ZIP8/ZIP14	Plasma membrane	Divalent ion/HCO_3^- symporters; transport metals across HCO_3^- gradient	Zn
Uptake	Citrate transporter	Plasma membrane	Chelates metals, including Mn	
Uptake	Choline transporter	Plasma membrane	Transports choline into neurons; transporter inhibited by Mn	
Uptake	Dopamine transporter	Plasma membrane	Transporter inhibited by Mn	
Uptake	Calcium channels	Plasma membrane	Voltage-gated, receptor, and store-operated ion channels	Ca
Efflux	Ferroportin	Plasma membrane	Removes Fe and Mn from cells	Fe
Efflux	NCX	Plasma membrane	Removes Ca from cells via influx of Na ions	Ca/Na
Efflux, subcellular	SLC30A10	Plasma membrane, Golgi, endosome	Cell-surface Mn export	Mn
Subcellular	Park9/ATP13A2	Lysosome	P-type ATPase; shuttles cations across lysosomal membrane	Mn
Subcellular	SPCA1	Golgi membrane	Ca^{2+}/Mn^{2+} ATPase; transports cytosolic Ca^{2+} and Mn^{2+} into Golgi lumen	Mn/Ca
Subcellular	HIP14/HIP14L	Golgi membrane	Transports divalent metals; palmitoylates Htt and synaptic proteins	Mg
Subcellular	Calcium channels	Golgi membrane	Voltage-gated, receptor, and store-operated ion channels	Ca

Table 1-1. **Types of Mn Transporters.** Abbreviations: ATP13A2, ATPase type 13A2; DMT1, divalent metal transporter 1; HCO_3, bicarbonate; HIP14/HIP14L, huntingtin-interacting protein 14/14-like; NCX, sodium-calcium exchanger; SLC, solute carrier; SPCA1, secretory pathway Ca^{2+}-ATPase isoform 1.

REGULATION OF CELLULAR AND SUBCELLULAR LEVELS

The mechanisms and details of intracellular Mn transport and storage are under active investigation. Most of the known transporters involved in transport of Mn into and within cells of the brain (including neurons and glia) are non-selective, and also transport other essential metals (see **Table 1-1** and **Figure 1-1**). As such, the known Mn transporters cannot explain how

intracellular Mn concentrations are selectively maintained without simultaneously strongly influencing the concentrations of other metals. Further, aside from a few notable exceptions [e.g., secretory pathway Ca2+-ATPase isoform 1 (SPCA1)], the manner by which known Mn transporters regulate uptake and efflux of Mn into the cells, versus the subcellular distribution of Mn is not well established. Indeed, Mn is the only essential metal for which cellular homeostatic processes are not defined, despite numerous Mn dependent enzymes throughout the cell. New research to generate novel chemical tools to probe mechanisms of Mn transport was performed via a high throughput screening approach [99]. A total of 41 small molecules were identified to be capable of significantly increasing or decreasing intracellular Mn content in a concentration dependent manner using a mouse striatal neural cell line [99]. Understanding the targets of these molecules may improve our understanding of cellular and intracellular Mn trafficking and the regulation of Mn homeostasis.

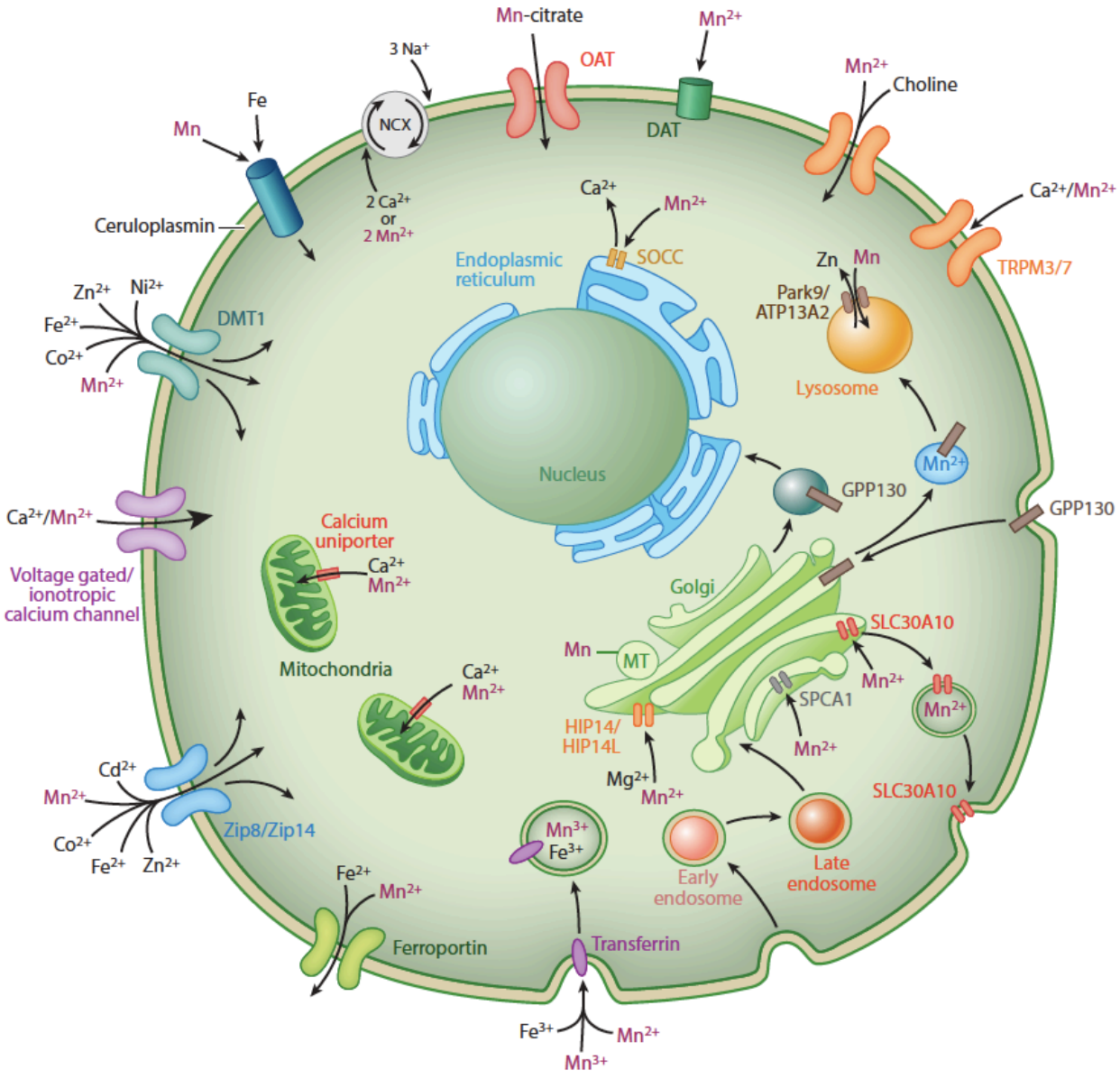

Figure 1-1. Known transporters and channels permeable to Mn within the brain and their cellular localizations. Other metals with affinities for each transporter are also listed. Abbreviations: DAT, dopamine transporter; Mn, manganese; MT, metallothionein; NCX, sodium-calcium exchanger; OAT, organic anion transporter; SOCC, store-operated calcium channel.

Mechanisms of Cellular Mn Uptake

DMT1 and the transferrin system. The divalent metal transporter (DMT1; previously known as NRAMP2, DCT1, or SLC11A2) is given its name for its ability to transport several metal cations such as Co^{2+}, Fe^{2+}, Mn^{2+}, Ni^{2+}, Pb^{2+}, and Zn^{2+} [100, 101]. Its function was first discovered in Belgrade rats, a breed lacking a functional DMT1 transporter, which is demarcated by microcytic anemia and impaired transport of Fe and Mn [101, 102]. Numerous studies have demonstrated that DMT1 is capable of transporting Mn^{2+}[45, 46, 103-106], and despite reports of its presence in the BBB [107], the choroid plexus [106], and in cells of the basal ganglia [108] where the highest amounts of Mn collect following exposure [109, 110], others still question the role that DMT1 plays in Mn transport in the brain. The pH that is required for Mn to be taken up into cells seems to be different than the pH at which DMT1 operates [71] and the mere existence of DMT1 in capillary endothelial cells has also been questioned [109, 111]. Despite having less than 1% of functional DMT1, Belgrade rats still have the same concentration of Mn in the brain compared to WT rats [71]. This, and other studies, [75, 112] at least suggest that DMT1 is not the major transporter of Mn in the brain. Recently, Seo and colleagues [113] noted that Mn accumulation increases both *in vitro* and *in vivo* neural models following Fe depletion, concurrent with the upregulation of DMT1 [113]. An alternative explanation to mediate conflicting results is that the presence of Fe diminishes the transport of Mn through a receptor independent of DMT1.

Although most biological free Mn appears to exist and be transported in its divalent state, a significant portion of Mn is transported as Mn^{3+} though a transferrin (Tf) mediated mechanism [64, 65, 68, 114, 115]. It was originally proposed that Mn was oxidized to a trivalent state and loaded onto transferrin via the oxidase protein ceruloplasmin, however Jursa and Smith [59] did not find any difference in trivalent Mn bound to transferrin between control and a

ceruloplasminemic mouse. As a side note, this study did find that mice lacking ceruloplasmin did distribute Mn throughout the body in a distribution that retained more Mn. The authors note an interaction of high Mn levels and greater oxidative stress in these mice [59]. This suggests that ceruloplasmin may have a capacity to influence Mn toxicity. A more recent study described these knock-out ceruloplasmin mice as developing a parkinsonism within 6 months of their life [116]. This phenotype could be reversed by treatment with the iron chelator deferiprone, or intravenous injection of ceruloplasmin.

Much like the case of DMT1, the mechanism by which Tf transports Mn is similar to its normal function of transporting Fe. Though it has been shown that Mn^{3+} can still compete with Fe^{3+} for Tf transport [65] the former transport occurs at a much slower rate. Despite the similarities of Mn and Fe in their biological activity, these metals differ in their preferred oxidation states, where Fe is much more stable in its trivalent form, and Mn its divalent form. The oxidative potential of Mn^{3+} is also stronger than that of Fe^{3+}, so following its deposition by Tf, Mn^{3+} may do unknown oxidative damage and contribute to Mn toxicity when in excess inside the cell [65]. Studies using transferrin-deficient mice note different distributions of Mn in several organs, but no changes from normal Mn concentrations in the brain, suggesting that transferrin is not the primary Mn transporter in the brain [114].

Because of the size of the transferrin complex, Mn or Fe bound to transferrin must be bound to a transferrin receptor and endocytosed in order to cross the plasma membrane. It has been suggested that the transferrin receptor (TfR) works in combination with DMT1 in a mechanism where the pH is lowered in the endosome via V-ATPase, causing the release of Mn from Tf and reduction to Mn^{2+}. DMT1 then is able to transport H^+ and Mn in its divalent state into the cytoplasm [65].

Zinc transporters. The SLC39 family of proteins are characterized by their variety of zinc transporters, but three in particular have been implicated in the regulation of Mn in cells. ZIP8 and ZIP14 are most closely related, both acting as divalent ion/HCO_3^- symporters that drive metals across a HCO_3^- gradient [117]. When expressed in HEK 293T cells or Xenopus oocytes, they are capable of transporting several divalent ions such as Co, Fe, Cd, and of course Zn [118]. Rat basophilic leukemia RBL-2H3 cells grown to be Mn-resistant show marked suppression of ZIP8 expression [119]. Knockdown of ZIP14 has shown reduction of Mn uptake in SH-SY5Y [120]. Stimulating inflammatory conditions with IL-6 stimulates the uptake of Mn while concurrently upregulating ZIP14 and downregulating SLC30A10 (105).

Citrate, choline, dopamine and calcium transporters. Crossgrove and colleagues (56) found that Mn citrate was able to cross the BBB at rates much faster than predicted for diffusion [69]. This suggests that a mechanism exists, at the very least in situ, for transport of Mn bound to citrate across the BBB and plasma membrane. The rates of Mn citrate transport were also significantly faster than Mn alone, indicating that it may be a major mechanism of Mn transport [69], and suggested to be facilitated perhaps through the organic ion transporter or the monocarboxylate transporter [57]. Suwalsky & Sotomayor [121] noted that exposure of Mn-citrate to the erythrocyte membrane induces far less structural damage than ionic Mn alone, arguably due to citrate's metal-chelating abilities. For this reason, and the large availability of citrate in serum compared to Mn [89], it would be logical that citrate is a reasonable source of Mn for the cell. However, the reality of citrate playing a meaningful role in Mn transport has not yet been further tested.

Another possible yet unconfirmed-significant route of Mn entrance into the brain is through the choline transporter. Exposure to Mn has been shown to inhibit choline uptake in perfused rodent brain by nearly 50% within in situ preparation [122]. More recently, Bagga & Patel [123] reported that chronic Mn exposure in mice was associated with decreased levels of choline in the hypothalamus and thalamus [123]. These areas were also marked by a reduction in glutamate, n-acetyl aspartate and N-acetyl aspartate. GABAergic disruption was only damaged in the basal ganglia.

Considering the numerous connections of Mn with parkinsonian disorders (see subsection *Mn excess in neurological disease)*, it is not surprising that Mn interacts with and is possibly transported by the dopamine transporter (DAT). Based on the observations that chronic exposure to Mn produces PD-like symptoms but spares the DAergic cells of the substantia nigra [124], it has been suggested that the mechanism would likely be acting at the presynaptic terminal, deactivating DAT [125]. Indeed, the amphetamine induced release of dopamine is prevented by Mn [126]. It has also been observed that the presence of Mn induces the internalization of DAT in transfected HEK cells [127].

Mn has often been used as a tool to observe the functionality of other transporters that transport divalent ions. For this reason, several calcium channels have been identified to be permeable to Mn, but their contribution to normal Mn transport, storage and homeostasis has not been adequately assessed. Examples of these include transient receptor potential cation channels, such as TRPM3 [128] and TRPM7 [129]. Voltage gated L-type Ca^{2+} channels [130, 131], ionotropic glutamate receptor channels [132], and store operated calcium channels [70, 129, 130, 133, 134] also have reported permeability to Mn.

Mechanisms of cellular Mn efflux

SLC30A10. Originally described as a zinc transporter (also called ZnT10) based on its family classification, analysis of its amino acid structure distinguishes SLC30A10 from other zinc transporters [135]. Immunohistochemical staining has indicated the localization of SLC30A10 at the plasma membrane and also throughout the secretory pathway- including the Golgi system and endosomes [136]. Transfections of the human SLC30A10 gene into Mn-sensitive yeast cells reversed the obstructed growth phenotype when exposed to Mn. Consistent with the support of SLC30A10 as a Mn transporter, inducing mutations into this gene reverted the cells back to their original Mn-sensitive phenotype [137]. Similar studies in *C. elegans*, HeLa cells, and primary cultures of mouse midbrain neurons have shown that expression of SLC30A10 yields protection from toxic Mn concentrations, and this effect is reversed when the gene is mutated [138].

Sodium-Calcium Exchanger. The permeability of the sodium-calcium exchanger (NCX) to Mn^{2+} was first demonstrated in myocardial cells as a surrogate to study Ca^{2+} efflux [139, 140]. More recently, the inhibition of the NCX channel for 24 hours was shown to increase cellular Mn levels in immortalized mouse striatal neuroprogenitors [141]. Efflux through NCX is a proposed dominant mechanism of Ca^{2+} efflux following an action potential [142-144], given the similar chemical properties of Mn^{2+} and Ca^{2+}, it is reasonable to postulate that Mn^{2+} can efflux the plasma membrane in the place of Ca^{2+} in exchange for the influx of three Na^{+} ions, all ions along their concentration gradients. The alteration of neuronal Mn content by NCX inhibition may be acting through blockage of Mn efflux, however additional studies are needed to determine the role of NCX under normal Mn neuronal homeostatic conditions.

Ferroportin. A third transporter of iron, ferroportin (FPN; also known as IREG1 or MTP1), allows for the efflux of both Fe and Mn from the cell [145, 146]. Mn is capable of inducing FPN mRNA expression in a dose dependent manner [146, 147]. Also understood as a compensatory mechanism, exposure to Mn or Fe has been shown to change FPN localization in the choroid plexus at the blood-cerebral spinal fluid barrier [106]. Recently, Mitchell and colleagues (2014) failed to reproducibly identify a difference of Mn efflux in *Xenopus* oocytes expressing FPN compared to those without FPN expression- finding an actual decrease of efflux of Mn in cells expressing FPN in some cases [148]. It is not yet understood whether or not this particular study accounts for the decreased accumulation of Mn in the FPN expressing cells as a reason for decreased efflux, as seen in a previous study using *Xenopus* oocytes [145]. Regardless, the role of FPN as an exporter of Mn has already been recognized in mouse brain *in vivo* [146] and its association remains much less controversial than a Mn role with DMT1 in the brain.

Regulation of Subcellular Distribution and Storage

Park9/ATP13A2. Park9, also known as ATP13A2, is a P-type ATPase primarily found in the neurons of the substantia nigra and is a putative cation shuttle across the lysosomal membranes [149-152]. The evidence supporting Park9 transport of Mn comes from studies showing that deletion of the yeast homolog, Ypk9, yields sensitivity to toxicity of heavy metals including Mn [151]. Similarly, a protective effect from Mn is seen when overexpressed in mammalian cell lines or rat primary cell cultures [152]. The mechanism behind the protective effect of ATP13A2 is not understood, but it has been proposed to help sequester toxic metals into vacuoles, or function as Zn/Mn pump as described by Kong [153]. A recent review [154] has criticized the proposal of

ATP13A2 as metal transporter, and suggests that it acts as a flippase aiding in vesicle creation and fusion. Whether this is true or not, it is clear that ATP13A2 in some fashion influences the proper movement of metals within the endosomes/lysosome transport process.

SPCA1 and GPP130. SPCA1 is a Ca^{2+}/Mn^{2+} ATPase expressed highly in the brain on the surface of the Golgi membrane that transports cytosolic Mn^{2} and Ca^{2+} into the Golgi lumen [155, 156]. By this mechanism, Ca^{2+} can be stored safely, and excess Mn^{2+} can be removed from the cytosol and exported through the secretory pathway. SPCA1 can transport one Mn^{2+} or Ca^{2+} ion at a time per hydrolyzed ATP. Considering its high affinity to Mn, comparable only equally to Ca [157, 158], SPCA1 is recognized as one of only two critical regulators of Mn known to date- the other being SLC30A10. Loss of function in the SPCA1 yeast homologue PMR1, leads to hypersensitivity to Mn toxicity [159]. In humans, the specificity to Mn is even higher than for the yeast protein [160]. The null mutant of SPCA1 in mice is lethal, with heterozygous mice having increased rates of apoptosis and demonstrating larger Golgi with diminished leaflets [161]. Rats exposed to chronic $MnCl_2$ (30mg/kg i.p. daily for 30 days) had twofold increased expression of SPCA in the mitochondrial proteome in the brain [162], in what can be assumed as a compensatory detoxification process. However higher concentrations of Mn^{2+} exposure (1mM) in cultured mouse neurons and glia have been shown to inhibit Ca^{2+} ATPase activity of SPCA1 to approximately 50% of vehicle without influencing expression [163]. The failure to see changes in SPCA1 expression are likely due to a timing difference (30 days as compared to 6 hours) or *in vivo*/*in vitro* differences, but what can be observed is that SPCA1 can be oversaturated by Mn and toxicity will result from presumably blocking normal Ca^{2+} sequestration. On a systems level, a significant amount of detoxification of Mn^{2+} may occur in the liver. Knockdown of SPCA1 in HEK293T cells

limited growth and decreased viability following Mn^{2+} exposure [164]. Overexpression of SPCA1 in these cells allowed for increased Mn^{2+} tolerance. Similarly, a mutation to increase the pore size of SPCA1 in yeast resulted in a hyperactive transporter with increased Mn^{2+} efflux and Mn^{2+} tolerance [165].

SPCA1 mRNA expression and protein show only modest increases across postnatal development in the hippocampus, cortex, and cerebellum of mice, however SPCA ATPase activity steadily increases over this time [166]. This discrepancy has been speculated to be due to differences in unknown activators of SPCA1, rather than SPCA2- a second isoform of SPCA that shares 64% of homology with SPCA1 [167] but whose expression in the brain is contentious [166, 168, 169], and has been reported to have little or no ATPase activity [170]. The relative amount of brain *SPCA1* expression compared to other tissues has been unclear. Wooten and colleagues [170] found that *SPCA1* mRNA expression and protein levels were highest in the rat brain, testis and germ cells compared to rat heart, lung, kidney, and liver, consistent with older data [171] prior to the identification of SPCA1's function, which also found rat RNA levels of *SPCA1* to be higher in the brain than any other tissues tested. Regardless, expression of *SPCA1* has been identified in neuronal, astroglial, ependymal, oligodendroglial, but not microglial cells [155]. The subcellular distribution of SPCA1 is predominantly reported in the Golgi [168, 172-174], though the exact subsection is uncertain, and strangely the amount of SPCA1 is not correlated with the amount of Golgi present in the cells [170].

The important discovery that Mn exposure induces the *cis*-Golgi glycolprotein GPP130 to traffic from the Golgi to multivesicular bodies and then to lysosomes for degradation [175] has defined a molecular and biological sensor for Mn that may be involved in Mn homeostatic regulation **(Figure 1-2)**. The normal function of GPP130 appears to involve the trafficking of

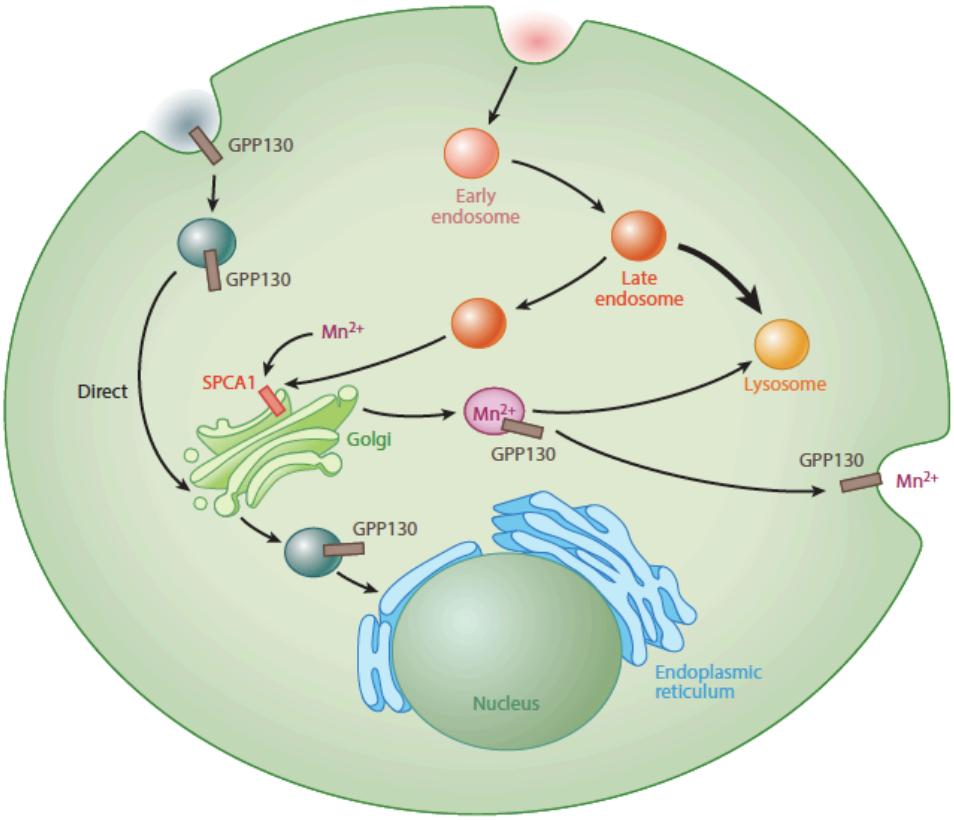

Figure 1-2. **Mechanism of Mn detection via SPCA1 and GPP130.** Endocytosed vesicles containing GPP130 are typically sorted directly to the late Golgi. SPCA1 transports Mn into the Golgi complex. In the presence of Mn and GPP130, vesicles are either guided to lysosomes, where Mn is sequestered, or are brought to the membrane, where Mn is then exocytosed. Abbreviations: GPP, *cis*-Golgi glycoprotein; Mn, manganese; SPCA1, secretory pathway Ca^{2+}-ATPase isoform 1.

vesicle directly from the endosomes to the Golgi bypassing late endosomes and pre-lysosomes [176]. Its sensitivity to Mn is delicate and specific to Mn rather than other metals. This mechanism has been recorded in neuronal cell lines and the degradation of GPP130 from Mn exposure has been demonstrated *in vivo* as well [177]. Recently, Tewari and colleagues [178] helped to elucidate this sorting mechanism by discovering that GPP130 binds to Mn, inducing oligomerization of the protein. SPCA1 is required for Mn^{2+} to reach the Golgi lumen and bind to GPP130, which provides a putative mechanism by which cells regulate excess cytosolic Mn. Increased cytosolic Mn may be pumped through SPCA1 to the Golgi lumen, where it binds to GPP130, induces its oligomerization, resulting in the sorting to the oligomer and secretion of Mn from the cell.

Metallothionein. The role that metallothioneins (MT) have in the storage, detoxification, or transport of Mn, as are the case of other metals, is unknown. Metallothioneins are Golgi-localized low molecular weight proteins that bind metals at the thiol groups of the cysteine rich residues. The literature on the relationship of Mn and MT is very sparse. Astrocyte exposure to Mn is known to decrease MT mRNA in a dose dependent fashion, assumingly due to a shift in metal metabolism [105]. MT is induced in the liver of mice following Mn exposure, however the metals bound to the induced MT was found to be mostly Zn, rather than Mn. Interestingly, this induction appears to be completely dependent on interleukin-6 (IL-6) production; mice lacking IL-6 did not have any MT response from Mn exposure [179].

MANGANESE NEURONAL HEALTH

Brain physiology and function

Mn is essential for brain physiology and biology via its role as a co-factor in numerous enzymatic processes. Furthermore, several Mn responsive pathways have been identified that may play a role in regulation of Mn cellular homeostasis and protection against neurotoxicity due to excess levels of Mn. It is likely that Mn, like other essential metals, must be carefully regulated to ensure proper health. The high levels of Mn that occur normally in brain (see above) argue for a particular role of Mn in brain physiology and function. Here we consider Mn-related neurobiological processes, and the consequences of insufficient and excessive brain Mn levels. Given the diverse set of cellular processes contingent on sufficient but controlled collection of Mn, the cellular demand for Mn is likely to change throughout development. Using small molecules

that perturb cellular Mn transport, a recent study showed that developing mesencephalic DAergic precursors alter their mechanisms of Mn transport between key neural developmental stages [99].

Mn-dependent and Mn-activated enzymes

Arginase is a Mn-dependent enzyme that catalyzes the hydrolysis of arginine to ornithine in the urea cycle. The two isozymes of arginase, ARG1 and ARG2, have the same function but differ in their expression. ARG1, which has been found at higher levels in the brain, is found primarily in the cytoplasm, while ARG2 is found primarily in the mitochondria [180]. ARG2 is expressed in neurons and glial cells of most brain structures, with particularly high levels of expression found in the neocortex, corpus callosum, putamen, and ventral striatum [181]. While metal requirements for arginases may differ between species, optimal catalytic function of human ARG1 specifically depends upon Mn^{2+} [182, 183]. Arginase is expressed in endothelial cells, where it controls the production of nitric oxide (NO) by mediating the bioavailability of arginine [184, 185]. The function of arginase in brain has not been fully characterized, though studies suggest neuroprotective effects. Depletion of arginine by ARG 1 promotes neuronal survival through inhibition of nitric oxide synthesis [186] and protein synthesis [187]. Arginase also plays a role in the neural immune response, contributing to neuronal protection and regeneration through microglial activation pathways [188] and polyamine synthesis pathways [189, 190].

Glutamine synthetase (GS) is also a very prevalent and significant Mn-dependent enzyme found primarily in astrocytes, where it catalyzes the conversion of the neurotransmitter glutamate (Glu) into glutamine (Gln), which can be released and subsequently taken up by neurons for use in the synthesis of glutamate [191-193]. Extracellular Glu is neurotoxic at high levels; accordingly, inhibited Glu uptake by astrocytes contributes to Glu neurotoxicity [194]. This process is

illustrated in **Figure 1-3.** Efficient Glu uptake relies on GS activity, indicating an important role for GS in normal synaptic function as well as a neuroprotective effect of this enzyme against Glu-induced excitotoxicity and neurodegeneration [195-197]. The finding that elevated levels of extracellular Glu increase GS expression and inhibit glial Glu transporters supports this conclusion [198]. Studies suggest that Mn neurotoxicity is associated with impaired Glu-Gln homeostatic mechanisms in the brain. Mn inhibits Gln transport into astrocytes [199, 200]. Counter-intuitively, Mn exposure has been found to reduce GS activity in the brain, particularly in the striatum and globus pallidus [201].

Mn-dependent superoxide dismutase/superoxide dismutase 2 (MnSOD/SOD2) is an antioxidant mitochondrial metalloenzyme that protects cells from oxidative stress by catalyzing the dismutation of superoxide anion radical to H_2O_2 and molecular oxygen, regulating cellular redox status and ROS generation [202]. By reducing oxidative stress, MnSOD has an important role in mediating physiological and pathological neuronal apoptosis and neurodegeneration [203, 204]. Overexpression of MnSOD in AD-model brains has been shown to reduce oxidative stress [205]. While Mn is required for the catalytic function of MnSOD, iron can also bind with high affinity to the Mn binding site of MnSOD [206]. Mn supplementation has been shown to increase MnSOD activity in human lymphocytes [207].

Also among critical enzymes requiring Mn, are pyruvate carboxylase (PC), and protein serine/threonine phosphatase-1 (PP1) [208]. PC is a Mn-dependent enzyme that converts pyruvate to the TCA-cycle intermediate, oxaloacetate [209-212]. PC deficiency can lead to accumulation of lactate in the bloodstream, causing lactic acidosis [213]. PP1 is needed to dephosphorylate serine and threonine residues, as it directly dephosphorylates AKT to regulate the AKT signaling transductions for cell survival and differentiation [214]. PP1 has also been shown to directly

dephosphorylate the apoptotic regulator, p53, thereby regulating the p53-dependent apoptotic pathway and promoting cell survival [215].

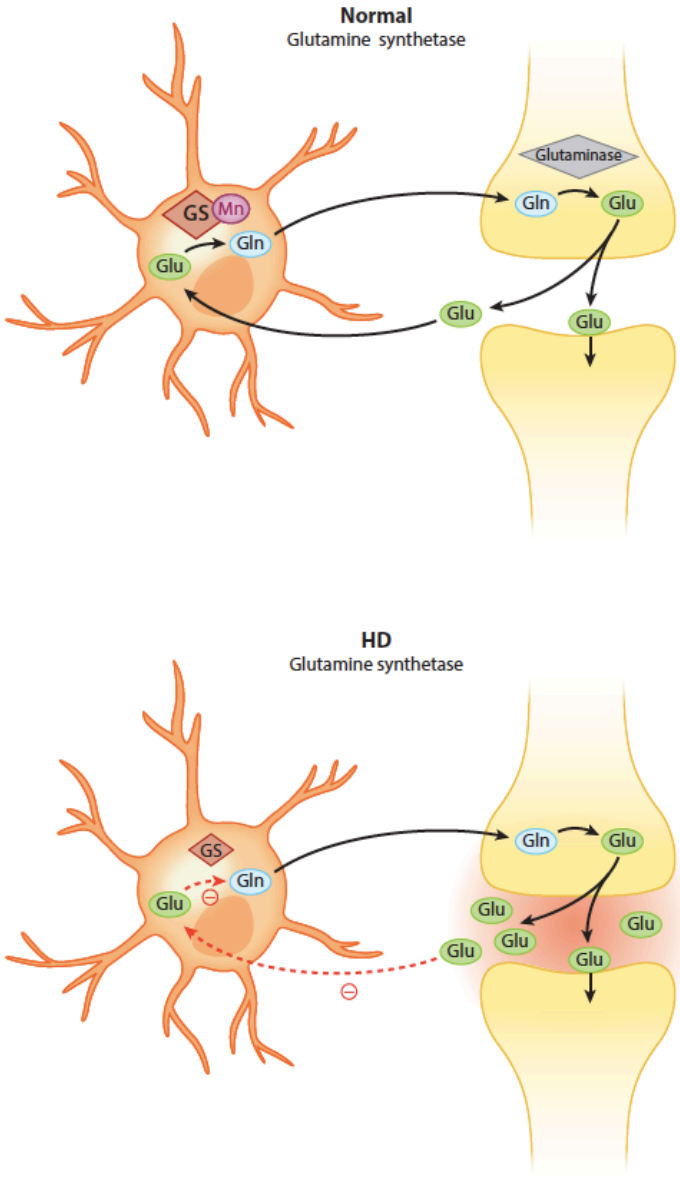

Figure 1-3. **Glutamine synthetase activity is diminished in Huntington's disease (HD).** Glutamine synthetase is a Mn-dependent enzyme. Efficient glutamate uptake by astrocytes relies on glutamine synthetase. In HD, where cellular Mn is reduced, impaired glutamine synthetase activity inhibits glutamate uptake. Abbreviations: Gln, glutamine; Glu, glutamate; GS, glutamine synthetase; Mn, manganese.

Mn-Responsive Pathways

ATM-p53 signaling pathway. Ataxia telangiectasia mutated (ATM) is a Mn-activated serine/threonine protein kinase involved in the cellular response to DNA damage and is mutated in Ataxia-telangiectasia, a neurodegenerative autosomal recessive disorder with impaired mitochondrial function and deficient mitochondrial DNA repair, indicating the importance of ATM for mitochondrial function in the brain [216, 217]. ATM has been shown to phosphorylate p53, H2AX and other targets in response to increased Mn levels, DNA damage and oxidative stress [141, 218, 219]. Ionizing radiation activates ATM to phosphorylate p53 in a Mn-dependent manner [220]. ATP has also been shown to activate ATM to phosphorylate p53 and other downstream substrates via an autophosphorylation mechanism that is specific to ATM kinase [221]. Mn is a strict *in vitro* requirement for phosphorylation by ATM of proteins involved in DNA damage pathways and cell-cycle checkpoints, including p53 [209]. This process is illustrated in **Figure 1-4**. During activation of ATM via double stranded DNA breakage, the DNA damage sensor complex MRN (Mre11, Rad50, Nbs1) is necessary. Mre11 has Mn-dependent exonuclease activity necessary for processing strand ends during non-homologous end joining repair. This nuclease activity requires Mn and cannot be substituted by magnesium or calcium [222-224]. However, nuclease activity-dead Mre11 mutants still undergo MRN complex binding to double stranded breaks and Mre11 dependent ATM phosphorylation [225]. A loss of Mn would likely result in stalled DSB strand repair, providing a longer active time to phosphorylate ATM, thus increasing its DNA damage response in cells.

Increased levels of p53 have been found in cortical neurons and glial cells from Mn-exposed non-human primates, and analysis of gene expression changes in cortical tissue from these Mn-exposed animals has revealed a prominent role of p53 in Mn-induced alterations in gene

expression [226, 227]. K-homology splicing regulator protein (KHSRP), a regulatory protein involved in neuronal apoptotic signaling, is upregulated in Mn-exposed striatum along with p53, providing further evidence of the role of p53 in Mn neurotoxicity [228]. Recently, a major p53 response to Mn exposure was found in mouse striatal cells and human neuroprogenitors. Activation of ATM kinase activity was shown to be sensitive to Mn at neurologically relevant concentrations, and inhibitors of ATM kinase decreased Mn-dependent p53 phosphorylation, confirming ATM-p53 as a significant Mn response pathway [141].

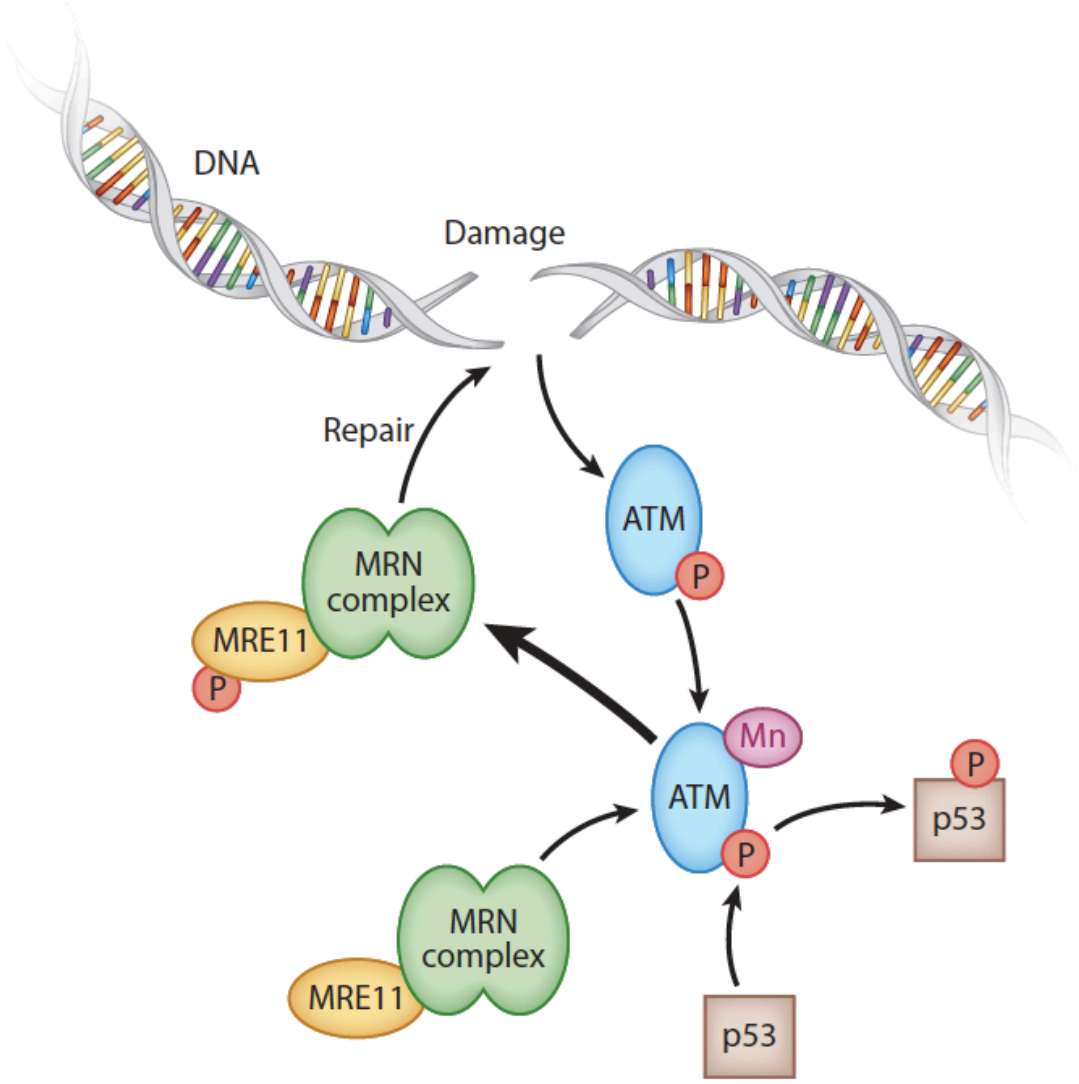

Figure 1-4. Mn-ATM-p53 pathway. Following double-stranded DNA damage, ATM is activated by Mn to phosphorylate p53 and Mre11 of the MRN complex. The MRN complex is then able to repair the DNA damage. Abbreviations: ATM, ataxia telangiectasia mutated; MRN, Mre11, Rad50, Nbs1.

Inflammatory Pathways. The neurotoxicity mechanism of Mn may in part be due to a resulting glial activation and neuro-inflammatory response (**Figure 1-5).** Pro-inflammatory cytokines such as IL-6, IL-1β and TNF-α are induced by endotoxins such as lipopolysaccharide (LPS), but potentiated in the presence of Mn [229]. Cytokine toxicity potentiated by Mn has been shown to depend upon the presence of astrocytes [230]. This is thought to be mediated by the activation nuclear factor kappa-light-chain-enhancer of activated B cells (NF-κB) and p38, reflecting how their pharmacological inhibition blocks this effect [231, 232]. However, microglia are capable of releasing these cytokines in response to Mn alone [232, 233]. Stressing the increased presence of microglia in the basal ganglia relative to any other areas throughout the brain [234], perhaps this in part can explain the sensitivity of the area to Mn toxicity. PD patients and animal models do demonstrate increased activation of microglia in these areas [235].

It is important to note the damage that continued glial cell activation can have primarily generating harmful ROS (discussed further below) and reactive nitrogen species (RNS) such as NO, but the overproduction of cytokines can lead to a cascade of further glial activation in the surrounding areas. Recently, it was noted that IL-6 could induce uptake of Mn while also upregulating the Mn-permeable ZIP14 zinc channels, and downregulating the Mn-exporter SLC30A10 [120]. Whether or not this can explain the potentiating effects of Mn with IL-6 and other cytokines is not yet clear.

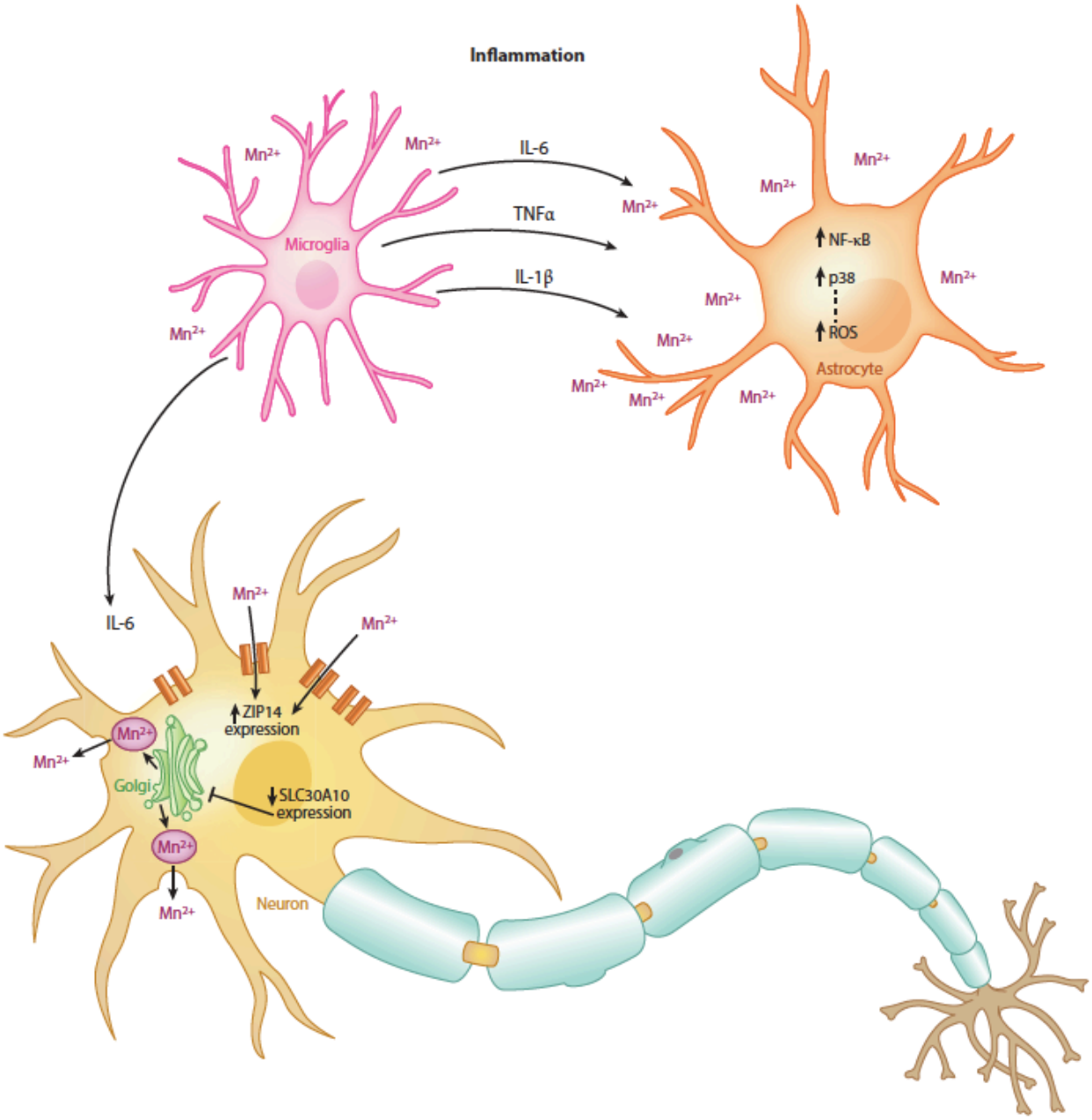

Figure 1-5. Inflammatory response induced by Mn. Mn exposure leads to the production of NF-κB and p38 in astrocytes, which increases reactive oxygen species. Inflammatory markers (IL-6, IL-1β, and TNF-α) are produced by microglia following Mn exposure. IN the presence of these markers and Mn, neurons have been found to increase expression of the Mn-permeable ZIP14 and decrease expression of the Mn exporter SLC30A10. Abbreviations: IL- β /6, interleukin-1 β /6; Mn, manganese; NF-κB, nuclear factor kappa-light-chain-enhancer of activated B cells; ROS, reactive oxygen species; SLC, solute carrier; TNF- α; tumor necrosis factor-alpha.

Neuropathological Consequences of Altered Mn Biology

Mn insufficiency in neurological disease. There are no known neurological conditions medically established to be due to Mn insufficiency. However, recent research on Huntington's disease (HD) has identified a deficiency in neuronal Mn handling associated with decreased neuronal Mn levels under both basal and elevated Mn exposure conditions [110, 141, 236-240]. While additional studies are needed to establish the relationship between alterations in Mn homeostasis and HD pathogenesis, several lines of evidence point to a potential role. For example, many critical Mn-dependent enzymes of the brain show diminished levels or activity in HD patients and other models of HD [241-244]. Of particular note, intracellular Mn levels are reduced in the striatum of HD patients and other HD models [245]. Mn-dependent activation of ATM signaling is impaired in both mouse and human neuronal models of HD and rescued by restoration of intracellular Mn levels [141]. Also, impairment of ATM-dependent repair pathways of DNA double-strand breaks (DSB) have been reported in irradiated HD human fibroblasts, suggesting that ATM may be implicated in HD pathology [246]. Consistent with the hypothesis of decreased Mn transport, HD cells have an increased tolerance to Mn toxicity [236]. The mechanism by which mutant Huntingtin protein (mutant HTT) impairs Mn transport is unknown. However, the changes of Mn levels in one cellular model of HD has been shown to be independent of transferrin or DMT1 activity, despite the known alterations of iron homeostasis in HD [110]. Of note, expression of ferroportin is increased and transferrin decreased in the cortex and striatum in mouse models of HD [247]. This may be a compensatory mechanism considering how iron concentrations are elevated in striatal neurons in HD.

Dietary Mn deficiency has been found to decrease arginase activity and increase the activity of nitric oxide synthases [248, 249]. Intracellular depletion of arginine by arginase may be

neuroprotective [250, 251]. While inhibition of ARG1 leads to increased NO production, which contributes to neuronal death, inhibition of NO by ARG1 contributes to neuronal survival, as demonstrated by a surviving subpopulation of motor neurons deprived of trophic factors [186]. Altered arginase activity (dependent on Mn as described above) has been implicated in the progression of Huntington's disease (HD). A urea cycle deficiency has been reported in HD. Increased ammonia and citrulline levels point to decreased arginase activity in these models [243]. Neuronal NOS and dietary L-arginine, the NO precursor, have been shown to mediate the time of symptom onset in HD [252, 253]. Diminished glutamine synthetase (GS) activity has also been observed in HD brain [254, 255]. Interestingly, decreased astrocytic GS expression and activity has been observed in the AD brain, especially in late stages of the disease [256-258].

Partial MnSOD deficiency has been shown to increase sensitivity to malonate and 3-nitropropionic acid, and both toxicants have been used to generate animal models for HD [259-261]. Decreased MnSOD activity from Mn deficiency may cause damage to the mitochondrial membrane via increased lipid peroxidation from free radicals [262]. Mitochondrial injury resulting from MnSOD deficiency contributes to neurodegeneration [263]. Loss of MnSOD activity has been shown to increase neuronal sensitivity to the mitochondrial toxin 3-nitropropionic acid (3NP), which leads to an HD-like neurodegenerative phenotype with degeneration of the medium spiny neurons of the striatum (caudate/putamen) in animal models and humans [259]. 3NP has also been shown to disturb glutaminergic and DAergic signaling in part by mediating the activity of serine/threonine phosphatases [264]. The PPM/PP2C family of protein phosphatases may regulate DAergic signaling in HD through AKT dephosphorylation of Htt protein in the G protein-dependent signaling pathway of the striatal dopamine D2 receptor (D2R) [265].

Alteration of neuronal Mn homeostasis in HD could also occur via the interaction of Htt

with HIP14 (huntingtin interacting protein 14) and HIP14L (Huntingtin interacting protein 14-like). Before their recognition as transporters for Mg^{2+} and other divalent metals like Mn^{2+} [266, 267], HIP14 and HIP14L were recognized as a required protein for the proper palmitoylation and thus proper cellular distribution of Htt and several synaptic localized proteins [268-272]. Down-regulation of HIP14 leads to increased inclusions in cells expressing either wild-type or mutant Htt [272]. Considering the connections between HD and altered Mn biology, a putative transporter of Mn that has an imperative role in proper Htt trafficking and proper response to Htt is a compelling link. Mice deficient in either HIP14 or HIP14L have been reported to have behavioral, motor, and neuropathological features [273, 274]. These proteins are found primarily in neurons within the Golgi complex, post-Golgi vesicles, and subplasmic membrane [266, 269]. Importantly, HIP14L is capable of palmitoylating HIP14, and HIP14 is capable of palmitoylating itself. The presence of wild-type Htt potentiates this effect, and mutant Htt is incapable of this potentiation, thus providing a potential mechanisms by which Mn transport is altered in Huntington's disease (see below) [275]. However, additional studies are needed to examine the functional relationship between HIP14/HIP14L and Mn biology.

Mn excess in neurological disease. Manganism/Mn poisoning/Mn-induced parkinsonism occurs primarily among industrial workers, such as welders, who are chronically exposed to Mn fumes or dust, the neurotoxic effects of which cause a PD-like syndrome. Chelating treatment with $CaNa_2EDTA$, along with sufficiently early removal from Mn exposure, has been found to effectively ameliorate symptoms in some workers with manganism, although irreversible cases have been reported [276]. The link between manganism and PD had been debated, with some patient studies reporting considerable overlap between the pathophysiology and clinical

characteristics of Mn-induced parkinsonism and PD, excepting age of onset [277, 278]. For example, symptoms of dystonia, impaired gait, psychosis, and emotional disturbances are common in both disorders. Significantly elevated levels of Mn have been found in the serum and CSF of PD patients [279, 280]. Mn-exposed non-human primates with motor abnormalities have dysfunctional DAergic systems. Positron Emission Tomography (PET) imaging of non-human primate brain has revealed impaired dopamine (DA) transmission, a feature of PD, in the striatum of Mn-exposed animals [126, 227]. PET imaging of asymptomatic Mn-exposed welders with 6-[18F]fluoro-L-dopa (FDOPA) also points to nigrostriatal DAergic dysfunction, but with a pattern of uptake inconsistent with that observed in patients with idiopathic PD [281]. Mn exposure at subtoxic levels has been found to amplify the neurotoxic effects of 1-Methyl-4-phenylpyridinium (MPP^+), which also contributes to a PD-like syndrome through the induction of ROS formation [282]. Despite the similarities and connections, the two disorders are distinguishable, as patients with manganism typically do not see an amelioration of symptoms with L-DOPA, as is seen in PD. The brains of manganism patients also lack Lewy bodies, a hallmark of PD absent in manganism (2, 3). The overwhelming consensus among the scientific community recognizes Mn-induced parkinsonism as a separate pathology from PD.

The E3 ligase, parkin, when overexpressed in SHSY5Y cells, is responsible for degrading 1B-DMT1 isoforms [283]. This degradation is protective against Mn toxicity. Parkin protein, encoded by *PARK2*, has been shown to accumulate in Mn-treated DAergic cells. Parkin may be critical for the attenuation of Mn-induced neuronal cell death, as overexpression of this protein has been found to protect DAergic neurons from the neurotoxic effects of Mn [284]. In response to Mn exposure, human lymphocytes lacking active parkin have demonstrated greater mitochondrial dysfunction and enhanced apoptotic signaling [285]. Workers who are repeatedly exposed to Mn

through welding fumes are at risk for parkinsonism. PARK genes may modulate the DAergic neurotoxicity of Mn-containing fumes, as exposure to Mn via fumes has been shown to cause mitochondrial dysfunction and alter DAergic PARK protein expression [286].

ATP13A2 (encoded by *PARK9,* introduced above) has been shown to protect cells from Mn toxicity by mediating intracellular Mn concentrations, an effect not observed in ATP13A2 mutants [152]. Variants in the ATP13A2 gene (described above) have been reported to be a risk factor for Mn neurotoxicity in humans [287]. Mutations of the ATP13A2 are known to cause a parkinsonian-like disease known as Kufor-Rakeb syndrome [288-290]. Increasing expression of ATP13A2 shows a protective effect against alpha-synuclein, and conversely, reduction of ATP13A2 results in elevated alpha synuclein accumulation.

More evidence for the association of Mn and parkinsonism is seen from the recent literature describing the selective cell-surface exporter of Mn identified as SLC30A10 [138]. The phenotype and age of onset observed by human patients with mutations in the SLC30A10 varies greatly, even within families with the same inherited mutation. The symptoms include hypermanganesemia, polycythemia, dystonia, and often also include chronic hepatic disease, cirrhosis, motor neuropathy, and behavioral disturbances with differing severity [291]. These symptoms have a large overlap with patients with PD; some studies have even found an increased occurrence of parkinsonism with suffers of cirrhosis up to 21% [292, 293]. Consistent with this idea, patients presenting parkinsonian symptoms that have decreased ability to excrete biliary Mn^{2+} suffer from Mn^{2+} induced neurotoxicity [292, 294]. It is important to note that affected individuals did not have any loss of striatal DAergic neurons in the striatum - which is the hallmark pathological feature in PD [136, 137, 295]. Lechpammer [295] describes in detail the pathology of one patient suffering from a mutations of SLC30A10 for the last 14 years of their life, and following their death at age

38, Mn levels in the basal ganglia were elevated 16-fold of control levels. There was marked loss of neurons in the medial and lateral globus pallidus, and increased activation of microglia, and astrocytes, myelin loss, and spongiosis. Although SLC30A10 has been shown to transport Zn and other cations other than Mn, it is remarkable that patients with mutations in SLC30A10 do not exhibit changes in concentrations in any other trace metals tested so far in the brain. Also interesting to note, expression of SLC30A10 has been found to be significantly reduced twofold in the frontal cortex of patients with AD- an observation also consistent in mouse models of AD [296].

Cellular redox pathways and neuronal oxidative stress. Production of ROS following excessive Mn exposure is a canonical response seen *in vitro* and *in vivo* [297]. The disabling of antioxidant defenses by Mn is also well characterized [85]. Recent work has shown that the toxicity of Mn is largely dependent upon the redox state, as glutathione levels can inversely predict toxicity upon Mn exposure [298]. Neuronal cell exposure to Mn induces oxidative damage to DNA, but this can be reversed with glutathione treatment [299]. Antioxidant treatment in chronically exposed rodents reverses not only toxicity but also motor deficits and signaling pathways activated by oxidative stress [300]. The signaling pathways associated with oxidative stress and Mn includes, PI3/Akt [300-302] protein kinase C, ERK1/2, p38, and JNK [303-305]. Interestingly, the phosphorylation of DARPP-32 at Thr34 is induced by Mn, which allows DARPP-32 to act as an inhibitor to protein phosphatase 1 (PP1; [301]). The production of ROS is thought to be the cause of nitric oxide synthase and NF-κB induction [306]. The autoxidation of dopamine by Mn is also well documented [307]. Monoamine oxidase (MAO) activity is increased as a result increased ROS, and this leads to a decrease in dopamine in the striatal cells affected. It has been noted that the

depletion of dopamine is independent of the ROS generation, as dopamine depletion has been observed to occur prior to ROS detection [78]. Glutamate uptake by the glutamate/aspartate transporter is inhibited by Mn, leading to higher extracellular glutamate [308]. Expression of GABA transporters are reduced with excess Mn, leading to increased extracellular GABA [309-311].

Mitochondria mediated toxicity is thought to occur in part by Mn^{2+} interfering with Ca^{2+} activation of ATP, leaving an energy deficit [312]. Mn has been shown to induce apoptosis-promoting caspase-12. Cytochrome *c*, and caspase-1, 3, 8, and 9 release also occurs following Mn exposure [313]. Not only does Mn induce apoptosis, but also the presence of dopamine potentiates apoptosis. This may in part explain the selective death of dopaminergic neurons following Mn exposure. One could argue that studies showing a reduction in tyrosine hydroxylase-positive cells (314, 315), or a reduction in other dopaminergic markers of cells following Mn exposure does not necessarily mean that these cells are dying; one could hypothesize that Mn simply reduces dopaminergic markers, not the cells themselves. However, combined with the evidence that Mn induces: ER stress (313), microglial activation and neuroinflammation (314, 316), caspase activation (313), and a reduction of total cell count in the substantia nigra pars compacta (315), this data suggest the neuronal apoptosis is a response to excessive Mn levels in the brain.

CONCLUSION

Mn is essential to human health. Given that Mn is required for a number of physiological functions but toxic at excessive levels, mechanisms of Mn homeostasis are critically important. Exposure to Mn is mainly dietary and occupational. While ingestion is the major route for exposure, Mn can also be inhaled, especially in certain industrial settings. Normally high levels of

Mn in the brain suggest that Mn plays a particularly important role in brain physiology and function and argue for the importance of elucidating mechanisms of Mn homeostasis. A number of candidates for cellular Mn uptake have been identified and investigated, including DMTI and the transferrin system, zinc transporters, as well as citrate, choline, dopamine, and calcium transporters. Likely candidates for cellular efflux of Mn include SLC30A10, the sodium-calcium exchanger (NCX), and ferroportin. Regulation of subcellular distribution and storage has been attributed to Park9/ATP13A2, SPCA1 and GPP130, and metallothioneins.

Mn is incorporated into a number of enzymes that are important for brain physiology and function. These include arginase, glutamine synthetase, MnSOD, pyruvate carboxylase, and protein serine/threonine phosphatases. Mn-responsive pathways have been identified, including the ATM-p53 pathway. Impaired neuronal Mn handling has been observed in HD. Impaired Mn homeostasis may alter the activity of Mn-dependent enzymes and Mn-sensitive pathways, contributing to neurotoxicity and the pathophysiology of neurodegenerative disorders including HD.

REFERENCES

1. ATSDR. TOXICOLOGICAL PROFILE FOR MANGANESE. In: SERVICES USDOHAH, editor. 2008.
2. Roth JA. Homeostatic and toxic mechanisms regulating manganese uptake, retention, and elimination. Biological research. 2006;39(1):45-57.
3. Aschner M, Guilarte TR, Schneider JS, Zheng W. Manganese: recent advances in understanding its transport and neurotoxicity. Toxicology and applied pharmacology. 2007;221(2):131-47.

4. Alves G, Thiebot J, Tracqui A, Delangre T, Guedon C, Lerebours E. Neurologic disorders due to brain manganese deposition in a jaundiced patient receiving long-term parenteral nutrition. JPEN J Parenter Enteral Nutr. 1997;21(1):41-5).
5. Iinuma Y, Kubota M, Uchiyama M, Yagi M, Kanada S, Yamazaki S, et al. Whole-blood manganese levels and brain manganese accumulation in children receiving long-term home parenteral nutrition. Pediatr Surg Int. 2003;19(4):268-72.
6. Siepler JK, Nishikawa RA, Diamantidis T, Okamoto R. Asymptomatic hypermanganesemia in long-term home parenteral nutrition patients. Nutr Clin Pract. 2003;18(5):370-3.
7. Zeron HM, Rodriguez MR, Montes S, Castaneda CR. Blood manganese levels in patients with hepatic encephalopathy. Journal of trace elements in medicine and biology : organ of the Society for Minerals and Trace Elements. 2011;25(4):225-9.
8. Smith EA, Newland P, Bestwick KG, Ahmed N. Increased whole blood manganese concentrations observed in children with iron deficiency anaemia. Journal of trace elements in medicine and biology : organ of the Society for Minerals and Trace Elements. 2012.
9. Fitsanakis VA, Zhang N, Avison MJ, Erikson KM, Gore JC, Aschner M. Changes in dietary iron exacerbate regional brain manganese accumulation as determined by magnetic resonance imaging. Toxicological sciences : an official journal of the Society of Toxicology. 2011;120(1):146-53.
10. Aschner JL, Aschner M. Nutritional aspects of manganese homeostasis. Molecular aspects of medicine. 2005;26(4-5):353-62.

11. Greger JL. Dietary standards for manganese: overlap between nutritional and toxicological studies. J Nutr. 1998;128(2 Suppl):368S-71S.

12. Medicine Io. Dietary Reference Intakes for Vitamin A, Vitamin K, Arsenic, Boron, Chromium, Copper, Iodine, Iron, Manganese, Molybdenum, Nickel, Silicon, Vanadium, and Zinc. 2001.

13. Rodriguez-Rodriguez E, Bermejo LM, Lopez-Sobaler AM, Ortega RM. [An inadequate intake of manganese may favour insulin resistance in girls]. Nutr Hosp. 2011;26(5):965-70.

14. Keen CL, Ensunsa JL, Watson MH, Baly DL, Donovan SM, Monaco MH, et al. Nutritional aspects of manganese from experimental studies. Neurotoxicology. 1999;20(2-3):213-23.

15. Friedman BJ, Freeland-Graves JH, Bales CW, Behmardi F, Shorey-Kutschke RL, Willis RA, et al. Manganese balance and clinical observations in young men fed a manganese-deficient diet. J Nutr. 1987;117(1):133-43.

16. Penland JG, Johnson PE. Dietary calcium and manganese effects on menstrual cycle symptoms. Am J Obstet Gynecol. 1993;168(5):1417-23.

17. Das A, Jr., Hammad TA. Efficacy of a combination of FCHG49 glucosamine hydrochloride, TRH122 low molecular weight sodium chondroitin sulfate and manganese ascorbate in the management of knee osteoarthritis. Osteoarthritis Cartilage. 2000;8(5):343-50.

18. Leffler CT, Philippi AF, Leffler SG, Mosure JC, Kim PD. Glucosamine, chondroitin, and manganese ascorbate for degenerative joint disease of the knee or low back: a randomized, double-blind, placebo-controlled pilot study. Mil Med. 1999;164(2):85-91.

19. Price CT, Langford JR, Liporace FA. Essential Nutrients for Bone Health and a Review of their Availability in the Average North American Diet. Open Orthop J. 2012;6:143-9.
20. Lonnerdal B. Nutritional aspects of soy formula. Acta Paediatr Suppl. 1994;402:105-8.
21. Ljung K, Palm B, Grander M, Vahter M. High concentrations of essential and toxic elements in infant formula and infant foods - A matter of concern. Food Chem. 2011;127(3):943-51.
22. Davidsson L, Cederblad A, Lonnerdal B, Sandstrom B. Manganese absorption from human milk, cow's milk, and infant formulas in humans. Am J Dis Child. 1989;143(7):823-7.
23. Wilson DC, Tubman TR, Halliday HL, McMaster D. Plasma manganese levels in the very low birth weight infant are high in early life. Biol Neonate. 1992;61(1):42-6.
24. Racette BA, Criswell SR, Lundin JI, Hobson A, Seixas N, Kotzbauer PT, et al. Increased risk of parkinsonism associated with welding exposure. Neurotoxicology. 2012;33(5):1356-61.
25. Criswell SR, Perlmutter JS, Huang JL, Golchin N, Flores HP, Hobson A, et al. Basal ganglia intensity indices and diffusion weighted imaging in manganese-exposed welders. Occupational and environmental medicine. 2012;69(6):437-43.
26. Andersen ME, Gearhart JM, Clewell HJ, 3rd. Pharmacokinetic data needs to support risk assessments for inhaled and ingested manganese. Neurotoxicology. 1999;20(2-3):161-71.
27. Elder A, Gelein R, Silva V, Feikert T, Opanashuk L, Carter J, et al. Translocation of inhaled ultrafine manganese oxide particles to the central nervous system. Environ Health Perspect. 2006;114(8):1172-8.

28. Sriram K, Jefferson AM, Lin GX, Afshari A, Zeidler-Erdely PC, Meighan TG, et al. Neurotoxicity following acute inhalation of aerosols generated during resistance spot weld-bonding of carbon steel. Inhal Toxicol. 2014;26(12):720-32.

29. Moberly AH, Czarnecki LA, Pottackal J, Rubinstein T, Turkel DJ, Kass MD, et al. Intranasal exposure to manganese disrupts neurotransmitter release from glutamatergic synapses in the central nervous system in vivo. Neurotoxicology. 2012;33(5):996-1004.

30. Roels H, Lauwerys R, Buchet JP, Genet P, Sarhan MJ, Hanotiau I, et al. Epidemiological survey among workers exposed to manganese: effects on lung, central nervous system, and some biological indices. Am J Ind Med. 1987;11(3):307-27.

31. Dorman DC, Struve MF, Clewell HJ, 3rd, Andersen ME. Application of pharmacokinetic data to the risk assessment of inhaled manganese. Neurotoxicology. 2006;27(5):752-64.

32. Loranger S, Zayed J. Environmental contamination and human exposure to airborne total and respirable manganese in Montreal. J Air Waste Manag Assoc. 1997;47(9):983-9.

33. Pellizzari ED, Clayton CA, Rodes CE, Mason RE, Piper LL, Fort B, et al. Particulate matter and manganese exposures in Toronto, Canada. Atmospheric Environment. 1999;33(5):721-34.

34. Pellizzari ED, Clayton CA, Rodes CE, Mason RE, Piper LL, Fort B, et al. Particulate matter and manganese exposures in Indianapolis, Indiana. J Expo Anal Environ Epidemiol. 2001;11(6):423-40.

35. Santos D, Batoreu C, Mateus L, Marreilha Dos Santos AP, Aschner M. Manganese in human parenteral nutrition: considerations for toxicity and biomonitoring. Neurotoxicology. 2014;43:36-45.

36. Frankel D. Supplementation of trace elements in parenteral nutrition: rationale and recommendations. Nutr Res. 1993;13:583-96.

37. Fallon EM, Le HD, Puder M. Prevention of parenteral nutrition-associated liver disease: role of omega-3 fish oil. Curr Opin Organ Transplant. 2010;15(3):334-40.

38. Graham MF, Tavill AS, Halpin TC, Louis LN. Inhibition of bile flow in the isolated perfused rat liver by a synthetic parenteral amino acid mixture: associated net amino acid fluxes. Hepatology. 1984;4(1):69-73.

39. Sax HC, Talamini MA, Brackett K, Fischer JE. Hepatic steatosis in total parenteral nutrition: failure of fatty infiltration to correlate with abnormal serum hepatic enzyme levels. Surgery. 1986;100(4):697-704.

40. Keen CL, Bell JG, Lonnerdal B. The effect of age on manganese uptake and retention from milk and infant formulas in rats. J Nutr. 1986;116(3):395-402.

41. Zlotkin SH, Atkinson S, Lockitch G. Trace elements in nutrition for premature infants. Clin Perinatol. 1995;22(1):223-40.

42. Davis CD, Zech L, Greger JL. Manganese metabolism in rats: an improved methodology for assessing gut endogenous losses. Proc Soc Exp Biol Med. 1993;202(1):103-8.

43. Finley JW, Johnson PE, Johnson LK. Sex affects manganese absorption and retention by humans from a diet adequate in manganese. Am J Clin Nutr. 1994;60(6):949-55.

44. Leblondel G, Allain P. Manganese transport by Caco-2 cells. Biological trace element research. 1999;67(1):13-28.

45. Bell JG, Keen CL, Lonnerdal B. Higher retention of manganese in suckling than in adult rats is not due to maturational differences in manganese uptake by rat small intestine. J Toxicol Environ Health. 1989;26(4):387-98.

46. Garrick MD, Dolan KG, Hobinski C, Ghio AJ, Higgins D, Porubcin M, et al. DMT1: A mammalian transporter for multiple metals. Biometals : an international journal on the role of metal ions in biology, biochemistry, and medicine. 2003;16:41-54.

47. Garcia-Aranda JA, Wapnir RA, Lifshitz F. In vivo intestinal absorption of manganese in the rat. J Nutr. 1983;113(12):2601-7.

48. Garcia SJ, Gellein K, Syversen T, Aschner M. Iron deficient and manganese supplemented diets alter metals and transporters in the developing rat brain. Toxicol Sci. 2007;95(1):205-14.

49. Hansen SL, Trakooljul N, Liu HC, Moeser AJ, Spears JW. Iron transporters are differentially regulated by dietary iron, and modifications are associated with changes in manganese metabolism in young pigs. J Nutr. 2009;139(8):1474-9.

50. Davidsson LA, Lonnerdal B. Fe-saturation and proteolysis of human lactoferrin: effect on brush-border receptor-mediated uptake of Fe and Mn. The American journal of physiology. 1989;257(6 Pt 1):G930-4.

51. Davidsson L, Cederblad A, Lonnerdal B, Sandstrom B. The effect of individual dietary components on manganese absorption in humans. Am J Clin Nutr. 1991;54(6):1065-70.

52. Stef DS, Gergen I. Effect of mineral-enriched diet and medicinal herbs on Fe, Mn, Zn, and Cu uptake in chicken. Chem Cent J. 2012;6(1):19.

53. Britton AA, Cotzias GC. Dependence of manganese turnover on intake. The American journal of physiology. 1966;211(1):203-6.

54. Dorman DC, Struve MF, James RA, McManus BE, Marshall MW, Wong BA. Influence of dietary manganese on the pharmacokinetics of inhaled manganese sulfate in male CD rats. Toxicological sciences. 2001;60(2):242-51.

55. Leggett RW. A biokinetic model for manganese. Sci Total Environ. 2011;409(20):4179-86.

56. Reaney SH, Kwik-Uribe CL, Smith DR. Manganese oxidation state and its implications for toxicity. Chem Res Toxicol. 2002;15(9):1119-26.

57. Yokel RA. Manganese flux across the blood-brain barrier. Neuromolecular medicine. 2009;11(4):297-310.

58. Scheuhammer AM, Cherian MG. Binding of manganese in human and rat plasma. Biochimica et biophysica acta. 1985;840(2):163-9.

59. Jursa T, Smith DR. Ceruloplasmin alters the tissue disposition and neurotoxicity of manganese, but not its loading onto transferrin. Toxicol Sci. 2009;107(1):182-93.

60. Harris WR, Chen Y. Electron paramagnetic resonance and difference ultraviolet studies of Mn2+ binding to serum transferrin. J Inorg Biochem. 1994;54(1):1-19.

61. Nischwitz V, Berthele A, Michalke B. Speciation analysis of selected metals and determination of their total contents in paired serum and cerebrospinal fluid samples: An approach to investigate the permeability of the human blood-cerebrospinal fluid-barrier. Anal Chim Acta. 2008;627(2):258-69.

62. Rabin O, Hegedus L, Bourre J, Smith QR. Rapid Brain Uptake of Manganese(I1) Across the Blood-Brain Barrier. Journal of neurochemistry. 1993;61(2):509-17.

63. Foradori AC, Bertinchamps A, Gulibon JM, Cotzias GC. The discrimination between magnesium and manganese by serum proteins. J Gen Physiol. 1967;50(9):2255-66.

64. Davidsson L, Loennerdal B, Sandstroem B, Kunz C, Keen CL. Identification of Transferrin as the Major Plasma Carrier Protein for Manganese Introduced Orally or

Intravenously or After In Vitro Addition in the Rat. Journal of Nutrition. 1989;119(10):1461-4.

65. Gunter TE, Gerstner B, Gunter KK, Malecki J, Gelein R, Valentine WM, et al. Manganese transport via the transferrin mechanism. Neurotoxicology. 2013;34:118-27.

66. Schroeder HA, Balassa JJ, Tipton IH. Essential trace metals in man: manganese, a study in homeostasis. J Chron Dis. 1996;19:545-71.

67. Cohn JR, Emmett EA. The excretion of trace metals in human sweat. Ann Clin Lab Sci. 1978;8(4):270-5.

68. Aschner M, Aschner JL. Manganese Transport Across the Blood-Brain Barrier: Relationship to Iron Homeostasis. Brain research bulletin. 1990;24:857-60.

69. Crossgrove JS, Allen DD, Bukaveckas BL, Rhineheimer SS, Yokel RA. Manganese Distribution Across the Blood–Brain Barrier I. Evidence for Carrier-Mediated Influx of Manganese Citrate as Well as Manganese and Manganese Transferrin. Neurotoxicology. 2003;24:3-13.

70. Crossgrove JS, Yokel RA. Manganese distribution across the blood-brain barrier. IV. Evidence for brain influx through store-operated calcium channels. Neurotoxicology. 2005;26(3):297-307.

71. Crossgrove JS, R.A. Y. Manganese distribution across the blood-brain barrier III. The divalent metal transporter-1 is not the major mechanism mediating brain manganese uptake. Neurotoxicology. 2004;25(3):451-60.

72. Fitsanakis VA, Piccola G, Aschner JL, Aschner M. Manganese transport by rat brain endothelial (RBE4) cell-based transwell model in the presence of astrocyte conditioned media. Journal of neuroscience research. 2005;81(2):235-43.

73. McCarthy RC, Kosman DJ. Mechanistic analysis of iron accumulation by endothelial cells of the BBB. Biometals : an international journal on the role of metal ions in biology, biochemistry, and medicine. 2012;25(4):665-75.

74. Fitsanakis VA, Piccola G, Aschner JL, Aschner M. Characteristics of manganese (Mn) transport in rat brain endothelial (RBE4) cells, an in vitro model of the blood-brain barrier. Neurotoxicology. 2006;27(1):60-70.

75. Bornhorst J, Wehe CA, Huwel S, Karst U, Galla HJ, Schwerdtle T. Impact of manganese on and transfer across blood-brain and blood-cerebrospinal fluid barrier in vitro. The Journal of biological chemistry. 2012;287(21):17140-51.

76. Yokel RA, Crossgrove JS, Bukaveckas BL. Manganese Distribution Across the Blood–Brain Barrier II. Manganese Efflux From the Brain Does not Appear to be Carrier Mediated. Neurotoxicology. 2003;24:15-22.

77. dos Santos AP, Milatovic D, Au C, Yin Z, Batoreu MC, Aschner M. Rat brain endothelial cells are a target of manganese toxicity. Brain research. 2010;1326:152-61.

78. Mishra G, Shukla R, Hasan M, Khanna SK, Das M. Potentiation of neurotoxicity of Lathyrus sativus by manganese: alterations in blood-brain barrier permeability. Toxicology mechanisms and methods. 2009;19(4):318-26.

79. Ramos P, Santos A, Pinto NR, Mendes R, Magalhaes T, Almeida A. Anatomical region differences and age-related changes in copper, zinc, and manganese levels in the human brain. Biological trace element research. 2014;161(2):190-201.

80. Boaru SG, Merle U, Uerlings R, Zimmermann A, Weiskirchen S, Matusch A, et al. Simultaneous monitoring of cerebral metal accumulation in an experimental model of

Wilson's disease by laser ablation inductively coupled plasma mass spectrometry. BMC neuroscience. 2014;15:98.

81. Akatsu H, Hori A, Yamamoto T, Yoshida M, Mimuro M, Hashizume Y, et al. Transition metal abnormalities in progressive dementias. Biometals : an international journal on the role of metal ions in biology, biochemistry, and medicine. 2012;25(2):337-50.

82. Finkelstein Y, Zhang N, Fitsanakis VA, Avison MJ, Gore JC, Aschner M. Differential Deposition of Manganese in the Rat Brain Following Subchronic Exposure to Manganese: a T1-Weighted Magnetic Resonance Imaging Study. Israel Medical Association Journal. 2008;10:793-8.

83. Robison G, Zakharova T, Fu S, Jiang W, Fulper R, Barrea R, et al. X-ray fluorescence imaging: a new tool for studying manganese neurotoxicity. PloS one. 2012;7(11):e48899.

84. Robison G, Zakharova T, Fu S, Jiang W, Fulper R, Barrea R, et al. X-ray fluorescence imaging of the hippocampal formation after manganese exposure. Metallomics : integrated biometal science. 2013;5(11):1554-65.

85. Liccione JJ, Maines MD. Selective vulnerability of glutathione metabolism and cellular defense mechanisms in rat striatum to manganese. The Journal of pharmacology and experimental therapeutics. 1988;247(1):156-61.

86. Gavin CE, Gunter KK, Gunter TE. Manganese and calcium efflux kinetics in brain mitochondria. Biochem J. 1990;266:329-34.

87. Kalia K, Jiang W, Zheng W. Manganese accumulates primarily in nuclei of cultured brain cells. Neurotoxicology. 2008;29(3):466-70.

88. Morello M, Canini A, Mattioli P, Sorge RP, Alimonti A, Bocca B, et al. Sub-cellular localization of manganese in the basal ganglia of normal and manganese-treated rats An

electron spectroscopy imaging and electron energy-loss spectroscopy study. Neurotoxicology. 2008;29(1):60-72.

89. Michalke B, Berthele A, Mistriotis P, Ochsenkuhn-Petropoulou M, Halbach S. Manganese species from human serum, cerebrospinal fluid analyzed by size exclusion chromatography-, capillary electrophoresis coupled to inductively coupled plasma mass spectrometry. Journal of trace elements in medicine and biology : organ of the Society for Minerals and Trace Elements. 2007;21 Suppl 1:4-9.

90. Reaney SH, Bench G, Smith DR. Brain accumulation and toxicity of Mn(II) and Mn(III) exposures. Toxicol Sci. 2006;93(1):114-24.

91. Carmona A, Roudeau S, Perrin L, Veronesi G, Ortega R. Environmental manganese compounds accumulate as Mn(II) within the Golgi apparatus of dopamine cells: relationship between speciation, subcellular distribution, and cytotoxicity. Metallomics. 2014;6(4):822-32.

92. Takeda AJ, Sawashita J, Okada S. Manganese concentration in rat brain: manganese transport from the peripheral tissues. Neuroscience Letters. 1998;242:45-8.

93. Krishna S, Dodd CA, Hekmatyar SK, Filipov NM. Brain deposition and neurotoxicity of manganese in adult mice exposed via the drinking water. Archives of toxicology. 2014;88(1):47-64.

94. Bowman AB, Aschner M. Considerations on manganese (Mn) treatments for in vitro studies. Neurotoxicology. 2014;41:141-2.

95. Doker S, Mounicou S, Dogan M, Lobinski R. Probing the metal-homeostatis effects of the administration of chromium(vi) to mice by ICP MS and size-exclusion chromatography-ICP MS. Metallomics : integrated biometal science. 2010;2(8):549-55.

96. Ergen K, Ince H, Duzova H, Karakoc Y, Emre MH. Acute effects of moderate and strenuous running on trace element distribution in the brain, liver, and spleen of trained rats. Balkan medical journal. 2013;30(1):105-10.

97. Fitsanakis VA, Zhang N, Anderson JG, Erikson KM, Avison MJ, Gore JC, et al. Measuring brain manganese and iron accumulation in rats following 14 weeks of low-dose manganese treatment using atomic absorption spectroscopy and magnetic resonance imaging. Toxicol Sci. 2008;103(1):116-24.

98. Hare DJ, George JL, Grimm R, Wilkins S, Adlard PA, Cherny RA, et al. Three-dimensional elemental bio-imaging of Fe, Zn, Cu, Mn and P in a 6-hydroxydopamine lesioned mouse brain. Metallomics : integrated biometal science. 2010;2(11):745-53.

99. Kumar KK, Lowe EW, Jr., Aboud AA, Neely MD, Redha R, Bauer JA, et al. Cellular manganese content is developmentally regulated in human dopaminergic neurons. Sci Rep. 2014;4:6801.

100. Forbes JR, Gros P. Iron, manganese, and cobalt transport by Nramp1 (Slc11a1) and Nramp2 (Slc11a2) expressed at the plasma membrane. Blood. 2003;102(5):1884-92.

101. Gunshin H, Mackenzie B, Berger UV, Gunshin Y, Romero MF, Boron WF, et al. Cloning and characterization of a mammalian proton-coupled metal-ion transporter. Nature. 1997;338.

102. Fleming MD, Romano MA, Su MA, Garrick LM, M.D. G, Andrews NC. Nramp2 is Mutated in the Anemic Belgrade (b) Rat: Evidence of a Role for Nramp2 in Endosomal Iron Transport. PNAS. 1998;95(3):1148-53.

103. Aschner M, Gannon M. Manganese (Mn) Transport Across the Rat Blood-Brain Barrier: Saturable and Transferrin-dependent Transport Mechanisms. Brain Research Bulletin. 1994;33:345-9.

104. Au C, Benedetto A, Anderson J, Labrousse A, Erikson K, Ewbank JJ, et al. SMF-1, SMF-2 and SMF-3 DMT1 orthologues regulate and are regulated differentially by manganese levels in C. elegans. PLoS One. 2009;4(11):e7792.

105. Erikson K, Aschner M. Manganese Causes Differential Regulation of Glutamate Transporter (GLAST) Taurine Transporter and Metallothionein in Cultured Rat Astrocytes. Neurotoxicology. 2002;23:595-602.

106. Wang X, Miller DS, Zheng W. Intracellular localization and subsequent redistribution of metal transporters in a rat choroid plexus model following exposure to manganese or iron. Toxicology and applied pharmacology. 2008;230(2):167-74.

107. Gruenheid S, Canonne-Hergaux F, Gauthier S, Hackam DJ, Grinstein S, Gros P. The Iron Transport Protein NRAMP2 Is an Integral Membrane Glycoprotein That Colocalizes with Transferrin in Recycling Endosomes. Journal of Experimental Medicine. 1999;189(5):831-41.

108. Huang E, Ong WY, Connor JR. Distribution of divalent metal transporter-1 in the monkey basal ganglia. Neuroscience. 2004;128(3):487-96.

109. Burdo JR, Menzies SL, Simpson IA, Garrick LM, Garrick MD, Dolan KG, et al. Distribution of Divalent Metal Transporter 1 and Metal Transport Protein 1 in the Normal and Belgrade Rat. Journal of neuroscience research. 2001;66:1198-207.

110. Williams BB, Kwakye GF, Wegrzynowicz M, Li D, Aschner M, Erikson KM, et al. Altered Manganese Homeostasis and Manganese Toxicity in a Huntington's Disease

Striatal Cell Model Are Not Explained by Defects in the Iron Transport System. Toxicological Sciences. 2010;117(1):169-79.

111. Wang XS, Ong WY, Connor JR. A light and electron microscopic study of the iron transporter protein DMT-1 in the monkey cerebral neocortex and hippocampus. J Neurocytol. 2001;30(4):353-60.

112. Crossgrove J, Zheng W. Manganese toxicity upon overexposure. NMR Biomed. 2004;17(8):544-53.

113. Seo YA, Li Y, Wessling-Resnick M. Iron depletion increases manganese uptake and potentiates apoptosis through ER stress. Neurotoxicology. 2013;38:67-73.

114. Dickinson TK, Devenyi AG, Connor JR. Distribution of injected ion 59 and manganese 54 in hypotransferrinemic mice. J Lab Clin Med. 1996;128(3):270-8.

115. Keefer RC, Barak AJ, Boyett JD. Binding of manganese and transferrin in rat serum. Biochimica et biophysica acta. 1970;221(2):390-3.

116. Ayton S, Lei P, Duce JA, Wong BXW, Sedjahtera A, Adlard PA, et al. Ceruloplasmin Dysfunction and Therapeutic Potential for Parkinson Disease. ANNALS of Neurology. 2013;73(4):554-9.

117. He L, Girijashanker K, Dalton TP, Reed J, Li H, Soleimani M, et al. ZIP8, member of the solute-carrier-39 (SLC39) metal-transporter family: characterization of transporter properties. Molecular pharmacology. 2006;70(1):171-80.

118. Wang CY, Jenkitkasemwong S, Duarte S, Sparkman BK, Shawki A, Mackenzie B, et al. ZIP8 is an iron and zinc transporter whose cell-surface expression is up-regulated by cellular iron loading. The Journal of biological chemistry. 2012;287(41):34032-43.

119. Fujishiro H, Ohashi T, Takuma M, Himeno S. Suppression of ZIP8 expression is a common feature of cadmium-resistant and manganese-resistant RBL-2H3 cells. Metallomics. 2013;5(5):437-44.

120. Fujishiro H, Yoshida M, Nakano Y, Himeno S. Interleukin-6 enhances manganese accumulation in SH-SY5Y cells: implications of the up-regulation of ZIP14 and the down-regulation of ZnT10. Metallomics : integrated biometal science. 2014;6(4):944-9.

121. Suwalsky M, Villena F, Sotomayor CP. Mn2+ exerts stronger structural effects than the Mn-citrate complex on the human erythrocyte membrane and molecular models. Journal of inorganic biochemistry. 2010;104(1):55-61.

122. Lockman PR, Roder KE, Allen DD. Inhibition of the rat blood brain barrier choline transporter by manganese chloride. Journal of Neurochemistry. 2001;79:588-94.

123. Bagga P, Patel AB. Regional cerebral metabolism in mouse under chronic manganese exposure: implications for manganism. Neurochemistry international. 2012;60(2):177-85.

124. Olanow CW, Good PF, Shinotoh H, Hewitt KA, Vingerhoets F, Snow BJ, et al. Manganese intoxication in the rhesus monkey: A clinical, imaging, pathologic, and biochemical study. Neurology. 1996;46:492-8.

125. Roth J, Ponzoni S, Aschner M. Manganese homeostasis and transport. Metal ions in life sciences. 2013;12:169-201.

126. Guilarte TR, Chen MK, McGlothan JL, Verina T, Wong DF, Zhou Y, et al. Nigrostriatal dopamine system dysfunction and subtle motor deficits in manganese-exposed non-human primates. Experimental neurology. 2006;202(2):381-90.

127. Roth JA, Li Z, Sridhar S, Khoshbouei H. The effect of manganese on dopamine toxicity and dopamine transporter (DAT) in control and DAT transfected HEK cells. Neurotoxicology. 2013;35:121-8.

128. Grimm C, Kraft R, Sauerbruch S, Schultz G, Harteneck C. Molecular and functional characterization of the melastatin-related cation channel TRPM3. J Biol Chem. 2003;278(24):21493-501.

129. Riccio A, Mattei C, Kelsell RE, Medhurst AD, Calver AR, Randall AD, et al. Cloning and functional expression of human short TRP7, a candidate protein for store-operated Ca2+ influx. The Journal of biological chemistry. 2002;277(14):12302-9.

130. Loutzenhiser K, Loutzenhiser R. Angiotensin II-Induced Ca2+ Influx in Renal Afferent and Efferent Arterioles Differeing Roles of Voltage Gated and Store Operated Ca2+ Entry. Circulation Research. 2000;87:551-7.

131. Lucaciu CM, Dragu C, Copa˘escu L, Morariu VV. Manganese transport through human erythrocyte membranes. An EPR study. Biochimica et biophysica acta. 1997;1328:90-8.

132. Kannurpatti SS, Joshi PG, Joshi NB. Calcium Sequestering Ability of Mitochondria Modulates Influx of Calcium through Glutamate Receptor Channel. Neurochemical Research. 2000;25(12):1527-36.

133. Guilbert A, Gautier M, Dhennin-Duthille I, Haren N, Sevestre H, Ouadid-Ahidouch H. Evidence that TRPM7 is required for breast cancer cell proliferation. Am J Physiol Cell Physiol. 2009;297(3):C493-502.

134. Xu SZ, Zeng F, Boulay G, Grimm C, Harteneck C, Beech DJ. Block of TRPC5 channels by 2-aminoethoxydiphenyl borate: a differential, extracellular and voltage-dependent effect. British journal of pharmacology. 2005;145(4):405-14.

135. Seve M, Chimienti F, Devergnas S, Favier A. In silico identification and expression of SLC30 family genes: An expressed sequence tag data mining strategy for the characterization of zinc transporters' tissue expression. BMC Genomics. 2004;5(1):32-40.

136. Quadri M, Federico A, Zhao T, Breedveld GJ, Battisti C, Delnooz C, et al. Mutations in SLC30A10 cause parkinsonism and dystonia with hypermanganesemia, polycythemia, and chronic liver disease. American journal of human genetics. 2012;90(3):467-77.

137. Tuschl K, Clayton PT, Gospe SM, Jr., Gulab S, Ibrahim S, Singhi P, et al. Syndrome of hepatic cirrhosis, dystonia, polycythemia, and hypermanganesemia caused by mutations in SLC30A10, a manganese transporter in man. American journal of human genetics. 2012;90(3):457-66.

138. Leyva-Illades D, Chen P, Zogzas CE, Hutchens S, Mercado JM, Swaim CD, et al. SLC30A10 Is a Cell Surface-Localized Manganese Efflux Transporter, and Parkinsonism-Causing Mutations Block Its Intracellular Trafficking and Efflux Activity. The Journal of neuroscience : the official journal of the Society for Neuroscience. 2014;34(42):14079-95.

139. Waghorn B, Schumacher A, Liu J, Jacobs S, Baba A, Matsuda T, et al. Indirectly probing Ca(2+) handling alterations following myocardial infarction in a murine model using T(1)-mapping manganese-enhanced magnetic resonance imaging. Magnetic resonance in medicine : official journal of the Society of Magnetic Resonance in Medicine / Society of Magnetic Resonance in Medicine. 2011;65(1):239-49.

140. Waghorn B, Yang Y, Baba A, Matsuda T, Schumacher A, Yanasak N, et al. Assessing manganese efflux using SEA0400 and cardiac T1-mapping manganese-enhanced MRI in a murine model. NMR in biomedicine. 2009;22(8):874-81.

141. Tidball AM, Bryan MR, Uhouse MA, Kumar KK, Aboud AA, Feist JE, et al. A novel manganese-dependent ATM-p53 signaling pathway is selectively impaired in patient-based neuroprogenitor and murine striatal models of Huntington's disease. Hum Mol Genet. 2014;. pii: ddu609 (Epub ahead of print).

142. Antoons G, Mubagwa K, Nevelsteen I, Sipido KR. Mechanisms underlying the frequency dependence of contraction and [Ca(2+)](i) transients in mouse ventricular myocytes. J Physiol. 2002;543(Pt 3):889-98.

143. Bassani JW, Bassani RA, Bers DM. Relaxation in rabbit and rat cardiac cells: species-dependent differences in cellular mechanisms. J Physiol. 1994;476(2):279-93.

144. Varro A, Negretti N, Hester SB, Eisner DA. An estimate of the calcium content of the sarcoplasmic reticulum in rat ventricular myocytes. Pflugers Arch. 1993;423(1-2):158-60.

145. Madejczyk MS, Ballatori N. The iron transporter ferroportin can also function as a manganese exporter. Biochimica et biophysica acta. 2012;1818(3):651-7.

146. Yin Z, Jiang H, Lee ES, Ni M, Erikson KM, Milatovic D, et al. Ferroportin is a manganese-responsive protein that decreases manganese cytotoxicity and accumulation. Journal of neurochemistry. 2010;112(5):1190-8.

147. Li X, Xie J, Lu L, Zhang L, Zhang L, Zou Y, et al. Kinetics of manganese transport and gene expressions of manganese transport carriers in Caco-2 cell monolayers. Biometals : an international journal on the role of metal ions in biology, biochemistry, and medicine. 2013;26(6):941-53.

148. Mitchell CJ, Shawki A, Ganz T, Nemeth E, Mackenzie B. Functional properties of human ferroportin, a cellular iron exporter reactive also with cobalt and zinc. American journal of physiology Cell physiology. 2014;306(5):C450-9.

149. Gitler AD, Chesi A, Geddie ML, Strathearn KE, Hamamichi S, Hill KJ, et al. Alpha-synuclein is part of a diverse and highly conserved interaction network that includes PARK9 and manganese toxicity. Nature genetics. 2009;41(3):308-15.

150. Ramonet D, Podhajska A, Stafa K, Sonnay S, Trancikova A, Tsika E, et al. PARK9-associated ATP13A2 localizes to intracellular acidic vesicles and regulates cation homeostasis and neuronal integrity. Human molecular genetics. 2012;21(8):1725-43.

151. Schmidt K, Wolfe DM, Stiller B, Pearce DA. Cd2+, Mn2+, Ni2+ and Se2+ toxicity to Saccharomyces cerevisiae lacking YPK9p the orthologue of human ATP13A2. Biochemical and biophysical research communications. 2009;383(2):198-202.

152. Tan J, Zhang T, Jiang L, Chi J, Hu D, Pan Q, et al. Regulation of intracellular manganese homeostasis by Kufor-Rakeb syndrome-associated ATP13A2 protein. The Journal of biological chemistry. 2011;286(34):29654-62.

153. Kong SM, Chan BK, Park JS, Hill KJ, Aitken JB, Cottle L, et al. Parkinson's disease-linked human PARK9/ATP13A2 maintains zinc homeostasis and promotes alpha-Synuclein externalization via exosomes. Human molecular genetics. 2014;23(11):2816-33.

154. van Veen S, Sorensen DM, Holemans T, Holen HW, Palmgren MG, Vangheluwe P. Cellular function and pathological role of ATP13A2 and related P-type transport ATPases in Parkinson's disease and other neurological disorders. Frontiers in molecular neuroscience. 2014;7:48.

155. Murin R, Verleysdonk S, Raeymaekers L, Kaplan P, Lehotsky J. Distribution of secretory pathway Ca2+ ATPase (SPCA1) in neuronal and glial cell cultures. Cell Mol Neurobiol. 2006;26(7-8):1355-65.

156. Missiaen L, Raeymaekers L, Dode L, Vanoevelen J, Van Baelen K, Parys JB, et al. SPCA1 pumps and Hailey-Hailey disease. Biochemical and biophysical research communications. 2004;322(4):1204-13.

157. Dode L, Andersen JP, Raeymaekers L, Missiaen L, Vilsen B, Wuytack F. Functional comparison between secretory pathway Ca2+/Mn2+-ATPase (SPCA) 1 and sarcoplasmic reticulum Ca2+-ATPase (SERCA) 1 isoforms by steady-state and transient kinetic analyses. J Biol Chem. 2005;280(47):39124-34.

158. Dode L, Andersen JP, Vanoevelen J, Raeymaekers L, Missiaen L, Vilsen B, et al. Dissection of the functional differences between human secretory pathway Ca2+/Mn2+-ATPase (SPCA) 1 and 2 isoenzymes by steady-state and transient kinetic analyses. J Biol Chem. 2006;281(6):3182-9.

159. Wei Y, Chen J, Rosas G, Tompkins DA, Holt PA, Rao R. Phenotypic screening of mutations in Pmr1, the yeast secretory pathway Ca2+/Mn2+-ATPase, reveals residues critical for ion selectivity and transport. J Biol Chem. 2000;275(31):23927-32.

160. Ton VK, Mandal D, Vahadji C, Rao R. Functional expression in yeast of the human secretory pathway Ca(2+), Mn(2+)-ATPase defective in Hailey-Hailey disease. J Biol Chem. 2002;277(8):6422-7.

161. Okunade GW, Miller ML, Azhar M, Andringa A, Sanford LP, Doetschman T, et al. Loss of the Atp2c1 secretory pathway Ca(2+)-ATPase (SPCA1) in mice causes Golgi stress,

apoptosis, and midgestational death in homozygous embryos and squamous cell tumors in adult heterozygotes. J Biol Chem. 2007;282(36):26517-27.

162. Zhang S, Fu J, Zhou Z. Changes in the brain mitochondrial proteome of male Sprague-Dawley rats treated with manganese chloride. Toxicology and applied pharmacology. 2005;202(1):13-7.

163. Sepulveda MR, Wuytack F, Mata AM. High levels of Mn(2)(+) inhibit secretory pathway Ca(2)(+)/Mn(2)(+)-ATPase (SPCA) activity and cause Golgi fragmentation in neurons and glia. J Neurochem. 2012;123(5):824-36.

164. Leitch S, Feng M, Muend S, Braiterman LT, Hubbard AL, Rao R. Vesicular distribution of Secretory Pathway Ca(2)+-ATPase isoform 1 and a role in manganese detoxification in liver-derived polarized cells. Biometals. 2011;24(1):159-70.

165. Mukhopadhyay S, Linstedt AD. Identification of a gain-of-function mutation in a Golgi P-type ATPase that enhances Mn2+ efflux and protects against toxicity. PNAS. 2011;108(2):858-63.

166. Sepulveda MR, Marcos D, Berrocal M, Raeymaekers L, Mata AM, Wuytack F. Activity and localization of the secretory pathway Ca2+-ATPase isoform 1 (SPCA1) in different areas of the mouse brain during postnatal development. Mol Cell Neurosci. 2008;38(4):461-73.

167. Wuytack F, Raeymaekers L, Missiaen L. Molecular physiology of the SERCA and SPCA pumps. Cell Calcium. 2002;32(5-6):279-305.

168. Vanoevelen J, Dode L, Van Baelen K, Fairclough RJ, Missiaen L, Raeymaekers L, et al. The secretory pathway Ca2+/Mn2+-ATPase 2 is a Golgi-localized pump with high affinity for Ca2+ ions. J Biol Chem. 2005;280(24):22800-8.

169. Xiang M, Mohamalawari D, Rao R. A novel isoform of the secretory pathway Ca2+,Mn(2+)-ATPase, hSPCA2, has unusual properties and is expressed in the brain. J Biol Chem. 2005;280(12):11608-14.

170. Wootton LL, Argent CC, Wheatley M, Michelangeli F. The expression, activity and localisation of the secretory pathway Ca2+ -ATPase (SPCA1) in different mammalian tissues. Biochimica et biophysica acta. 2004;1664(2):189-97.

171. Gunteski Hamblin AM, Clarke DM, Shull GE. Molecular cloning and tissue distribution of alternatively spliced mRNAs encoding possible mammalian homologues of the yeast secretory pathway calcium pump. Biochemistry. 1992;31(33):7600-8.

172. Micaroni M, Perinetti G, Berrie CP, Mironov AA. The SPCA1 Ca2+ pump and intracellular membrane trafficking. Traffic. 2010;11(10):1315-33.

173. Reinhardt TA, Lippolis JD, Shull GE, Horst RL. Null mutation in the gene encoding plasma membrane Ca2+-ATPase isoform 2 impairs calcium transport into milk. J Biol Chem. 2004;279(41):42369-73.

174. Sepulveda MR, Vanoevelen J, Raeymaekers L, Mata AM, Wuytack F. Silencing the SPCA1 (secretory pathway Ca2+-ATPase isoform 1) impairs Ca2+ homeostasis in the Golgi and disturbs neural polarity. J Neurosci. 2009;29(39):12174-82.

175. Mukhopadhyay S, Bachert C, Smith DR, Linstedt AD. Manganese-induced Trafficking and Turnover of the cis-Golgi Glycoprotein GPP130. Molecular Biology of the Cell. 2010;21:1282-92.

176. Puri S, Bachert C, Fimmel CJ, Linstedt AD. Cycling of early Golgi proteins via the cell surface and endosomes upon lumenal pH disruption. Traffic. 2002;3(9):641-53.

177. Masuda M, Braun-Sommargren M, Crooks D, Smith DR. Golgi phosphoprotein 4 (GPP130) is a sensitive and selective cellular target of manganese exposure. Synapse. 2013;67(5):205-15.

178. Tewari R, Jarvela T, Linstedt AD. Manganese induces oligomerization to promote down-regulation of the intracellular trafficking receptor used by Shiga toxin. Mol Biol Cell. 2014;25(19):3049-58.

179. Kobayashi K, Kuroda J, Shibata N, Hasegawa T, Seko Y, Satoh M, et al. Induction of metallothionein by manganese is completely dependent on interleukin-6 production. The Journal of pharmacology and experimental therapeutics. 2007;320(2):721-7.

180. Yu H, Iyer RK, Kern RM, Rodriguez WI, Grody WW, Cederbaum SD. Expression of arginase isozymes in mouse brain. Journal of neuroscience research. 2001;66(3):406-22.

181. Braissant O, Gotoh T, Loup M, Mori M, Bachmann C. L-arginine uptake, the citrulline–NO cycle and arginase II in the rat brain: an in situ hybridization study. Molecular Brain Research. 1999;70:231-41.

182. Kanyo ZF, Scolnick LR, Ash DE, Christianson DW. Structure of a unique binuclear manganese cluster in arginase. Nature. 1996;383(6600):554-7.

183. D'Antonio EL, Hai Y, Christianson DW. Structure and function of non-native metal clusters in human arginase I. Biochemistry. 2012;51(42):8399-409.

184. Yang J, Gonon AT, Sjoquist PO, Lundberg JO, Pernow J. Arginase regulates red blood cell nitric oxide synthase and export of cardioprotective nitric oxide bioactivity. Proceedings of the National Academy of Sciences of the United States of America. 2013;110(37):15049-54.

185. Berkowitz DE, White R, Li D, Minhas KM, Cernetich A, Kim S, et al. Arginase reciprocally regulates nitric oxide synthase activity and contributes to endothelial dysfunction in aging blood vessels. Circulation. 2003;108(16):2000-6.

186. Estevez AG, Sahawneh MA, Lange PS, Bae N, Egea M, Ratan RR. Arginase 1 regulation of nitric oxide production is key to survival of trophic factor-deprived motor neurons. The Journal of neuroscience : the official journal of the Society for Neuroscience. 2006;26(33):8512-6.

187. Esch FL, K.; Hills, A.; Zaman, K.; Baraban, J.; Chatterjee, S.; Rubin, L.; Ash, D.E.; Ratan, R.R. Purification of a Multipotent Antideath Activity from Bovine Liver and Its Identification as Arginase: Nitric Oxide-Independent Inhibition of Neuronal Apoptosis. Journal of Neuroscience. 1998;18(11):4083-95.

188. Colton CA, Mott RT, Sharpe H, Xu Q, Van Nostrand WE, Vitek MP. Expression profiles for macrophage alternative activation genes in AD and in mouse models of AD. J Neuroinflammation. 2006;3:27.

189. Kuo HS, Tsai MJ, Huang MC, Chiu CW, Tsai CY, Lee MJ, et al. Acid fibroblast growth factor and peripheral nerve grafts regulate Th2 cytokine expression, macrophage activation, polyamine synthesis, and neurotrophin expression in transected rat spinal cords. J Neurosci. 2011;31(11):4137-47.

190. Deng K, He H, Qiu J, Lorber B, Bryson JB, Filbin MT. Increased synthesis of spermidine as a result of upregulation of arginase I promotes axonal regeneration in culture and in vivo. J Neurosci. 2009;29(30):9545-52.

191. Norenberg MD. Distribution of glutamine synthetase in the rat central nervous system. Journal of Histochemistry & Cytochemistry. 1979;27(3):756-62.

192. Hertz LY, A.; Svenneby, G.; Kvamme, E.; Fosmark, H.; Schousboe, A. Absence of preferential glutamine uptake into neurons--an indication of a net transfer of TCA constituents from nerve endings to astrocytes? Neuroscience Letters. 1980;16:103-9.

193. Hassel BB, H.; Jones, P.; Fonnum, F.; Sonnewald, U. Trafficking of Amino Acids Between Neurons and Glia In Vivo. Effects of Inhibition of Glial Metabolism by Fluoroacetate. Journal of Cerebral Blood Flow and Metabolism. 1997;17:1230-8.

194. Zou JY, Crews FT. TNF alpha potentiates glutamate neurotoxicity by inhibiting glutamate uptake in organotypic brain slice cultures: neuroprotection by NF kappa B inhibition. Brain Res. 2005;1034(1-2):11-24.

195. Zou J, Wang YX, Dou FF, Lu HZ, Ma ZW, Lu PH, et al. Glutamine synthetase down-regulation reduces astrocyte protection against glutamate excitotoxicity to neurons. Neurochem Int. 2010;56(4):577-84.

196. Shaked IB-D, I.; Vardimon, L. Glutamine synthetase enhances the clearance of extracellular glutamate by the neural retina. Journal of Neurochemistry. 2002;83:574-80.

197. Gorovitz RA, N.; Avisar, N.; Shaked, I.; Vardimon, L. Glutamine synthetase protects against neuronal degeneration in injured retinal tissue. Proc Natl Acad Sci USA. 1997;94:7024-9.

198. Lehmann C, Bette S, Engele J. High extracellular glutamate modulates expression of glutamate transporters and glutamine synthetase in cultured astrocytes. Brain Res. 2009;1297:1-8.

199. Sidoryk-Wegrzynowicz M, Lee E, Albrecht J, Aschner M. Manganese disrupts astrocyte glutamine transporter expression and function. J Neurochem. 2009;110(3):822-30.

200. Milatovic D, Yin Z, Gupta RC, Sidoryk M, Albrecht J, Aschner JL, et al. Manganese induces oxidative impairment in cultured rat astrocytes. Toxicological sciences : an official journal of the Society of Toxicology. 2007;98(1):198-205.

201. Morello M, Zatta P, Zambenedetti P, Martorana A, D'Angelo V, Melchiorri G, et al. Manganese intoxication decreases the expression of manganoproteins in the rat basal ganglia: an immunohistochemical study. Brain research bulletin. 2007;74(6):406-15.

202. Buettner GRN, C.F.; Wang, M.; Rodgers, V.G.J.; Schafer, F.Q. A New Paradigm: Manganese Superoxide Dismutase Influences the Production of H2O2 in Cells and Thereby Their Biological State. Free Radic Biol Med 2006;41(8):1338-50.

203. Shan XC, L.; Ke, Y.; Luo, C.; Qian, S.; Gozal, D.; Liu, R. Manganese Superoxide Dismutase Protects Mouse Cortical Neurons From Chronic Intermittent Hypoxia-Mediated Oxidative Damage. Neurobiol Dis. 2007;28(2):206-15.

204. Keller JNK, M.S.; Holtsberg, F.W.; St. Clair, D.K.; Yen, H.; Germeyer, A.; Steiner, S.M.; Bruce-Keller, A.J.; Hutchins, J.B.; Mattson, M.P. Mitochondrial Manganese Superoxide Dismutase Prevents Neural Apoptosis and Reduces Ischemic Brain Injury: Suppression of Peroxynitrite Production, Lipid Peroxidation, and Mitochondrial Dysfunction. Journal of Neuroscience. 1998;18(2):687-97.

205. Dumont M, Wille E, Stack C, Calingasan NY, Beal MF, Lin MT. Reduction of oxidative stress, amyloid deposition, and memory deficit by manganese superoxide dismutase overexpression in a transgenic mouse model of Alzheimer's disease. FASEB J. 2009;23(8):2459-66.

206. Mizuno K, Whittaker MM, Bachinger HP, Whittaker JW. Calorimetric studies on the tight binding metal interactions of Escherichia coli manganese superoxide dismutase. The Journal of biological chemistry. 2004;279(26):27339-44.

207. Davis CD, Greger JL. Longitudinal changes of manganese-dependent superoxide dismutase and other indexes of manganese and iron status in women. Am J Clin Nutr. 1992;55:747-52.

208. Wozniak-Celmer E, Oldziej S, Ciarkowski J. Theoretical models of catalytic domains of protein phosphatases 1 and 2A with Zn2+ and Mn2+ metal dications and putative bioligands in their catalytic centersBF. Acta Biochimica Polonica. 2001;48(1):35-52.

209. Chan DW. Purification and Characterization of ATM from Human Placenta. A MANGANESE-DEPENDENT, WORTMANNIN-SENSITIVE SERINE/THREONINE PROTEIN KINASE. Journal of Biological Chemistry. 2000;275(11):7803-10.

210. Midvan AS, Scrutton MC, Utter MF. Pyruvate Carboxylase: VII. A POSSIBLE ROLE FOR TIGHTLY BOUND MANGANESE. J Biol Chem. 1966;241:3488-98.

211. Scrutton MC, Utter MF. Pyruvate Carboxylase III. SOME PHYSICAL AND CHEMICAL PROPERTIES OF THE HIGHLY PURIFIED ENZYME. The Journal of biological chemistry. 1965;240(1):1-9.

212. Scrutton MC, Utter MF, Mildvan AS. Pyruvate Carboxylase: VI. THE PRESENCE OF TIGHTLY BOUND MANGANESE. Journal of Biological Chemistry. 1966;241:3480-7.

213. Mochel F, DeLonlay P, Touati G, Brunengraber H, Kinman RP, Rabier D, et al. Pyruvate carboxylase deficiency: clinical and biochemical response to anaplerotic diet therapy. Molecular genetics and metabolism. 2005;84(4):305-12.

214. Xiao L, Gong LL, Yuan D, Deng M, Zeng XM, Chen LL, et al. Protein phosphatase-1 regulates Akt1 signal transduction pathway to control gene expression, cell survival and differentiation. Cell death and differentiation. 2010;17(9):1448-62.

215. Li DW, Liu JP, Schmid PC, Schlosser R, Feng H, Liu WB, et al. Protein serine/threonine phosphatase-1 dephosphorylates p53 at Ser-15 and Ser-37 to modulate its transcriptional and apoptotic activities. Oncogene. 2006;25(21):3006-22.

216. Ambrose M, Goldstine JV, Gatti RA. Intrinsic mitochondrial dysfunction in ATM-deficient lymphoblastoid cells. Hum Mol Genet. 2007;16(18):2154-64.

217. Sharma NK, Lebedeva M, Thomas T, Kovalenko OA, Stumpf JD, Shadel GS, et al. Intrinsic mitochondrial DNA repair defects in Ataxia Telangiectasia. DNA Repair (Amst). 2014;13:22-31.

218. Banin S, Moyal L, Shieh S, Taya Y, Anderson CW, Chessa L, et al. Enhanced phosphorylation of p53 by ATM in response to DNA damage. Science. 1998;281(5383):1674-7.

219. Guo ZK, S.; Lavin, M.F.; Person, M.D.; Paull, T.T. ATM activation by oxidative stress. Science. 2010;330(6003):517-21.

220. Canman CEL, D.S.; Cimprich, K.A.; Taya, Y.; Tamai, K.; Sakaguchi, K.; Appella, E.; Kastan, M.B.; Siliciano, J.D. Activation of the ATM kinase by ionizing radiation and phosphorylation of p53. Science. 1998;281(5383):1677-9.

221. Kozlov S. ATP Activates Ataxia-Telangiectasia Mutated (ATM) in Vitro. Importance of Autophosphorylation. Journal of Biological Chemistry. 2003;278(11):9309-17.

222. Hopfner K, Karcher A, Craig L, Woo TT, Carney JP, Tainer JA. Structural Biochemistry and Interaction Architecture of the DNA Double-Strand Break Repair Mre11 Nuclease and Rad50-ATPase. Cell. 2001;105:473-85.

223. Paull TT, Gellert M. The 3' to 5' Exonuclease Activity of Mre11 Facilitates Repair of DNA Double-Strand Breaks. Molecular cell. 1998;1:969-79.

224. Trujillo KM, Yuan SSF, Lee EYHP, Sung P. Nuclease Activities in a Complex of Human Recombination and DNA Repair Factors Rad50, Mre11, and p95. Journal of Biological Chemistry. 1998;273(34):21447-50.

225. Limbo O, Moiani D, Kertokalio A, Wyman C, Tainer JA, Russell P. Mre11 ATLD17/18 mutation retains Tel1/ATM activity but blocks DNA double-strand break repair. Nucleic acids research. 2012;40(22):11435-49.

226. Guilarte TR. APLP1, Alzheimer's-like pathology and neurodegeneration in the frontal cortex of manganese-exposed non-human primates. Neurotoxicology. 2010;31(5):572-4.

227. Guilarte TR, Burton NC, Verina T, Prabhu VV, Becker KG, Syversen T, et al. Increased APLP1 expression and neurodegeneration in the frontal cortex of manganese-exposed non-human primates. J Neurochem. 2008;105(5):1948-59.

228. Shi S, Zhao J, Yang L, Nie X, Han J, Ma X, et al. KHSRP Participates in Manganese-Induced Neurotoxicity in Rat Striatum and PC12 Cells. Journal of molecular neuroscience : MN. 2014.

229. Zhang P, Lokuta KM, Turner DE, Liu B. Synergistic dopaminergic neurotoxicity of manganese and lipopolysaccharide: differential involvement of microglia and astroglia. J Neurochem. 2010;112(2):434-43.

230. Spranger M, Schwab S, Desiderato S, Bonmann E, Krieger D, Fandrey J. Manganese augments nitric oxide synthesis in murine astrocytes: a new pathogenetic mechanism in manganism? Exp Neurol. 1998;149(1):277-83.

231. Crittenden PL, Filipov NM. Manganese-induced potentiation of in vitro proinflammatory cytokine production by activated microglial cells is associated with persistent activation of p38 MAPK. Toxicol In Vitro. 2008;22(1):18-27.

232. Filipov NM, Seegal RF, Lawrence DA. Manganese potentiates in vitro production of proinflammatory cytokines and nitric oxide by microglia through a nuclear factor kappa B-dependent mechanism. Toxicological sciences : an official journal of the Society of Toxicology. 2005;84(1):139-48.

233. Liu M, Cai T, Zhao F, Zheng G, Wang Q, Chen Y, et al. Effect of microglia activation on dopaminergic neuronal injury induced by manganese, and its possible mechanism. Neurotox Res. 2009;16(1):42-9.

234. Lawson LJ, Perry VH, Dri P, Gordon S. Heterogeneity in the distribution and morphology of microglia in the normal adult mouse brain. Neuroscience. 1990;39(1):151-70.

235. Czlonkowska A, Kohutnicka M, Kurkowska-Jastrzebska I, Czlonkowski A. Microglial reaction in MPTP (1-methyl-4-phenyl-1,2,3,6-tetrahydropyridine) induced Parkinson's disease mice model. Neurodegeneration. 1996;5(2):137-43.

236. Williams BB, Li D, Wegrzynowicz M, Vadodaria BK, Anderson JG, Kwakye GF, et al. Disease-toxicant screen reveals a neuroprotective interaction between Huntington's disease and manganese exposure. J Neurochem. 2010;112(1):227-37.

237. Wegrzynowicz M, Holt HK, Friedman DB, Bowman AB. Changes in the striatal proteome of YAC128Q mice exhibit gene-environment interactions between mutant huntingtin and manganese. J Proteome Res. 2012;11(2):1118-32.

238. Madison JL, Wegrzynowicz M, Aschner M, Bowman AB. Disease-toxicant interactions in manganese exposed Huntington disease mice: early changes in striatal neuron morphology and dopamine metabolism. PLoS One. 2012;7(2):e31024.

239. Stansfield KH, Bichell TJ, Bowman AB, Guilarte TR. BDNF and Huntingtin protein modifications by manganese: implications for striatal medium spiny neuron pathology in manganese neurotoxicity. J Neurochem. 2014;131(5):655-66.

240. Bowman AB, Kwakye GF, Herrero Hernandez E, Aschner M. Role of manganese in neurodegenerative diseases. Journal of trace elements in medicine and biology : organ of the Society for Minerals and Trace Elements. 2011;25(4):191-203.

241. Carter CJ. Glutamine synthetase activity in Huntington's disease. Life Sci. 1982;31(11):1151-9.

242. Butterworth J. Changes in nine enzyme markers for neurons, glia, and endothelial cells in agonal state and Huntington's disease caudate nucleus. J Neurochem. 1986;47(2):583-7.

243. Chiang MC, Chen HM, Lee YH, Chang HH, Wu YC, Soong BW, et al. Dysregulation of C/EBPalpha by mutant Huntingtin causes the urea cycle deficiency in Huntington's disease. Human molecular genetics. 2007;16(5):483-98.

244. Chiang MC, Chen HM, Lai HL, Chen HW, Chou SY, Chen CM, et al. The A2A adenosine receptor rescues the urea cycle deficiency of Huntington's disease by enhancing the activity of the ubiquitin-proteasome system. Hum Mol Genet. 2009;18(16):2929-42.

245. Rosas HD, Chen YI, Doros G, Salat DH, Chen NK, Kwong KK, et al. Alterations in brain transition metals in Huntington disease: an evolving and intricate story. Arch Neurol. 2012;69(7):887-93.

246. Ferlazzo ML, Sonzogni L, Granzotto A, Bodgi L, Lartin O, Devic C, et al. Mutations of the Huntington's disease protein impact on the ATM-dependent signaling and repair pathways of the radiation-induced DNA double-strand breaks: corrective effect of statins and bisphosphonates. Molecular neurobiology. 2014;49(3):1200-11.

247. Chen J, Marks E, Lai B, Zhang Z, Duce JA, Lam LQ, et al. Iron accumulates in Huntington's disease neurons: protection by deferoxamine. PloS one. 2013;8(10):e77023.

248. Brock AA, Chapman SA, Ulaman EA, Wu G. Dietary Manganese Deficiency Decreases Rat Hepatic Arginase Activity. American Insititue of Nutrition. 1993:340-4.

249. Ensunsa JL, J.D. S, Lanoue L, Schrader HR, Keen CL. Reducing arginase activity via dietary manganese deficiency enhances endothelium-dependent vasorelaxation of rat aorta. Exp Biol Med. 2004;229(11):1143-53.

250. Esch F, Lin K, Hills A, Baraban JM, Chatterjee S, Rubin L, et al. Purification of a Multipotent Antideath Activity from Bovine Liver and Its Identification as Arginase: Nitric Oxide-Independent Inhibition of Neuronal Apoptosis. The Journal of Neuroscience. 1998;18(11):4083-95.

251. Lee J, Ryu H, Ferrante RJ, Morris SM, Jr., Ratan RR. Translational control of inducible nitric oxide synthase expression by arginine can explain the arginine paradox. Proceedings of the National Academy of Sciences of the United States of America. 2003;100(8):4843-8.

252. Deckel AW, Tang V, Nuttal D, Gary KA, Elder R. Altered neuronal nitric oxide synthase expression contributes to disease progression in Huntington's disease transgenic mice. Brain research. 2002;939:76-86.

253. Deckel AW, Volmer P, Weiner R, Gary KA, Covault J, Sasso D, et al. Dietary arginine alters time of symptom onset in Huntington's disease transgenic mice. Brain research. 2000;875:187-95.

254. Behrens PF, Franz P, Woodman B, Lindenberg KS, Landwehrmeyer GB. Impaired glutamate transport and glutamate± glutamine cycling: downstream effects of the Huntington mutation. Brain. 2002;125:1908-22.

255. Carter CJ. Glutamine Synthetase Activity in Huntington's Disease. Life Sciences. 1982;31:1151-9.

256. Kulijewicz-Nawrot M, Sykova E, Chvatal A, Verkhratsky A, Rodriguez JJ. Astrocytes and glutamate homoeostasis in Alzheimer's disease: a decrease in glutamine synthetase, but not in glutamate transporter-1, in the prefrontal cortex. ASN Neuro. 2013;5(4):273-82.

257. Olabarria M, Noristani HN, Verkhratsky A, Rodriguez JJ. Age-dependent decrease in glutamine synthetase expression in the hippocampal astroglia of the triple transgenic Alzheimer's disease mouse model: mechanism for deficient glutamatergic transmission? Molecular Neurodegeneration. 2011;6(55).

258. Robinson SR. Neuronal expression of glutamine synthetase in Alzheimer's disease indicates a profound impairment of metabolic interactions with astrocytes. Neurochemistry International. 2000;36:471-82.

259. Andreassen OA, Ferrante RJ, Dedeoglu A, Albers DW, Klivenyi P, Carlson EJ, et al. Mice with a partial deficiency of manganese superoxide dismutase show increased vulnerability to the mitochondrial toxins malonate, 3-nitropropionic acid, and MPTP. Experimental neurology. 2001;167(1):189-95.

260. Schulz JB, Matthews RT, Klockgether T, Dichgans J, Beal MF. The role of mitochondrial dysfunction and neuronal nitric oxide in animal models of neurodegenerative diseases. Mol Cell Biochem. 1997;174(1-2):193-7.

261. Brouillet E. The 3-NP Model of Striatal Neurodegeneration. Curr Protoc Neurosci. 2014;67:9.48.1-14.

262. Zidenberg-Cherr S, Keen CL, Lönnerdal B, Hurley LS. Superoxide dismutase activity and lipid peroxidation in the rat: developmental correlations affected by manganese deficiency. Journal of Nutrition. 1983;113(12):2498-504.

263. Lebovitz RM, Zhang H, Vogel H, Cartwright JJ, Dionne L, Lu N, et al. Neurodegeneration, myocardial injury, and perinatal death in mitochondrial superoxide dismutase-deficient mice. PNAS. 1996;93:9782-7.

264. Napolitano M, Centonze D, Gubellini P, Rossi S, Spiezia S, Bernardi G, et al. Inhibition of mitochondrial complex II alters striatal expression of genes involved in glutamatergic and dopaminergic signaling: possible implications for Huntington's disease. Neurobiology of disease. 2004;15(2):407-14.

265. Marion S, Urs NM, Peterson SM, Sotnikova TD, Beaulieu JM, Gainetdinov RR, et al. Dopamine D2 receptor relies upon PPM/PP2C protein phosphatases to dephosphorylate huntingtin protein. The Journal of biological chemistry. 2014;289(17):11715-24.

266. Goytain A, Hines RM, Quamme GA. Huntingtin-interacting proteins, HIP14 and HIP14L, mediate dual functions, palmitoyl acyltransferase and Mg2+ transport. The Journal of biological chemistry. 2008;283(48):33365-74.

267. Quamme GA. Molecular identification of ancient and modern mammalian magnesium transporters. Am J Physiol Cell Physiol. 2010;298(3):C407-29.

268. Huang K, Yanai A, Kang R, Arstikaitis P, Singaraja RR, Metzler M, et al. Huntingtin-interacting protein HIP14 is a palmitoyl transferase involved in palmitoylation and trafficking of multiple neuronal proteins. Neuron. 2004;44(6):977-86.

269. Ohyama T, Verstreken P, Ly CV, Rosenmund T, Rajan A, Tien AC, et al. Huntingtin-interacting protein 14, a palmitoyl transferase required for exocytosis and targeting of CSP to synaptic vesicles. The Journal of cell biology. 2007;179(7):1481-96.

270. Sanders SS, Mui KK, Sutton LM, Hayden MR. Identification of binding sites in Huntingtin for the Huntingtin Interacting Proteins HIP14 and HIP14L. PloS one. 2014;9(2):e90669.

271. Singaraja RR, Hadano S, Metzler M, Givan S, Wellington CL, Warby S, et al. HIP14, a novel ankyrin domain-containing protein, links huntingtin to intracellular trafficking and endocytosis. Human molecular genetics. 2002;11(23):2815-28.

272. Yanai A, Huang K, Kang R, Singaraja RR, Arstikaitis P, Gan L, et al. Palmitoylation of huntingtin by HIP14 is essential for its trafficking and function. Nature neuroscience. 2006;9(6):824-31.

273. Singaraja RR, Huang K, Sanders SS, Milnerwood AJ, Hines R, Lerch JP, et al. Altered palmitoylation and neuropathological deficits in mice lacking HIP14. Hum Mol Genet. 2011;20(20):3899-909.

274. Sutton LM, Sanders SS, Butland SL, Singaraja RR, Franciosi S, Southwell AL, et al. Hip14l-deficient mice develop neuropathological and behavioural features of Huntington disease. Hum Mol Genet. 2013;22(3):452-65.

275. Huang K, Sanders SS, Kang R, Carroll JB, Sutton L, Wan J, et al. Wild-type HTT modulates the enzymatic activity of the neuronal palmitoyl transferase HIP14. Hum Mol Genet. 2011;20(17):3356-65.

276. Herrero Hernandez E, Discalzi G, Valentini C, Venturi F, Chio A, Carmellino C, et al. Follow-up of patients affected by manganese-induced Parkinsonism after treatment with CaNa2EDTA. Neurotoxicology. 2006;27(3):333-9.

277. Racette BA, McGee-Minnich L, Moerlein SM, Mink JW, Videen TO, Perimutter JS. Welding-related parkinsonism. Neurology. 2001;56:8-12.

278. Racette BA, Antenor JA, McGee-Minnich L, Moerlein SM, Videen TO, Kotagal V, et al. [18F]FDOPA PET and clinical features in parkinsonism due to manganism. Movement disorders : official journal of the Movement Disorder Society. 2005;20(4):492-6.

279. Ahmed SS, Santosh W. Metallomic profiling and linkage map analysis of early Parkinson's disease: a new insight to aluminum marker for the possible diagnosis. PloS one. 2010;5(6):e11252.

280. Hozumi I, Hasegawa T, Honda A, Ozawa K, Hayashi Y, Hashimoto K, et al. Patterns of levels of biological metals in CSF differ among neurodegenerative diseases. Journal of the neurological sciences. 2011;303(1-2):95-9.

281. Criswell SR, Perlmutter JS, Videen TO, Moerlein SM, Flores HP, Birke AM, et al. Reduced uptake of [18F]FDOPA PET in asymptomatic welders with occupational manganese exposure. Neurology. 2011;76:1296-301.

282. Wang R, Zhu X. Subtoxic concentration of manganese synergistically potentiates 1-methyl-4-phenylpyridinium-induced neurotoxicity in PC12 cells. Brain Research. 2003;961:131-8.

283. Roth JA, Singleton S, Feng J, Garrick M, Paradkar PN. Parkin regulates metal transport via proteasomal degradation of the 1B isoforms of divalent metal transporter 1. J Neurochem. 2010;113(2):454-64.

284. Higashi Y, Asanuma M, Miyazaki I, Hattori N, Mizuno Y, Ogawa N. Parkin attenuates manganese-induced dopaminergic cell death. Journal of neurochemistry. 2004;89(6):1490-7.

285. Roth JA, Ganapathy B, Ghio AJ. Manganese-induced toxicity in normal and human B lymphocyte cell lines containing a homozygous mutation in parkin. Toxicology in vitro : an international journal published in association with BIBRA. 2012;26(7):1143-9.

286. Sriram K, Lin GX, Jefferson AM, Roberts JR, Wirth O, Hayashi Y, et al. Mitochondrial dysfunction and loss of Parkinson's disease-linked proteins contribute to neurotoxicity of manganese-containing welding fumes. FASEB journal : official publication of the Federation of American Societies for Experimental Biology. 2010;24(12):4989-5002.

287. Rentschler G, Covolo L, Haddad AA, Lucchini RG, Zoni S, Broberg K. ATP13A2 (PARK9) polymorphisms influence the neurotoxic effects of manganese. Neurotoxicology. 2012;33(4):697-702.

288. Ramirez A, Heimbach A, Grundemann J, Stiller B, Hampshire D, Cid LP, et al. Hereditary parkinsonism with dementia is caused by mutations in ATP13A2, encoding a lysosomal type 5 P-type ATPase. Nat Genet. 2006;38(10):1184-91.

289. Tsunemi T, Krainc D. Zn(2)(+) dyshomeostasis caused by loss of ATP13A2/PARK9 leads to lysosomal dysfunction and alpha-synuclein accumulation. Human molecular genetics. 2014;23(11):2791-801.

290. Ugolino J, Fang S, Kubisch C, Monteiro MJ. Mutant Atp13a2 proteins involved in parkinsonism are degraded by ER-associated degradation and sensitize cells to ER-stress induced cell death. Hum Mol Genet. 2011;20(18):3565-77.

291. Delnooz CC, Wevers RA, Quadri M, Clayton PT, Mills PB, Tuschl K, et al. Phenotypic variability in a dystonia family with mutations in the manganese transporter gene. Movement disorders : official journal of the Movement Disorder Society. 2013;28(5):685-6.

292. Burkhard PR, Delavelle J, Pasquier RD, Spahr L. Chronic Parkinsonism Associated With Cirrhosis A Distinct Subset of Acquired Hepatocerebral Degeneration. Archives of Neurology. 2003;60:521-8.

293. Noone ML, Kumar P, Ummer K, Achambat L, Salam KA. Cirrhosis presenting as Parkinsonism. Annals of Indian Academy of Neurology. 2008;11:179-81.

294. Aggarwal A, Vaidya S, Shah S, Singh J, Desai S, Bhatt M. Reversible Parkinsonism and T1W pallidal hyperintensities in acute liver failure. Mov Disord. 2006;21(11):1986-90.

295. Lechpammer M, Clegg MS, Muzar Z, Huebner PA, Jin LW, Gospe SM, Jr. Pathology of inherited manganese transporter deficiency. Ann Neurol. 2014;75(4):608-12.

296. Bosomworth HJ, Adlard PA, Ford D, Valentine RA. Altered Expression of ZnT10 in Alzheimer's Disease Brain. PloS one. 2013;8(5):e65475.

297. Parenti M, Rusconi L, Cappabianca V, Parati EA, Groppetti A. Role of dopamine in manganese neurotoxicity. Brain Res. 1988;473(2):236-40.

298. Stredrick DL, Stokes AH, Worst TJ, Freeman WM, Johnson EA, Lash LH, et al. Manganese-induced cytotoxicity in dopamine-producing cells. Neurotoxicology. 2004;25(4):543-53.

299. Stephenson AP, Schneider JA, Nelson BC, Atha DH, Jain A, Soliman KF, et al. Manganese-induced oxidative DNA damage in neuronal SH-SY5Y cells: attenuation of thymine base lesions by glutathione and N-acetylcysteine. Toxicol Lett. 2013;218(3):299-307.

300. Cordova FM, Aguiar AS, Jr., Peres TV, Lopes MW, Goncalves FM, Pedro DZ, et al. Manganese-exposed developing rats display motor deficits and striatal oxidative stress that are reversed by Trolox. Arch Toxicol. 2013;87(7):1231-44.

301. Cordova FM, Aguiar AS, Jr., Peres TV, Lopes MW, Goncalves FM, Remor AP, et al. In vivo manganese exposure modulates Erk, Akt and Darpp-32 in the striatum of developing rats, and impairs their motor function. PLoS One. 2012;7(3):e33057.

302. McDougall SA, Der-Ghazarian T, Britt CE, Varela FA, Crawford CA. Postnatal manganese exposure alters the expression of D2L and D2S receptor isoforms: relationship to PKA activity and Akt levels. Synapse. 2011;65(7):583-91.

303. Cai T, Che H, Yao T, Chen Y, Huang C, Zhang W, et al. Manganese induces tau hyperphosphorylation through the activation of ERK MAPK pathway in PC12 cells. Toxicological sciences : an official journal of the Society of Toxicology. 2011;119(1):169-77.

304. Crittenden PL, Filipov NM. Manganese modulation of MAPK pathways: effects on upstream mitogen activated protein kinase kinases and mitogen activated kinase phosphatase-1 in microglial cells. J Appl Toxicol. 2011;31(1):1-10.

305. Hirata Y, Furuta K, Miyazaki S, Suzuki M, Kiuchi K. Anti-apoptotic and pro-apoptotic effect of NEPP11 on manganese-induced apoptosis and JNK pathway activation in PC12 cells. Brain Res. 2004;1021(2):241-7.

306. Prabhakaran K, Ghosh D, Chapman GD, Gunasekar PG. Molecular mechanism of manganese exposure-induced dopaminergic toxicity. Brain Res Bull. 2008;76(4):361-7.

307. Subhash MN, Padmashree TS. Regional Distribution of Dopamine beta-hydroxylase and Monoamine Oxidase in the Brains of Rats Exposed to Manganese. Fd Chem Toxic. 1990;28(8):567-70.

308. Erikson KM, Suber RL, Aschner M. Glutamate/Aspartate Transporter (GLAST), Taurine Transporter and Metallothionein mRNA Levels are Differentially Altered in Astrocytes Exposed to Manganese Chloride, Manganese Phosphate or Manganese Sulfate. Neurotoxicology. 2002;23:281-8.

309. Anderson JG, Fordahl SC, Cooney PT, Weaver TL, Colyer CL, Erikson KM. Manganese exposure alters extracellular GABA, GABA receptor and transporter protein and mRNA levels in the developing rat brain. Neurotoxicology. 2008;29(6):1044-53.

310. Dydak U, Jiang YM, Long LL, Zhu H, Chen J, Li WM, et al. In Vivo Measurement of Brain GABA Concentrations by Magnetic Resonance Spectroscopy in Smelters Occupationally Exposed to Manganese. Environmental Health Perspective. 2011;119(2):219-24.

311. Fordahl SC, Anderson JG, Cooney PT, Weaver TL, Colyer CL, Erikson KM. Manganese exposure inhibits the clearance of extracellular GABA and influences taurine homeostasis in the striatum of developing rats. Neurotoxicology. 2010;31(6):639-46.

312. Gunter TE, Gavin CE, Aschner M, Gunter KK. Speciation of manganese in cells and mitochondria: a search for the proximal cause of manganese neurotoxicity. Neurotoxicology. 2006;27(5):765-76.

313. Chun HS, Lee HH, Son JH. Manganese induces endoplasmic reticulum (ER) stress and activates multiple caspases in nigral dopaminergic neuronal cells, SN4741. Neuroscience Letters. 2001;316:5-8.

314. Fang Zhao, Tongjian Cai, Mingchao Liu, Gang Zheng, Wenjing Luo, Jingyuan Chen, Manganese Induces Dopaminergic Neurodegeneration via Microglial Activation in a Rat Model of Manganism, *Toxicological Sciences*, Volume 107, Issue 1, January 2009, Pages 156–164.

315. Stanwood GD, Leitch DB, Savchenko V, Wu J, Fitsanakis VA, Anderson DJ, Stankowski JN, Aschner M, McLaughlin B. Manganese exposure is cytotoxic and alters dopaminergic and GABAergic neurons within the basal ganglia. J Neurochem. 2009 Jul;110(1):378-89. doi: 10.1111/j.1471-4159.2009.06145.x. Epub 2009 May 5.

316. Ivleva I, Pestereva N, Zubov A, Karpenko M. Intranasal exposure of manganese induces neuroinflammation and disrupts dopamine metabolism in the striatum and hippocampus. Neurosci Lett. 2020;738:135344.

A selection of the following chapter, including text and figures, has previously been published in Molecules. 2021; 26(4):1175, as “Identification of Three Small Molecules That Can Selectively Influence Cellular Manganese Levels in a Mouse Striatal Cell Model”.
DOI 10.3390/molecules26041175

CHAPTER II

CHARACTERIZATION OF THE MANGANESE TOOLBOX

INTRODUCTION

Occupational and environmental exposure to manganese (Mn) increases risk for parkinsonism, and genetic risk factors for early onset Parkinson's Disease (PD) alter cellular susceptibility to Mn toxicity (1–8). Under normal conditions, the brain and especially structures of the basal ganglia, have relatively high levels of Mn- but are subject to heightened susceptibility to Mn-induced neurotoxicity (9–12). Excess exposure to Mn results in a condition with extrapyramidal symptoms similar to PD, known as manganism (13–15). Considering how Mn is an essential metal required for the activity of several critical neural enzymes (e.g. arginase and glutamine synthase), but in excess can be neurotoxic, it is likely that there is active regulation of Mn distribution in place within neurons (16). However, the extent to which neurons actively regulate control and distribution of intracellular Mn is poorly understood. All but one of the known Mn transporters (SLC30A10, a Mn efflux transporter and PD genetic risk factor) predominantly regulates levels of another divalent metal (16–20). Despite the abundant knowledge of genetic factors that influence neurodegeneration of basal ganglia structures and the vulnerability of these same brain structures to Mn toxicity, there is a lack of knowledge regarding the gene-environment interface that leads to neuronal vulnerability.

The mechanisms of intracellular Mn transport and storage require active investigation. Most of the known transporters involved in transport of Mn into and within cells of the brain (including neurons and glia) are non-selective, and also transport other essential metals. As such,

the known Mn transporters cannot explain how intracellular Mn concentrations are selectively maintained without simultaneously strongly influencing the concentrations of other metals (21). Aside from a few notable exceptions (e.g. DMT1 (22–24), TfR (25,26), SLC30A10(17,27,28)), the manner by which known Mn transporters regulate uptake and efflux of Mn into the cells, versus the subcellular distribution of Mn is not well established. Indeed, Mn is the only essential metal for which cellular homeostatic processes are not defined, despite numerous Mn dependent enzymes throughout the cell. New research to generate novel chemical tools to probe mechanisms of Mn transport was performed previously by our lab via a high throughput screening approach. Research to generate novel chemical tools to probe Mn transport mechanisms was performed previously by our lab using a high throughput screening approach (29). The Fura-2-based fluorescent assay is referred to as the Cellular Fura-2 Manganese Extraction Assay, or CFMEA (30,31). In brief, cells are exposed to extracellular Mn and incubated at physiological conditions before washing away the excess extracellular Mn in calcium-free buffer and using detergent to lyse open the cells. The released Mn is detected by the added fluorophore, Fura-2, and its fluorescence is quenched in a quantifiable, concentration-dependent matter at the calcium isosbestic point ($360_{Ex}/535_{Em}$) so that cellular calcium co-released with the Mn does not influence the fluorescence signal. While it is possible other endogenous divalent metals that alter Fura-2 fluorescence could interfere with Mn determination, the CFMEA was previously validated for accuracy of Mn quantification in the absence of elevated exposures to other divalent metals beyond what is normally found in cell culture media (30,31). This is likely due to the fact that normal cellular levels of other divalent metals (aside from calcium) are too low to alter Fura-2 signals. This assay was subsequently optimized for a high-throughput screening format (32), and then subsequently used to screen ~40,000 small molecules across a diverse set of libraries (29). The

libraries screened include the National Institutes of Health (NIH) Clinical Collection I/II, Microsource Spectrum Collection, three different kinase inhibitor libraries, a bioactive lipid library, a non-steroidal anti-inflammatory library, as well as the ChemBridge and ChemDiv libraries; more details of the small molecule libraries screened and all compound structures examined in this paper are available in the original publication of the screen (29).

However, though validated and identified, their targets and mechanisms of these small molecules remained unknown. This set of small molecules was coined the "Mn toolbox", as we hoped to use each molecule as a chemical tool to investigate Mn homeostasis in neuronal cells. We set out to test the hypothesis that cell-level homeostatic processes regulate intracellular Mn to avoid hazardous concentrations in the brain. Understanding how cells selectively control intracellular Mn to avoid an excess or deficit is critical; when these processes are impaired, as they appear to be in PD and HD, our understanding of Mn homeostasis could illuminate curative solutions to these devastating diseases. We sought to test the hypothesis that the 41 small molecules which alter intracellular Mn act on multiple and diverse biological targets in human neurons that are susceptible to death in HD and PD. The goal of this was to functionally classify the 41 small molecules that alter intracellular Mn by observing its effects on Mn-dependent cell biology. Using our fluorescent assay of intracellular Mn uptake (CFMEA) as a readout, pharmacological characteristics were to be established for each small molecule (e.g. duration of effect, specificity for Mn versus other metals). This would allow us to determine if the small molecules alter uptake or efflux of Mn. Also using CFMEA, epistatic experiments using both Mn-increasers (small molecules that would overall increase Mn uptake in cells for a given endogenous Mn-exposure exposure) and Mn-decreasers (small molecules that would overall decrease Mn uptake in cells for a given endogenous Mn-exposure exposure) in the same exposure will help

delineate the order that each small molecule may be acting in the pathway of interest. We expected to define functional groups of small molecules that share common activity patterns representative of multiple distinct mechanisms of Mn transport.

RESULTS

Small molecule functional stability and effectiveness in buffer and stability

As the Mn toolbox had only previously been tested and validated under one condition, (in HBSS for 3 hours at 33 degrees), it was important to know if the small molecules would work under other conditions that might be useful to study. For an optimally controlled environment, the toolbox was previously validated in Hanks Balanced Buffer Solution (HBSS), but the question remained if the small molecules could work to influence Mn while the cells were in DMEM. The utility of this was that cells in DMEM were in a more natural and complete environment, and cells could continuously be cultured long-term in their media instead, which is not possible in HBSS. Therefore, we tested the toolbox in the cells' normal medium (10% FBS, 1% Penicillin/Streptomycin in High Glucose DMEM; see methods for further details). As a control, and an attempt to confirm the results of the original screen, the toolbox was run in their standard conditions (HBSS for 3 hours with 125μM Mn co-incubation at 33° C), seen in **Figure** 2-**1A**. Brown-Forsythe ANOVA and Welch's ANOVA tests were performed to confirm whether a small molecule significantly increased or decreased Mn uptake in cells compared to vehicle (DMSO). Small molecules boxed in red were molecules that were **not** confirmed by Dunnett's T3 multiple comparison test to be significantly different from vehicle, with an adjusted *P* value less than 0.1. A total of six small molecules did not confirm under standard conditions (**Fig 1A**). Three of these were previously found to decrease Mn uptake in the Q7 cells, while the other three were previously identified as Mn-increasers. Two Mn-decreasers and 28 Mn-increasers were confirmed in total.

A comparison of the entire toolbox in HBSS (**Fig 2-1A**) to the toolbox in media (**Fig 2-1B**), using a Two-Way ANOVA, reveals a clear main effect of the buffer used ($P<0.0001$), comprising of 26% of the variation, with an equally significant interaction between buffer and small molecule, comprising of 28% of the total variation. There was an overall decrease in effectiveness of the small molecules (decrease in fold change) when used in DMEM- an average loss of 2.6-fold change was measured. Accordingly, there were an additional two Mn-decreasers and twelve Mn-increasers that were not significantly different from vehicle when measured using Brown-Forsythe ANOVA and Welch's ANOVA tests with Dunnett's T3 multiple comparisons. These small molecules are also boxed in red (**Figure 2-1B**). What remained were zero Mn-decreasers and seventeen Mn-increasers that were capable of influencing Mn uptake while in media.

To test if any of these small molecules have Mn-altering activity for prolonged periods, the entire toolbox was tested for activity in media for 18 hours (**Figure 2-1C**). There was an interesting interaction between 3 hours and 18 hours in media- where some small molecules that were not active in media at 3 hours had a significant effect after 18 hours (boxed in purple). Two Mn-increasers (VU0041803, VU0050661) and two Mn-decreasers (VU0047355, VU0244366) displayed this effect. Even more interesting were four small molecules that changed *directions* of Mn after 18 hours. Decreaser VU0063088 and increasers VU0026977, VU0135086, and VU024305 had modest increases and decreases to vehicle, respectively (boxed in blue). Those that were inactive in media after 18 hours are boxed in red. In total, only eight small molecules maintained their significant effect on Mn uptake in media after 3 or 18 hours, not including the four that changed directionality of their effect. An additional four had activity in media at 18 hours but not at 3 hours.

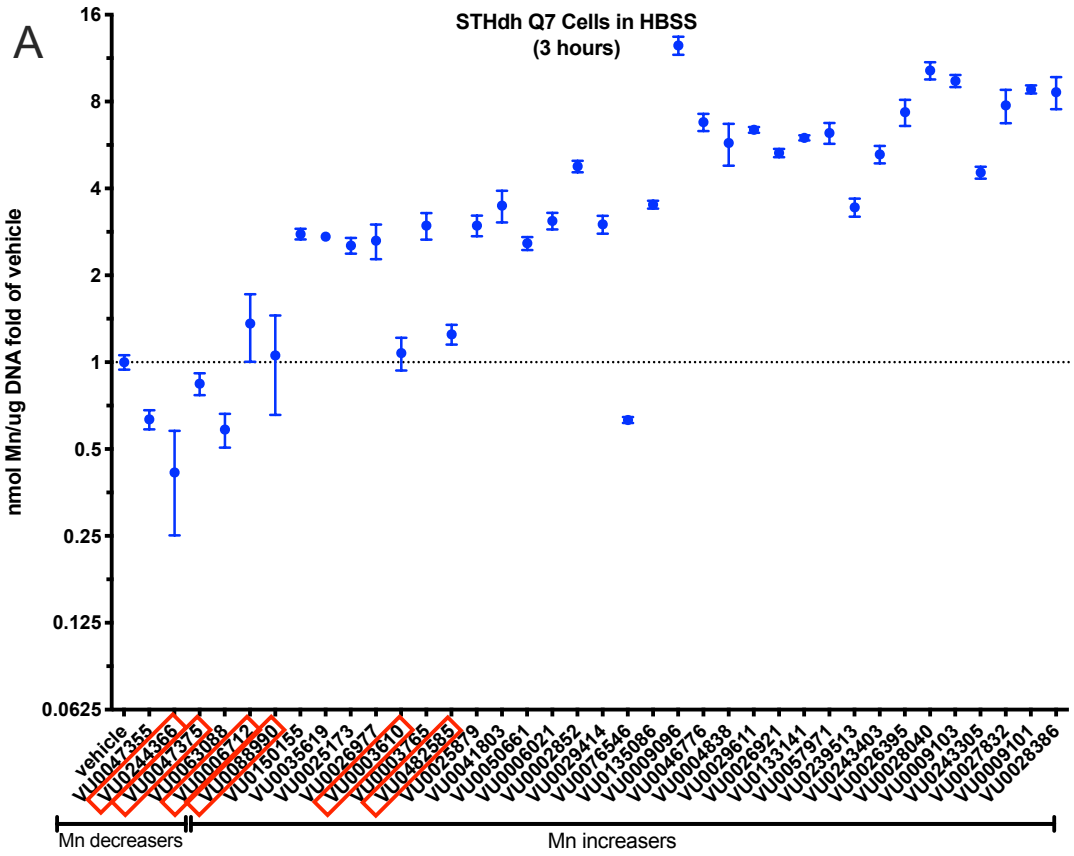
A
STHdh Q7 Cells in HBSS
(3 hours)
nmol Mn/ug DNA fold of vehicle
16
8
4
2
1
0.5
0.25
0.125
0.0625
vehicle
VU0047355
VU0244366
VU0047375
VU0063088
VU0006712
VU0088990
VU0150155
VU0035619
VU0025173
VU0026977
VU0003610
VU0003765
VU0482585
VU0025879
VU0041803
VU0050661
VU0006021
VU0002852
VU0029414
VU0076546
VU0135086
VU0009096
VU0046776
VU0004838
VU0029611
VU0026921
VU0133141
VU0057971
VU0239513
VU0243403
VU0026395
VU0028040
VU0009103
VU0243305
VU0027832
VU0009101
VU0028386
Mn decreasers
Mn increasers

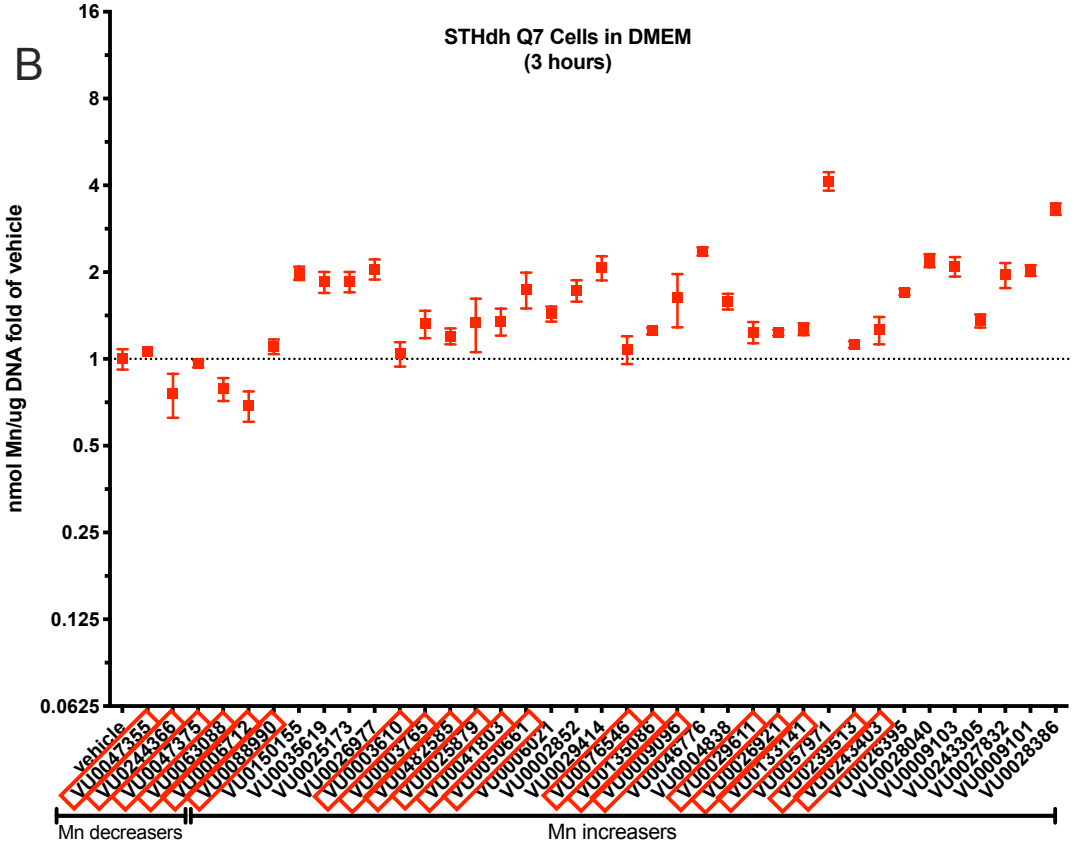
B
STHdh Q7 Cells in DMEM
(3 hours)
nmol Mn/ug DNA fold of vehicle
16
8
4
2
1
0.5
0.25
0.125
0.0625
vehicle
VU0047355
VU0244366
VU0047375
VU0063088
VU0006712
VU0088990
VU0150155
VU0035619
VU0025173
VU0026977
VU0003610
VU0003765
VU0482585
VU0025879
VU0041803
VU0050661
VU0006021
VU0002852
VU0029414
VU0076546
VU0135086
VU0009096
VU0046776
VU0004838
VU0029611
VU0026921
VU0133141
VU0057971
VU0239513
VU0243403
VU0026395
VU0028040
VU0009103
VU0243305
VU0027832
VU0009101
VU0028386
Mn decreasers
Mn increasers

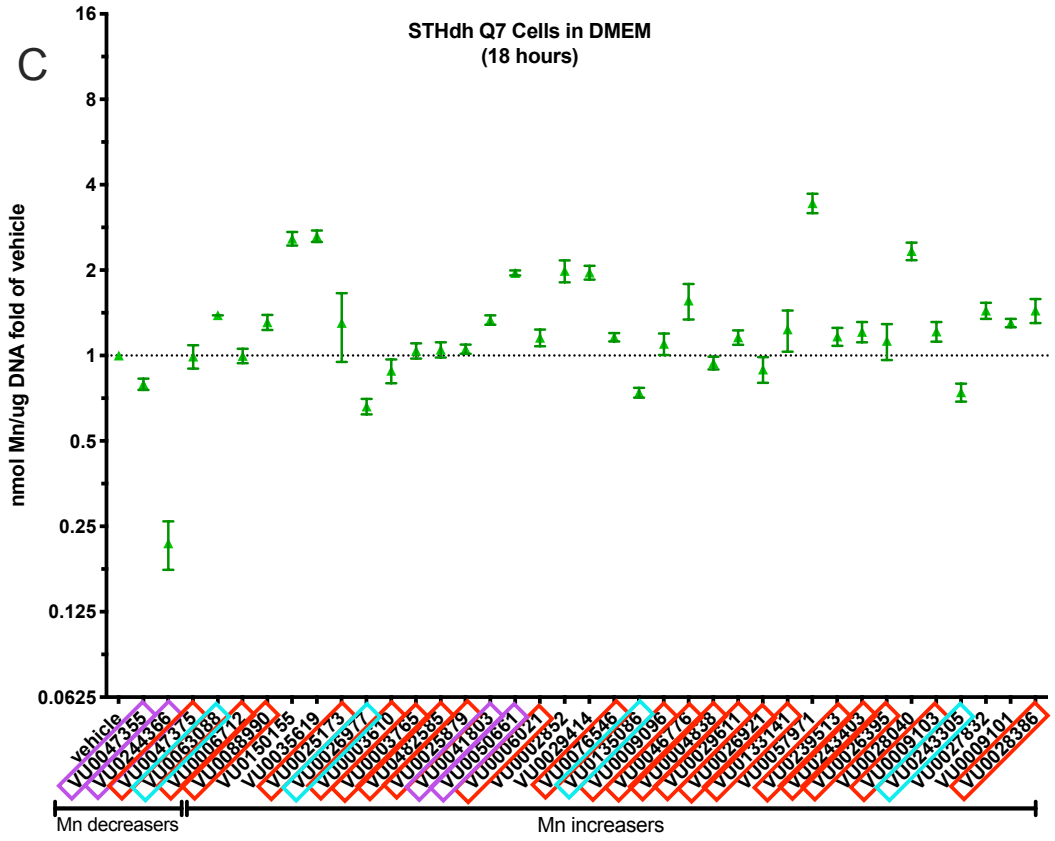

Figure 2-1: Small molecule modifiers of manganese have a tendency to lose their efficacy when exposed in media. The set of small molecules identified to influence intracellular Mn in a high throughput screen (see reference 29), commonly referred to as the "Mn Toolbox", are confirmed independently (A). All Mn exposures were at 125μM for 3 hours or 18 hours where noted. A red box around each small molecule, identified using its assigned VU identity number denotes non-significance as determined by a Brown-Forsythe ANOVA and Welch's ANOVA tests with Dunnett's T3 multiple comparisons. The number of compounds that did not reach statistical significance increases when exposed in DMEM rather than HBSS (B). When incubated in media for 18 hours (C), several small molecules had an impact on Mn when there was previously none statistically at 3 hours (boxed in purple). Several small molecules changed directions (Mn-increaser to decreaser, or decreaser to increaser), which are denoted by a box in blue. Error bars represent standard deviation of three biological replicates.

The Role of the SV40 Large T-Antigen in Mn Uptake

We next tested the hypothesis that the SV40 Large T-antigen, that which our Q7 (STHdh) neuronal cell line was immortalized with, was responsible for the mechanism(s) by which the small molecules of the toolbox influenced intracellular Mn (**Figure 2-2**). It was previously posited that the T-antigen could affect cellular Mn uptake. This was based on some differences seen in Mn uptake between HEK 293 and HEK 293T cells (data never published). Thus, to rule out or rule in this as mechanism of action for a given small molecule, we wanted to see if any of the small molecules were T-antigen dependent. We would also see if any of the small molecules Mn-influencing activity was an artifact of the Q7 cells that were used. Thirdly, the results of the small molecule uptake at 33° C may be expected to confirm the results of the high-throughput screen that originally formed the Mn toolbox, however the molecules in this case were used in DMEM instead of HBSS.

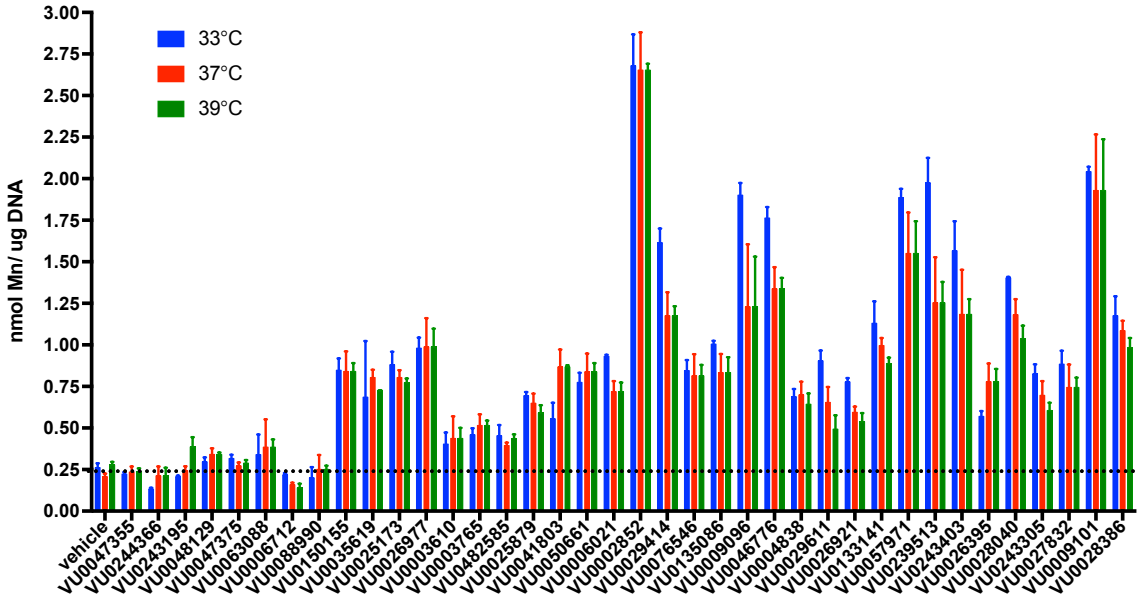

Figure 2-2: Mechanisms of Mn 'toolbox' small molecules are in part independent of SV40 Large T-antigen. Cells are grown at 33°C to maintain T-antigen activity and allow cell division. Cells were exposed to 125μM Mn for 3 hours in HBSS. At 39°C, the temperature at which the T-antigen is inactivated, small molecules are still effective. A Two-Way ANOVA plotting small molecules against temperature assayed revealed that small molecule, temperature, and an interaction of the two contributed significantly to the variation among the data (main effect with $p<0.0001$ in all cases).

The T-antigen is temperature dependent so that at 39 degrees the T-antigen is no longer stable. Therefore, we tested the small molecules at 37, 39, and 33 degrees (as a control). To control for cell growth (the inactivation of the T-antigen slows cell division), the amount of Mn was normalized to DNA per well. We discovered a few interesting things. First, a Two-Way ANOVA plotting small molecules against temperature assayed revealed that small molecule, temperature, and an interaction of the two contributed significantly to the variation among the data (main effect with $P < 0.0001$ in all cases). The temperature was attributed to only 0.89% of the source variation, with an interaction contributing 3.56%. Post-hoc Sidak's multiple comparison tests did not show a significant effect of temperature under vehicle conditions, but eleven small molecules did show an effect of temperature (See **Table 2-1**).

Small Molecule	Temperature Comparison	P value
VU0041803	33 vs 39	$P < 0.005$
VU0029414	33 vs 39	$P < 0.0001$
VU0009096	33 vs 39	$P < 0.0001$
VU0046776	33 vs 39	$P < 0.0001$
VU0029611	33 vs 39	$P < 0.0001$
VU0026921	33 vs 39	$P < 0.05$
VU0133141	33 vs 39	$P < 0.05$
VU0057971	33 vs 39	$P < 0.01$
VU0239513	33 vs 39	$P < 0.0001$
VU0243403	33 vs 39	$P < 0.001$
VU0028040	33 vs 39	$P < 0.001$

Table 2-1: List of small molecules whose ability to influence Mn is significantly altered by temperature.

For VU0041803, a Mn-increaser, an increase in temperature actually increased the effectiveness of the small molecule in Mn-uptake. For the other significant ten, all Mn-increasers, the amount of Mn measured in cells at higher temperatures was significantly less than at 33 degrees. These ten exhibited a trend where 33 degrees was the maximum for each small molecule, followed by 37, and then 39 with the least. However, in all 11 molecules that had significant changes at the post-hoc level, the result of 39 degrees never completely blocked the effectiveness of the small molecule to increase. There was never more than a 50% decrease in uptake, and on

average the reduction of Mn uptake was approximately 20%. There were no Mn-decreaser small molecules that were significantly affected by temperature.

Mn Chelation Experiments

Based on established knowledge that molecules with the quinolinol functional group could chelate divalent metal ions (33), and given that five members of the toolbox were in fact quinolinols, we used two different assays of measuring Mn chelation properties of the small molecules. The first was an *in vitro* assay of competition between Fura-2 and the small molecule for Mn. Mn quenches Fura-2 fluorescence so that 1μM quenches approximately 50% of the signal. Small molecules were added to 1μM Mn in buffer with 0-10μM of compound with 0.5μM Fura-2. The idea was that if the small molecule chelates Mn, it would compete with Fura-2 for Mn, and the Fura-2 fluorescence signal would be unquenched. EDTA, a known Mn chelator, was used as a positive control to provide proof of principle. There was not one small molecule that decreased Fura-2 quenching (increased fluorescence of the Fura-2 signal) in a concentration-dependent manner (**Figure 2-3**), indicating that no small molecules could compete with Fura-2 for Mn at 10μM or below.

A second, *in vivo* assay for chelation was also run for the Mn toolbox. Lillian Juttukonda performed these experiments, from Dr. Eric Skaar's lab. The assay was a growth assay of WT *s. aureus* compared to *s. aureus* with the mntH/C transporter KO. This ΔmntH/C strain struggles to grow in Mn-poor environments, so their growth is markedly reduced in the presence of a Mn-chelator. Compounds that reduced growth in the ΔmntH/C strain but did not impact WT were identified as chelators. **Table 2-2** shows the small molecules that were "designated" as chelators, negative for chelation, or those that fell "in between" in this assay. Six were designated as

"definite" chelators, in contrast to the zero that were identified in the *in vitro* experiment. Twenty-two were definitively not chelators, and the remaining 11 fell into the "possible/likely chelator" category.

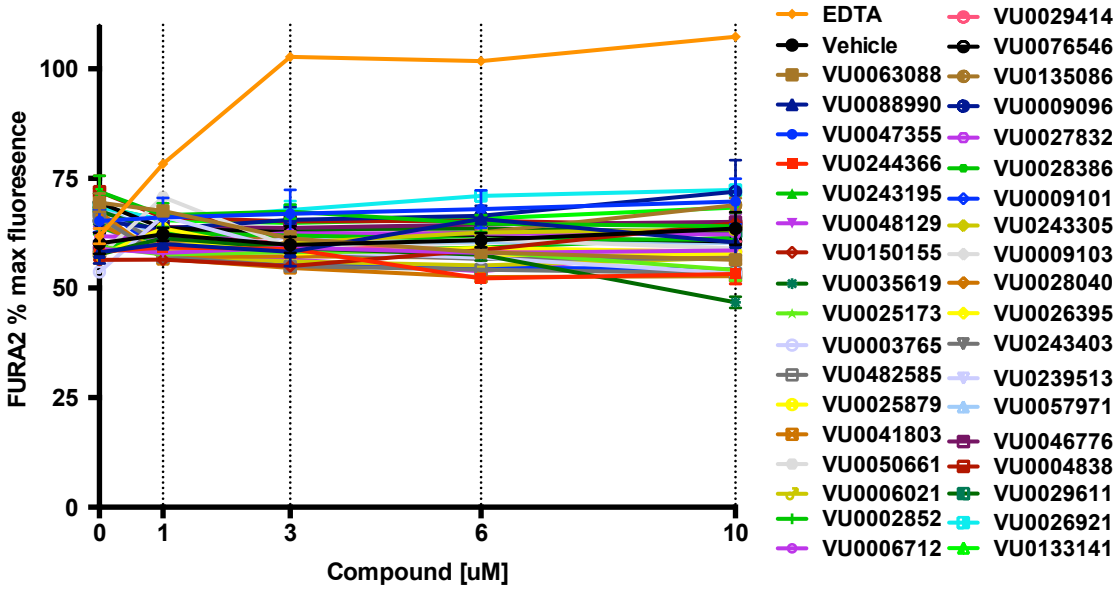

Figure 2-3: Unlike EDTA, all small molecules of the Mn toolbox fail to sequester Mn from Fura-2 while *in vitro*. Small molecules at varying concentrations (1-10uM) were added to 1uM Mn in the presence of Fura-2. EDTA, a Mn chelator, is able to sequester Mn from Fura-2 to prevent it's fluorescence quenching. None of the 39 small molecules tested presented a concentration dependent reversal of Fura-2 quenching. This is evidence against a chelating mechanism of Mn-influence.

Table 2-2: List of small molecules classified as Mn chelators as measured by bacterial growth assay.

Compound	Inhibitory at 100 uM	Inhibitory at 50 uM	Chelator at 10uM or lower	Chelator?	Log EC50	EC50 (uM)	structure
VU0243195	No	No		No	-5.752	1.7701	
VU0035619	Yes	Yes		No	-5.968	1.0765	
VU0150155	No	No		No	-5.917	1.2106	
VU0076546	No	No		No	-6.294	0.5082	
VU0088990	No	No		No	-6.412	0.3873	
VU0029414	No	No		No	-6.377	0.4198	
VU0003610	No	No		No	-6.834	0.1466	
VU0047355	No	No		No	-5.687	2.0559	
VU0047375	No	No		No	-6.385	0.4121	
VU0025173	No	No		No	-5.808	1.556	
VU0006712	No	No		No	-6.677	0.2104	
VU0244366	Yes	Yes		No	-5.92	1.2023	
VU0048129	No	No		No	-5.834	1.4655	
VU0057971	Yes	Yes	Maybe	No	-6.286	0.5176	
VU0133141	Yes	Yes		No	-5.416	3.8371	
VU0028386	WT only	No		No	-5.744	1.803	
VU0063088	No	No		No	-7.043	0.0906	
VU0050661	No	No		No	-5.078	8.356	
VU0026395	No	No		No	-4.082	82.7942	
VU0026977	No	No		No	-5.501	3.155	
VU0046776	No	No		**No**	-5.899	1.2618	quinolinol
VU0003765	No	No		No	-5.723	1.8923	
VU0006021	Yes	Yes		Possible	-5.451	3.54	
VU0025879	mnt only	No		Possible	-5.332	4.6559	
VU0135086	Yes	Yes	Yes	Possible	-5.638	2.3014	
VU0026921	Yes	Yes	Yes	Possible	-5.324	4.7424	benzo-hydrazide
VU0004838	Yes	Yes	Maybe	Likely	-6.338	0.4592	
VU0028040	Yes	Yes	Yes	Likely	-7.274	0.0532	differ only by methyl/ethyl and hydroxy
VU0027832	Yes	Yes	Yes	Likely	-5.501	3.155	differ only by methyl/ethyl and hydroxy
VU0482585	mnt only	No		Likely	-5.927	1.183	
VU0041803	Yes	Yes	Maybe	Likely	-5.454	3.5156	
VU0009103	Yes	Yes		Likely	-5.61	2.4547	acetohydrazide
VU0029611	Yes	Yes		Likely	-7.271	0.0536	acetohydrazide
VU0009101	Yes	Yes	Yes	**Yes**	-5.629	2.3496	acetohydrazide
VU0009096	Yes	Yes	Yes	**Yes**	-5.706	1.9679	acetohydrazide
VU239513	Yes	mnt only	Yes	**Yes**	-5.36	4.3652	quinolinol
VU0002852	Yes	Yes	Yes	**Yes**	-5.457	3.4914	quinolinol acetate

VU0243403	Yes	Yes	Yes	**Yes**	-5.747	1.7906	quinolinol
VU0243305	Yes	Yes	Yes	**Yes**	-5.713	1.9364	quinolinol

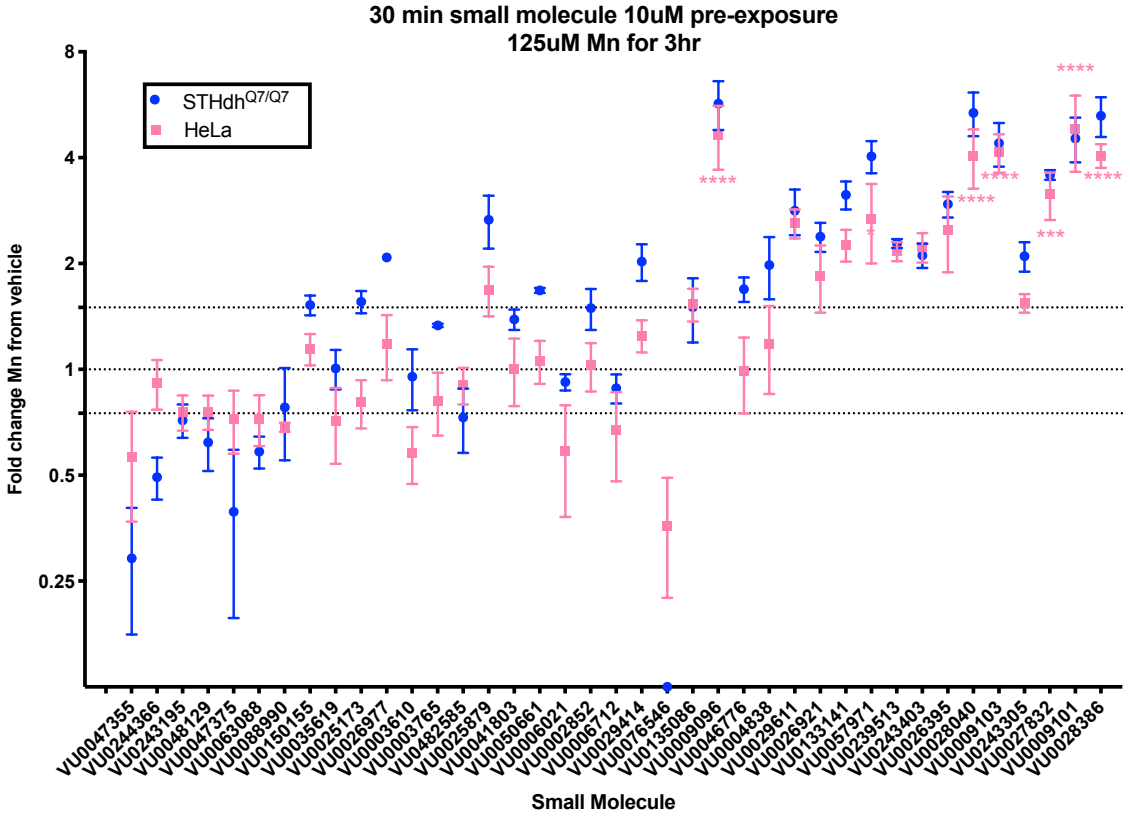

Figure 2-4: The majority of the Mn toolbox are able to influence intracellular Mn in HeLa cells. Cells (STHdh Q7 or HeLa) were pre-exposed to small molecule at 10uM for 30 minutes before exposure to 125uM Mn. Fold change, relative to vehicle is plotted. Significance in fold change between cell type for a given small molecule is denoted with pink stars (*** P<0.001, **** P<0.0001) as determined by a Two-Way ANOVA with Sidak's multiple comparisons test.

Activity of the Mn Toolbox in Other Cell Types

Since the toolbox was initially established with a neuronal mouse cell line (STHdh Q7/Q7), we wanted to know if any of the small molecules were an artifact of the cell type used. It would be particularly useful to know if a given small molecule maintained Mn-altering activity in a human cell line, and a non-neuronal cell line. For this reason, the toolbox was assessed for activity in HeLa cells (**Figure 2-4**).

HeLa cells and Q7 cells (as a control) were pre-exposed to 10μM of each small molecule for 30 minutes, then exposed to 125μM Mn for 3 hours. The fold change of intracellular Mn accumulated relative to vehicle was plotted and analyzed by Two-Way ANOVA with Sidak's multiple comparisons tests. Of the 39 tested, only seven (VU0009096, VU0057971, VU0028040, VU0009103, VU0027832, VU0009101, VU0028386) were significantly different from vehicle in the HeLa cells. (Significance is marked in pink asterisks). However, a multiple comparisons test between cell types noted **zero** small molecules that had significantly different fold change from one cell type compared to the other. Due to this conflicting data, cut-offs were set at 0.75 and 1.5-fold, so that any small molecule with a mean fold-change in between 0.75 and 1.5-fold would be considered "inactive". This eliminated 11 small molecules (VU0244366, VU0243195, VU0048129, VU0150155, VU0025173, VU0026977, VU0482585, VU0050661, VU0029414, VU0046776, VU0004838) that otherwise had activity in the STHdh Q7 cells. Interestingly, four small molecules (VU0088990, VU0003610, VU0006021, VU0006712) appeared to significantly decrease Mn in the HeLa cells but not Q7 cells. Three small molecules (VU0003765, VU0041803, VU0002852) were marked as "inactive" in both Q7s and HeLa cells. The remaining 21 small molecules were listed as "active" in both Q7 and HeLa cells.

In order to differentiate whether the small molecules that are inactive in HeLa cells are inactive due to a species difference or a difference in cell differentiation, we sought to test the Mn toolbox on a human neuronal line: SH-SY5Y (**Figure 2-5**). Similar to the HeLa experiments, Q7 cells were run in parallel to the SH-SY5Y cells as a control. In contrast to the HeLa cells, small molecules VU0243195, VU0048129, VU0088990, VU0050661, and VU0004838 significantly altered Mn uptake in SH-SY5Ys. Sixteen other small molecules in the toolbox significantly altered Mn uptake in the SH-SY5Y's. These were statistically significant from vehicle, and over the 1.5-

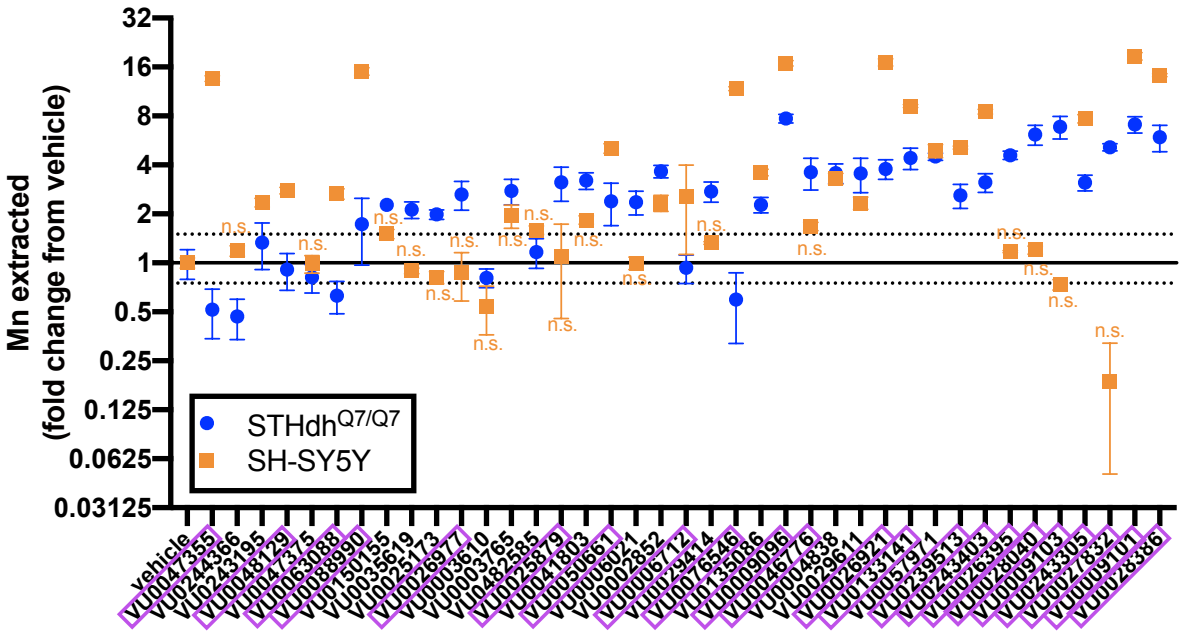

Figure 2-5: SH-SY5Y cells are impacted by the Mn toolbox differently than STHdh cells. Cells were exposed to 125μM Mn for 3 hours in HBSS. Thirty of the small molecules had significantly different Mn fold-change in SH-SY5Y's compared to Q7 cells as determined by Two-Way ANOVA, Sidak's multiple comparisons test. These are indicated in purple boxes. Small molecules that did not induce statistically significant changes from vehicle in the SH-SY5Y cells are noted with "n.s." in

fold change cut-offs. Notably, a Mn-decreaser in the Q7's, VU0047355, was a strong Mn-increaser in the SH-SY5Ys, with an increase more than 13-fold over vehicle. VU0088990, a modest "increaser" in the Q7's, had a fold change more than 15-fold over vehicle. Though not statistically significant, VU0027832 decreased Mn to less than 0.2-fold of vehicle on average, despite being a strong "increaser" in Q7's. There was an overall trend of the Mn-toolbox performing much differently in the SH-SY5Y's compared to the Q7's. Of the 39 tested, 30 of the small molecules had significantly different fold-change in SH-SY5Y's compared to Q7 cells. These 30 small molecules are labeled with a purple box surrounding their ID numbers in Figure 5. Those that were not significantly different from vehicle in the SH-SY5Y's are labeled "n.s." in orange.

Further Refinement of the Mn Toolbox

It was noted that despite repeated washing with PBS, there was always a set amount of Mn left behind in the wells of the 96-well plates that was independent of cellular uptake. Given that some of the small molecules bind Mn, we wanted to make sure that our CFMEA assay was not confounded by small molecules that would increase or decrease the amount of Mn that is left behind, bound to the plastic or cellular debris, after washing. To address this concern, we ran a "stickiness assay" to see if the small molecules in the toolbox were leaving Mn behind. Since there is a deficit in Mn uptake in the STHdh Q111 cells, these cells may "handle" Mn differently (i.e. differential Mn being bound to the cell surface). Therefore, both cell lines were used in the assay. Cells were plated in 96 well plates and allowed to grow for 16hours, before the plate was fixed with 4% paraformaldehyde. Mn was added to the terminated cells with small molecule and incubated for 3 hours, before washing and continuing a regular CFMEA assay. The amount of Mn left behind with or without a given small molecule was quantified by Fura-2 quenching (**Figure 2-6**). Five small molecules (VU0002852, VU0004838, VU0009096, VU0009101, and VU0009103) were shown to be "sticky": they significantly increased the amount of Mn left over in the wells despite the cells being dead. This was 2 to 6-fold higher than the Mn left over with vehicle (DMSO).

At this time, it was noted that VU0076546 appeared to decrease the Mn bound to the well. Upon further review, it was found that the small molecule itself was fluorescent at the same wavelength that Fura-2 is read (Ex/Em 365/535), creating an illusion that there was less Mn. (The presence of Mn quenches Fura-2 fluorescence, so the addition of fluorescence would make it appear that there was less Mn present.) During the high-throughput screening process, VU0076546 was noted to be fluorescent but not removed as a false positive despite this since it appeared to

increase Mn at high concentrations. In all previous and subsequent experiments, VU0076546 did not appear to increase Mn uptake at any concentration. VU0076546 was removed from the Mn toolbox in subsequent experiments.

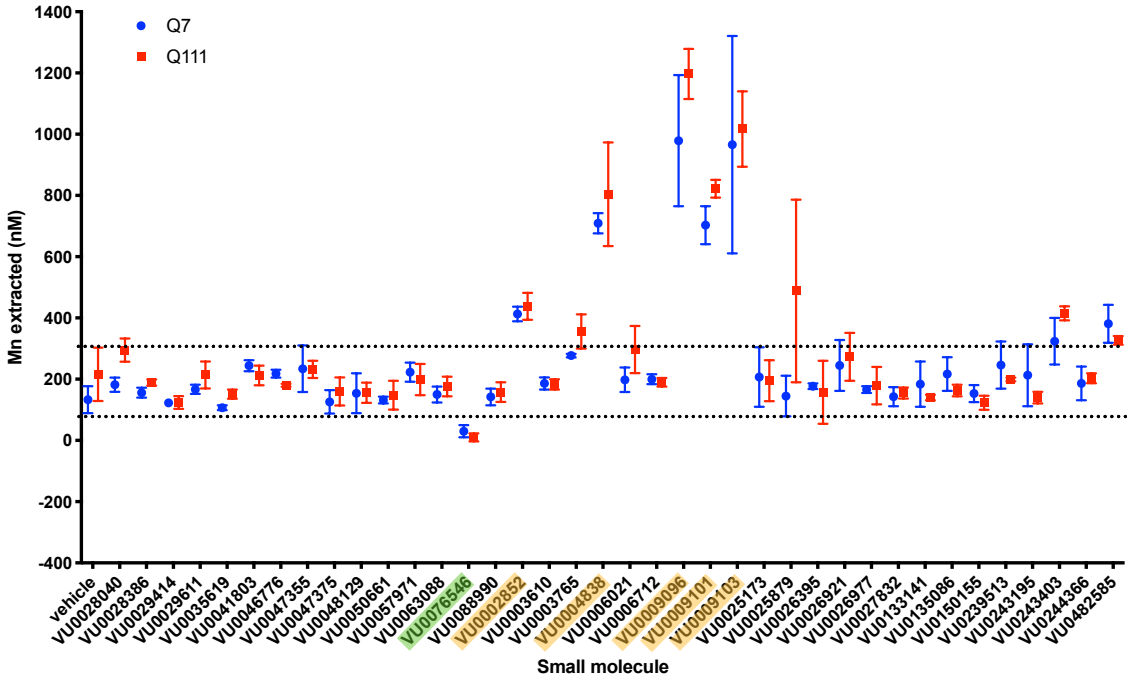

Figure 2-6: False positives in the Mn toolbox were identified by their induction of "Mn uptake" in dead cells. Prior to co-exposing small molecules with Mn, STHdh Q7 and Q111 cells were fixed with 4% paraformaldehyde dissolved in PBS for 20 minutes at room temperature. The fixed cells were washed three times with PBS before adding the Mn and/or small molecule. Exposures were 125 µM Mn for 3 hours in HBSS. Small molecules highlighted are those that were significantly above (yellow) or below (green) Vehicle levels, as measured by a Two-Way ANOVA, Sidak's multiple comparisons.

Assigning Small Molecules to Specific Mn Transport Pathways with Epistasis Experiments

Lastly, we tested the hypothesis that the small molecules could be categorized into distinct Mn-level altering functional pathways by performing a pathway analysis through epistasis experiments. We used the STHdh cells, where all the molecules are active, and tested two molecules at a time, at saturation, to see if their effects were additive, or if one molecule was epistatic to another. We started with six small molecules and confirmed that they were at saturation at 4 µM. The results can be seen in **Figure 2-7A.** All six molecules were at saturation at 4 µM,

considering that their influence on intracellular Mn (as measured by CFMEA) was not any different at 8 μM. Next, STHdh cells were exposed to Mn and 4 μM of small molecule(s) alone or in combination with another small molecule at 4 μM. Intracellular Mn was also quantified by CFMEA. Additive and epistatic relationships of small molecule combinations can be seen in **Figure 2-7B**. Of note is molecule VU0243195, or abbreviated "195", which was epistatic to 4 of the 5 small molecules tested. The exception was small molecule VU0029414, abbreviated "414", which had an additive effect with VU0243195. This suggested that "195" operated downstream from the other four small molecules, but "414" operated on an independent Mn pathway. Small molecule "VU0028386" or abbreviated "386" also appeared to be downstream from small molecule VU0244366 ("366"), based on the same logic.

Next, we wanted to see if the Mn decreaser VU0243195 operated downstream of the other small molecules in the toolbox, so these combinations were made and intracellular Mn was assayed by CFMEA after a 3 hour Mn/small molecule co-incubation (**Figure 2-7C**). Small molecule VU0243195 appeared to be epistatic to the majority of the toolbox, and the rest with an additive relationship. There were two exceptions: increasers VU0057971 ("971") and VU0026395 ("395"). Small molecule "971" was tested on the original five small molecules ("414", "386", "086", "366", and "195") and found to be epistatic to all five (**Figure 2-7D**). This highlights a dominant role of Mn uptake played by "971", and places it further downstream from small molecule "195". Ultimately, we began delineating an extensive step-wise chemical biology pathway regulating intracellular Mn, and established a foundation for future epistatic experiments to build on. We demonstrated that epistasis can be used to delineate Mn trafficking and homeostasis pathways at a cellular level.

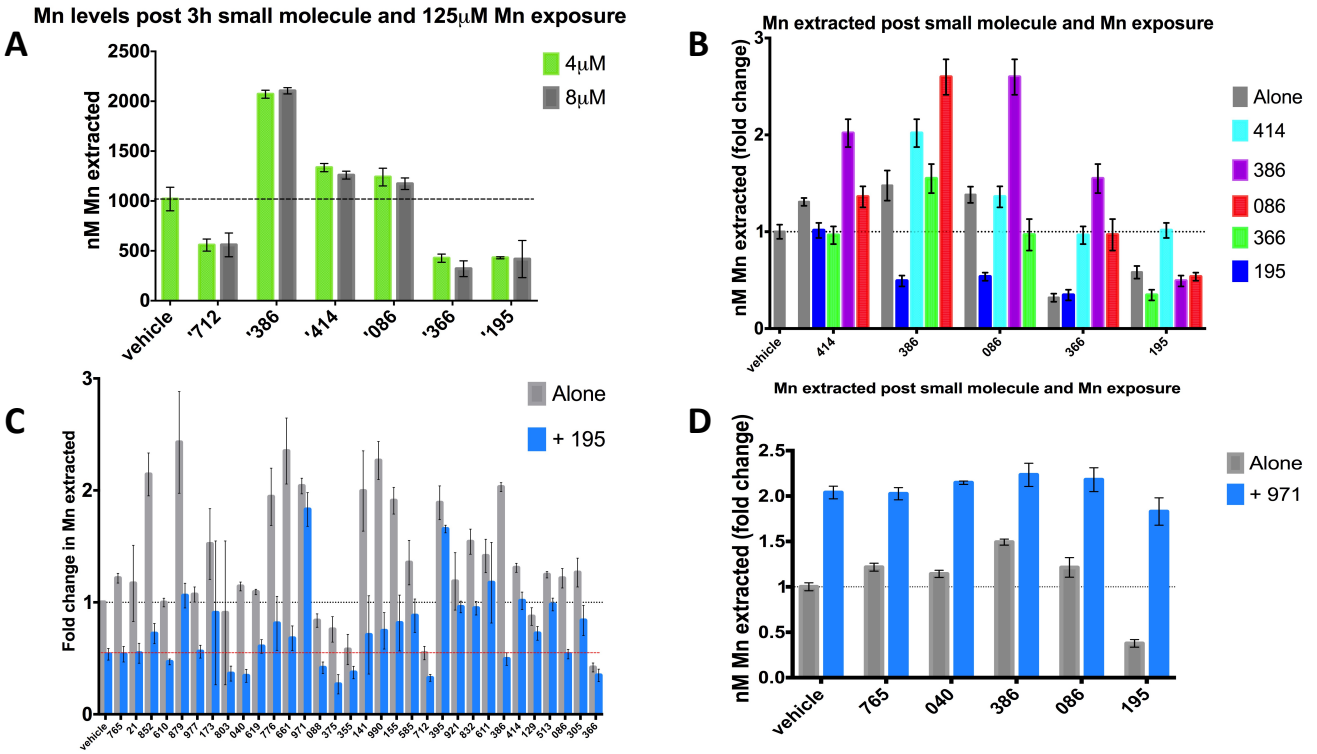

Figure 2-7: Epistasis experiments can delineate small molecule "pathways" without knowing the molecular targets. Six small molecules were tested to confirm that they were at saturation at 4μM (A). By combining these six with each other, two at a time, we could test which combinations were additive and which were epistatic (B). VU0243195 or '195' appeared to be epistatic (downstream/dominant) to the majority of the toolbox (C). One exception was the small molecule VU0057971, which acted downstream of '195' and several other molecules. An illustration of the combined order can be seen in Figure 11. Each Mn exposure was 125μM for 3 hours. Each bar represents 5-7 technical replicates.

VU0243195 and other Platinum Compounds

Considering the increased interest in VU0243195, as both an epistatically dominant molecule and SLC30A10 targeting candidate (see **Chapter IV**), we were especially concerned with the structure of the given molecule. Unfortunately, we were uncertain of its true molecular identity. It was officially cataloged as the platinum-based chemotherapy medication, cisplatin (34,35), but was then subsequently and perhaps incorrectly, published as platinum II chloride. The results of **Figure 2-8** were unclear as to whether VU0243195 was unique in its ability to decrease intracellular Mn accumulation, compared to other anti-cancer homologs. (We had initially made

the assumption that VU0243195 was indeed cisplatin). The results varied between biological replicates, but we can hypothesize on why the time in between the experiments may have mattered. The biological replicates in **Figure 2-8** are separated to show this difference. VU0243195 or a cisplatin homolog was pre-exposed to STHdh Q7 cells for 30 minutes before adding Mn for 3 hours. The impact of the small molecules was compared to the amount of Mn accumulated in these cells by CFMEA under vehicle conditions. As expected, VU0243195 decreased net Mn uptake by approximately 0.5-fold both times when assayed, though the cisplatin homologs had varying effects between the first and second biological replicate. Several homologs had no appreciable influence on intracellular Mn the first round but appeared to slightly increase Mn when assayed

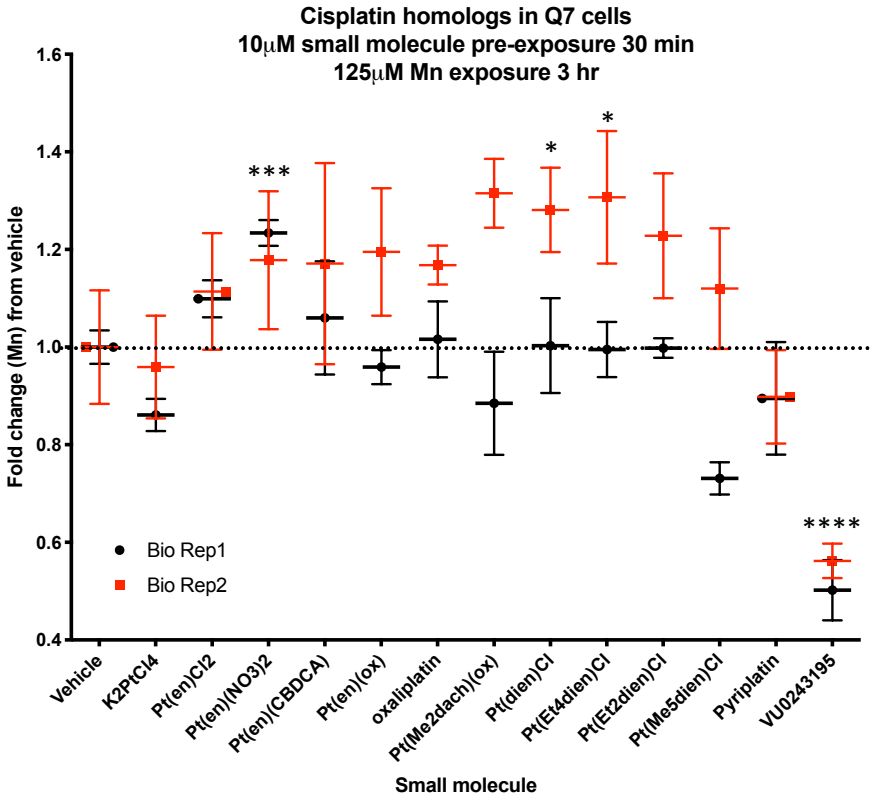

Figure 2-8: Pt-based chemotherapy drugs like cisplatin may alter Mn homeostasis. STHdh cells were pre-treated with a Pt-based chemotherapy drug for 30 minutes and then exposed to 125μM Mn for 3 hours, as if each was a member of the Mn-toolbox. Fold change over vehicle Mn accumulation was plotted as measured by CFMEA. Significance by One-Way ANOVA, Sidak's multiple comparisons is denoted by *, $p < 0.05$; **, $p<0.01$; ***, $p<0.001$; ****, $p<0.0001$. N=2 of biological replicates. Error bars reflect standard deviation of experimental replicates (4) per biological replicate.

days later, where stocks were frozen and thawed. This difference remained a mystery until reading the Hall et al 2014 (36) manuscript which described the degradation and inactivation of cytotoxicity in cisplatin and other platinum complexes while dissolved in dimethyl sulfoxide (DMSO). We hypothesized that a similar mechanism was occurring with these cisplatin homologs and wondered if it occurred with VU0243195.

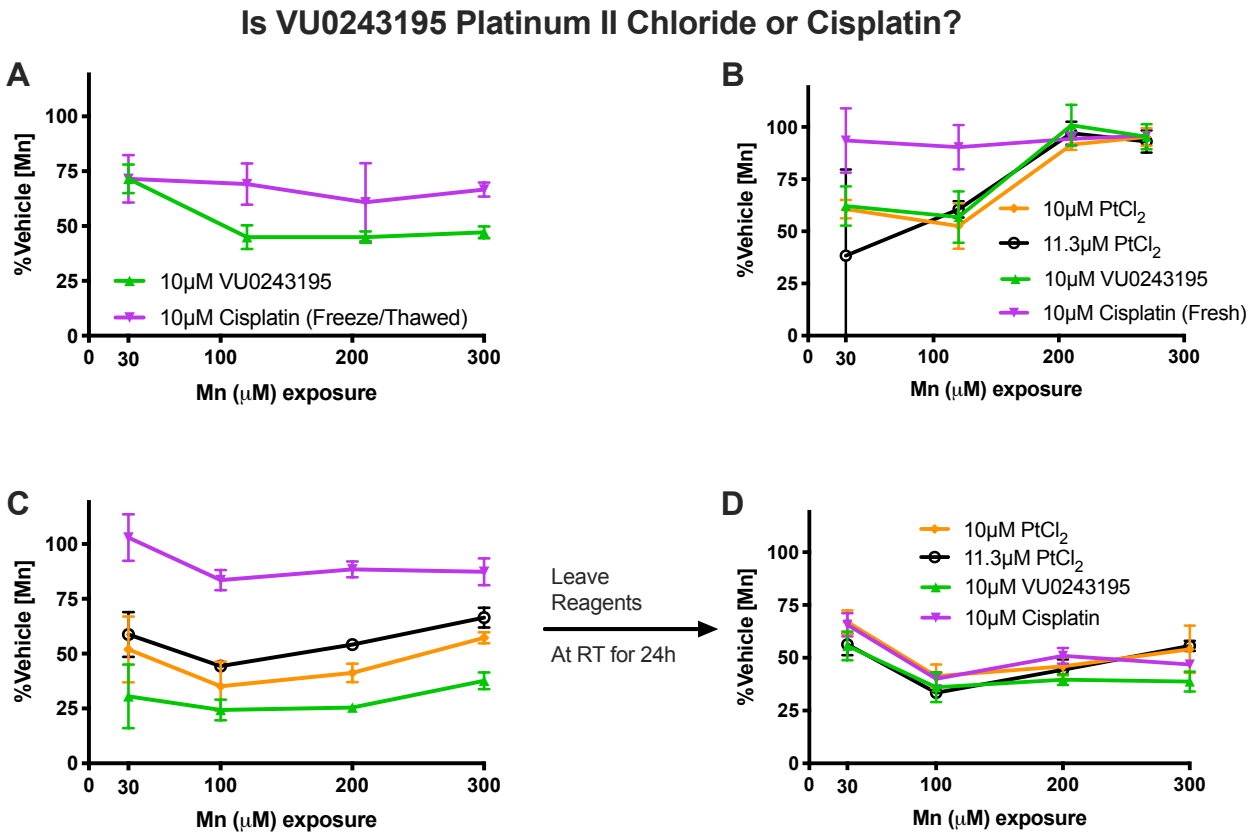

Figure 2-9: Cisplatin degrades into a bioactive Mn-reducer similar to $PtCl_2$ when stored in DMSO. Cisplatin, Platinum II Chloride, and VU0243195 were all tested to see their influence on Mn accumulation relative to Vehicle, as measured by CFMEA in STHdh (Q7) cells. Cells were co-exposed with small molecule and varying Mn concentrations for 3 hours at 37°C. Small molecule stock solutions were typically stored at -20 °C or -80°C between experiments. However, stocks of each small molecule were left at room temperature for 24 hours in between the experiments seen in (C) and (D). Each point is one biological replicate consisting of 4-6 technical replicates.

Considering the idea that cisplatin may degrade to $PtCl_2$ in DMSO, and the potential that VU0243195 was actually $PtCl_2$, we independently secured both cisplatin and platinum II chloride to compare their functional influence, if any, on net intracellular Mn accumulation. This can be seen in **Figure 2-9**. Our old cisplatin stock was first compared to VU0243195 alone, under varying Mn exposures to compare efficacy (**Figure 2-9A**). Cisplatin reduced Mn uptake (at all concentrations, to approximately 75% vehicle), but was not quite as effective as VU0243195. Freshly made cisplatin (also dissolved in DMSO) did not effectively reduce Mn uptake (**Figure 2-9B**), though VU0243195 and $PtCl_2$ (also dissolved in DMSO) worked to reduce Mn uptake at similar capacities when assayed (**Figure 2-9B**, **Figure 2-9C**). Following the experiment in Figure 12C, the reagents were left out at room temperature for 24hrs instead of being frozen as usual. When used 24 hours later, $PtCl_2$, Cisplatin, and VU0243195 all inhibited Mn uptake in cells effectively (**Figure 2-9D**). We concluded that cisplatin either degrades to platinum II chloride when stored in DMSO, or that it degrades into something functionally similar to platinum II chloride, as platinum II chloride certainly influences Mn accumulation. To be sure that $PtCl_2$ was not interfering with the way in which Mn is measured by CFMEA, *in vitro* curves of Mn were performed in the presence of varying concentrations of PtCl2 (**Figure 2-10**). A correlation analysis of Fura2 fluorescence with PtCl2 concentrations was not significant at all Mn concentrations tested.

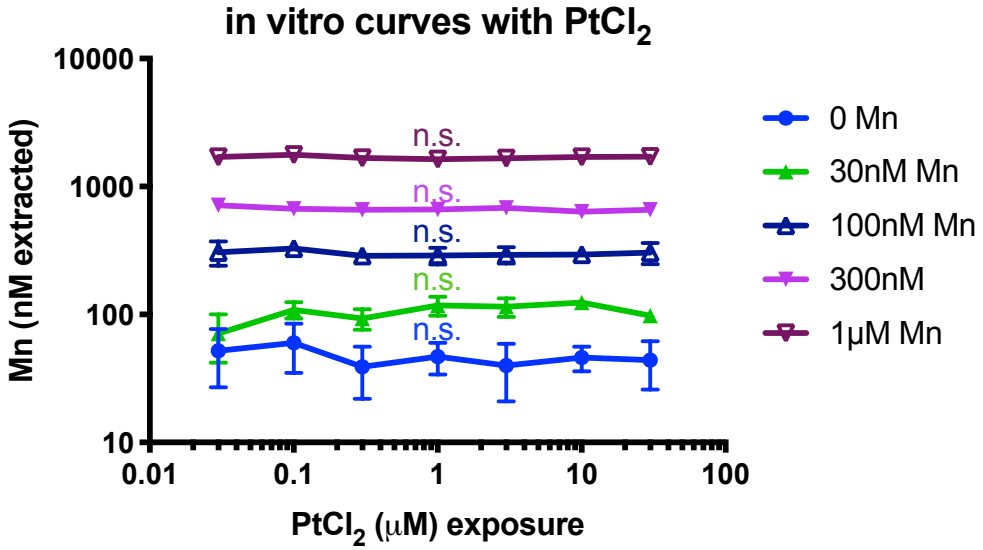

Figure 2-10: Platinum chloride does not influence Fura-2 fluorescence. Varying concentrations of platinum chloride were incubated in the presence of varying Mn concentrations to see if there was an effect on Fura-2. Mn concentrations were measured by fluorescence (Ex/Em 365nm/535nm) as if it was assayed by CFMEA. The lack of correlation (n.s.) between Mn measured and $PtCl_2$ concentration confirms that $PtCl_2$ does not interfere with the measurement of Mn by CFMEA.

DISCUSSION

The results of **Figure 1** demonstrate the varying utility of the small molecules in the Mn toolbox. A quick comparison of **Fig 1A** to **1B** shows a steep decline in fold change. It is not surprising that many small molecules lose efficacy in media from buffer- it is likely that the molecule is simply being bound to protein in the serum. Those that remain active do indeed have lower EC_{50}'s, and the concentrations used between conditions were static at 10 μM. Albumin-binding assays should be used in the future to confirm this hypothesis. In brief, a fluorescent probe targeted to bind albumin will fluoresce in the presence of albumin but will compete with the small molecules of the toolbox for the albumin binding site. Dose dependent curves of varying small molecule concentrations can be used to observe any percent inhibition the small molecule may have on the probe fluorescence. This can then be compared with the amount of apparent inhibition of small molecule effect on intracellular Mn concentrations. This is most important to verify the loss of potency for the molecule VU0028386 (MESM) in **Figure 2B**, which is specifically studied

in more detail **Chapter V**. If MESM or other small molecules that lose potency in complete medium unexpectedly do not demonstrate significant albumin binding, then a new hypothesis regarding small molecule degradation or another mechanism must be evaluated.

The observation that some small molecules switched direction of activity in HBSS media versus DMEM cell culture media (**Figure 2-1**) indicates that they are capable of influencing mechanisms of Mn homeostasis, rather than relying on a chelation mechanism, for example. Such small molecules may be prioritized in future studies that assess changes to candidate proteins known to induce changes in intracellular Mn. Further, it will be important to clarify how small molecule activities are influenced by the duration of treatment, the type of extracellular media, and the concentration of extracellular Mn and other metals. Here, the concentrations of metals tested were selected based on their ability to detectably alter Fura-2 fluorescence in cell lysates, and thus are not matched to each other. In addition, to better replicate previously published data, the Mn exposure concentrations at 3 h in HBSS and media were both 125 μM. To avoid toxicity, however, the concentration of Mn used in the 18-h studies was 50 μM. While previously all of these small molecules were validated in HBSS for 37 μM and 125 μM Mn, it conceptually makes sense that some molecules may not be able to influence Mn at concentrations not relevant to physiological conditions. This may be why Mn-decreasers such as VU0047355 and VU0244366 were active at 18 h (50 μM Mn) but not at 3 h (125 μM Mn). Stability of the molecules themselves at 33 vs. 37 ºC may also be a contributing factor. Thus, with more detailed stability assessment of each molecule, the longevity of the molecule stability versus longevity of a molecule's downstream effects can be better parsed.

The results of **Figure 2-2** suggest that while the inclusion of the SV40 T-Antigen may play a role in Mn-uptake, it is not the sole mechanism of any small molecule effect. None of the seven Mn-decreasers were affected by the temperature-dependent ejection of the SV40 T-Antigen from the cell, though eleven of the Mn-increasers were impacted. None of the eleven molecules completely lost effectiveness to alter Mn, suggesting that multiple Mn-altering mechanisms are at play. It is not a surprise that many of the small molecules have multiple chemical and biological targets. The only piece of evidence that argues against this idea is the small molecule VU0244366. This Mn-decreaser was the one small molecule of the 41 that appeared to have effectiveness (to decrease Mn uptake) at 33 degrees but lose all effectiveness (remain at vehicle levels) at higher temperatures. This result was not statistically significant, but merely places that small molecule as a suspect. Also, of note was the lack of effectiveness seen in the Mn-decreasers, even at 33 degrees, in this study. This is likely due to the already-small fold change being lost in media. (Previous experiments have already noted the lack of activity of these Mn-decreasers when applied in medium.)

Small molecules of similar structure (for example, the quinolinols: VU0243305, VU0243403, VU239513, VU0046776) had similar trends based on temperature. VU0243305 was not statistically significantly different at different temperatures but had a *P* value of 0.0549 comparing 33 vs 39. It was initially thought that the quinolinols were altering Mn by a chelation effect, but the data in part supports the idea that part of the effect is due to the T-Antigen. An alternative hypothesis would raise the issue that a myriad of factors could be affected by temperature- not just the T-Antigen. For instance, the binding affinities of ligand to receptor are often mutable based on temperature.

Assays to measure the chelation effect of the quinolinols (and all molecules) have had conflicting results. Unlike the *s. aureus* growth assay, the *in vitro* assay yielded no Mn chelators. This could be due to the assay buffers- undoubtedly the *s. aureus* experiment is closer to biological conditions. The Mn toolbox works best in HBSS, as we've seen, but has not been tested to influence Mn in cells while in PBS (which is what was used in the *in vitro* study). It is not a case of concentration, as the *s. aureus* growth assay determined that EC_{50} of each molecule, with only one exception, was under 10μM. Perhaps the small molecules that act as chelators can simultaneously chelate Mn but not interfere with Fura-2 quenching, however this is not the case for EDTA.

Regardless, the results of the *s. aureus* growth assay are interesting and consistent with the literature. As mentioned above, four out of the five quinolinols in the toolbox were marked chelators. Two other structurally similar molecules (VU0027832 and VU0028040), which differ only by a methyl and a hydroxyl group, were both listed as "Likely" chelators. Of the four acetohydrazides, two were marked as chelators and the other two were listed as "Likely" chelators. A benzo-hydrazide, VU0026921, was marked as a "Possible" chelator, but displayed remarkable toxicity in both the WT and the mnt-transporter KO bacteria. Follow-up experiments (by Lillian Juttukonda) would later reveal that this toxicity was selectively rescued by Mn. This sparked great interest and generated subsequent experiments on this small molecule (see **Appendix**).

Of all the small molecules tested in HeLa cells, only seven of the 39 were statistically significant from vehicle. All of these molecules are relatively robust increasers in STHdh Q7 cells. The data was misleading, however, in that none of the small molecules had significantly different fold-change activity between cell types. This indicated a lack of power to detect smaller changes

in Mn uptake. Rather than rely on statistical significance or lack thereof, cutoffs of fold change were used to designate a small molecule "active" in influencing Mn uptake, or inactive. The results of these cutoffs implicate 11 small molecules in the toolbox that may be only mouse or neuronal-specific, as these actively influenced Mn in the STHdh cells but not the HeLa cells. Three other small molecules were active in neither, so conclusions can't be drawn from these as the control cells could not confirm activity. However, an interesting trend of four small molecules that normally increase Mn in Q7 cells appeared to decrease Mn in HeLa cells. Of these four, two molecules (VU0088990 and VU0006021) are highly fluorescent. We did not anticipate that the nine fluorescent small molecules in the toolbox would appear to decrease Mn, if they fail to increase Mn. This is because Mn levels are based on Fura2 quenching; a decrease in fluorescence is associated with more Mn present. An increase in fluorescence, from Fura-2 or any other source, would be interpreted as less Mn. The other two small molecules (VU0006712 and VU0003610) are not fluorescent, so their apparent decrease in Mn uptake appears to be a real but unexpected effect. Given that 23 of the 39 small molecules retained some sort of activity in HeLa cells suggests that majority of the Mn toolbox works ubiquitously across mammalian cell types, regardless of species or differentiation. There were five small molecules (VU0243195, VU0048129, VU0088990, VU0050661, VU0004838) that had activity in the SH-SY5Y's (and Q7's) but had no activity in the HeLa cells. It is therefore possible to consider their targets as neural-specific. In support of this idea, there were not any small molecules that were significantly different in the HeLa cells but did not have activity in the SH-SY5Y's.

Though the five "sticky" molecules in **Figure 2-6** may, in actuality, act to biologically influence Mn uptake, their biological mechanism versus their "stickiness" would always be

difficult to parse in previous and future CFMEA experiments. It was for this reason that led to the decision to remove them from the Mn toolbox. The fluorescence of VU0076546 would not immediately cause us to eliminate it from the toolbox, but it appeared to lose the ability to increase Mn uptake in the Q7 cells despite this. The amount of Mn quantified with its co-exposure would not be the true amount, but the molecule could still be useful if it was also increasing Mn. Since subsequent experiments with new stock of VU0076546 failed to see an increase in Mn uptake with co-exposure, the molecule was removed from the Mn toolbox. Regardless of whether if co-exposure with the small molecule increased Mn uptake due to random chance in previous experiments, or the molecule is unstable, it no longer has use in the Mn toolbox.

The epistasis experiments provide a necessary proof-of-concept step in its early attempts to decipher biological target pathways. Based on the results in **Figure 2-7**, a working model schematic of a biological pathway has been drawn to better visualize the data (**Figure 2-11**). The benefits of these initial experiments alone could assist in future pharmacological experiments, once the target of one of the small molecules is found. For example, we already know that molecule 195 (VU0243195) was found to be downstream of several small molecules, and upstream of one small molecule 971 (VU0057971). We already know from the SLC30A10 screen data (see **Chapter III**) that 195 appears to enhance Mn efflux via SLC30A10. If we know that 971 can operate downstream of 195 from the epistatic experiments in **Figure 2-7**, then we should be able to negate the effect of SLC30A10 induction with 971, without even knowing the target of 971. This is consistent with the data in **Chapter IV**; small molecule 971 (boxed in purple) is able to increase cellular Mn levels regardless of SLC30A10 genotype. Unlike nearly all the other small molecule Mn-increasers, 971 increases the cellular levels of Mn in the WT SLC30A10 overexpressing HEK cells. Considering this and its interruption of the V-phenotype, one could argue that 971 blocks

the function of SLC30A10. For this reason, future experiments should also look at SLC30A10 function in the presence of 971, and 096 (VU0009096), which displays a similar phenotype. The epistasis experiments can add insight and aid in future experiments like described above and can also add support to data from other completed experiments.

On the other hand, however, by the same reasoning above, the several small molecules which are upstream of 195 (VU0135086, VU0003765, VU0028040, VU0002852, VU0050661, VU0088990) should also have an impact of SLC30A10. There is no evidence of this in **Chapter III**. Instead, we may consider the possibility that 195 interacts with and functionally degrades these small molecules. According to experiments in **Figure 2-10**, small molecule 195 (VU0243195) is simply platinum II chloride. As cisplatin degrades to platinum II chloride, it is possible that platinum II chloride interacts with other molecules. Indeed, platinum chloride and other cisplatin reagents are very reactive with intracellular molecules containing thiols or other sulfur nucleophiles (37).

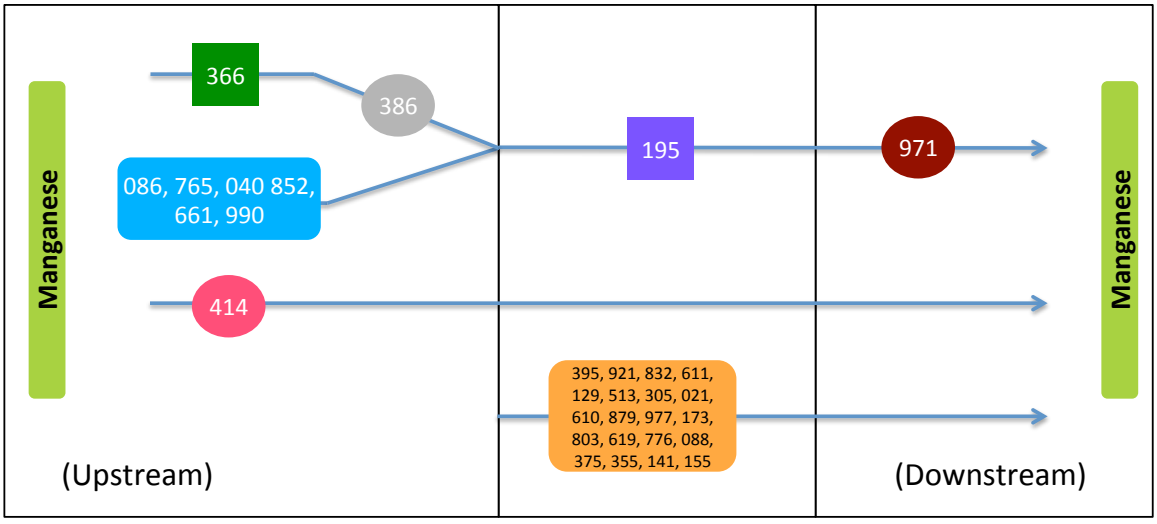

Figure 2-11: Working model showing possible small molecule pathways altering Mn trafficking and homeostasis. Small molecules toward the right of the model are downstream and have a dominant Mn-altering effect. Mn increasers and decreasers are represented with circles and squares, respectively.

While it is possible that 195 is not functionally downstream from these several small molecules as outlined in **Figure 11**, it is undeniable that 195 is able to influence Mn, most likely via SLC30A10 or SLC30A10-similar processes. For this reason, future chemical studies (via mass-spectrometry or by other non-functional measures should investigate whether $PtCl_2$ interacts/reacts with the small molecules that are hypothesized to be epistatic from it.

With the insights from **Figures 3-8, 3-9,** and **3-10**, it is possible that the other Pt-based chemotherapy medications tested in **Figure 3-8** are degrading into platinum II chloride-based complex as well. Future studies (mass spectrometry/NMR/etc.) should confirm that the result of cisplatin in DMSO is $PtCl_2$. Alternatively, it could be a product between $PtCl_2$ as predicted in the Hall et al paper: $[Pt(NH_3)_2(Cl)(DMSO)]^+$, $[Pt(NH_3)(Cl)(DMSO)_2]^+$, or μNH_2-$[Pt(NH_3)(Cl)(DMSO)]_2^+$ (36). Dissolving cisplatin in water and waiting 24 hours at room temperature before pre-exposing it to cells could test this idea. ($PtCl_2$ is insoluble in water, but perhaps in dilute HCl.)

In conclusion, the major findings implicate a handful of small molecules that should be placed on high priority to discover their molecular targets. In addition to a variety of biochemical methods have been proposed, bioinformatics methods (proteomics, metabolomics) would be the most comprehensive and deterministic methods. This would apply to the Pt-based Mn-decreaser VU0243195, which can be generated by the degradation of cancer-treatment drugs in DMSO and can also act downstream of most of the other small molecules in the Mn toolbox.

MATERIALS AND METHODS

Cell Culture

STHdh$^{Q7/Q7}$ wild-type immortalized murine striatal derived cells and STHhh$^{Q111/Q111}$ cells were obtained from Coriell Cell Repository (Camden, NJ). They were plated at a density of 10,000 and 12,000 cells per well, respectively, of a 96-well plate and incubated at 33°C with 5% CO_2 in complete Dulbecco's Modified Eagles Medium (DMEM; high glucose Sigma-Aldrich; D6546; St. Louis, MO) with 10% Fetal Bovine Serum (FBS; Atlanta Biologicals; Flowery Branch, GA), 1% Penicillin/Streptomycin (15140-122; Life Technologies; Carlsbad, CA), 2mM GlutaMAX (Life Technologies), 0.5 mg/mL G418 Sulfate, (Life Technologies) 1X Non-essential Amino Acids Solution (Life Technologies), 14mM HEPES (Life Technologies) for 16-24 hours prior to the assay. Cells were dissociated using 0.05% Trypsin-EDTA solution (Life Technologies). In Figure 6, STHdh cells were fixed with 4% paraformaldehyde dissolved in PBS for 20 minutes at room temperature, and then washed three times with PBS prior to the assay. SH-SY5Y cells were obtained from ATCC and cultured in a 1:1 mix of DMEM:F12 (10565-018; Gibco) with 10% FBS. HeLa cells were cultured in DMEM (10-013CV; Corning) containing 10% FBS.

Cellular Mn level assay and extraction with triton/ Cellular Fura-2 Manganese Extraction Assay (CFMEA)

Cell cultures were exposed to varying Mn concentrations ($MnCl_2 \cdot 4H_2O$ stock dissolved in sterile water), in HBSS unless otherwise noted. Exceptions were STHdh cells exposed to Mn in cell medium (complete DMEM; see above) in Figure 1B and 1C. Cells were typically plated in a 96-well format, with final volume in each well at 100µL. Incubations were at 33°C degrees for all STHdh cell cultures, except in Figure 2, exposures were also done at 37°C and 39°C. All other cell

cultures (HEK, HeLa, SH-SY5Y) were incubated at 37°C. Incubation times of Mn exposures varied by experiment but were typically 2-3 hours unless otherwise noted. Often, other small molecules (stocks dissolved in DMSO) were co-incubated with the Mn in the HBSS/medium to assess their impact on Mn accumulation levels. Percent DMSO levels incubated with cells never exceed 0.1% and experiments always included a DMSO (vehicle-only) control. All CFMEA experiments necessitated a no-Mn control for normalization of Fura-2 maximum fluorescence. After Mn and/or small molecule incubations, the cells were washed three times with PBS (without Ca^{2+} and Mg^{2+}) to remove the extracellular Mn and small molecule-modifiers. *Extraction buffer* (PBS containing 0.1% TritonX100; Sigma-Aldrich; T8787; St. Louis, MO and 500nM Fura-2) was added to lyse the cells. The fluorescence of the Fura-2 in the extraction buffer was then measured at 360nm/535nm (Ex/Em) so that Mn could be quantified.

Manganese Quantification by Fura-2

A percent max of Fura-2 fluorescence 360nm/535nm (Ex/Em) was calculated for each condition as the corresponding zero Mn condition was defined as 100%. Background fluorescence was subtracted from all values. The concentration of Mn (nM) was calculated with the equation:

$[Mn] = 1138 \times ((1 / \%max) - 1)^{0.9682}$, which was generated based on a standard curve of Mn quenching Fura-2 signal (32). The absolute values were calculated by multiplying by the concentration by volume.

DNA Quantification and Normalization

Cells were lysed with 0.1% triton and 5µL (of 100µL) from each well was added to 95µL Tris-EDTA buffer (Corning; 46-009-CM) with 1:800 PicoGreen Reagent (final; Quant-iT PicoGreen

dsDNA Assay Kit; Invitrogen; P7589). Fluorescence of each sample well was measured at $490_{Ex}/525_{Em.}$ DNA content for each well was quantified based on an equation of linear regression generated by the fluorescence of a DNA standard curve containing equal amounts of PicoGreen reagent and 0.1% triton. Mn concentrations were normalized to DNA levels to control for cell growth between groups and observe possible cell loss from washing steps or toxicity (see Figure 2).

Mn-Chelation Experiments

Concentration curves (1 to 10μM) for each small molecule were run in a 96 well format –without cells, in the presence of 0.5μM Fura-2 and 1 μM Mn dissolved in HBSS. A concentration curve of EDTA in HBSS was used as a positive control. EDTA, a Mn chelator, is able to sequester Mn from Fura-2 to prevent its fluorescence quenching.

Statistical Analysis

All data was analyzed statistically by GraphPad Prism 8. Statistical significance was determined by paired t-tests, Ordinary One-Way ANOVAs, Two-Way ANOVAs with Sidak's multiple comparisons, or Tukey's multiple comparisons where not

REFERENCES

1. Roth JA, Ganapathy B, Ghio AJ. Lymphocyte Cell Lines Containing a Homozygous Mutation in Parkin. Toxicol Vitr. 2013;26(7):1143–9.
2. Chen MK, Lee JS, McGlothan JL, Furukawa E, Adams RJ, Alexander M, et al. Acute manganese administration alters dopamine transporter levels in the non-human primate striatum. Neurotoxicology. 2006;27(2):229–36.
3. Chakraborty S, Chen P, Bornhorst J, Schwerdtle T, Schumacher F, Kleuser B, et al. Loss of pdr-1/parkin influences Mn homeostasis through altered ferroportin expression in C. elegans. Metallomics [Internet]. 2015;7(5):847–56. Available from: http://dx.doi.org/10.1039/C5MT00052A
4. Mukhopadhyay S. Familial manganese-induced neurotoxicity due to mutations in SLC30A10 or SLC39A14. Neurotoxicology [Internet]. 2018;64:278–83. Available from: http://dx.doi.org/10.1016/j.neuro.2017.07.030
5. Ramonet D, Podhajska A, Stafa K, Sonnay S, Trancikova A, Tsika E, et al. PARK9-associated ATP13A2 localizes to intracellular acidic vesicles and regulates cation homeostasis and neuronal integrity. Hum Mol Genet. 2012;21(8):1725–43.
6. Chun HS, Lee H, Son JH. Manganese induces endoplasmic reticulum (ER) stress and activates multiple caspases in nigral dopaminergic neuronal cells, SN4741. Neurosci Lett. 2001;316(1):5–8.
7. Rentschler G, Covolo L, Ahmadi Haddad A, Lucchini RG, Zoni S, Broberg K. ATP13A2 (PARK9) polymorphisms influence the neurotoxic effects of manganese. Neurotoxicology. 2012;33(4):697–702.

8. Gorell JM, Johnson CC, Rybicki BA, Peterson EL, Kortsha GX, Brown GG, et al. Occupational exposure to manganese, copper, lead, iron, mercury and zinc and the risk of Parkinson's disease. Neurotoxicology. 1999;
9. Thompson KJ, Molina RM, Donaghey T, Savaliya S, Schwob JE, Brain JD. Manganese uptake and distribution in the brain after methyl bromide-induced lesions in the olfactory epithelia. Toxicol Sci [Internet]. 2011 Mar [cited 2014 Nov 20];120(1):163–72. Available from: http://www.pubmedcentral.nih.gov/articlerender.fcgi?artid=3044207&tool=pmcentrez&rendertype=abstract
10. Finkelstein Y, Zhang N, Fitsanakis VA, Avison MJ, Gore JC, Aschner M. Differential deposition of Manganese in the rat brain following subchronic exposure to manganese: A T1-weighted magnetic resonance imaging study. Isr Med Assoc J. 2008;10(11):793–8.
11. Pfalzer AC, Bowman AB. Relationships Between Essential Manganese Biology and Manganese Toxicity in Neurological Disease. Curr Environ Heal reports. 2017;4(2):223–8.
12. Michalke B, Fernsebner K. New insights into manganese toxicity and speciation. J Trace Elem Med Biol [Internet]. 2014 Apr [cited 2014 Nov 8];28(2):106–16. Available from: http://www.ncbi.nlm.nih.gov/pubmed/24200516
13. Tuschl K, Mills PB, Clayton PT. Manganese and the brain. [Internet]. 1st ed. Vol. 110, International review of neurobiology. Elsevier Inc.; 2013 [cited 2014 Oct 15]. 277–312 p. Available from: http://www.ncbi.nlm.nih.gov/pubmed/24209443
14. Chang Y, Jin S-U, Kim Y, Shin KM, Lee HJ, Kim SH, et al. Decreased brain volumes in manganese-exposed welders. Neurotoxicology [Internet]. 2013 Jul [cited 2014 Nov

19];37:182–9. Available from: http://www.ncbi.nlm.nih.gov/pubmed/23685157

15. Guilarte TR, Burton NC, Mcglothan JL, Verina T, Zhou Y, Alexander M, et al. Implications to manganese-induced parkinsonism. 2013;107(5):1236–47.

16. Horning KJ, Caito SW, Tipps KG, Bowman AB, Aschner M. Manganese Is Essential for Neuronal Health. Annu Rev Nutr [Internet]. 2015;35(1):71–108. Available from: http://www.annualreviews.org/doi/10.1146/annurev-nutr-071714-034419

17. DeWitt MR, Chen P, Aschner M. Manganese efflux in Parkinsonism: insights from newly characterized SLC30A10 mutations. Biochem Biophys Res Commun [Internet]. 2013 Mar 1 [cited 2014 May 2];432(1):1–4. Available from: http://www.pubmedcentral.nih.gov/articlerender.fcgi?artid=3594538&tool=pmcentrez&rendertype=abstract

18. Aschner M, Liu C, Smith DR, Shawlot W, Taylor CA, Mukhopadhyay S, et al. SLC30A10 transporter in the digestive system regulates brain manganese under basal conditions while brain SLC30A10 protects against neurotoxicity. J Biol Chem. 2018;294(6):1860–76.

19. Mills PB, Bhatia KP, Stamelou M, Clayton PT, Burroughs AK, Tuschl K, et al. Dystonia with brain manganese accumulation resulting from SLC30A10 mutations: A new treatable disorder . Mov Disord. 2012;27(10):1317–22.

20. Leyva-Illades D, Chen P, Zogzas CE, Hutchens S, Mercado JM, Swaim CD, et al. SLC30A10 Is a Cell Surface-Localized Manganese Efflux Transporter, and Parkinsonism-Causing Mutations Block Its Intracellular Trafficking and Efflux Activity. J Neurosci [Internet]. 2014 Oct 15 [cited 2014 Nov 20];34(42):14079–95. Available from: http://www.ncbi.nlm.nih.gov/pubmed/25319704

21. Williams BB, Kwakye GF, Wegrzynowicz M, Li D, Aschner M, Erikson KM, et al. Altered manganese homeostasis and manganese toxicity in a Huntington's disease striatal cell model are not explained by defects in the iron transport system. Toxicol Sci [Internet]. 2010 Sep [cited 2014 Oct 28];117(1):169–79. Available from: http://www.pubmedcentral.nih.gov/articlerender.fcgi?artid=2923282&tool=pmcentrez&rendertype=abstract

22. Burdo JR, Menzies SL, Simpson IA, Garrick LM, Garrick MD, Dolan KG, et al. Distribution of Divalent Metal Transporter 1 and Metal Transport Protein 1 in the Normal and Belgrade Rat. 2001;1207(July):1198–207.

23. Illing AC, Shawki A, Cunningham CL, Mackenzie B. Substrate profile and metal-ion selectivity of human divalent metal-ion transporter-1. J Biol Chem. 2012;287(36):30485–96.

24. Garrick MD, Dolan KG, Horbinski C, Ghio AJ, Higgins D, Porubcin M, et al. DMT1: A mammalian transporter for multiple metals. BioMetals. 2003;16(1):41–54.

25. Gunter TE, Gerstner B, Gunter KK, Malecki J, Gelein R, Valentine WM, et al. Manganese transport via the transferrin mechanism. Neurotoxicology [Internet]. 2013 Jan [cited 2014 Nov 20];34:118–27. Available from: http://www.pubmedcentral.nih.gov/articlerender.fcgi?artid=3576891&tool=pmcentrez&rendertype=abstract

26. Crossgrove JS, Allen DD, Bukaveckas BL, Rhineheimer SS, Yokel RA. Manganese distribution across the blood-brain barrier. I. Evidence for carrier-mediated influx of manganese citrate as well as manganese and manganese transferrin. Neurotoxicology. 2003;24(1):3–13.

27. Chen P, Bowman AB, Mukhopadhyay S, Aschner M. SLC30A10 : A novel manganese transporter. 2015;4(3):4–7.

28. Zaki MS, Issa MY, Elbendary HM, El-Karaksy H, Hosny H, Ghobrial C, et al. Hypermanganesemia with dystonia, polycythemia and cirrhosis in 10 patients: Six novel SLC30A10 mutations and further phenotype delineation. Clin Genet. 2018;93(4):905–12.

29. Kumar KK, Lowe EW, Aboud A a, Neely MD, Redha R, Bauer J a, et al. Cellular manganese content is developmentally regulated in human dopaminergic neurons. Sci Rep [Internet]. 2014 Jan [cited 2014 Nov 2];4:6801. Available from: http://www.ncbi.nlm.nih.gov/pubmed/25348053

30. Kwakye GF, Li D, Kabobel OA, Bowman AB. Cellular fura-2 Manganese Extraction Assay (CFMEA). Curr Protoc Toxicol. 2011;2651(SUPPL.48):1–26.

31. Kwakye GF, Li D, Bowman AB. Novel high-throughput assay to assess cellular manganese levels in a striatal cell line model of Huntington's disease confirms a deficit in manganese accumulation. Neurotoxicology. 2011;32(5):630–9.

32. Kumar KK, Aboud AA, Patel DK, Aschner M, Bowman AB. Optimization of Fluorescence Assay of Cellular Manganese Status for High Throughput Screening. J Biochem Mol Toxicol [Internet]. 2013 Jan;27(1):42–9. Available from: http://doi.wiley.com/10.1002/jbt.21457

33. Prachayasittikul V, Prachayasittikul S, Ruchirawat S, Prachayasittikul V. 8-Hydroxyquinolines: A review of their metal chelating properties and medicinal applications. Drug Des Devel Ther. 2013;7:1157–78.

34. Drucker J, New EJ, Ma H-YM, Shen C, Eljack ND, Hambley TW, et al. Mechanisms of cell uptake and toxicity of the anticancer drug cisplatin. Metallomics. 2014;6(11):2126–

33.

35. Basu A, Krishnamurthy S. Cellular Responses to Cisplatin-Induced DNA Damage. J Nucleic Acids. 2010;2010:1–16.

36. Hall MD, Telma KA, Chang KE, Lee TD, Madigan JP, Lloyd JR, et al. Say no to DMSO: Dimethylsulfoxide inactivates cisplatin, carboplatin, and other platinum complexes. Cancer Res. 2014;74(14):3913–22.

37. Hermanson G. Bioconjugate Techniques. In: 3rd ed.

A version of the following chapter, including text and figures, have previously been published in Molecules. 2021; 26(4):1175, as “Identification of Three Small Molecules That Can Selectively Influence Cellular Manganese Levels in a Mouse Striatal Cell Model”.
DOI 10.3390/molecules26041175

CHAPTER III

IDENTIFICATION OF THREE SMALL MOLECULES THAT CAN SELECTIVELY INFLUENCE CELLULAR MANGANESE LEVELS IN A MOUSE STRIATAL CELL MODEL AND THEIR RELATIOSHIP TO THE HUNTINGTON'S DISEASE MN PHENOTYPE

INTRODUCTION

In recent years, a cellular deficit of the essential metal manganese (Mn) has been implicated in the pathogenesis of Huntington's disease (HD), a fatal neurodegenerative disease characterized by the expression of mutant huntingtin. Deficient Mn handling in neurons has been reported in cellular and *in vivo* models Huntington's disease (HD) (1,2). HD is a devastating neurodegenerative disorder characterized by involuntary hyperactive limb movements, psychiatric disturbances, cognitive decline, and the loss of GABAergic medium spiny neurons in the striatum; a part of the motor area of the brain. Although its cause is known: an expansion of the poly-glutamine (polyQ) tract in the huntingtin protein (HTT), the disease has no known cure, and treatments to alleviate symptoms are poor and do not slow disease progression (3). In recent years, a cellular deficit of the essential metal manganese (Mn) has been implicated in the pathogenesis of HD. Mn is an essential metal, required as a cofactor for numerous kinases and several fundamental enzymes such as glutamine synthetase, Mn superoxide dismutase, and arginase (4). Deficiencies in arginase enzymatic activity of the urea cycle in HD have been noted previously in our lab (2). The recycling of the neurotransmitter glutamate is mediated by the Mn-dependent enzyme glutamine synthetase, and its reduced enzymatic activity in HD has also been noted (5,6).

These deficiencies occur in (but are not limited to) the striatum- where Mn selectively accumulates over time, and the same area that degenerates in HD (7). Recent studies have linked the Mn bioavailability deficiency in HD as the culprit surrounding impaired autophagy (8) and insulin signaling (9).

Much like other biological trace metals, sufficient Mn needs to be achieved while avoiding excess, toxic amounts. However, unlike other essential metals, the proteins and mechanisms known to maintain Mn homeostasis are exceedingly sparse. Since it has become likely that reduced bioavailability of Mn in HD contributes to cellular pathologies, exactly how that Mn deficiency occurs and whether it could be targeted for therapeutic treatments have become pertinent questions. Although some iron transporters are capable of trafficking Mn with some affinity, without Mn specificity they alone are insufficient to explain how cells maintain a homeostatic balance of Mn under normal conditions (10). Only recently has the first Mn-specific transporter been described (11). Understanding how cells maintain appropriate Mn concentrations in the brain under normal conditions is vital to understanding how a Mn deficit may occur in HD. Complicating matters further, HTT is known to interact with hundreds of proteins of various functions, but its exact function isn't clear (12,13). Understanding how cells maintain appropriate Mn concentrations in the brain under normal conditions is vital to understanding how a Mn deficit may occur in HD. Considering the dearth of information between the two fields, and our interest in bridging them together, a more exploratory and comprehensive approach was warranted.

A set of 41 individual small molecules, capable of influencing intracellular Mn accumulation were identified by our lab in 2014 using the Cellular Fura-2 Manganese Extraction Assay (CFMEA) method with a high throughput screening approach (14). This set of small molecules was coined the "Mn toolbox", as each molecule may be used as a chemical tool to

investigate Mn homeostasis in neuronal cells. Of the original 41 molecules previously identified, 37 are presently available and were examined in this study. We had previously validated in vivo activity for two molecules of the Mn toolbox (VU0063088 and VU0026921), that were shown to modulate Mn levels in *C. elegans,* through mechanisms independent of the species DMT-2 homologue, and induce protection from Mn neurotoxicity (15).

Though they have been confirmed to increase or decrease Mn accumulation in STHdh$^{Q7/Q7}$ cells, or Q7 cells, a WT immortalized model of striatal neurons, we were unsure of their selectivity towards influencing Mn over other divalent transition metals. Since the metal deficit in HD is specific to Mn, we hypothesized that any small molecules that are Mn selective may be ineffective in the cellular HD model: STHdh$^{Q111/Q111}$, or Q111 cells. These are the HD-counterparts to the Q7 cells, which differ only in the number of CAG repeats in the expanded polyglutamine tract in exon 1 of the huntingtin gene (a pathological 111 repeats compared to a non-pathological 7 repeats). Here, using a modified version of the CFMEA assay (16) we find that of the set of small molecules tested, only three appear to be Mn-selective. Of these three, two of them are effective increasers in the WT Q7 cells but are ineffective in the HD Q111 cells. The results indicate that the target(s) of these two small molecules are the very mechanisms of Mn transport that are deficient in HD.

RESULTS

Evaluation of the selectivity of small molecules for divalent metals

Despite the fact that all of the molecules in the Mn toolbox are able to influence intracellular Mn accumulation, there was no guarantee that the small molecules were acting on mechanisms that are used specifically for Mn homeostasis. Rather than perform the costly analysis of ICP-MS for 30-40 small molecules each, per divalent metal, we applied the same principle of CFMEA (16) to other divalent metals to screen the Mn toolbox. This allowed us to screen 33 of

the small molecules from the Mn toolbox against all four of these divalent metals (cobalt, copper, nickel, zinc) with the workflow displayed in **Figure 3-1**. Although 37 of the small molecules were available for use, three molecules (VU0009101, VU0009103, VU0239513) were retained because they were close structural homologs of other molecules in the toolbox, and one (VU0076546) was later identified to be a false positive and was subsequently removed from the Mn toolbox completely. In brief, CFMEA allows cells to be incubated with extracellular Mn, before washing any remaining extracellular Mn with PBS (without Ca and Mg). The cells are then lysed open with 0.1% triton containing Fura-2, a fluorescent indicator of Mn concentration. Fura-2 fluorescence is quantitatively quenched in the presence of Mn when measured at the calcium isosbestic point-360nm/535nm (Ex/Em). It was previously observed (17) that several other essential and divalent metals: cobalt (Co), nickel (Ni), zinc (Zn) and copper (Cu), could similarly influence Fura-2 fluorescence when added in excess. Though this was not quantified to an intracellular concentration of each divalent, we sought to find small molecules that significantly increased or decreased Fura-2 fluorescence by One-Way ANOVA with Dunnett's multiple comparisons test

(P< 0.05) with a fold change greater than or less than two standard deviations from the Vehicle mean. The %Fura-2 signal compared to vehicle is shown in **Figure 3-2**.

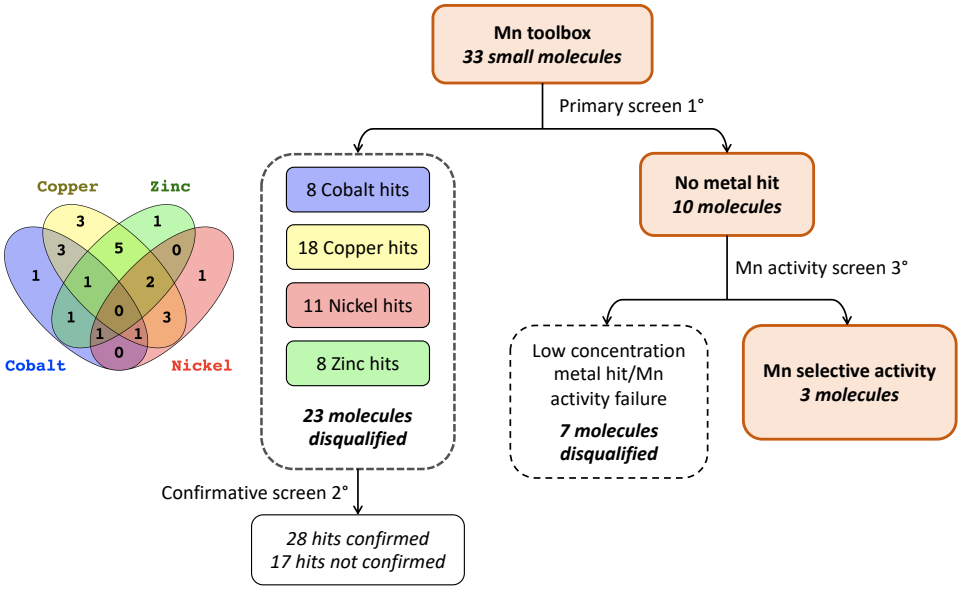

Figure 3-1: Screening paradigm for small molecule activity against other divalent metals. A primary screen of 33 small molecules was completed, assaying each molecule for fluctuations in Fura-2 fluorescence after Co, Cu, Zn, and Ni exposure (see Supplementary Table 1). Significant deviations (by one-way ANOVA, Sidak's multiple comparisons) were detected in 23 of the small molecules, leaving 10 that were not significantly different (and within two standard deviations from the vehicle mean; see Supplementary Table 2). These 10 were tested in the presence of lower concentrations of each metal, and it was confirmed that they could indeed influence intracellular Mn levels. Three molecules remained.

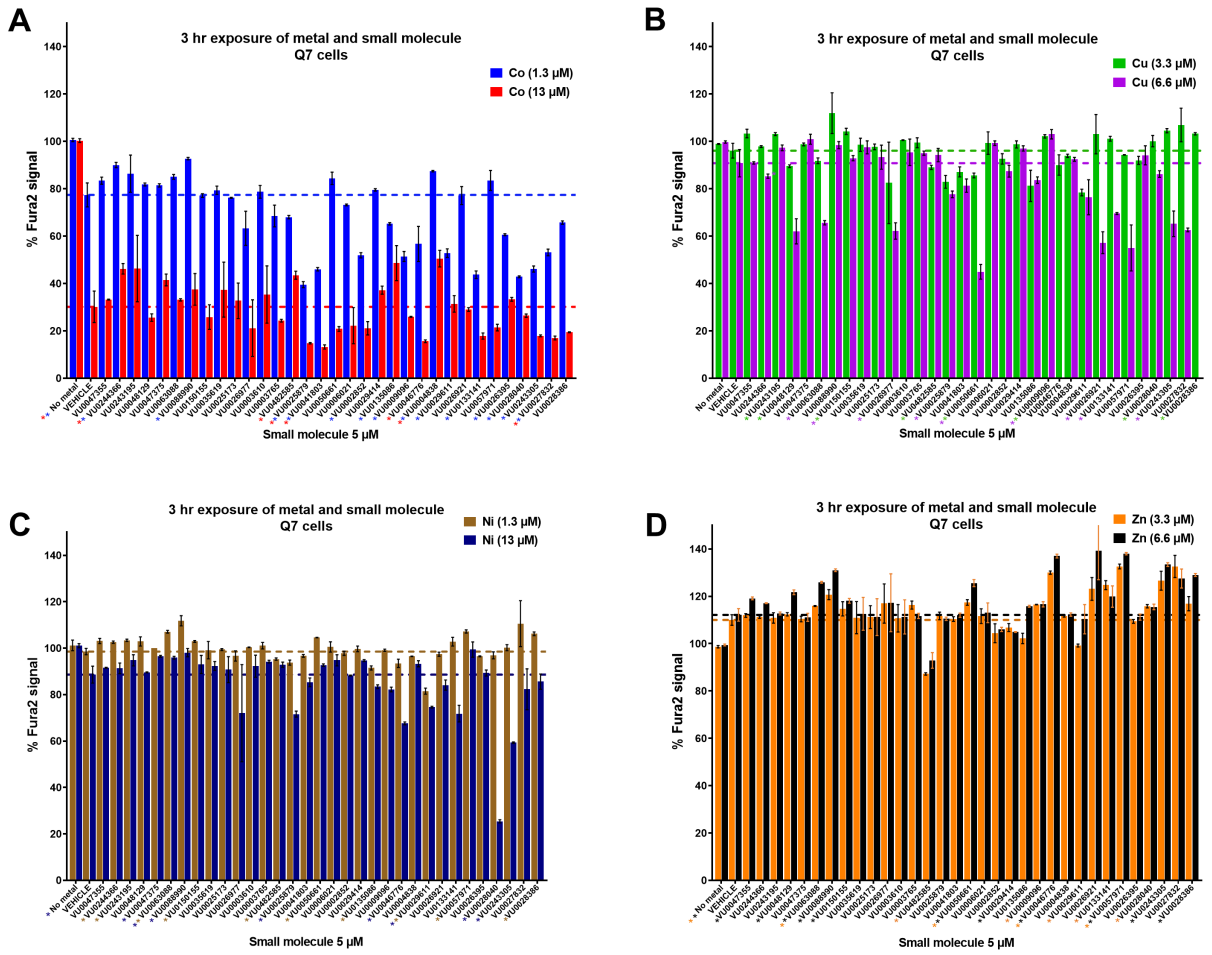

Figure 3-2: Cellular Fura-2 Divalent Metal Extraction Assay (CFDMEA) screen with toolbox. Cells were pre-exposed with small molecule (5 μM), then the metal (A: Cobalt, B: Copper; C: Nickel; D: Zinc) was added. After 3 h, the cells were washed with PBS and lysed open with 0.1% Triton containing Fura-2. The presence of divalent metal quenches the Fura-2 signal in a concentration-dependent manner. We compared the Fura-2 signal of metals taken up by cells (Q7s) under vehicle conditions and determined whether the Fura-2 signal was significantly different when cells were co-exposed with a small molecule. Cells were exposed to a small molecule and metal in HBSS. The dotted line shows vehicle levels for a given metal concentration. A one-way ANOVA for each metal concentration tested was run, with post-hoc Dunnett's T3 multiple comparisons test.

While it was our intent to cluster small molecules by their functionality in these CFMEA-like experiments (i.e. one might see patterns of similar structure/function influencing the same metals in the same direction), our primary outcome of interest was whether these small molecules

were specific to Mn or influenced other divalents. Small molecules that displayed a significant influence on Fura-2 signal compared to vehicle (divalent hits) were disqualified and went through a secondary screen for confirmation of their activity (see **Table 3-1**). Molecules that did not hit any given metals were subjected to a third screen in which lower concentrations of metals were applied and their activity on Mn were confirmed (**Table 3-2**).

TABLE 3-1. Primary and Secondary Screen of Small Molecules With Other Divalents

Ordinary One-Way ANOVA, Dunnett's multiple comparisons p <0.05 with a mean difference of a least 2 standard deviations								
VU ID	**Cobalt 1°**	**Cobalt 2°**	**Copper 1°**	**Copper 2°**	**Zinc 1°**	**Zinc 2°**	**Nickel 1°**	**Nickel 2°**
VU0047355	n.s.	/	n.s.	/	n.s.	/	n.s.	/
VU0244366	n.s.	/	n.s.	/	n.s.	/	n.s.	/
VU0243195	decrease	not confirmed	decrease	**confirmed**	n.s.	/	n.s.	/
VU0048129	n.s.	/	increase	**confirmed**	increase	not confirmed	n.s.	/
VU0047375	n.s.	/	decrease	not confirmed	n.s.	/	n.s.	/
VU0063088	n.s.	/	increase	not confirmed	increase	not confirmed	n.s.	/
VU0088990	n.s.	/	decrease	not confirmed	increase	not confirmed	n.s.	/
VU0150155	n.s.	/	n.s.	/	n.s.	/	n.s.	/
VU0035619	n.s.	/	n.s.	/	n.s.	/	n.s.	/
VU0025173	n.s.	/	n.s.	/	n.s.	/	n.s.	/
VU0026977	n.s.	/	increase	**confirmed**	n.s.	/	increase	**confirmed**
VU0003610	n.s.	/	n.s.	/	n.s.	/	n.s.	/
VU0003765	n.s.	/	n.s.	/	n.s.	/	n.s.	/
VU0482585	decrease	**confirmed**	n.s.	/	decrease	not confirmed	n.s.	/
VU0025879	increase	**confirmed**	increase	**confirmed**	n.s.	/	increase	**confirmed**
VU0041803	increase	**confirmed**	increase	**confirmed**	n.s.	/	n.s.	/
VU0050661	n.s.	/	increase	**confirmed**	increase	not confirmed	n.s.	/
VU0006021	n.s.	/	decrease	not confirmed	n.s.	/	n.s.	/
VU0002852	n.s.	/	n.s.	/	n.s.	/	n.s.	/
VU0029414	n.s.	/	n.s.	/	n.s.	/	n.s.	/
VU0135086	decrease	**confirmed**	increase	**confirmed**	n.s.	/	n.s.	/
VU0009096	n.s.	/	decrease	not confirmed	n.s.	/	n.s.	/
VU0046776	increase	**confirmed**	n.s.	/	increase	**confirmed**	increase	**confirmed**
VU0004838	decrease	not confirmed	n.s.	/	n.s.	/	n.s.	/
VU0029611	n.s.	/	increase	**confirmed**	n.s.	/	increase	**confirmed**
VU0026921	n.s.	/	increase	**confirmed**	increase	not confirmed	n.s.	/
VU0133141	n.s.	/	increase	**confirmed**	n.s.	/	increase	**confirmed**
VU0057971	n.s.	/	increase	**confirmed**	increase	not confirmed	decrease	not confirmed
VU0026395	n.s.	/	n.s.	/	n.s.	/	n.s.	/
VU0028040	n.s.	/	n.s.	/	n.s.	/	increase	**confirmed**
VU0243305	n.s.	/	increase	**confirmed**	increase	**confirmed**	increase	**confirmed**
VU0027832	increase	**confirmed**	increase	**confirmed**	increase	not confirmed	n.s.	/
VU0028386	n.s.	/	n.s.	/	increase	not confirmed	n.s.	/

TABLE 3-2 Confirmation Screen of Small Molecules With Other Divalents

Ordinary One-Way ANOVA, Dunnett's multiple comparisons p <0.05 with a mean difference of a least 2 standard deviations					
VU ID	**Cobalt 3° (low: 1.3µM)**	**Copper 3° (low: 3.3µM)**	**Zinc 3° (low: 3.3µM)**	**Nickel 3° (low: 1.3µM)**	**Mn control**
VU0047355	n.s.	n.s.	n.s.	decrease	decrease
VU0244366	decrease	n.s.	n.s.	n.s.	decrease
VU0150155	n.s.	n.s.	n.s.	decrease	increase
VU0035619	n.s.	n.s.	n.s.	n.s.	increase
VU0025173	n.s.	n.s.	n.s.	n.s.	increase
VU0003610	n.s.	n.s.	n.s.	n.s.	n.s.
VU0003765	n.s.	n.s.	n.s.	n.s.	n.s.
VU0002852	increase	n.s.	n.s.	n.s.	increase
VU0029414	n.s.	n.s.	n.s.	n.s.	increase
VU0026395	increase	n.s.	n.s.	n.s.	increase

This left us with just three small molecules (VU0035619, VU0025173, and VU0029414), highlighted in green in Table **3-2**, that influenced Mn but not Co, Cu, Zn, or Ni. They were all associated with relatively small Mn increasers (~1.5 fold). Two small molecules (VU0003610 and VU0003765) did not confirm Mn activity. A replicate CFDMEA was performed where the activities of the three selected molecules were confirmed at higher extracellular concentrations (**Figure 3-4**). As shown in **Figure 3-4A**, none of the three molecules had a significant influence on the intracellular levels of Co, Cu, Zn, or Ni. Meanwhile, all three molecules decreased %Fura-2 fluorescence signal compared to vehicle, indicating an increased cellular Mn uptake when cells were exposed to Mn with the presence of these three small molecules. The structure of these Mn-selective molecules is provided in **Figure 3-4B**. This experiment confirmed the Mn selectivity of the three small molecules determined from the divalent metal activity screen.

Two of the three small molecules which are Mn-selective are differentially affected in HD phenotype

We tested the hypothesis that Mn-selective small molecules may have differential "activity" in the STHdh Q111 cells, which are the Huntington's disease model cell line counterparts of the Q7 cells. In comparison to the Q7 cells that have a mere seven poly-glutamine repeats in the huntingtin gene, the Q111 cells express mutant huntingtin with 111 poly-glutamine repeats. The Q111 cells present a Mn-phenotype which protects them from Mn toxicity (1,10). This results in the Q111 cells taking up approximately half the amount that Q7's take up for a given Mn-exposure. This phenotype can be seen at "Vehicle", where the final concentration of Mn left behind is on average 385μM for Q7's and 185μM for Q111's.

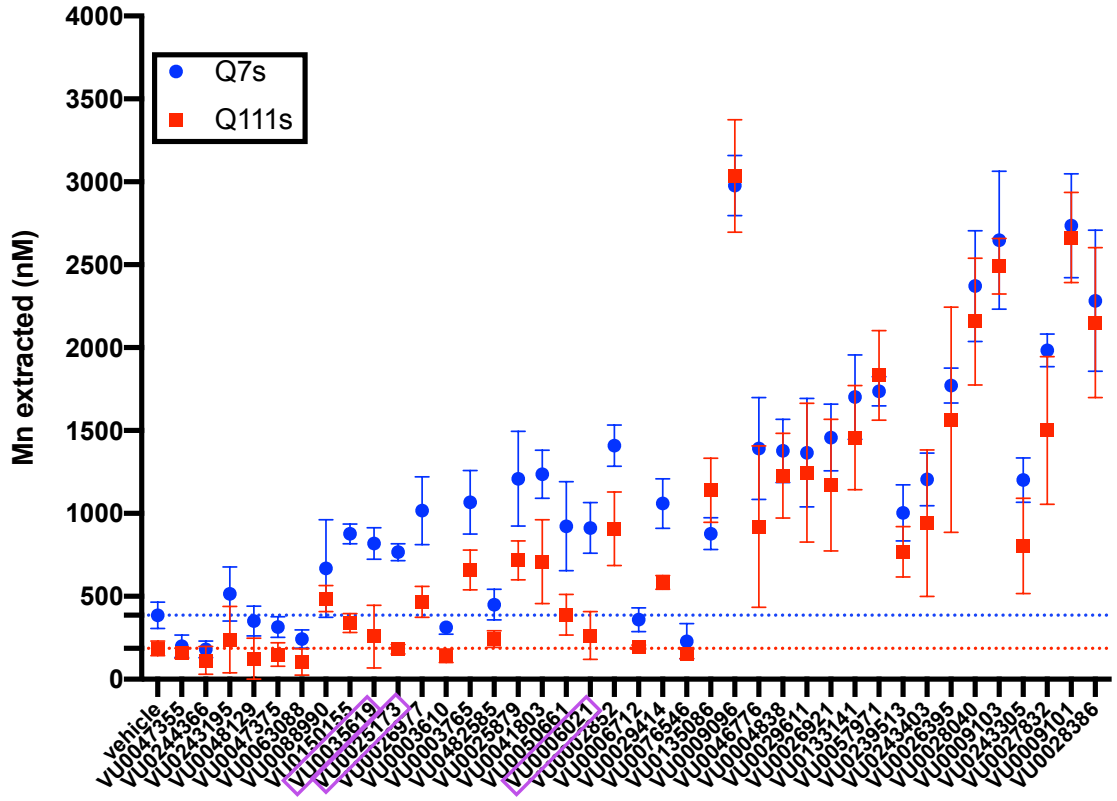

Figure 3-3: Three small molecules of the Mn toolbox impact the Huntington's disease genotype Q111 cells differentially. STHdh cells (both Q7 and Q111) were incubated at 37° C with 125μM Mn for 3 hours. Significance between Mn extracted in Q7 cells compared to Q111 cells, as denoted by a Two-Way ANOVA, Sidak's multiple comparisons test, were denoted by the VU ID boxed in purple. N=3.

We were interested to see if any of the small molecules could influence Q7's but not Q111's, or were more influential on Q111's than Q7's. This would suggest that the small molecule's target is the determining factor that is responsible for the Mn-deficit phenotype seen in the Q111's. It is still unknown what transporter or channel is responsible for this deficit. Nevertheless, if we knew that a small molecule was targeting that protein, we would be a step closer to finding a way to rescue the phenotype. As seen in **Figure 3-3**, there were five small molecules (VU0047355, VU0244366, VU0035619, VU0025173, VU0006021) that were inactive in Q111 cells but active in the Q7 cells. Two of these (VU0047355, VU0244366) were Mn-decreasers that decreased Mn to Q111 levels in the Q7's but did not influence Q111 levels. This

may be due to a type of a cellular “floor effect”, as the physiological concentration of intracellular Mn may only be able to get so low. The Mn level in the Q7’s for these two molecules were statistically indistinguishable from Q111’s; however, the majority of the toolbox (36 of 39) was indistinguishable between Q7’s and Q111’s as measured by Two-Way ANOVA with Sidak’s multiple comparisons test. The remaining three that were significantly different were the Mn-increasers that increase Mn in the Q7’s but do not in the Q111’s (VU0035619, VU0025173, VU0006021; boxed in purple). Importantly, of the three Mn-selective small molecules identified in **Table 3-2**, two of them happen to be ineffective in Q111 cells (**Figure 3-3**). A Chi-square test is significant with a P value of 0.0003, and an odds ratio of 58.00, meaning that a molecule is 58 times more likely to be Mn selective if its activity is significantly different between Q7’s and Q111’s.

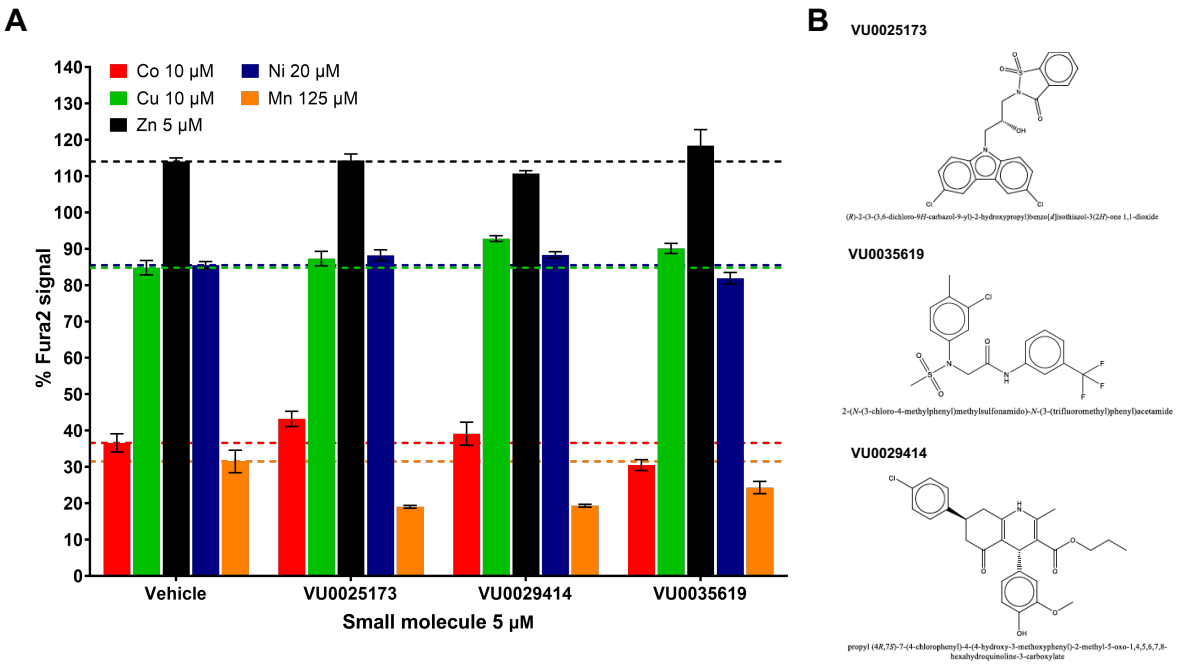

Figure 3-4. The divalent metal profiles of the Mn-selective small molecules VU0025173, VU0035619, and VU0029414. The profiles of the Mn-selective small molecules VU0025173, VU0035619, and VU0029414. Q7 cells were exposed in HBSS with DMSO vehicle or small molecules (5 µM) with a single divalent metal (Co 10 µM; Cu 10 µM; Zn 5 µM; Ni 20 µM; or Mn 125 µM) for 2 h at 37°C. Following the exposure, cells were washed with PBS and lysed open with PBS + 0.1% Triton for CFDMEA. Figure 4A shows the %Fura-2 signal of CFDMEA with means ± standard deviations. For ease of visualization a colored dashed line is shown at the %Fura-2 signal of the vehicle control for each metal. Figure 4B shows the chemical structures of the molecules.

DISCUSSION

The results of **Figure 3-3** identify five small molecules of interest that may act on the targets that are also disrupted in the Q111 cells, and thus may be contributing to the changes in Mn transport in these cells compared to wild-type control. Two of these (VU0047355 and VU0244366) bring Q7 Mn levels down to Q111-vehicle levels- mimicking the Q111 phenotype. They are both relatively small Mn increasers (~1.5 fold). They also have nearly identical effect sizes/direction in HEK, HeLas, and SH-SY5Ys. They are structurally very different but appear to act on the same mechanism. These small molecules may activate a channel the effluxes Mn faster from the cell, for example, which may be over-active or already open in the Q111 cells.

Alternatively, the three small molecules (VU0035619, VU0025173, VU0006021) that had significant activity in the Q7 cells but not in the Q111 cells may act on a Mn importer that is not expressed or functional in the Q111 cells.

Follow-up studies to these small molecules should be attempts to find the small molecule's target. This can be done in a variety of direct and indirect ways, based on the resources available. Perhaps the most direct way would be using an affinity-based pull-down; using agarose beads, biotin, or a photoreactive group and linker conjugated to the small molecule would allow for mass analysis of the target protein via mass spectrometry. This would be dependent on the structure-activity relationships of each small molecule, so a linker could be placed on the small molecule without compromising its activity to increase/decrease intracellular Mn. Considering the small size of some of these molecules, finding an active analog with an affinity linker attached might not be possible. An alternative method would be to use a label-free target identification approach. The proteome could be co-incubated with the small molecule and allow for proteolysis to occur. The small-molecule-protein complex should be protected against proteolysis, and this band could be identified on a gel and then removed for mass analysis. Target identification using phage display or mRNA display technology could also be used.

Our study was limited to a neuronal murine cell line (STHdh), which was also used in our original 2014 HTS screen to generate the Mn toolbox; future studies should confirm the activity and specificity of these molecules in primary cell cultures or in vivo systems. In addition, while the CFMEA assay is validated for Mn accuracy, the CFDMEA outcomes for individual molecules should ultimately be confirmed by other methods for determining intracellular metal levels such as inductively coupled mass spectrometry (ICP-MS) or atomic absorption spectroscopy (AAS).

Despite the fact that the novel interaction between Mn and Huntington's disease has been published nearly a decade ago (1), and numerous subsequent studies have noted the rescue of HD phenotypes by the reinstatement of bioavailable Mn (2,8,9,18,19), the cause of this reduced Mn bioavailability is still unknown. The results of this study provide an unobstructed avenue towards finally identifying the culprit that causes Mn deficiency in HD. These Mn-selective molecules will also provide therapeutic options for activating these Mn-deficient mechanisms.

MATERIALS AND METHODS

Cell Culture

STHdh$^{Q7/Q7}$ wild-type immortalized murine striatal derived cells and STHhh$^{Q111/Q111}$ cells were obtained from Coriell Cell Repository (Camden, NJ). They were plated at a density of 10,000 and 12,000 cells per well, respectively, of a 96-well plate and incubated at 33°C with 5% CO_2 in Dulbecco's Modified Eagles Medium (DMEM; high glucose Sigma-Aldrich; D6546; St. Louis, MO) with 10% Fetal Bovine Serum (FBS; Atlanta Biologicals; Flowery Branch, GA), 1% Penicillin/Streptomycin (15140-122; Life Technologies; Carlsbad, CA), 2mM GlutaMAX (Life Technologies), 0.5 mg/mL G418 Sulfate, (Life Technologies) 1X Non-essential Amino Acids Solution (Life Technologies), 14mM HEPES (Life Technologies) for 24 hours prior to the assay. Cells were dissociated using 0.05% Trypsin-EDTA solution (Life Technologies).

Cellular Fura-2 Manganese Extraction Assay (CFMEA)

STHdh cells were exposed to 125μM Mn, and incubated at 37° C (5% CO_2) in HBSS for 3 hours. This generated "Vehicle" values when Mn was co-incubated with representative amounts of DMSO (Sigma-Aldrich; D8418). Often other small molecules were co-incubated with the 125μM

Mn in the HBSS to assess their impact on Mn levels. After incubation, the cells were washed three times with PBS (without Ca^{2+} and Mg^{2+}) to remove the extracellular Mn. *Extraction buffer* (PBS containing 0.1% TritonX100; Sigma-Aldrich; T8787; St. Louis, MO and 500nM Fura-2) was added to lyse the cells. The fluorescence of the Fura-2 in the extraction buffer was then measured at 360nm/535nm (Ex/Em) so that Mn could be quantified.

Manganese Quantification by Fura-2

A percent max of Fura-2 fluorescence 360nm/535nm (Ex/Em) was calculated for each condition as the corresponding zero Mn condition was defined as 100%. Background fluorescence was subtracted from all values. The concentration of Mn (nM) was calculated with the equation: $[Mn] = 1138 \times ((1 / \%max) - 1)^{0.9682}$, which was generated based on a standard curve of Mn quenching Fura-2 signal (20). The absolute values were calculated by multiplying by the concentration by volume.

Cellular Fura-2 Divalent Metal Extraction Assay (CFDMEA)

STHdh cells were exposed to varying concentrations of cobalt, nickel, zinc, or copper, and incubated at 37° C in HBSS for 2 hours. This generated "Vehicle" values when the divalent metal was co-incubated with representative amounts of DMSO (Sigma-Aldrich; D8418). Often other small molecules were co-incubated with the divalent metal in the HBSS to assess their impact on that metal's relative levels. After incubation, the cells were washed three times with PBS (without Ca^{2+} and Mg^{2+}) to remove the extracellular metal. *Extraction buffer* (PBS containing 0.1% TritonX100; Sigma-Aldrich; T8787; St. Louis, MO and 500nM Fura-2) was added to lyse the cells.

The fluorescence of the Fura-2 in the extraction buffer was then measured at 360nm/535nm (Ex/Em).

Statistical Analysis

All analyses were made using GraphPad Prism 8 software with either One-Way ANOVA with post-hoc Dunnett's multiple comparisons, or Sidak's multiple comparisons test. One exception is the Chi-square test, also analyzed using GraphPad Prism 8, using Baptista-Pike methods to calculate odds ratio.

REFERENCES

1. Williams BB, Li D, Wegrzynowicz M, Vadodaria BK, Anderson JG, Kwakye GF, et al. Disease-toxicant screen reveals a neuroprotective interaction between Huntington's disease and manganese exposure. J Neurochem [Internet]. 2010 Jan;112(1):227–37. Available from: http://doi.wiley.com/10.1111/j.1471-4159.2009.06445.x
2. Bichell TJ V., Wegrzynowicz M, Tipps KG, Bradley EM, Uhouse MA, Bryan M, et al. Reduced bioavailable manganese causes striatal urea cycle pathology in Huntington's disease mouse model. Biochim Biophys Acta - Mol Basis Dis [Internet]. 2017;1863(6):1596–604. Available from: http://dx.doi.org/10.1016/j.bbadis.2017.02.013
3. Arning L, Epplen JT. Genetic modifiers of Huntington's disease: beyond CAG. Future Neurol [Internet]. 2012 Jan 15;7(1):93–109. Available from: http://www.interscience.wiley.com/jpages/0885-3185%7B%25%7D0Ahttp://ovidsp.ovid.com/ovidweb.cgi?T=JS%7B&%7DPAGE=reference%7B&%7DD=emed16%7B&%7DNEWS=N%7B&%7DAN=600189275

4. Horning KJ, Caito SW, Tipps KG, Bowman AB, Aschner M. Manganese Is Essential for Neuronal Health. Annu Rev Nutr [Internet]. 2015;35(1):71–108. Available from: http://www.annualreviews.org/doi/10.1146/annurev-nutr-071714-034419
5. Behrens PF, Franz P, Woodman B, Lindenberg KS, Landwehrmeyer GB. Impaired glutamate transport and glutamate-glutamine cycling: downstream effects of the Huntington mutation. Brain [Internet]. 2002 Aug;125(Pt 8):1908–22. Available from: http://www.ncbi.nlm.nih.gov/pubmed/12135980
6. Carter CJ. Glutamine synthetase activity in Huntington's disease. Life Sci [Internet]. 1982 Sep 13;31(11):1151–9. Available from: http://www.ncbi.nlm.nih.gov/pubmed/6128649
7. Tarohda T, Yamamoto M, Amamo R. Regional distribution of manganese, iron, copper, and zinc in the rat brain during development. Anal Bioanal Chem. 2004;380(2):240–6.
8. Bryan MR, Brien MTO, Nordham KD, Rose DIR, Foshage AM, Joshi P, et al. Acute manganese treatment restores defective autophagic cargo loading in Huntington ' s disease cell lines. 2019;28(22):3825–41.
9. Bryan MR, Nordham KD, Rose DIR, Brien MTO, Joshi P, Foshage AM, et al. Manganese Acts upon Insulin / IGF Receptors to Phosphorylate AKT and Increase Glucose Uptake in Huntington ' s Disease Cells. 2020;1570–93.
10. Williams BB, Kwakye GF, Wegrzynowicz M, Li D, Aschner M, Erikson KM, et al. Altered manganese homeostasis and manganese toxicity in a Huntington's disease striatal cell model are not explained by defects in the iron transport system. Toxicol Sci [Internet]. 2010 Sep [cited 2014 Oct 28];117(1):169–79. Available from: http://www.pubmedcentral.nih.gov/articlerender.fcgi?artid=2923282&tool=pmcentrez&rendertype=abstract

11. Leyva-Illades D, Chen P, Zogzas CE, Hutchens S, Mercado JM, Swaim CD, et al. SLC30A10 Is a Cell Surface-Localized Manganese Efflux Transporter, and Parkinsonism-Causing Mutations Block Its Intracellular Trafficking and Efflux Activity. J Neurosci [Internet]. 2014 Oct 15 [cited 2014 Nov 20];34(42):14079–95. Available from: http://www.ncbi.nlm.nih.gov/pubmed/25319704

12. Saudou F, Humbert S. The Biology of Huntingtin. Neuron. 2016;89(5):910–26.

13. Schulte J, Littleton JT. The biological function of the Huntingtin protein and its relevance to Huntington's Disease pathology. Curr Trends Neurol [Internet]. 2011;1(5):65–78. Available from: https://www.ncbi.nlm.nih.gov/pmc/articles/PMC3237673/pdf/nihms-341899.pdf

14. Kumar KK, Lowe EW, Aboud A a, Neely MD, Redha R, Bauer J a, et al. Cellular manganese content is developmentally regulated in human dopaminergic neurons. Sci Rep [Internet]. 2014 Jan [cited 2014 Nov 2];4:6801. Available from: http://www.ncbi.nlm.nih.gov/pubmed/25348053

15. Peres T V, Horning KJ, Bornhorst J, Schwerdtle T, Bowman AB, Aschner M. Small Molecule Modifiers of In Vitro Manganese Transport Alter Toxicity In Vivo. Biol Trace Elem Res [Internet]. 2018 Sep 28; Available from: http://link.springer.com/10.1007/s12011-018-1531-7

16. Kwakye GF, Li D, Kabobel OA, Bowman AB. Cellular fura-2 Manganese Extraction Assay (CFMEA). Curr Protoc Toxicol. 2011;2651(SUPPL.48):1–26.

17. Kwakye GF, Li D, Bowman AB. Novel high-throughput assay to assess cellular manganese levels in a striatal cell line model of Huntington's disease confirms a deficit in manganese accumulation. Neurotoxicology. 2011;32(5):630–9.

18. Tidball AM, Bryan MR, Uhouse MA, Kumar KK, Aboud AA, Feist JE, et al. A novel manganese-dependent ATM-p53 signaling pathway is selectively impaired in patient-based neuroprogenitor and murine striatal models of Huntington's disease. Hum Mol Genet. 2014;24(7):1929–44.

19. Bryan MR, Uhouse MA, Nordham KD, Joshi P, Rose DIR, O'Brien MT, et al. Phosphatidylinositol 3 kinase (PI3K) modulates manganese homeostasis and manganese-induced cell signaling in a murine striatal cell line. Neurotoxicology [Internet]. 2018;64:185–94. Available from: https://doi.org/10.1016/j.neuro.2017.07.026

20. Kumar KK, Aboud AA, Patel DK, Aschner M, Bowman AB. Optimization of Fluorescence Assay of Cellular Manganese Status for High Throughput Screening. J Biochem Mol Toxicol [Internet]. 2013 Jan;27(1):42–9. Available from: http://doi.wiley.com/10.1002/jbt.21457

CHAPTER IV

IDENTIFICATION OF SMALL MOLECULES THAT ALTER A SLC30A10 PHENOTYPE

INTRODUCTION

Mutations in SLC30A10 lead to the development of a familial manganese-induced parkinsonism (27), first characterized and identified by Tuschl et al (22, 24) as a syndrome involving hepatic cirrhosis, dystonia, polycythemia, and hypermanganesemia. SLC30A10 protein (ZnT10) is a cell surface-localized Mn-efflux transporter capable of protecting neurons and a variety of other cell models from Mn-toxicity (15). Levy et al. recently demonstrated that this Mn extrusion is driven by a active Ca^{2+} coupled exchange, in contrast to most mammalian ZnT transporters that exchange metal for H^{+} (14). Whole-body knockouts, in combination with clinical mutation data suggests that SLC30A10 transporter is responsible for the primary excretion of systemic Mn into bile (17, 18).

Curiously, all other eight members of the SLC30A cation diffusion superfamily of metal transporters facilitate the movement of zinc (8, 10), however, there is ample evidence that SLC30A10 transports manganese selectively rather than zinc. First, all patients identified with SLC30A10 mutations have increased blood Mn levels, but no changes of zinc in the blood or brain (13, 20, 22, 24). Expression of WT SLC30A10 in cell culture and *C. elegans* reduces intracellular Mn and protects against Mn-induced toxicity, but not zinc toxicity (3, 15). Indeed, evidence relating to the structural elements in the transmembrane and cytoplasmic domains of SLC30A10 appear to be considerably different from the other SLC30 proteins (27). However, ZnT10 (encoded

by SLC30A10) is still often mischaracterized as a zinc transporter, leading to conclusions about zinc homeostasis where Mn is most likely a key player (9).

Exactly how SLC30A10 operates in a system to maintain Mn homeostasis is an area of emerging research. Recently, a mutation in another metal transporter gene (SLC39A14; encoding for ZIP14) have been identified (18, 23), as these familial mutations also lead to hypermanganesemia, dystonia, polycythemia and cirrhosis; a syndrome often referred to as HMDPC (25). Both Zip8 and Zip14, coded by SLC39A8 and SLC39A14 respectively, are cell surface transporters that have been implicated in cellular Mn uptake by animal models and clinical studies (1, 2, 4, 7, 11, 16, 19, 26). It is believed that Mn is taken up from the blood by ZIP14 in the liver and secreted into the bile by SLC30A10, and Mn is subsequently removed from the bile by ZIP8 (28).

A zebrafish model of SLC30A10 deficiency was used in a study that led to the discovery of a novel compensatory mechanism involving ATP2C1 (also known as SPCA1; ATPase secretory pathway Ca2+ transporting 1), whose expression protected zebrafish embryos and HeLa cells from Mn toxicity prior to the expression of SLC30A10 (25). The zebrafish model of SLC30A10 deficiency is interesting as SLC30A10's function as a Mn exporter is conserved, and deficiency also leads to hepatic pathology, polycythemia, and neurological defects such as rigidity, bradykinesia, and disrupted GABAergic and dopaminergic signaling (25). While EDTACaNa2 chelation treatment partially rescues this phenotype, targeting ATP2C1 also appears to have therapeutic potential (25). Known regulators of SLC30A10 expression include interleukin-6, which down-regulates SLC30A10 while upregulating ZIP14 and increasing Mn accumulation in SH-SY5Y cells (6). Recently, β-napthoflavone, an exogenous ligand of aryl hydrocarbon receptor, was noted to decrease SLC30A10 expression about 50% in HepG2 cells (9).

Understanding the mechanisms behind SLC30A10's ability to selectively efflux Mn is important for three main reasons (27). From an epidemiological perspective, the fact that SNPs in SLC30A10 can affect blood Mn levels suggest that other polymorphisms in this gene could put the general population at a higher risk for manganese toxicity. Secondly, a clear understanding of the structural elements that makes a protein selective to Mn, rather than another metal, have implications for substrate specificity of ion transporters. There is a gap in knowledge to be addressed in basic science regarding principles dictating whether a given structure confers Mn specificity- in a world where SLC30A10 is the only ion transporter identified to date that selectively transports Mn. Lastly, and most relevant here, is the translational viewpoint. Small molecule tools that target SLC30A10 activity may have therapeutic potential for patients with SLC30A10 polymorphisms or patients suffering from hypermanganesemia for a variety of reasons. Previous studies have demonstrated the potential of targeting SLC30A10 by showing that overexpression of SLC30A10 reduces cellular Mn toxicity. Even without an understanding of SLC30A10 mechanisms, a tool that targets this transporter, if not specifically, is a solid step in drug development. Here, we provide evidence that an increase in intracellular, rather than extracellular Mn activates SLC30A10, and identify several small molecules that may interact with SLC30A10. We also propose models by which SLC30A10 activation or suppression can occur with a small molecule-influencer.

RESULTS

Overexpression of WT or mutant SLC30A10 yields a small phenotype of Mn accumulation in HEK cells following exposure

Thanks to collaborators at the University of Texas at Austin (Somshuvra Mukhopadhyay lab), we were able to screen the toolbox against HEK293 cells overexpressing WT or mutant (E25A) SLC30A10. These E25A mutants do not change localization of the protein, but inactivates Mn transport (27). Untransfected HEK293 cells were used as a control. When exposed to Mn, and measured by CFMEA, the WT HEK293 cells that overexpress SLC30A10 tend to accumulate less Mn than the mutant SLC30A10 cells or the untransfected cells (**Figure 4-1**). A Two-Way ANOVA yielded a significant main effect for Mn concentration (****, $p < 0.0001$), but no main effect for cell type ($p = 0.1215$), and no interaction. One can begin to see by eye that a "V" shape of the 3-point line graph appears at higher concentrations between cell types, where untransfected cells accumulate about equal Mn as the mutants, but the SLC30A10 WT HEKs accumulate less than both. This "V" phenotype makes intuitive sense, as the WT cells are equipped with an overexpression of a Mn efflux transporter, so they will accumulate less Mn than cells without this surplus of efflux transporter (untransfected) or those with an inactive transporter (E25A mutants). When comparing individual biological replicates (N=4), the "V" phenotype can be seen three out of four times at 50μM, two out of four times at 100μM $MnCl_2$, and four out of four times at 200μM $MnCl_2$. Despite this, there was no significant main effect for cell type. The Two-Way ANOVA attributed 7.6% of the variation due to cell type.

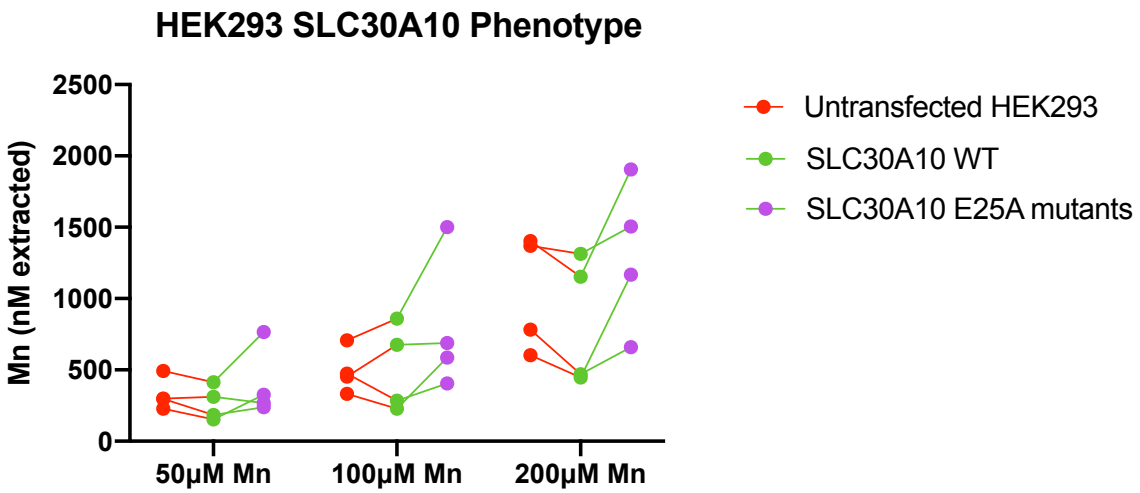

Figure 4-1: Mn exposures to HEK cells with WT or mutant SLC30A10 present a notable "V phenotype" in Mn uptake at higher concentrations. Cells were plated at 300K cells/mL 24 hours prior to a 3 hour incubation with Mn at 37°C. Individual dots represent one biological replicate consisting of an average of five technical replicates. Lines drawn between dots represent comparisons from the same biological replicate. N=4 biological replicates. A Two-Way ANOVA showed a significant main effect for Mn concentration (****, $p < 0.0001$), no main effect for cell type ($p = 0.1215$), and no interaction between genotype and Mn concentration.

Application of small molecule modifiers of intracellular Mn to SLC30A10 HEK cells exacerbates or modifies the phenotype

Though the higher exposure yielded the largest magnitude phenotype in **Figure 4-1**, the three HEK293 cell types were not screened with small molecules at 200μM $MnCl_2$ but rather 100μM. This was an effort to avoid Mn toxicity, expose closer to physiologically relevant Mn levels, and to see if small molecule exposure could potentiate a stronger phenotype. Cells were plated at 600,000 cells per mL for three hours. We hypothesized that an interruption of the "V" phenotype, or whichever phenotype the vehicle conditions normally displayed, would suggest a small molecule interaction with SLC30A10. The results of the screen can be seen in **Figure 4-2**. A Two-Way ANOVA found significance in a main effect of cell type ($p < 0.0001$) and small molecule ($p < 0.0001$), including a significant interaction between the two ($p < 0.0001$). Tukey's multiple comparisons tests revealed statistical significance between cell types (untransfected vs

WT, untransfected vs mutant, WT vs mutant) in multiple instances for multiple molecules (see **Table 4-1**), but statistical significance could not readily demonstrate the "V" phenotype or deviations from it**.** For each small molecule, Tukey's multiple comparisons tests asked if three different comparisons were significant or not: untransfected versus WT; untransfected versus mutant; and WT versus mutant. To help classify functionality and phenotype, small molecules were sorted into groups based on the answers to these questions (significant between genotypes or not). The small molecules could be classified into five groups (see **Table 2**):

1) **Vehicle**; (No, Yes, Yes):
    a. Not statistically different between untransfected and WT; "No"
    b. Statistically different between untransfected and mutant; "Yes"
    c. Statistically different between WT and mutant; "Yes"
2) **Dominant negative phenotype**; (No, No, Yes):
    a. Not statistically different between untransfected and WT; "No"
    b. Not statistically different between untransfected and mutant; "No"
    c. Statistically different between WT and mutant; "Yes"
3) **Perfect V phenotype**; (Yes, No, Yes):
    a. Statistically different between untransfected and WT; "Yes"
    b. Not statistically different between untransfected and mutant; "No"
    c. Statistically different between WT and mutant; "Yes"
4) **Altered V phenotype**; (Yes, Yes, Yes):
    a. Statistically different between untransfected and WT; "Yes"
    b. Statistically different between untransfected and mutant; "Yes"
    c. Statistically different between WT and mutant; "Yes"

5) **"No" phenotype**; (No, No, No):

a. Not statistically different between untransfected and WT; "No"

b. Not statistically different between untransfected and mutant; "No"

c. Not statistically different between WT and mutant; "No"

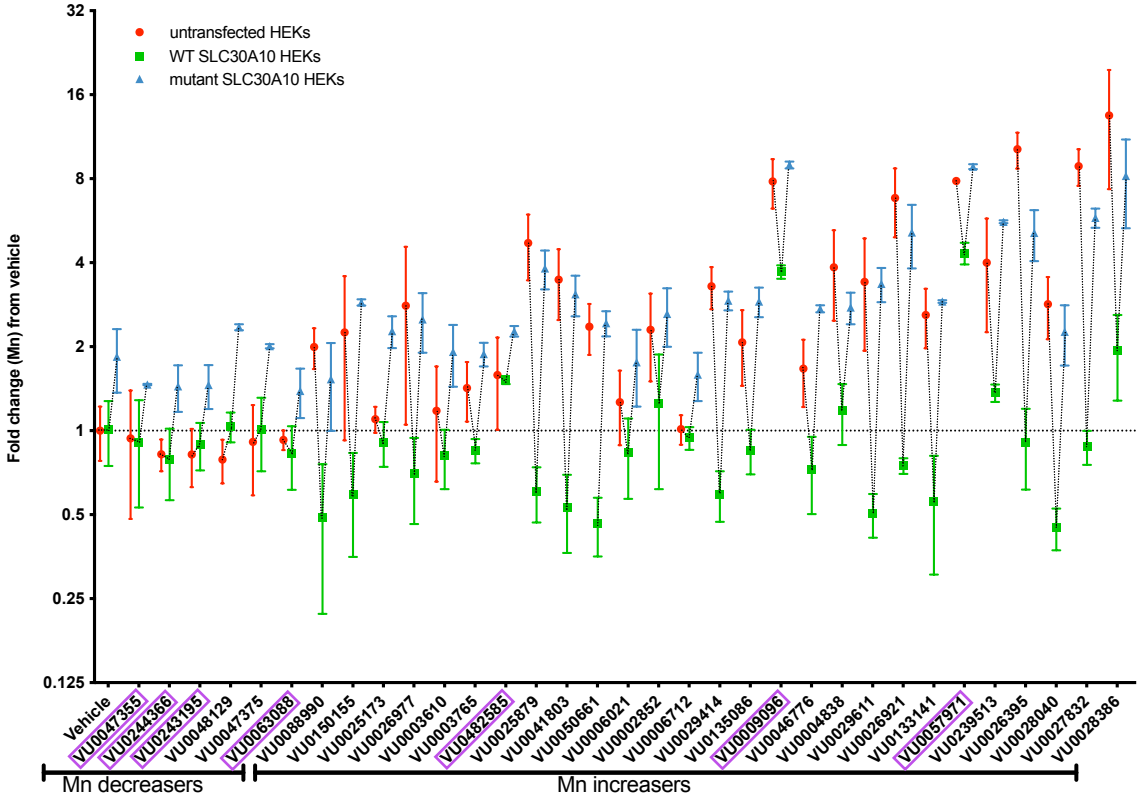

Figure 4-2: Small molecules that interrupt the "Perfect V phenotype" or Vehicle phenotype may interact with SLC30A10. Data is normalized Mn fold change to the vehicle of untransfected cells, set at 1. Individual dots represent one biological replicate consisting of an average of five technical replicates. Lines drawn between dots represent comparisons from the same biological replicate. Small molecules that are suspected of interacting with SLC30A10 are boxed in purple.

TABLE 4-1: Tukey's Multiple Comparisons Tests From SLC30A10 Screen					
Tukey's multiple comparisons test	**Predicted (LS) mean diff.**	**95.00% CI of diff.**	**Significant?**	**Summary**	**Adjusted P Value**
Vehicle					
untransfected HEKs vs. WT SLC30A10 HEKs	-0.01191	-0.4947 to 0.4709	**No**	ns	0.9982
untransfected HEKs vs. mutant SLC30A10 HEKs	-0.8404	-1.323 to -0.3575	**Yes**	***	0.0001
WT SLC30A10 HEKs vs. mutant SLC30A10 HEKs	-0.8284	-1.311 to -0.3456	**Yes**	***	0.0002
VU0047355					
untransfected HEKs vs. WT SLC30A10 HEKs	0.02974	-0.9359 to 0.9953	No	ns	0.9971
untransfected HEKs vs. mutant SLC30A10 HEKs	-0.5257	-1.491 to 0.4399	No	ns	0.4082
WT SLC30A10 HEKs vs. mutant SLC30A10 HEKs	-0.5555	-1.521 to 0.4101	No	ns	0.3679
VU0244366					
untransfected HEKs vs. WT SLC30A10 HEKs	0.03289	-0.7555 to 0.8213	No	ns	0.9947
untransfected HEKs vs. mutant SLC30A10 HEKs	-0.6186	-1.407 to 0.1698	No	ns	0.1567
WT SLC30A10 HEKs vs. mutant SLC30A10 HEKs	-0.6515	-1.440 to 0.1369	No	ns	0.1282
VU0243195					
untransfected HEKs vs. WT SLC30A10 HEKs	-0.07165	-0.8601 to 0.7168	No	ns	0.9752
untransfected HEKs vs. mutant SLC30A10 HEKs	-0.6363	-1.425 to 0.1522	No	ns	0.1409
WT SLC30A10 HEKs vs. mutant SLC30A10 HEKs	-0.5646	-1.353 to 0.2238	No	ns	0.2131
VU0048129					
untransfected HEKs vs. WT SLC30A10 HEKs	-0.2468	-1.212 to 0.7188	No	ns	0.8203
untransfected HEKs vs. mutant SLC30A10 HEKs	-1.562	-2.527 to -0.5963	Yes	***	0.0005
WT SLC30A10 HEKs vs. mutant SLC30A10 HEKs	-1.315	-2.281 to -0.3495	Yes	**	0.0041
VU0047375					
untransfected HEKs vs. WT SLC30A10 HEKs	-0.1029	-1.068 to 0.8627	No	ns	0.9661
untransfected HEKs vs. mutant SLC30A10 HEKs	-1.097	-2.063 to -0.1317	Yes	*	0.0212
WT SLC30A10 HEKs vs. mutant SLC30A10 HEKs	-0.9944	-1.960 to -0.02877	Yes	*	0.0418

Tukey's multiple comparisons test	Predicted (LS) mean diff.	95.00% CI of diff.	Significant?	Summary	Adjusted P Value
VU0063088					
untransfected HEKs vs. WT SLC30A10 HEKs	0.1018	-0.6866 to 0.8902	No	ns	0.9507
untransfected HEKs vs. mutant SLC30A10 HEKs	-0.4616	-1.250 to 0.3268	No	ns	0.355
WT SLC30A10 HEKs vs. mutant SLC30A10 HEKs	-0.5634	-1.352 to 0.2250	No	ns	0.2145
VU0088990					
untransfected HEKs vs. WT SLC30A10 HEKs	1.506	0.7180 to 2.295	Yes	****	<0.0001
untransfected HEKs vs. mutant SLC30A10 HEKs	0.4664	-0.3220 to 1.255	No	ns	0.3474
WT SLC30A10 HEKs vs. mutant SLC30A10 HEKs	-1.04	-1.828 to -0.2516	Yes	**	0.0057
VU0150155					
untransfected HEKs vs. WT SLC30A10 HEKs	1.658	0.6928 to 2.624	Yes	***	0.0002
untransfected HEKs vs. mutant SLC30A10 HEKs	-0.631	-1.597 to 0.3346	No	ns	0.2756
WT SLC30A10 HEKs vs. mutant SLC30A10 HEKs	-2.289	-3.255 to -1.324	Yes	****	<0.0001
VU0025173					
untransfected HEKs vs. WT SLC30A10 HEKs	0.1914	-0.5971 to 0.9798	No	ns	0.8364
untransfected HEKs vs. mutant SLC30A10 HEKs	-1.174	-1.963 to -0.3859	Yes	**	0.0014
WT SLC30A10 HEKs vs. mutant SLC30A10 HEKs	-1.366	-2.154 to -0.5773	Yes	***	0.0002
VU0026977					
untransfected HEKs vs. WT SLC30A10 HEKs	2.103	1.314 to 2.891	Yes	****	<0.0001
untransfected HEKs vs. mutant SLC30A10 HEKs	0.2985	-0.4899 to 1.087	No	ns	0.6477
WT SLC30A10 HEKs vs. mutant SLC30A10 HEKs	-1.804	-2.592 to -1.016	Yes	****	<0.0001
VU0003610					
untransfected HEKs vs. WT SLC30A10 HEKs	0.3653	-0.4231 to 1.154	No	ns	0.5222
untransfected HEKs vs. mutant SLC30A10 HEKs	-0.7373	-1.526 to 0.05114	No	ns	0.0725
WT SLC30A10 HEKs vs. mutant SLC30A10 HEKs	-1.103	-1.891 to -0.3142	Yes	**	0.003

Tukey's multiple comparisons test	Predicted (LS) mean diff.	95.00% CI of diff.	Significant?	Summary	Adjusted P Value
VU0003765					
untransfected HEKs vs. WT SLC30A10 HEKs	0.5717	-0.2168 to 1.360	No	ns	0.2051
untransfected HEKs vs. mutant SLC30A10 HEKs	-0.462	-1.250 to 0.3264	No	ns	0.3544
WT SLC30A10 HEKs vs. mutant SLC30A10 HEKs	-1.034	-1.822 to -0.2453	Yes	**	0.0061
VU0482585					
untransfected HEKs vs. WT SLC30A10 HEKs	0.0619	-0.9037 to 1.027	No	ns	0.9876
untransfected HEKs vs. mutant SLC30A10 HEKs	-0.6905	-1.656 to 0.2751	No	ns	0.2141
WT SLC30A10 HEKs vs. mutant SLC30A10 HEKs	-0.7524	-1.718 to 0.2132	No	ns	0.1607
VU0025879					
untransfected HEKs vs. WT SLC30A10 HEKs	4.098	3.310 to 4.887	Yes	****	<0.0001
untransfected HEKs vs. mutant SLC30A10 HEKs	0.8873	0.09889 to 1.676	Yes	*	0.0228
WT SLC30A10 HEKs vs. mutant SLC30A10 HEKs	-3.211	-4.000 to -2.423	Yes	****	<0.0001
VU0041803					
untransfected HEKs vs. WT SLC30A10 HEKs	2.949	2.161 to 3.737	Yes	****	<0.0001
untransfected HEKs vs. mutant SLC30A10 HEKs	0.3979	-0.3905 to 1.186	No	ns	0.4629
WT SLC30A10 HEKs vs. mutant SLC30A10 HEKs	-2.551	-3.339 to -1.763	Yes	****	<0.0001
VU0050661					
untransfected HEKs vs. WT SLC30A10 HEKs	1.894	1.105 to 2.682	Yes	****	<0.0001
untransfected HEKs vs. mutant SLC30A10 HEKs	-0.06852	-0.8569 to 0.7199	No	ns	0.9773
WT SLC30A10 HEKs vs. mutant SLC30A10 HEKs	-1.962	-2.751 to -1.174	Yes	****	<0.0001
VU0006021					
untransfected HEKs vs. WT SLC30A10 HEKs	0.4272	-0.3612 to 1.216	No	ns	0.4117
untransfected HEKs vs. mutant SLC30A10 HEKs	-0.4953	-1.284 to 0.2931	No	ns	0.3038
WT SLC30A10 HEKs vs. mutant SLC30A10 HEKs	-0.9225	-1.711 to -0.1341	Yes	*	0.0169

Tukey's multiple comparisons test	Predicted (LS) mean diff.	95.00% CI of diff.	Significant?	Summary	Adjusted P Value
VU0002852					
untransfected HEKs vs. WT SLC30A10 HEKs	1.054	0.2659 to 1.843	Yes	**	0.005
untransfected HEKs vs. mutant SLC30A10 HEKs	-0.3183	-1.107 to 0.4701	No	ns	0.6104
WT SLC30A10 HEKs vs. mutant SLC30A10 HEKs	-1.373	-2.161 to -0.5842	Yes	***	0.0001
VU0006712					
untransfected HEKs vs. WT SLC30A10 HEKs	0.07087	-0.7175 to 0.8593	No	ns	0.9758
untransfected HEKs vs. mutant SLC30A10 HEKs	-0.5752	-1.364 to 0.2132	No	ns	0.2011
WT SLC30A10 HEKs vs. mutant SLC30A10 HEKs	-0.646	-1.434 to 0.1424	No	ns	0.1327
VU0029414					
untransfected HEKs vs. WT SLC30A10 HEKs	2.696	1.908 to 3.485	Yes	****	<0.0001
untransfected HEKs vs. mutant SLC30A10 HEKs	0.3657	-0.4227 to 1.154	No	ns	0.5215
WT SLC30A10 HEKs vs. mutant SLC30A10 HEKs	-2.331	-3.119 to -1.542	Yes	****	<0.0001
VU0135086					
untransfected HEKs vs. WT SLC30A10 HEKs	1.222	0.2563 to 2.187	Yes	**	0.0085
untransfected HEKs vs. mutant SLC30A10 HEKs	-0.8312	-1.797 to 0.1344	No	ns	0.1079
WT SLC30A10 HEKs vs. mutant SLC30A10 HEKs	-2.053	-3.019 to -1.087	Yes	****	<0.0001
VU0009096					
untransfected HEKs vs. WT SLC30A10 HEKs	4.121	3.155 to 5.086	Yes	****	<0.0001
untransfected HEKs vs. mutant SLC30A10 HEKs	-1.137	-2.102 to -0.1711	Yes	*	0.016
WT SLC30A10 HEKs vs. mutant SLC30A10 HEKs	-5.257	-6.223 to -4.292	Yes	****	<0.0001
VU0046776					
untransfected HEKs vs. WT SLC30A10 HEKs	0.9413	-0.02428 to 1.907	No	ns	0.0579
untransfected HEKs vs. mutant SLC30A10 HEKs	-1.066	-2.032 to -0.1003	Yes	*	0.0262
WT SLC30A10 HEKs vs. mutant SLC30A10 HEKs	-2.007	-2.973 to -1.042	Yes	****	<0.0001

Tukey's multiple comparisons test	Predicted (LS) mean diff.	95.00% CI of diff.	Significant?	Summary	Adjusted P Value
VU0004838					
untransfected HEKs vs. WT SLC30A10 HEKs	2.673	1.885 to 3.462	Yes	****	<0.0001
untransfected HEKs vs. mutant SLC30A10 HEKs	1.088	0.2993 to 1.876	Yes	**	0.0035
WT SLC30A10 HEKs vs. mutant SLC30A10 HEKs	-1.586	-2.374 to -0.7973	Yes	****	<0.0001
VU0029611					
untransfected HEKs vs. WT SLC30A10 HEKs	2.908	2.120 to 3.696	Yes	****	<0.0001
untransfected HEKs vs. mutant SLC30A10 HEKs	0.05382	-0.7346 to 0.8422	No	ns	0.986
WT SLC30A10 HEKs vs. mutant SLC30A10 HEKs	-2.854	-3.643 to -2.066	Yes	****	<0.0001
VU0026921					
untransfected HEKs vs. WT SLC30A10 HEKs	6.07	5.282 to 6.858	Yes	****	<0.0001
untransfected HEKs vs. mutant SLC30A10 HEKs	1.687	0.8987 to 2.476	Yes	****	<0.0001
WT SLC30A10 HEKs vs. mutant SLC30A10 HEKs	-4.383	-5.171 to -3.595	Yes	****	<0.0001
VU0133141					
untransfected HEKs vs. WT SLC30A10 HEKs	2.04	1.075 to 3.006	Yes	****	<0.0001
untransfected HEKs vs. mutant SLC30A10 HEKs	-0.3055	-1.271 to 0.6601	No	ns	0.7384
WT SLC30A10 HEKs vs. mutant SLC30A10 HEKs	-2.346	-3.311 to -1.380	Yes	****	<0.0001
VU0057971					
untransfected HEKs vs. WT SLC30A10 HEKs	3.516	2.550 to 4.482	Yes	****	<0.0001
untransfected HEKs vs. mutant SLC30A10 HEKs	-0.996	-1.962 to -0.03038	Yes	*	0.0414
WT SLC30A10 HEKs vs. mutant SLC30A10 HEKs	-4.512	-5.478 to -3.546	Yes	****	<0.0001
VU0239513					
untransfected HEKs vs. WT SLC30A10 HEKs	2.637	1.672 to 3.603	Yes	****	<0.0001
untransfected HEKs vs. mutant SLC30A10 HEKs	-1.601	-2.567 to -0.6357	Yes	***	0.0003
WT SLC30A10 HEKs vs. mutant SLC30A10 HEKs	-4.239	-5.204 to -3.273	Yes	****	<0.0001

Tukey's multiple comparisons test	Predicted (LS) mean diff.	95.00% CI of diff.	Significant?	Summary	Adjusted P Value
VU0026395					
untransfected HEKs vs. WT SLC30A10 HEKs	9.296	8.507 to 10.08	Yes	****	<0.0001
untransfected HEKs vs. mutant SLC30A10 HEKs	5.091	4.302 to 5.879	Yes	****	<0.0001
WT SLC30A10 HEKs vs. mutant SLC30A10 HEKs	-4.205	-4.994 to -3.417	Yes	****	<0.0001
VU0028040					
untransfected HEKs vs. WT SLC30A10 HEKs	2.392	1.603 to 3.180	Yes	****	<0.0001
untransfected HEKs vs. mutant SLC30A10 HEKs	0.5791	-0.2093 to 1.368	No	ns	0.1968
WT SLC30A10 HEKs vs. mutant SLC30A10 HEKs	-1.813	-2.601 to -1.024	Yes	****	<0.0001
VU0027832					
untransfected HEKs vs. WT SLC30A10 HEKs	7.994	7.206 to 8.783	Yes	****	<0.0001
untransfected HEKs vs. mutant SLC30A10 HEKs	3.082	2.293 to 3.870	Yes	****	<0.0001
WT SLC30A10 HEKs vs. mutant SLC30A10 HEKs	-4.913	-5.701 to -4.124	Yes	****	<0.0001
VU0028386					
untransfected HEKs vs. WT SLC30A10 HEKs	11.55	10.76 to 12.34	Yes	****	<0.0001
untransfected HEKs vs. mutant SLC30A10 HEKs	5.307	4.518 to 6.095	Yes	****	<0.0001
WT SLC30A10 HEKs vs. mutant SLC30A10 HEKs	-6.242	-7.031 to -5.454	Yes	****	<0.0001

TABLE 4-1. Tukey's Multiple Comparisons Tests Following Two Way ANOVA Small Molecule SLC30A10 Screen.

TABLE 4-2: SUMMARY OF SMALL MOLECULE CLASSIFICATIONS BY TUKEY'S MULTIPLE COMPARISONS STATISTICAL PHENOTYPES				
VEHICLE	**DOMINANT NEGAVTIVE PHENOTYPE**	**PERFECT V PHENOTYPE**	**ALTERED V PHENOTYPE**	**"NO" PHENOTYPE**
VU0048129	VU0003610	VU0088990	VU0025879	VU0047355*
VU0047375	VU0003765	VU0150155	VU0004838	VU0244366*
VU0025173	VU0006021	VU0026977	VU0009096*	VU0243195*
VU0046776		VU0041803	VU0026921	VU0063088*
		VU0050661	VU0057971*	VU0482585*
		VU0002852	VU0239513	VU0006712
		VU0029414	VU0026395	
		VU0135086	VU0027832	
		VU0029611	VU0028386	
		VU0133141		
		VU0028040		

Table 4-2. Summary of small molecule classifications by Tukey's multiple comparisons statistical phenotypes. Small molecule Mn "decreasers" are in blue, with Mn "increasers" in red. Small molecules with the potential to target SLC30A10 have an * next to the VUID.

The classification of small molecules into five groups accomplishes three things: First, it reveals the trend for the Mn-decreasers to cluster together in the "No" phenotype (no point is statistically different from another) or remain statistically indistinguishable from the Vehicle phenotype. Second, it reveals that the majority of the Mn-increasers (20 of 27) create a "V" phenotype consistent with the expected effect of increasing intracellular Mn in cells with little, excess, and null SLC30A10 functioning protein. In nearly every instance, the SLC30A10 WT cells start with increased intracellular Mn (due to a Mn-increasing small molecule; what appears to happen in the control untransfected cells), but are able to compensate with its Mn-efflux ability to accumulate less Mn (below 1-fold) than untransfected vehicle controls. Combined with the data from **Figure 4-1**, this indicates that it is intracellular Mn concentrations, not extracellular Mn, which induces activation of SLC30A10. Lastly, the classification in **Table 4-2** clusters together

small molecules that have the potential to interact with SLC30A10 function. Other clustering analyses (classical hierarchy, k-means) fail to cluster the molecules of interest appropriately.

DISCUSSION

The results of **Figure 4-2** summarized in **Table 4-2** identify seven small molecule suspects that may affect SLC30A10 or related targets. Of these seven, three are "Mn-increasers" in the toolbox. The addition of Mn to the cells, and then the subsequent increase of Mn by a small molecule appears to induce SLC30A10 activation in the WT SLC30A10 cells, as the majority of small molecules that induce the "V" phenotype see a decrease in intracellular Mn accumulated in the SLC30A10 WT cells, relative to vehicle, following the addition of what should be a Mn-increaser. The exceptions to this trend are interesting as they suggest an interaction between them and SLC30A10. The most striking examples are VU0009096 and VU0057971, which present a V phenotype suggesting induction of WT SLC30A10, but this bottom point of the V shape lies well above the 1-fold line.

There are two possible explanations for this altered V phenotype. First, it is possible that the increase of intracellular Mn is so great and/or rapid that the overexpression of WT SLC30A10 cannot compensate. Indeed, the fold change increase in Mn for their untransfected Mn is higher than most other small molecules; though molecules VU0026921, VU0026395, and VU0027832 see similar fold change increases in their untransfected controls while the WT SLC30A10 cells remain at or below the 1-fold threshold. The second, more likely option is that VU0009096 and VU0057971 are blocking SLC30A10 efflux function. They both fall into the "altered V phenotype" in **Table 4-2**, since the mutants are significantly different from the untransfected. This isn't abundantly clear since the y-scale is in a log-2 format, but the mutants lie significantly above

the untransfected controls. This is consistent with a blockage of both WT and mutant SLC30A10. While mutant SLC30A10 has a dominant negative effect in most situations, it shows residual activity in other small molecule increasers, where the mutants have significantly lower Mn than untransfected controls (seen in VU0025879, VU0004838, VU0026921, and others; see **Table 4-1**).

Conversely, VU0028386 demonstrates a similar phenotype (raised V) to VU0009096 and VU0057971, but is not believed to block SLC30A10. VU0028386 has been identified as a selective Mn ionophore (MESM; see Chapter 5). For this reason, VU0028386 is not an interesting molecule in the context of SLC30A10. In addition, if VU0009096 and VU0057971 block SLC30A10 function it is not selective; these molecules are likely blocking other Mn efflux mechanisms. We do not believe that blocking the little endogenous SLC30A10 in untransfected controls is responsible for such a large increase in Mn. This may however be the case for VU0482585, which also appears to block SLC30A10 albeit in a more modest degree. A previous screen of the Mn-toolbox on Mn efflux in Q7 cells did not indicate any reduced Mn efflux in the presence of VU0009096, VU0057971, or VU0482585 (see Chapter 5), however this screen was in calcium-deficient conditions, while SLC30A10 is a Mn^{2+}/Ca^{2+} symporter (14). Neither molecule has been previously noted as molecule of interest based on previous characterizations, with the exception of VU0057971, which was the sole molecule in the toolbox found to be epistatic from VU00243195 (See **Chapter II**).

The four small molecules that are classified as “Vehicle” are not statistically significant from Vehicle, and therefore are of little interest in the context of SLC30A10. The difference between these small molecules and the three molecules in the “Dominant Negative” phenotype is subtle in that the only difference is non-significance between untransfected cells and mutant. They

are characterized only by a significant difference between WT and mutant, but this difference tended to not be large in magnitude. From a translational perspective, small molecules that could activate SLC30A10 function without increasing intracellular Mn are of most interest. This fits in best with the "No" phenotype, where all three points tend to cluster together and overall decrease intracellular Mn. Not surprisingly these are all typical "Mn-decreasers" in the toolbox. Their influence is small, but their little activity may be a good starting point for a more potent activator of SLC30A10. Future studies should combine the exposures of these four molecules (VU0047355, VU024366, VU0243195, VU0063088) to see if there is a combined effect or if each molecule is working on the same mechanism.

A model of what we believe to be happening during the various phenotypes can be seen in **Figure 4-3**. In the proposed model for the Perfect V-phenotype, a Mn-increaser small molecule acts on an (unknown) Mn importer target, activating it and increasing Mn influx. This increases intracellular Mn in the untransfected cells, but the increase of Mn in the cells is handily rescued by the overexpression of SLC30A10 efflux in the SLC30A10 WT HEK293 cells. The E25A mutant SLC30A10 HEK293 cells, which presumably have the same Mn-efflux capabilities as the untransfected controls, accumulate just as much Mn as the untransfected controls. The intracellular Mn levels of each cell type are normalized to their own Mn levels following DMSO/Mn exposure in **Figure 4-2**. This means that the decreases in Mn accumulation (below 1-fold) in the WT SLC30A10 cells are further decreases in intracellular Mn than seen in their smaller "V" phenotype in **Figure 4-1**. It follows that the initial increase in intracellular Mn from the Mn-increaser in these WT SLC30A10 cells "activates" more SLC30A10 efflux activity. Whether this is due to changes in SLC30A10 structure conformation, expression at the cell surface, protein translation, or some

other mechanism, is currently unknown. This marks a mechanism of Mn homeostasis that remains unexplored.

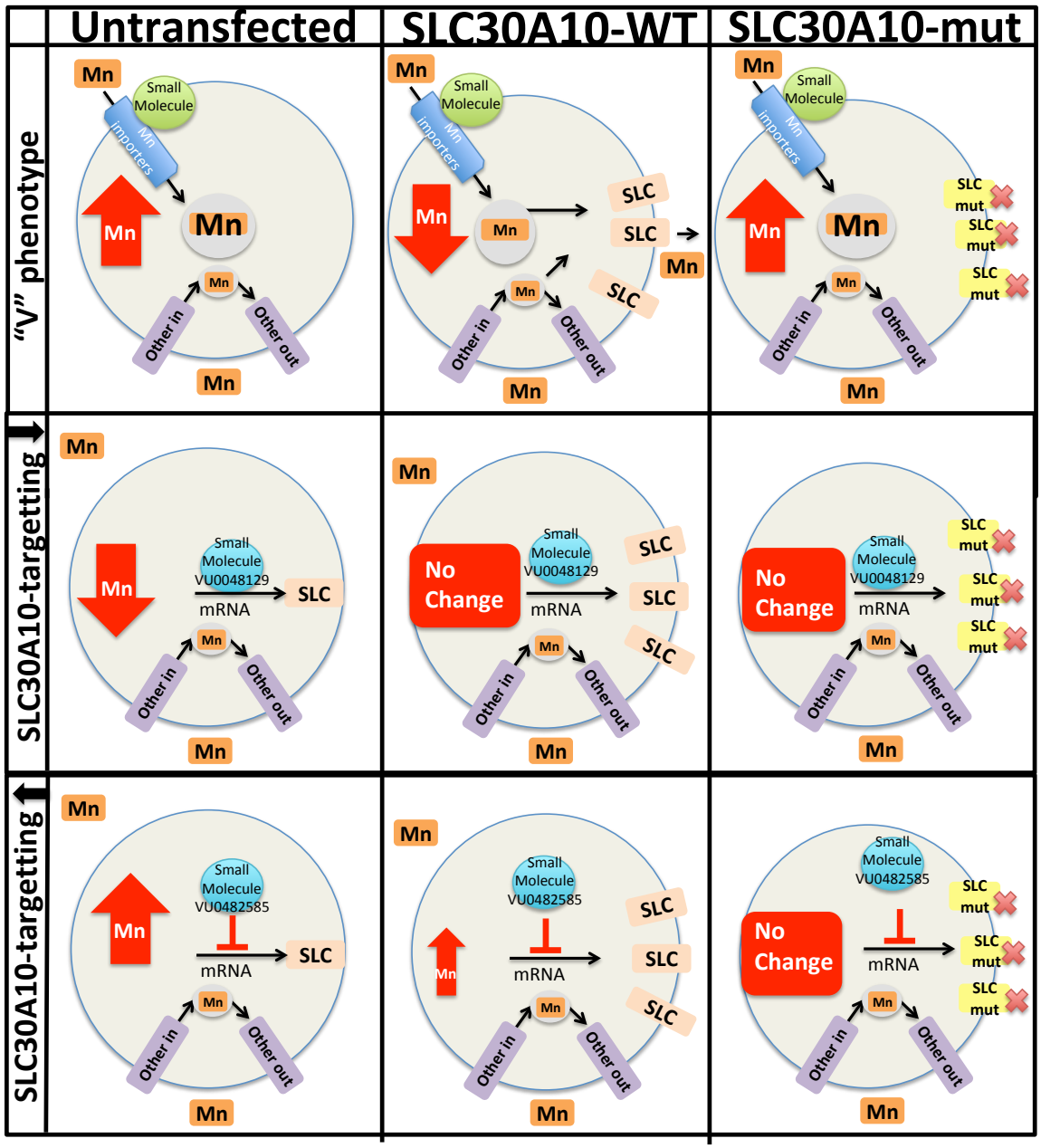

Figure 4-3: Proposed model of how small molecules that influence Mn may influence SLC30A10.

The exceptions in the "V" phenotype seen in **Figure 4-2** are interesting as they either represent an inactive molecule in HEK293 cells, such as the case for VU0006712, or they represent

a small molecule that targets some aspect of SLC30A10 functionality. The clearest cases are for VU0243195 and VU0048129. These Mn-decreasers seem to induce the activation of the little endogenous SLC30A10 that exists in the untransfected HEK293 cells. An example of this could be a ligand (small molecule) that enhances protein translation, such as a riboswitch. This is illustrated in the middle panel of **Figure 4-3**. SLC30A10 WT cells already are keeping intracellular Mn levels low, so increased expression of SLC30A10 does little or no change to intracellular Mn concentrations. Finally, the E25A mutants have increased SLC0A10 protein expression as a result of the small molecule, but because this mutant protein is not functional, there is no change to intracellular Mn in these cells. An opposite mechanism might be proposed for a small molecule such as VU0482585. Instead of promoting SLC30A10 activity, it blocks it, as illustrated in the bottom row of **Figure 4-3**. This produces a modest increase in untransfected cells, and a more mild increase in the WT cells. Since SLC30A10 is already inactive in the mutants, it fails to see a change in intracellular Mn in these cells. Future experiments should utilize SLC30A10 antibodies and immunofluorescence to confirm changes in expression and localization following Mn/small molecule exposure in both WT SLC30A10 and untransfected HEK293 cells.

However, for the small molecules that appear to work on SLC30A10 in the HEK cells, these small molecules would not be expected to be active in HeLa cells, as these cells lack endogenous SLC30A10. This is true in the case of the Mn-decreasers VU0048129, VU0243195, and Mn-increaser VU0482585 (See Chapter II). These three small molecules lack Mn-altering activity in cells that don't express endogenous SLC30A10, and also alter the SLC30A10 "V" phenotype. These small molecules, especially the Mn-decreasers that appear to activate endogenous SLC30A10, should be confirmed in other models for their targeting of SLC30A10.

Considering the case of Mn toxicity, and the lack of treatment options there are with those affected by Mn dyshomeostasis (5, 15, 18), this should be a high priority.

Treatment options for patients with HMDPC are limited, however a case study from 2019 found that regular treatment of infusions of disodium calcium edetate and oral iron compounds led to decreased serum manganese and returned hemoglobin levels to normal values. In addition, significant resolution of MRI lesions, and partial improvement of neurological symptoms were seen (21).

MATERIALS AND METHODS

Cell Culture

Untransfected HEK293 cells were obtained from ATCC and plated at a density of 60,000 cells per well of a 96-well plate and incubated at 37°C with 5% CO_2 in DMEM (10-013CV; Corning) containing 10% Fetal Bovine Serum (FBS; Atlanta Biologicals; Flowery Branch, GA) and 1% Penicillin/Streptomycin (15140-122; Life Technologies; Carlsbad, CA) for 24 hours prior to the assay. WT SLC30A10 Overexpressing cells and E25A mutants were a gift from Somshuvra Mukhopadhyay. Cells were dissociated using 0.05% Trypsin-EDTA solution (Life Technologies).

Cellular Mn level assay and extraction with triton/ Cellular Fura-2 Manganese Extraction Assay (CFMEA)

All HEK cell genotypes were exposed to varying Mn concentrations, at 37 degrees or on ice, in HBSS for 2 hours. Often other small molecules were co-incubated with the Mn in the HBSS to assess their impact on Mn levels, as in **Figure 4-2**. After incubation, the cells were washed three times with PBS (without Ca^{2+} and Mg^{2+}) to remove the extracellular Mn. *Extraction buffer* (PBS

containing 0.1% TritonX100; Sigma-Aldrich; T8787; St. Louis, MO and 500nM Fura-2) was added to lyse the cells. The fluorescence of the Fura-2 in the extraction buffer was then measured at 360nm/535nm (Ex/Em) so that Mn could be quantified.

Manganese Quantification by Fura-2

A percent max of Fura-2 fluorescence 360nm/535nm (Ex/Em) was calculated for each condition as the corresponding zero Mn condition was defined as 100%. Background fluorescence was subtracted from all values. The concentration of Mn (nM) was calculated with the equation: $[Mn] = 1138 \times ((1 / \%max) - 1)^{0.9682}$, which was generated based on a standard curve of Mn quenching Fura-2 signal (12). The absolute values were calculated by multiplying by the concentration by volume.

REFERENCES

1. Aydemir TB, Cousins RJ. 2018. The multiple faces of the metal transporter ZIP14 (SLC39A14). *J. Nutr.* 148(2):174–84
2. Aydemir TB, Kim M-H, Kim J, Colon-Perez LM, Banan G, et al. 2017. Metal Transporter *Zip14* (*Slc39a14*) Deletion in Mice Increases Manganese Deposition and Produces Neurotoxic Signatures and Diminished Motor Activity. *J. Neurosci.* 37(25):5996–6006
3. Chen P, Bowman AB, Mukhopadhyay S, Aschner M. 2015. SLC30A10 : A novel manganese transporter. . 4(3):4–7
4. Choi EK, Nguyen TT, Gupta N, Iwase S, Seo YA. 2018. Functional analysis of SLC39A8 mutations and their implications for manganese deficiency and mitochondrial disorders. *Sci. Rep.* 8(1):1–17

5. DeWitt MR, Chen P, Aschner M. 2013. Manganese efflux in Parkinsonism: insights from newly characterized SLC30A10 mutations. *Biochem. Biophys. Res. Commun.* 432(1):1–4

6. Fujishiro H, Yoshida M, Nakano Y, Himeno S. 2014. Interleukin-6 enhances manganese accumulation in SH-SY5Y cells: implications of the up-regulation of ZIP14 and the down-regulation of ZnT10. *Metallomics*. 6(4):944–49

7. He L. 2006. ZIP8, member of the solute-carrier-39 (SLC39) metal-transporter family: characterization of transporter properties. *Mol. Pharmacol.* 70(1):171–80

8. Huang L, Tepaamorndech S, Editor G, Hediger MA. 2013. Molecular Aspects of Medicine The SLC30 family of zinc transporters – A review of current understanding of their biological and pathophysiological roles q. *Mol. Aspects Med.* 34(2–3):548–60

9. Ishida T, Takechi S. 2019. β-Naphthoflavone , an exogenous ligand of aryl hydrocarbon receptor , disrupts zinc homeostasis in human hepatoma. . 44(10):711–20

10. Kambe T, Tsuji T, Hashimoto A, Itsumura N. 2015. THE PHYSIOLOGICAL, BIOCHEMICAL, AND MOLECULAR ROLES OF ZINC TRANSPORTERS IN ZINC HOMEOSTASIS AND METABOLISM. *Worm*, pp. 749–84

11. Koike A, Sou J, Ohishi A, Nishida K, Nagasawa K. 2017. Inhibitory effect of divalent metal cations on zinc uptake via mouse Zrt-/Irt-like protein 8 (ZIP8). *Life Sci.* 173:80–85

12. Kumar KK, Aboud AA, Patel DK, Aschner M, Bowman AB. 2013. Optimization of Fluorescence Assay of Cellular Manganese Status for High Throughput Screening. *J. Biochem. Mol. Toxicol.* 27(1):42–49

13. Lechpammer M, Clegg MS, Muzar Z, Huebner P a, Jin L-W, Gospe SM. 2014. Pathology of inherited manganese transporter deficiency. *Ann. Neurol.* 75(4):608–12

14. Levy M, Elkoshi N, Barber-Zucker S, Hoch E, Zarivatch R, et al. 2019. Zinc transporter

10 (ZnT10)-dependent extrusion of cellular Mn2+ is driven by an active Ca2+-coupled exchange. *J. Biol. Chem.* 10:jbc.RA118.006816

15. Leyva-Illades D, Chen P, Zogzas CE, Hutchens S, Mercado JM, et al. 2014. SLC30A10 Is a Cell Surface-Localized Manganese Efflux Transporter, and Parkinsonism-Causing Mutations Block Its Intracellular Trafficking and Efflux Activity. *J. Neurosci.* 34(42):14079–95
16. Lin W, Vann DR, Doulias PT, Wang T, Landesberg G, et al. 2017. Hepatic metal ion transporter ZIP8 regulates manganese homeostasis and manganese-dependent enzyme activity. *J. Clin. Invest.* 127(6):2407–17
17. Mercadante CJ, Rao DB, Thomas B, Mercadante CJ, Prajapati M, et al. 2019. Manganese transporter Slc30a10 controls physiological manganese excretion and toxicity Find the latest version : Manganese transporter Slc30a10 controls physiological manganese excretion and toxicity. . 129(12):5442–61
18. Mukhopadhyay S. 2018. Familial manganese-induced neurotoxicity due to mutations in SLC30A10 or SLC39A14. *Neurotoxicology*. 64:278–83
19. Park JH, Hogrebe M, Fobker M, Brackmann R, Fiedler B, et al. 2018. SLC39A8 deficiency: Biochemical correction and major clinical improvement by manganese therapy. *Genet. Med.* 20(2):259–68
20. Quadri M, Federico A, Zhao T, Breedveld GJ, Battisti C, et al. 2012. Mutations in SLC30A10 Cause Parkinsonism and Dystonia with Hypermanganesemia , Polycythemia , and Chronic Liver Disease. , pp. 467–77
21. Tavasoli A, Rafsanjani KA, Hemmati S, Mojbafan M, Zarei E. 2019. A case of dystonia with polycythemia and hypermanganesemia caused by SLC30A10 mutation : a treatable

inborn error of manganese metabolism. , pp. 1–6

22. Tuschl K, Clayton PT, Gospe SM, Gulab S, Ibrahim S, et al. 2012. Syndrome of Hepatic Cirrhosis , Dystonia , Polycythemia , and Hypermanganesemia Caused by Mutations in SLC30A10 , a Manganese Transporter in Man. *Am. J. Hum. Genet.* 90(3):457–66

23. Tuschl K, Meyer E, Valdivia LE, Zhao N, Dadswell C, et al. 2016. Mutations in SLC39A14 disrupt manganese homeostasis and cause childhood-onset parkinsonism-dystonia. *Nat. Commun.* 7(May):1–16

24. Tuschl K, Mills PB, Parsons H, Malone M, Fowler D, et al. 2008. Hepatic cirrhosis , dystonia , polycythaemia and hypermanganesaemia — A new metabolic disorder. , pp. 151–63

25. Xia Z, Wei J, Li Y, Wang J, Li W, et al. 2017. Zebrafish slc30a10 deficiency revealed a novel compensatory mechanism of Atp2c1 in maintaining manganese homeostasis. *PLoS Genet.* 13(7):

26. Xin Y, Gao H, Wang J, Qiang Y, Imam MU, et al. 2017. Manganese transporter Slc39a14 deficiency revealed its key role in maintaining manganese homeostasis in mice. *Cell Discov.* 3:17025

27. Zogzas CE, Aschner M, Mukhopadhyay S. 2016. Structural elements in the transmembrane and cytoplasmic domains of the metal transporter SLC30A10 are required for its manganese efflux activity. *J. Biol. Chem.* 291(31):15940–57

28. Zogzas CE, Mukhopadhyay S. 2017. Inherited Disorders of Manganese Metabolism. In *Handbook of Clinical Neurology*. 131:35–49

CHAPTER V

IDENTIFICATION OF A SELECTIVE MANGANESE IONOPHORE THAT ENABLES NONLETHAL QUANTIFICATION OF CELLULAR MANGANESE

INTRODUCTION

Manganese (Mn) is an essential metal required as a cofactor for numerous kinases and other enzymes such as glutamine synthetase, Mn superoxide dismutase (Mn-SOD), and arginase (1). Similar to other biological trace metals, sufficient Mn needs to be retained while avoiding excess, toxic amounts. In the brain, this appears to be a narrow window: estimated concentrations of physiological Mn in the brain are in the range of 20-55 μM Mn, whereas neurotoxic responses begin at concentrations corresponding to 60-160 μM Mn (2). However, mechanistic information on how cells maintain Mn homeostasis is exceedingly sparse.

Cellular Mn transport was initially thought to be only co-regulated by iron (Fe) transporters such as divalent metal transporter-1 (DMT1) or the transferrin receptor (TfR) (1). A third transporter of Fe, ferroportin, is able to efflux both Fe and Mn from the plasma membrane (3). As mRNA expression of ferroportin is induced in a dose-dependent manner upon Mn exposure- it can act as a compensatory mechanism to prevent Mn toxicity (4,5). However, a recent study noted that very low expression of ferroportin in mice did not impact Mn levels, suggesting that ferroportin may not play a role in Mn homeostasis at basal conditions (6). Although these Fe transporters are capable of trafficking Mn with some efficacy, without Mn specificity they alone are insufficient to explain how cells maintain a homeostatic balance of Mn (7).

Only recently has the first Mn-selective transporters been described (8). This cell surface Mn-efflux transporter, SLC30A10, was first identified when patients suffering the symptoms of Mn- toxicity (motor impairment, cirrhosis, high blood Mn content) were matched with mutations in the gene expressing the SLC30A10 protein (9–11). A set of cell surface transporters, Zip8 and Zip14, coded by SLC39A8 and SLC39A14, have also been implicated in cellular Mn uptake based on clinical studies and recent animal models through a similar process (12–20). Based on these clinical loss-of-function mutation studies and animal data, a model of how these three transporters work together to regulate whole-body Mn homeostasis and detoxification has been proposed (21). Mn is taken up from blood via ZIP14 in the liver and secreted into bile via SLC30A10. Hepatocytes are then able to take up Mn from the bile via ZIP8. The uptake of Mn by ZIP8 has been shown to be essential for the proper functioning of Mn-dependent enzymes throughout the whole-body (14). This model is also consistent with the neuroprotective role of SLC30A10, as whole-body knockout mice have elevated brain Mn levels (22). The absorption of Mn from the blood is also neuroprotective, as mutations of ZIP14 lead to increased Mn accumulation in the brain, as well as increases in blood, bone, heart, and kidney Mn levels (23).

Mn has been shown to play a role in neurodevelopment. Epidemiological studies show that varying Mn exposures in children result in cognitive deficits (24–26). Patients suffering from Mn-toxicity due to a genetic disorder (described above) present with similar symptoms to a syndrome known as manganism: a Parkinsonian-like condition that occurs in welders and other industrial workers chronically exposed to Mn. They share overlapping symptoms of the motor, cognitive, and emotional abnormalities seen in Parkinson's disease (27). However, instead of responding to

common Parkinson's disease treatments, amelioration of the symptoms is only seen upon treatment with the calcium (Ca^{2+}) disodium salt of the chelating agent EDTA [$CaNa_2EDTA$] (28).

A cellular *deficit* of Mn has been implicated in the pathogenesis of Huntington's disease (HD), a fatal neurodegenerative disease characterized by the expression of mutant huntingtin protein and death of medium spiny neurons in the corpus striatum. The rescue of HD phenotypes by Mn has been seen both *in vitro* and *in vivo* (29–31). These findings support the idea that a Mn deficiency may be occurring and contributing to the pathology of HD. Understanding how cells maintain appropriate Mn concentrations in the brain under normal conditions is vital to understanding how a Mn deficit may occur in HD, or how excess Mn might be corrected due to environmental exposure or other genetic mutations.

Though non-lethal, the use of the Ca^{2+} fluorescent indicator Fura-2 AM can measure intracellular Mn, but only in relative quantities (32–37). Fura-2 AM quantification works by loading cells full of membrane-soluble Fura-2, so that it directly interacts with intracellular Mn. Fura-2 fluorescence is quenched based on the Mn present in the cytosol, so that cells containing more Mn will have lesser fluorescence. However, the amount of Fura-2 that is loaded into the cells will vary between experiments and between cell types, making full quantification of Mn concentrations impossible. Furthermore, the amount of Mn that is quantified is based only where Fura-2 AM has access to in the cytosol; Mn stored subcellularly is not considered. Beyond this, Fura-2 AM as well would need to be repeatedly loaded into cells to enable longitudinal studies. This loading would quite likely change cellular status and be toxic to the cells - thus it has not allowed such analysis.

Therefore, the most practical standard (in terms of throughput and financial cost) for Mn quantification up until now has been the Cellular Fura-2 Mn Extraction Assay (CFMEA), which relies on the use of a detergent to lyse open cells, and then the ability to quantify the now-extracellular Mn by a concentration-dependent quenching mechanism of the fluorophore Fura-2 (38). CFMEA is the cost-effective preferred method for measuring Mn in cells, which unlike Fura-2AM methods, allows for full quantification of Mn. The single disadvantage of the CFMEA method is one of the same disadvantages affecting the gold standards of spectrometry or spectroscopy- it requires the lysis and death of the cells being measured. In addition, alternative methods to measure Mn concentrations such as inductively coupled plasma mass spectrometry (ICP-MS) or atomic absorption spectroscopy (AAS) are prohibitively expensive for the number of samples- costing ~$10 per/sample, versus ~$1 per 100 samples by CFMEA in 96-well plate format. Moreover, AAS and ICP-MS are hampered by detection limits precluding multi-titer plate cell culture based experimental designs. With the exception using Fura-2 AM (for semi-quantitative Mn determination within an experiment), other techniques require the lysis and destruction of the biological sample, limiting longitudinal studies. This is important as the ability to look at Mn changes over time, while limiting all other variables is not possible. The alternative is performing multiple experiments in parallel, greatly increasing the cells, resources, and financial costs required. Developing a non-lethal assay that bypasses these problems would facilitate the ability to explore new questions and mechanistic details of Mn transport, toxicity and homeostasis. Here we report the development of such a non-lethal multi-titer plate assay, and the discovery of a novel small molecule to selectively and rapidly release total accumulated intracellular Mn for extracellular detection by a Fura-2 based method similar in concept and cost to CFMEA.

RESULTS

Small molecule VU0028386 (MESM) rapidly evokes cellular efflux of Mn

A set of small molecules that were found to alter net Mn levels (39) were screened to determine if their mechanism of action was due to an influence in Mn efflux rates. We found that the majority of these small molecules could in fact influence Mn efflux rates (**Figure 5-1A-C)**. Most notably, the small molecule VU0028386 (which henceforth we'll call MESM; Manganese-Extracting Small Molecule) greatly facilitated Mn efflux from cells almost immediately, and after 15 minutes released nearly all of the intracellular Mn **(Figure 5-1C)**. In comparison, an analogous amount of effluxed Mn was not reached under vehicle conditions even after 6 hours. The time for 50% of the total Mn to be released under vehicle conditions was 79.1 minutes ($t_{1/2}$) with 95% CI falling between 70.73 to 89.87 minutes.

In contrast, the rate at which Mn effluxes in the presence of MESM is extremely fast to the point t hat a $t_{1/2}$ cannot be accurately calculated. Considering the lag period between assay and first measurement, we can estimate that the $t_{1/2}$ value is less than 2 minutes. This is based on recordings of the length of this period from adding small molecule to the first plate reader data point which yielded an average of 94.4 ± 4.72 SD seconds (n=5; data not shown). Taking this into consideration, since a true zero cannot be recorded, we imputed a 0 sec time, 0% Mn efflux point in all of the graphs 94 seconds before the first measured point. We compare MESM's effects on efflux with another small molecule (VU0026921) that was also screened and previously referred to as a "Mn-increaser" (**Figure 5-1B)**.

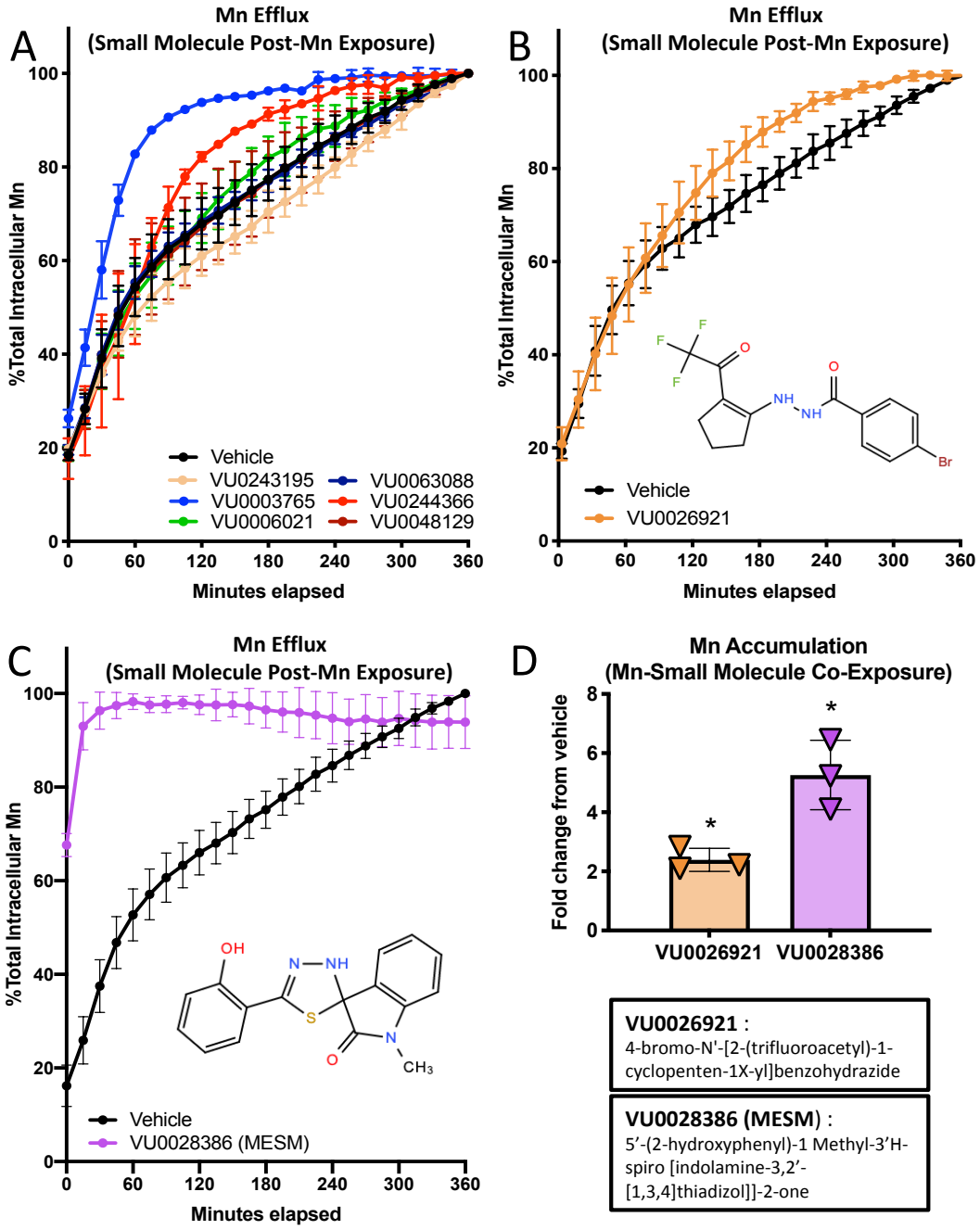

VU0026921 :
4-bromo-N'-[2-(trifluoroacetyl)-1-cyclopenten-1X-yl]benzohydrazide

VU0028386 (MESM) :
5'-(2-hydroxyphenyl)-1 Methyl-3'H-spiro [indolamine-3,2'-[1,3,4]thiadizol]]-2-one

Figure 5-1. Small molecule VU0028386 (MESM) rapidly induces cellular efflux of Mn. Cells of the murine striatal neuron lineage, STHdh$^{Q7/Q7}$ (Q7) were pre-exposed to 125μM $MnCl_2$ for 2 hours in HBSS (Hanks Balanced Buffer Solution) before washing away the extracellular Mn and allowing the cells to efflux their intracellular Mn to the extracellular space in PBS (lacking Ca^{2+} and Mg) with co-incubation of a small molecule (10μM). Fluorescent dye (Fura-2; 500nM) was added to the PBS so its fluorescence could be quenched by effluxed Mn. Fluorescence of Fura-2 was measured at 360/535 (Ex/Em) every 15 minutes for 6 hours at 37°C and Mn was calculated based on percent fluorescence quenching. The maximum quantity of Mn effluxed after 6 hours was normalized to 100%. (**A**) A representative sample from a partial screen of small molecules performed in duplicate was performed (all 22 molecules can be seen in *Figure S1*). (**B)** Following the screen, small molecule VU0026921 was assayed again (total N=3) as another "Mn-increaser" to compare to VU0028386 (MESM) which was also assayed again (total N=6) for confirmation of its efflux kinetics (**C**). A sum of squares F-test comparison of MESM and Vehicle data sets, using a nonlinear regression model of one phase exponential decay determined both data sets fit significantly different curves ($P < 0.001$). The biological half-life ($t_{1/2}$) of Mn efflux in Vehicle was calculated at 79.11 minutes. In comparison, the efflux of Mn with MESM is so fast a half-life value can't be accurately calculated as the 50% mark occurs before measurement begins. Considering the lag time between assay and measurement, we can estimate the half-life value is less than 2 minutes. Error bars are the standard deviation of the biological replicates from each experiment. **(D**) STHdh$^{Q7/Q7}$ (Q7) were co-incubated with a known "Mn-increaser" VU0028386 or VU0026921 at 10μM or 0.1% DMSO (Vehicle) with 125μM $MnCl_2$ for 2 hours in HBSS (Hanks Balanced Buffer Solution). Cells were washed 5 times in PBS to remove extracellular Mn. Cells were lysed open with triton and intracellular Mn was quantified using the CMFEA method (described previously; (38)). Mn levels were normalized to Vehicle levels and their fold change is plotted (N=3). Error bars shown represent standard deviation (**A-D**). An Ordinary One Way ANOVA with Dunnett's multiple comparisons test to Vehicle to show statistical significance for intracellular Mn accumulation increases (*, $p < 0.05$).

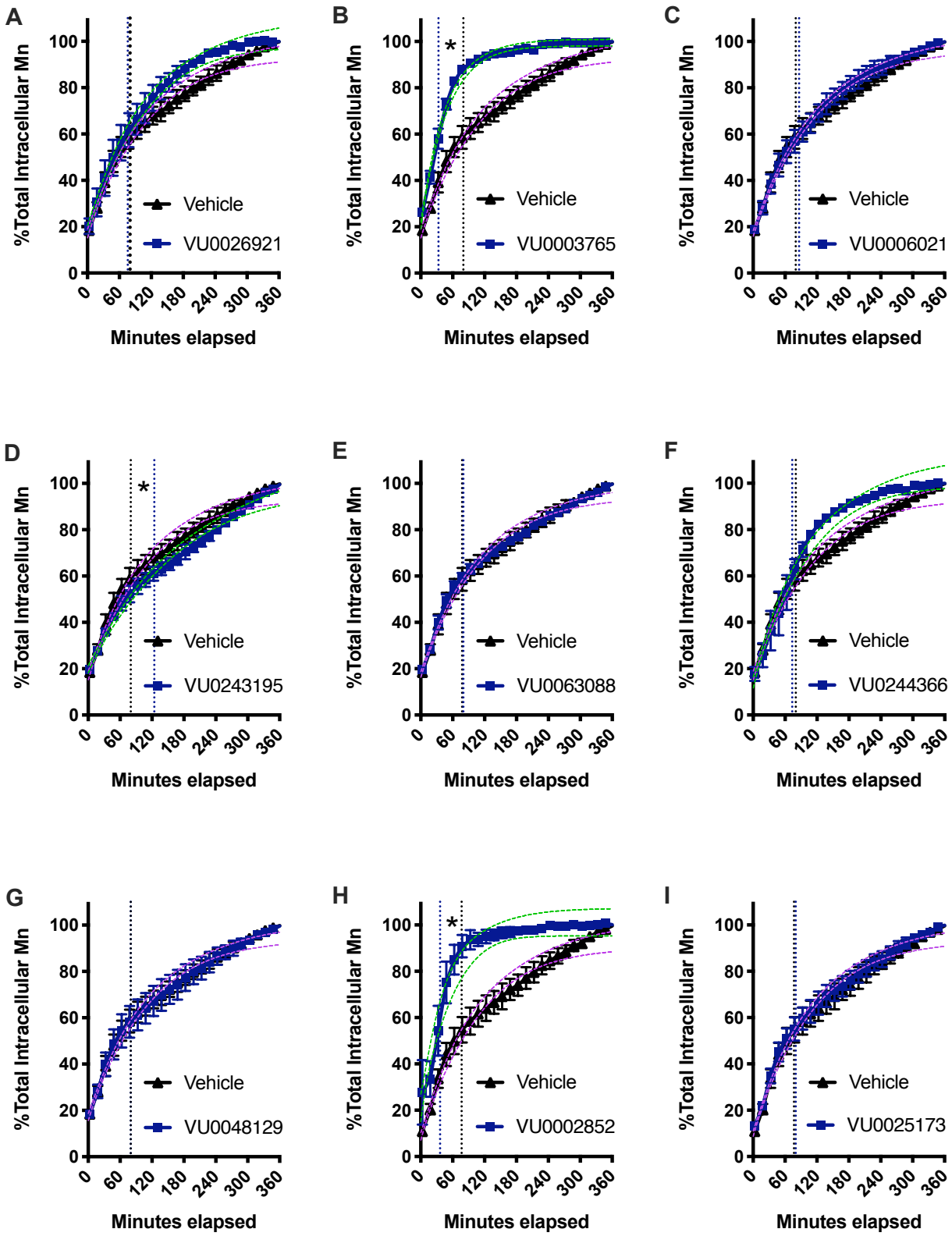
A
%Total Intracellular Mn
Minutes elapsed
Vehicle
VU0026921
B
*
Vehicle
VU0003765
C
Vehicle
VU0006021
D
*
Vehicle
VU0243195
E
Vehicle
VU0063088
F
Vehicle
VU0244366
G
Vehicle
VU0048129
H
*
Vehicle
VU0002852
I
Vehicle
VU0025173

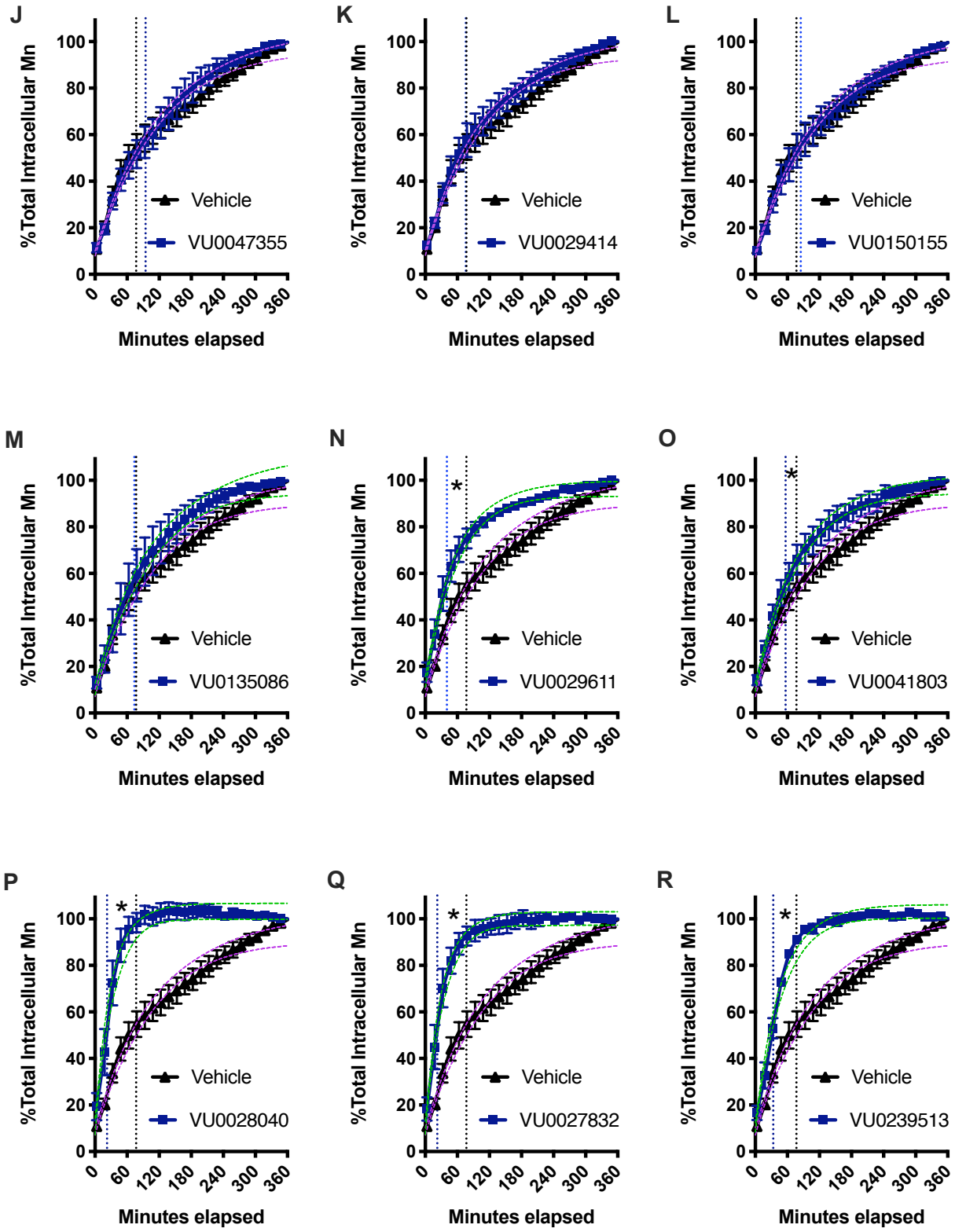
J
K
L
M
N
O
P
Q
R
%Total Intracellular Mn
Minutes elapsed
Vehicle
VU0047355
VU0029414
VU0150155
VU0135086
VU0029611
VU0041803
VU0028040
VU0027832
VU0239513
*

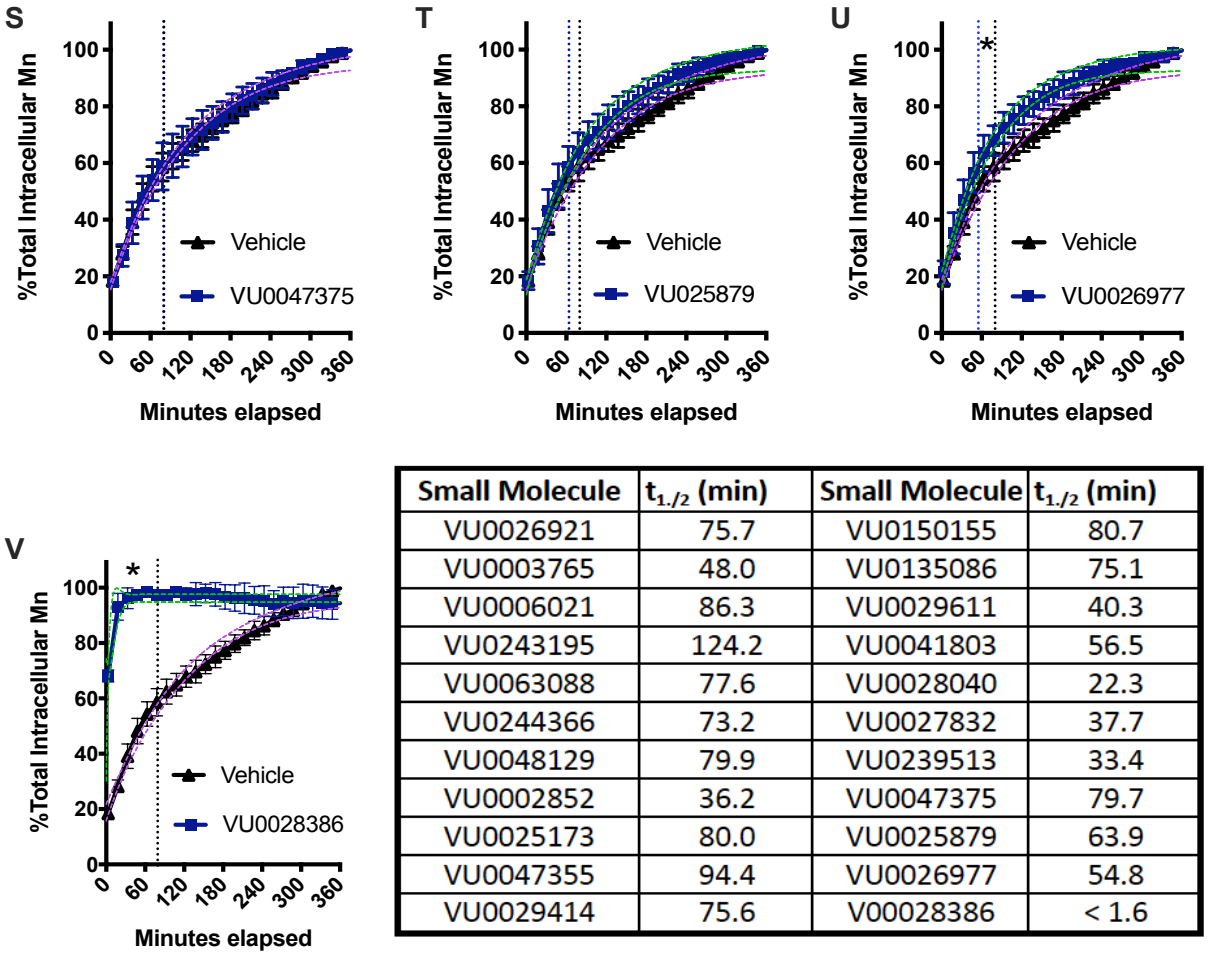

Small Molecule	$t_{1./2}$ (min)	Small Molecule	$t_{1./2}$ (min)
VU0026921	75.7	VU0150155	80.7
VU0003765	48.0	VU0135086	75.1
VU0006021	86.3	VU0029611	40.3
VU0243195	124.2	VU0041803	56.5
VU0063088	77.6	VU0028040	22.3
VU0244366	73.2	VU0027832	37.7
VU0048129	79.9	VU0239513	33.4
VU0002852	36.2	VU0047375	79.7
VU0025173	80.0	VU0025879	63.9
VU0047355	94.4	VU0026977	54.8
VU0029414	75.6	V00028386	< 1.6

Figure 5-1. Efflux screens show other efflux facilitators, but all lack the fast kinetics of MESM. Cells of the murine striatal neuron lineage, STHdh$^{Q7/Q7}$ (Q7) were pre-exposed to 125μM $MnCl_2$ for 2 hours in HBSS (Hanks Balanced Buffer Solution) before washing away the extracellular Mn and allowing the cells to efflux their intracellular Mn to the extracellular space in PBS (lacking Ca^{2+} and Mg^{2+}) with co-incubation of a small molecule (10 μM). Fluorescent dye (Fura-2; 500nM) was added to the PBS so its fluorescence could be quenched by effluxed Mn. Fluorescence of Fura-2 was measured at 360/535 (Ex/Em) every 15 minutes for 6 hours at 37°C and Mn was calculated based on percent fluorescence quenching. The maximum quantity of Mn effluxed after 6 hours was normalized to 100%. A one-phase exponential decay model of nonlinear regression was used and compared if one curve could adequately fit both data sets (small molecule and vehicle). Least squares regression fitting was used with weighting $1/Y^2$. Green dotted curves of 95% confidence intervals are drawn for every significant curve fit by using an extra sum of squares F-test. ($p < 0.01$). Purple dotted curves of 95% confidence intervals are drawn for fit curves to vehicle and curves not significantly different than vehicle. A (*) is placed in every instance where the calculated $t_{1/2}$ value and 95% confidence intervals are non-overlapping. Of the 22 screened, only 8 small molecules did not have a significant impact on efflux rates. The $t_{1/2}$ values of each small molecule are summarized in a table at the bottom.

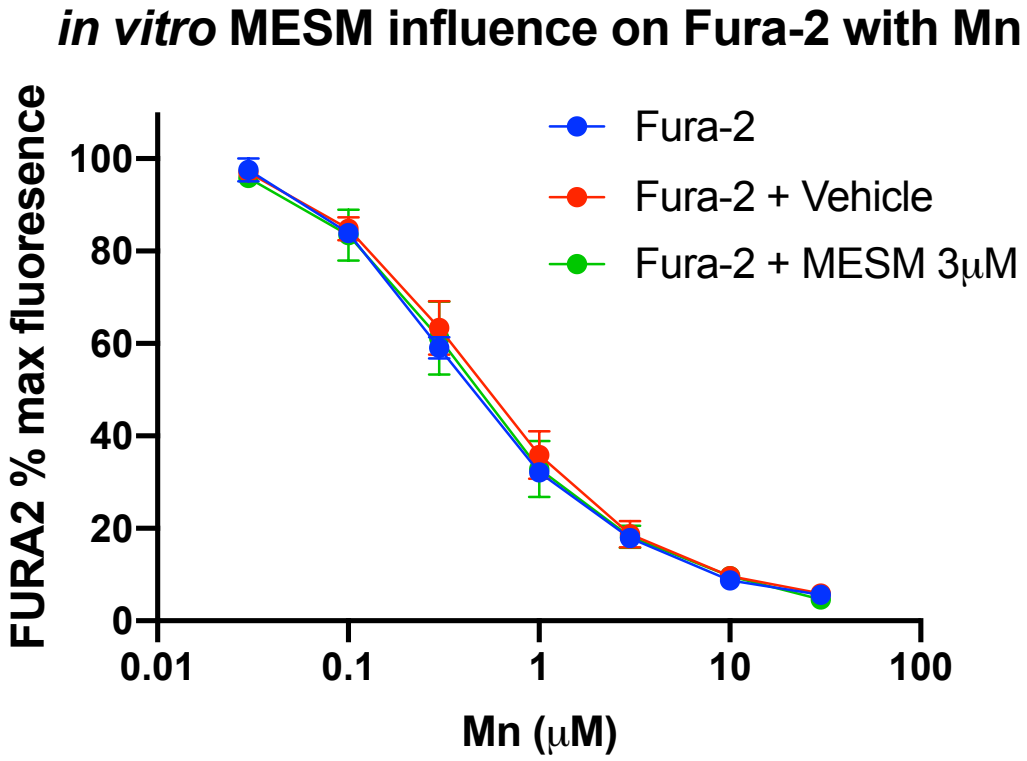

Figure 5-2. MESMER does not interfere with Fura-2 based Mn quantification. Various concentrations of Mn were added to empty wells (no cells) in PBS (without Ca^{2+} and Mg) in the presence of Fura-2 (0.5μM), Fura-2 with 3μM MESM, or Fura-2 with an equivalent DMSO vehicle. The plates were read at 360nm/535nm Ex/Em as earlier described. N=3 of individual replicates performed on different days, with four technical replicate wells for each condition each day. Error bars shown represent standard deviation of the three independent replicate averages. As expected a Two-Way ANOVA yielded a significant main effect for Mn concentration ($p < 0.0001$), but no main effect of MESM or interaction. Sidak's multiple comparisons test yielded no significant differences in Fura-2 % fluorescence between groups at each Mn concentration ($p > 0.05$).

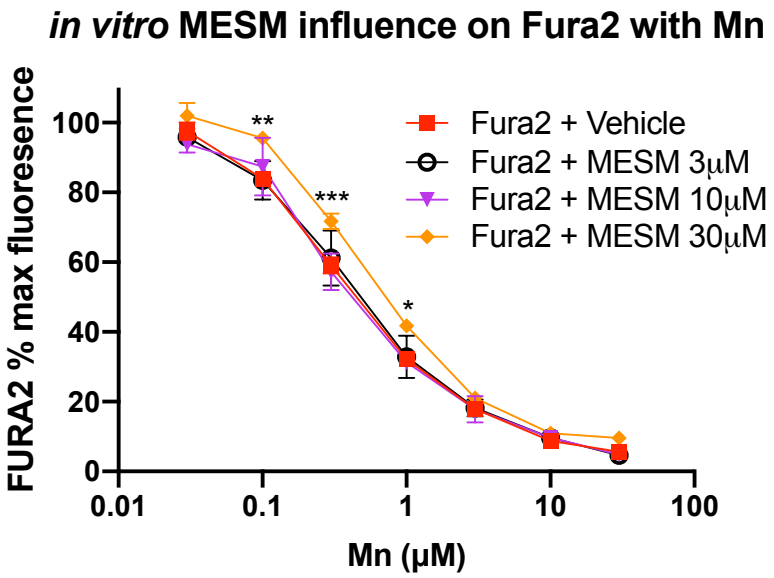

Figure 5-2S. Higher than optimal concentrations of MESM interfere with Mn quantification. Various concentrations of Mn were added to empty wells (no cells) in PBS (without Ca^{2+} and Mg^{2+}) in the presence of Fura-2 (0.5μM), Fura-2 with 10μM MESM, or Fura-2 with an equivalent DMSO vehicle. The plates were read at 360nm/535nm Ex/Em as earlier described. N=3 of individual replicates performed on different days, with four technical replicate wells for each condition each day. Error bars shown represent standard deviation of the three independent replicate averages. A Two-Way ANOVA yielded a significant main effect for Mn concentration ($p < 0.0001$), and a main effect for MESM concentration ($p < 0.0001$). Sidak's multiple comparisons tests found significant differences between 30 μM MESM and Vehicle Fura-2 % fluorescence at 0.1, 0.3, and 1.0 μM Mn concentrations. (*, $p < 0.05$; **, $p < 0.01$; *** $p < 0.001$). These concentrations are 10-fold higher than required for Mn extraction, but the parabolic effect seen in this MESM concentration curve suggests a competition for Mn binding between MESM and Fura-2.

Since MESM was originally identified as a "Mn increaser" in terms of net cellular uptake (39), we sought to confirm that MESM does in fact increase Mn levels in cells when incubated with extracellular Mn at the same time (**Figure 5-1D**). The difference between the two experiments is the cellular concentration gradient of Mn during MESM exposure. When cells are pre-exposed to Mn to increase intracellular Mn levels, and extracellular Mn concentration is low during the MESM treatment - MESM facilitates Mn to move to the extracellular space (**Figure 5-1C**). When MESM is co-incubated with high extracellular Mn levels, intracellular Mn levels are increased compared to Mn co-incubation with vehicle alone (**Figure 5-1D**). In summary, MESM can induce

Mn influx in conditions where extracellular Mn concentrations are higher than its intracellular concentration.

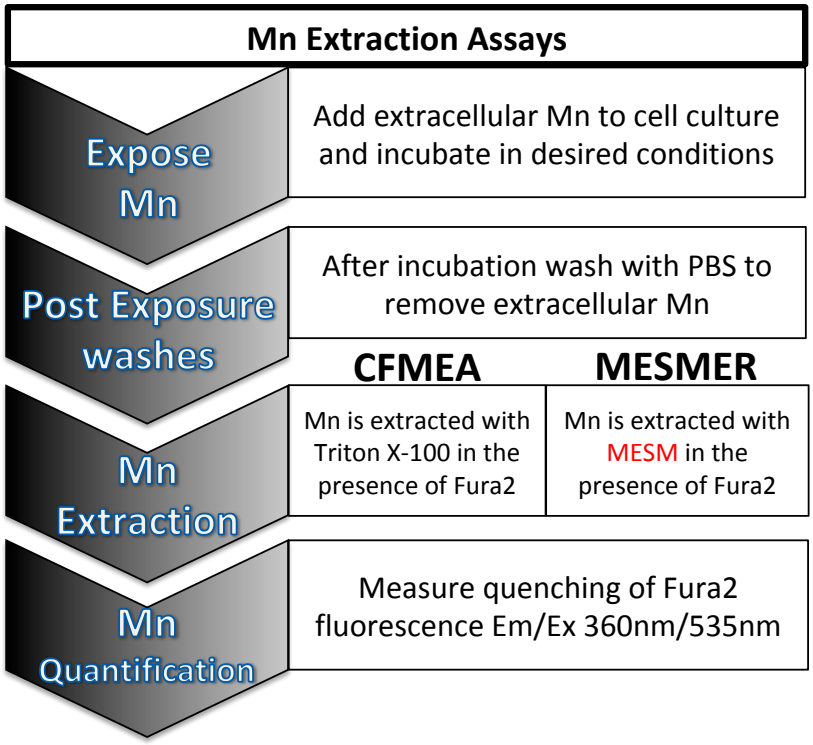

Figure 5-3. The already-validated CFMEA (Cellular Fura-2 Manganese Extraction Assay) method and the proposed MESMER (Manganese Extracting Small Molecule Estimation Route) method differ only at their extraction step. In both assays cells are "loaded" with Mn by an extracellular Mn concentration. After this incubation, this extracellular Mn is washed away so that only intracellular Mn remains. In the CFMEA method, PBS with 0.1% triton is used to lyse open the cells and release intracellular Mn, while 0.5μM Fura-2 is also present to act as fluorescent Mn indicator. In contrast, the MESMER assay extracts Mn using a small molecule, VU0028386, or MESM, while also in the presence of Fura-2. The last step remains the same, as Mn is quantified by measuring the quenching of the Fura-2 signal at Em/Ex 360nM/535nm.

MESM can also induce Mn efflux when extracellular Mn concentration is lower than intracellular Mn. To establish that the effect of MESM on apparent Mn levels was not an artifact of interfering with the quantification of Mn (which is a function of the quenching of the fluorophore Fura-2), *cell-free* concentration curves of Mn to quench Fura-2 were generated in the presence or absence of MESM (**Figure 5-2**). The data showed no evidence that MESM alone

impacted Fura-2 fluorescence at the concentrations being used for extraction. This supports the conclusion that MESM was yielding the true quantities of intracellular Mn from cells via efflux rather than non-Mn dependent changes in Fura-2 fluorescence. While MESM was used at 3-10μM concentrations for Mn extractions throughout these studies, at concentrations 30μM and higher there was evidence of an interaction that is consistent with a competition for binding of Mn to both MESM and Fura-2 (**Figure 5-S2**).

Using MESM as a tool to extract and quantify Mn

As noted above, current quantitative methods of assessing intracellular Mn are cell lethal, as the cells ultimately need to be lysed open for Mn to be quantified. The most high throughput and inexpensive way this can be presently carried out is using the Cellular Fura-2 Manganese Extraction Assay (CFMEA; **Figure 5-3**). CFMEA relies on the lysis of cells with detergent to release Mn and quantify it by the quenching of Fura-2 fluorescence (38,40). The lysis of cells every time Mn levels are quantified severely limits the type of experiments that are possible. Examples of such limited experiments are longitudinal or large multiplexed experiments. There are also time and financial burdens of cell lethal assays, especially in human induced pluripotent stem cell (hiPSC) model systems that are expensive to maintain and take weeks to differentiate. Thus, there is a strong appeal for an assay that could extract Mn in a non-lethal approach. We reasoned that a non-toxic small molecule that leads to rapid efflux of total cellular Mn, could be used to develop such an assay. Therefore we sought to develop a new assay- MESMER (Manganese-Extracting Small Molecule Estimation Route) using the MESM molecule to rapidly extract and quantify cellular Mn content by a non-lethal alternative method based upon the CFMEA assay (**Figure 5-3**). The only difference between the two methods is the extraction step,

in which MESMER uses the small molecule MESM instead of detergent lysis. Considering the rate of efflux seen in **Figure 5-1C**, we selected 15 minutes as the time for incubating MESM with the cells, as this time was sufficient to release >93.0 ± 5.1% of total cellular Mn.

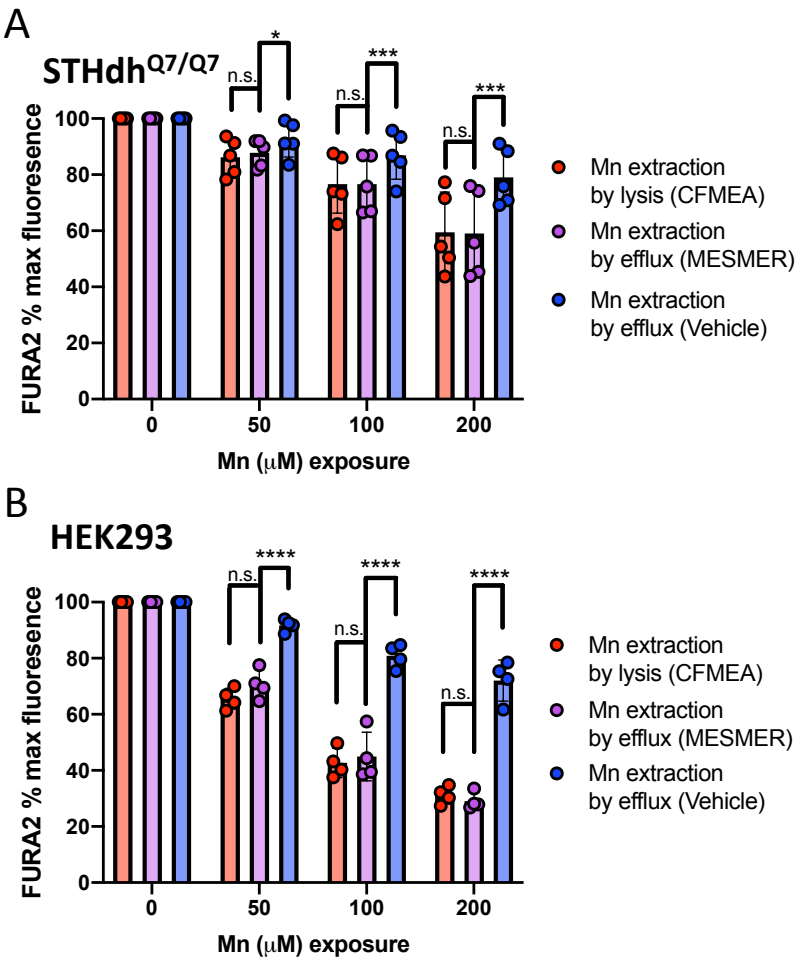

Figure 5-4. The MESMER assay yields comparable readouts as current CFMEA method standard. Murine striatal neuron lineage STHdh Q7 cells (**A**) or Human Embryonic Kidney (HEK) cells (**B**) were exposed to 0, 50, 100 or 200μM Mn for two hours at 37°C. Q7 cells (N=5) were exposed to Mn in HBSS and HEK cells (N=4) in DMEM, respectively. The cells were then washed in PBS (lacking Ca^{2+} and Mg^{2+}) and then exposed to 3μM MESM (MESMER), a DMSO vehicle equivalent (Vehicle), or 0.1% triton in PBS (CFMEA). All solutions contained 0.5μM Fura-2. After 15 minutes at 37°C, the plates were read at 360/535nm (see Figure 3). Error bars shown represent standard deviation. Statistical significance was determined by Two Way ANOVA and is denoted by (n.s., not significant; *, $p < 0.05$; ***, $p < 0.001$; ****, $p < 0.0001$).

MESMER extractions are specific to Mn and are comparable to the CFMEA assay and ICP-MS quantification

To test whether MESMER could be used to quantify Mn accurately, the levels of Mn in cells were compared between the new assay and the AAS-validated CFMEA assay (38). In both cell types tested (STHdh$^{Q7/Q7}$, and HEK293), MESMER demonstrated a Mn concentration-dependent effect similar to CFMEA, with comparable %max values of Fura-2 in each condition (**Figure 5-4A-B**). The %max in all cases was defined as the fluorescence measured divided by maximum fluorescence of Fura-2 (Ex/Em 360nm/535nm) seen in the absence of additional extracellular Mn added to the base culture media. In the STHdh and HEK293 cells, the %max Fura-2 quenching at each Mn exposure was statistically indistinguishable between the MESMER and CFMEA extractions (**Figure 5-4A-B**). To ensure that the MESM molecule was responsible for this effect, extraction was attempted with efflux buffer using just the DMSO vehicle that MESM is dissolved in instead at the same dilution. This method did not yield a Mn-concentration dependent effect, and was statistically different from both CFMEA and MESMER extractions in all conditions (**Figure 5-4A-B**).

To fully confirm that MESMER is in fact quantifying Mn accurately and specifically, STHdh cells were exposed to 50μM $MnCl_2$ for two hours in media. After washing with PBS, intracellular Mn content was measured by MESMER or ICP-MS. ICP-MS was also run on samples that had already been quantified by MESMER as a control (**Figure 5-5A**). A One-Way ANOVA showed no significant difference in Mn content as measured by MESMER or ICP-MS. In contrast, samples that had Mn extracted by MESMER and then assayed by ICP-MS had significantly less Mn than either MESMER or ICP-MS alone. When cells were not exposed to extracellular Mn, but exposed to MESM prior to measurement by ICP-MS, the intracellular Mn content of those cells

was significantly lower (>95%) than those exposed to vehicle (**Figure 5-5B**). This indicated that MESM could quantitatively release intracellular concentrations of Mn into the extracellular environment.

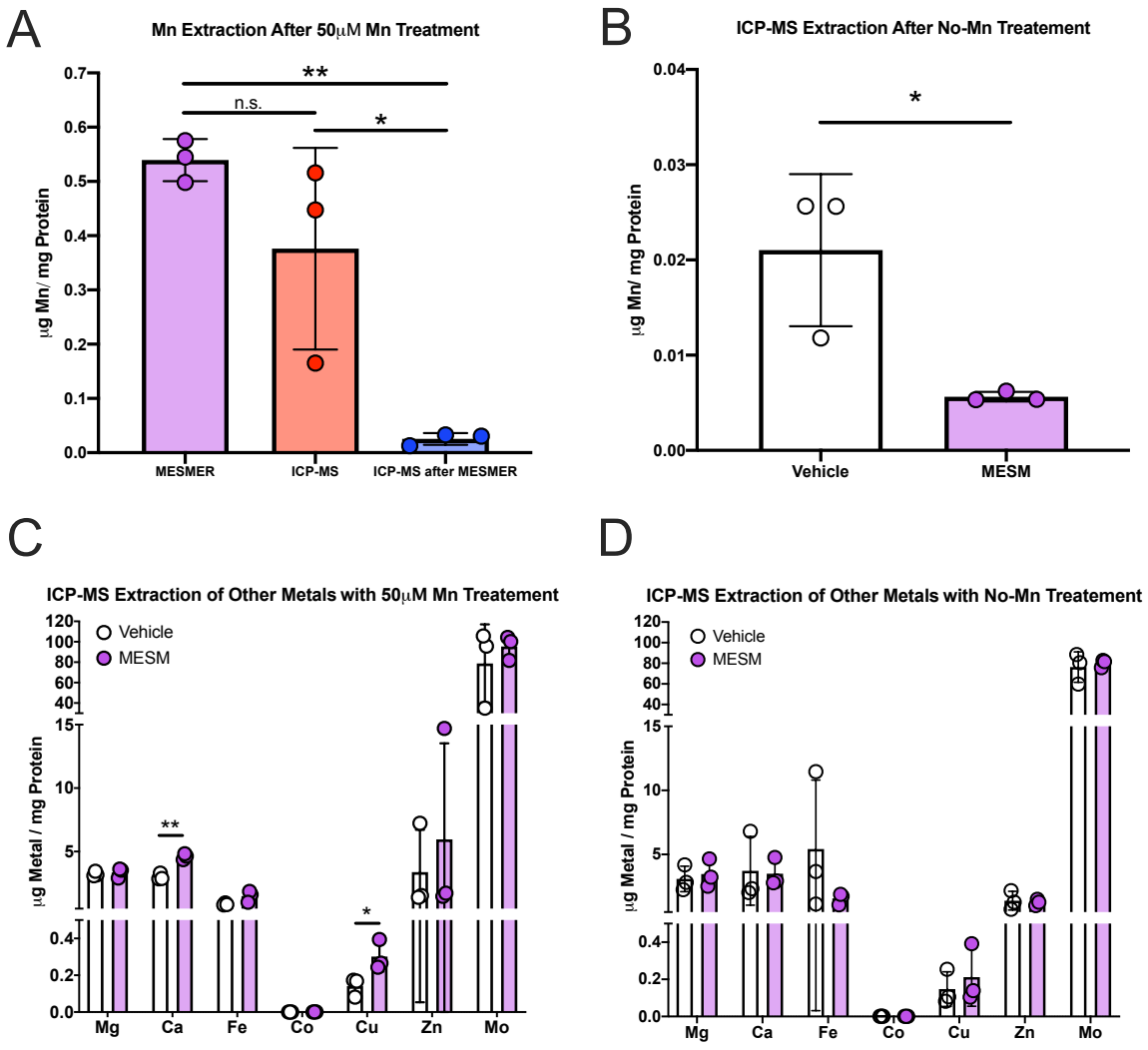

Figure 5-5. The MESMER assay yields comparable readouts to ICP-MS and is Mn-specific. Murine striatal neuron lineage STHdh Q7 cells were exposed to 50μM Mn in DMEM for 2 hours before being washed in PBS. Samples were subjected to MESMER, ICP-MS, or both (**A**). For comparison, some cells were not exposed to any extracellular Mn in DMEM, and received MESM or Vehicle prior to sample preparation for ICP-MS (**B**). Data was normalized to protein via a BCA assay of the samples. A One-Way ANOVA with Tukey's multiple comparison tests revealed a significant difference between the samples that were extracted with MESMER prior to ICP-MS compared to those samples that were just extracted with ICP-MS (*, $p < 0.05$). These samples extracted with MESMER prior to ICP-MS were also significantly different from samples that were just extracted with MESMER alone (**, $p < 0.01$). Importantly, there was no significant difference between the samples that were measured by MESMER alone or ICP-MS alone (n.s.). For the cells that received no Mn treatment in DMEM (**B**), there was a significant decrease of extracted Mn in those treated with MESM prior to ICP-MS, compared to those treated with Vehicle as measured by a two-tailed t-test (*, $p < 0.05$). ICP-MS for other divalents was analyzed in the samples that had Mn pre-exposed prior to extraction (**C**) or with Mn pre-exposure (**D**). There was a significant difference in Ca and Cu in (**C**) as measured by Student's two-tailed t-test (*, $p<0.05$; **, $p< 0.01$).

To understand the specificity of the effect that MESM might have on other essential metals, the content of magnesium, calcium, iron, cobalt, copper, zinc, and molybdenum were also measured by ICP-MS in the samples that were +/- MESM and +/- Mn. Since MESM is able to facilitate the movement of Mn out of the cell to the extracellular space, it was reasoned that it might do the same to other divalent metals. There was no statistical decrease in the levels of any other metal tested by ICP-MS when treated with 50μM extracellular Mn (**Figure 5-5C**) or no-Mn treatment (**Figure 5-5D**). As of result of MESM, the only statistically significant difference seen besides a decrease in Mn levels was a significant but small *increase* in calcium and copper levels limited to cells that have been previously exposed to Mn (**Figure 5-5 C, D**). The ionophore activity of MESM therefore appears to be Mn-specific.

MESMER and CFMEA extractions in hiPSC-derived cells

There exists a great value in developing a non-lethal method in hiPSCs given their utility for longitudinal studies across developmental trajectories. For example: being able to follow cells as they proceed from pluripotent state to post-mitotic neuroprogenitors, then to immature and mature neurons. Considering the model that stem cells can provide in terms of neurodevelopment toxicity (41), we sought to confirm that MESMER could provide quantification of Mn in hiPSC-derived Islet-1 positive striatal like neuroprogenitors (NPCs). Islet-1 positive striatal-like NPCs were exposed to varying concentrations of Mn for 1, 3, or 6 hours. After 6 hours, cells were returned back to Mn-free media for 1 or 6 more hours before being assayed. MESMER was able to detect expected concentration-dependent effects of Mn-exposure (**Figure 5-S3A**). Consistent and predictable time-dependent differences in Mn levels were also evident in these cells (**Fig. 5-S3B**). The cells that were returned to Mn-free medium before being assayed showed time-

dependent effects, where those allowed to incubate longer in Mn-free media had less cellular Mn measured.

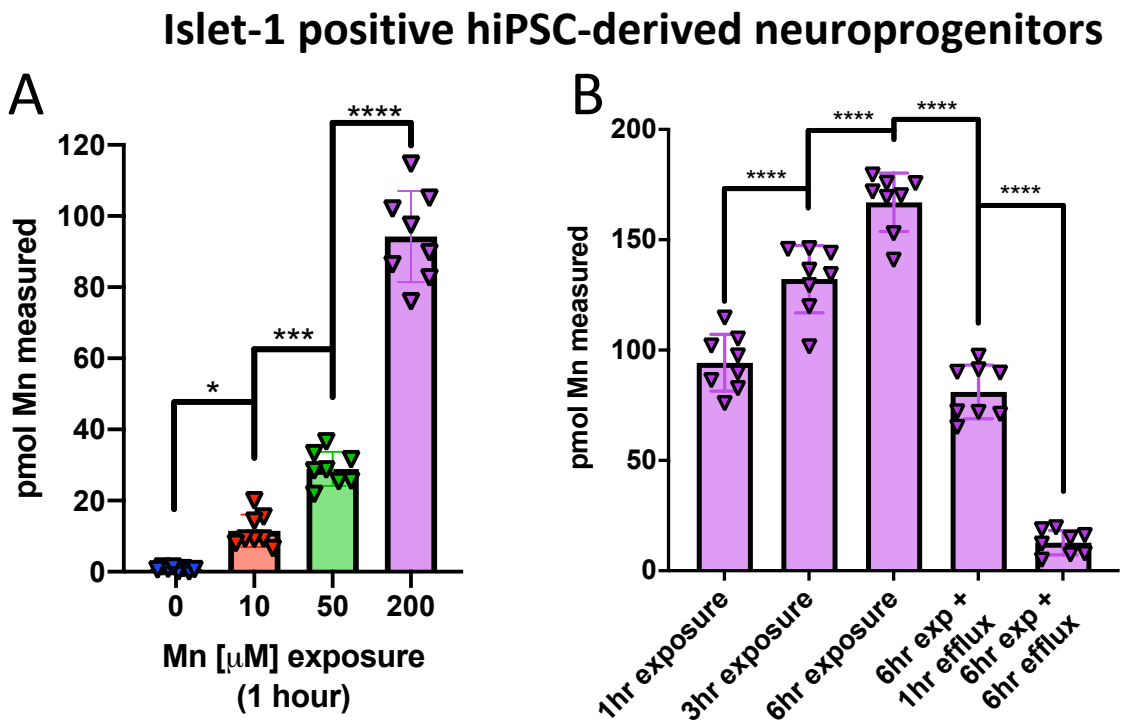

Figure 5-3S. Manganese extraction by MESMER in hiPSC-derived cells differentiated to day 11 striatal-like lineage, Islet-1-positive, neuroprogenitors, show time- and concentration-dependent effects of Mn exposure.
(A) Islet-1-positive NPCs were exposed to various concentrations (10, 50, 200μM) of Mn in medium for one hour. Two independent differentiations with 4 individual wells each, for a total N=8. Ordinary One-Way ANOVA with Tukey's multiple comparisons test. (*, $p < 0.05$; ***, $p < 0.001$); ****, $p<0.0001$). (**B**) At the highest concentration (200μM), cells were exposed for 1, 3, or 6 hours, combined with efflux conditions, where after Mn exposure, the medium was replaced with medium without Mn for 1 or 6 hours, thus allowing free efflux of Mn from cells, before assaying intracellular Mn with MESMER. MESMER was able to detect increases in intracellular Mn concentrations with increasing exposure times, and subsequent time-dependent decreases in Mn, after allowing Mn efflux from cells. Two independent differentiations with 4 individual wells each, for a total of N=8. Ordinary One-Way ANOVA with Sidak's multiple comparisons. (****, $p<0.0001$).

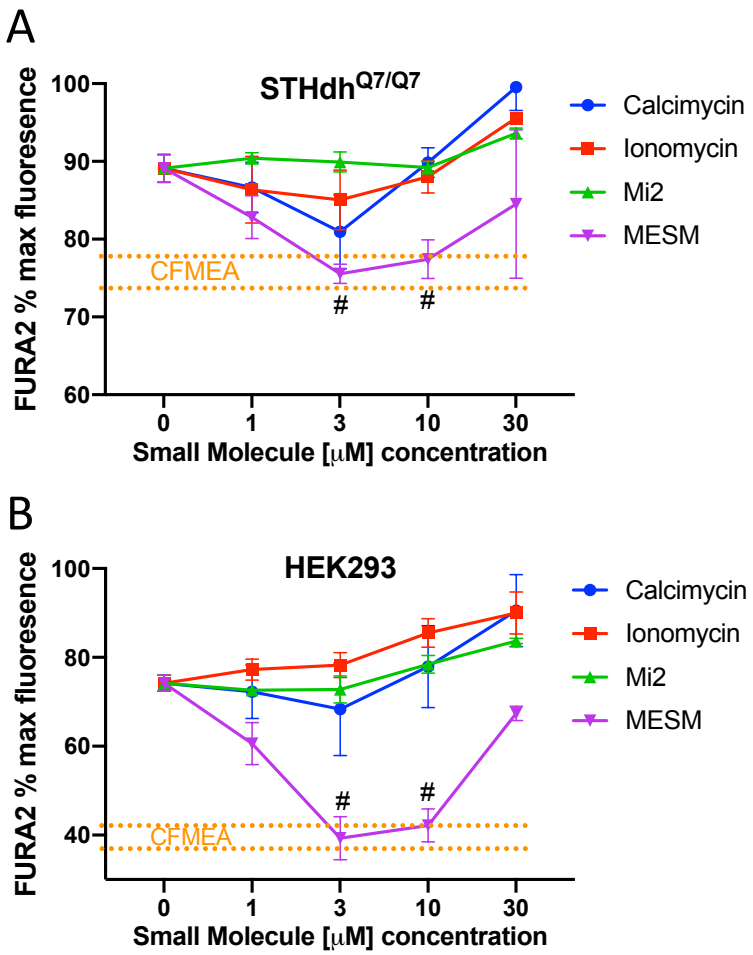

Figure 5-6. Extraction with MESM is comparable to CFMEA output from 3-to 10μM and outperforms other known Mn-ionophores. Murine striatal neuron lineage Q7 cells (**A**) or Human Embryonic Kidney (HEK) cells (**B**) were exposed to 100μM Mn for two hours at 37°C. Q7 cells (N=3-6) were exposed to Mn in HBSS and HEK cells (N=3) in DMEM, respectively. The cells were then washed five times in PBS (lacking Ca^{2+} and Mg^{2+}) and then exposed to 0.5μM Fura-2 and varying concentrations of calcimycin, ionomycin, Manganese Ionophore II (Mi2) or MESM for 15 minutes before reading at 360nm/535nm Ex/Em. A separate group of cells had Mn extracted by traditional CFMEA means after Mn exposure, for comparison. CFMEA dotted lines (in orange) denote range of one standard deviation from CFMEA average. Each point outside the orange lines is significantly different from CFMEA, as determined by a Two-Way ANOVA with Sidak's multiple comparisons. The points within the orange lines are not significantly different from CFMEA levels and labeled with a (#). Error bars represent standard deviation of all biological replicates.

MESM extracts Mn more efficiently than known Mn-ionophores without cellular toxicity

Despite its name, calcimycin (also known as A23187) is an ionophore with a higher affinity towards Mn^{2+} than Ca^{2+} (42,43). Of similar relation and function, ionomycin is another ionophore often paired with calcimycin (44,45). We tested if known Mn-ionophores such as ionomycin, calcimycin, or a commercially available molecule named Manganese Ionophore II (Mi2) could extract Mn in similar way as MESM. Effectively, the MESMER assay was performed except instead of MESM, ionophores (calcimycin, ionomycin, Mi2) were used at varying concentrations. MESM at varying concentrations were used as a control and a CFMEA performed at the same time for comparison (**Figure 5-6 A, B)**. Although there was an effect of concentration of calcimycin in the STHdh cells that approached the amount of Fura-2 quenching seen in the CFMEA, neither ionomycin, calcimycin, nor Mi2 yielded quenching of Fura-2 to the same degree as measured by CFMEA detergent lysis of the cells, at any concentration between 1 and 30µM. In contrast, Mn extraction by MESM was not significantly different from CFMEA at 3µM and 10µM in both cell types tested (**Figure 5-6 A, B**). Calcimycin continued to extract more Mn over time (as indicated by Fura-2 quenching), but even after 45 minutes failed to reach the CFMEA range (**Figure 5-4S**).

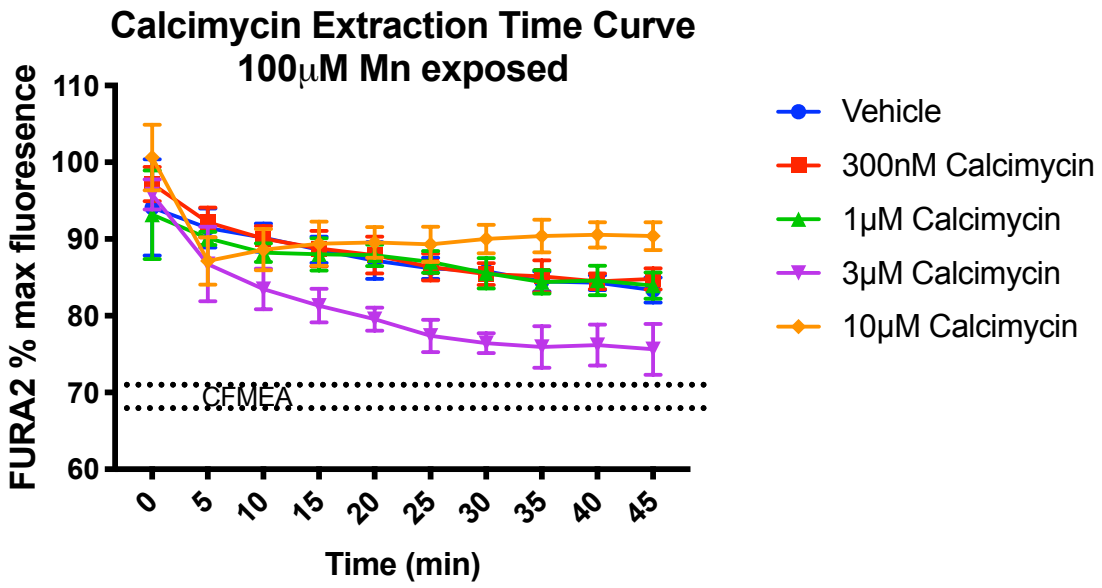

Figure 5-4S. Calcimycin continuously extracts Mn over time, but fails to reach the CFMEA range. Murine striatal neuron lineage Q7 cells were exposed to 100μM Mn in HBSS for two hours at 37°C. Cells were then washed five times in PBS (lacking Ca^{2+} and Mg^{2+}) and then exposed to 0.5μM Fura-2 and varying concentrations of calcimycin for 45 minutes. Fluorescence was read every 5 minutes at 360nm/535nm Ex/Em. A separate group of cells had Mn extracted by traditional CFMEA means after Mn exposure, for comparison. CFMEA dotted lines (in black) denote range of one standard deviation from CFMEA average. Each point outside the black dotted lines is significantly different from CFMEA, as determined by a Two-Way ANOVA with Sidak's multiple comparisons. Error bars represent standard deviation of all biological replicates.

Following the exposure to ionophores of different concentrations, the STHdh and HEK cells were tested for viability using the Cell-Titer Blue (CTB) Assay. Viability is significantly reduced in STHdh and HEK293 cells with concentrations of calcimycin 3μM and higher (**Figure 5-7 A, B**). Ionomycin also reduces cell viability at concentrations at or above 10μM in HEK293 cells and above 30μM in STHdh cells. As previously demonstrated (39), MESM does not significantly alter viability in STHdh cells or in HEK293 cells below 10μM (**Fig. 7a-b**). In an assay of membrane integrity, neither MESM nor the other ionophores were significantly different than vehicle. As a positive control, triton was used to disrupt membrane integrity (**Fig. 7c**).

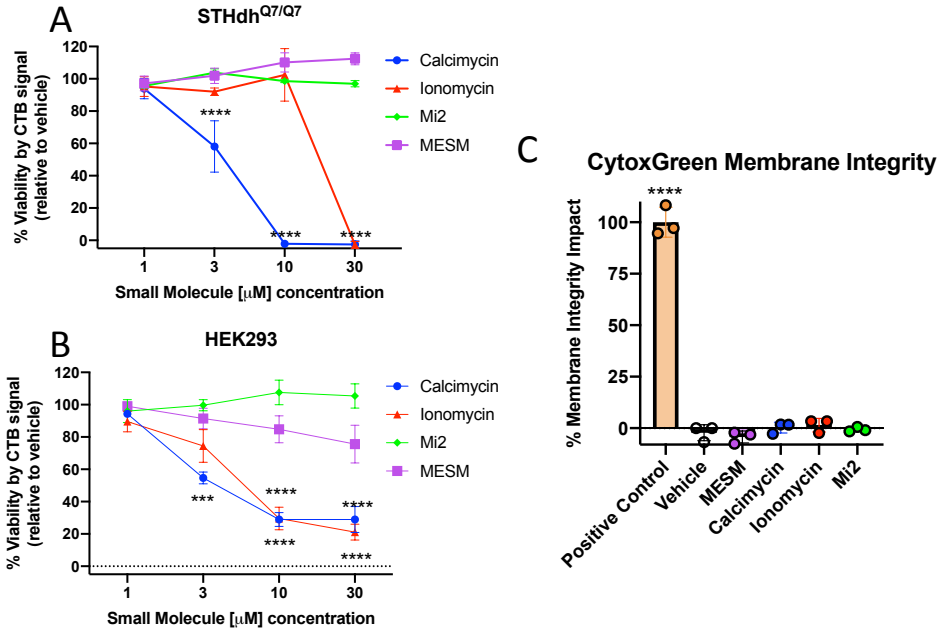

Figure 5-7. MESM exposure during the assay does not affect viability as measured by the Cell Titer Blue Assay (CTB) or membrane integrity as measured by CytoTox Green Assay. Following Mn treatment and ionophore extraction/treatment the ionophore/PBS mixture was removed from Q7 cells (**A**) or HEK cells (**B**) and were put back into their regular DMEM for 24 hours at 37°C. An injection of 20μL of CTB reagent was added to each well and returned to the incubator for another 2 hours before measuring the absorbance of each well at 590nm. N=3-6 biological replicates for Q7 cells (**A**), N=5 for HEK cells (**B**) The Cell Titer Blue Assay relies on viable cells to reduce the reagent resazurin to a fluorescent product- see methods section. Signal of vehicle conditions were normalized to 100%, and a Two-Way ANOVA with Sidak's multiple comparisons test to vehicle for every condition was used. Significance from vehicle denoted by (*, $p < 0.05$; **, $p < 0.01$; ****, $p < 0.0001$). (**C**) A separate measure of toxicity was used as validation at the most effective extraction and least toxic by CTB conditions (3μM compound) in Q7 cells called CytoTox Green. It is based on membrane integrity, so that a dye will fluoresce if it binds DNA- see methods. N=3 of independent biological replicates for all. Error bars shown represent standard deviation of average across biological replicates. One-Way ANOVA with Dunnetts multiple comparisons only shows significant statistical difference from vehicle in the positive control, which was 0.1% triton X100.

MESM facilitates the transport of Mn independent of cellular metabolism or cell surface proteins

The ability of MESM to transport Mn in or out of a cell based on a concentration gradient suggests an activity consistent with an ionophore. An ionophore would not be expected to be dependent on cellular metabolism for its mechanism. To test the hypothesis that MESM does not depend on cellular metabolism to move Mn across cell membranes, STHdh cells were co-exposed with MESM and Mn at 37°C or on ice to limit cellular energetics and ATP metabolism. In

comparison to cells co-incubated with MESM and Mn at 37°C, cells co-incubated with MESM and Mn while on ice accumulated Mn by the same quantity (**Figure 5-8A**). This is in contrast to other known "Mn-increasers" such as VU0026921 or VU003765, which have significant decreases in net Mn uptake when co-incubated on ice.

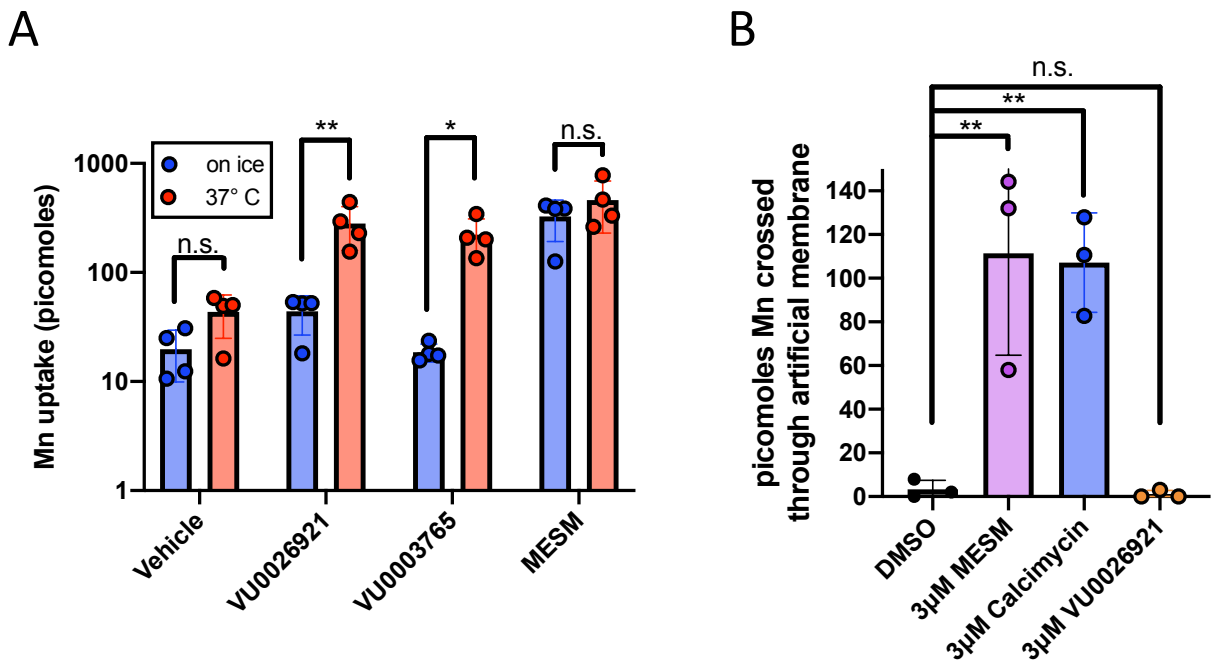

Figure 5-8. MESM transports Mn independent of cellular metabolism or transmembrane proteins. (**A**) Q7 cells were co-incubated with 100μM Mn and 10μM MESM, two other known "Mn-increasers" (VU0026921 and VU0003765) or equivalent vehicle for 2 hours at 37°C or on ice (N=4). Cells were then washed 5 times in PBS and then CFMEA extraction was performed. In contrast to the other "Mn-increasers", MESM does not lose any ability to move Mn into the cell while on ice and ATP is limited. Significance from a Two-Way ANOVA with multiple Sidak's comparisons test is denoted by (*, $p < 0.05$; **, $p < 0.01$). (**B**) A parallel artificial membrane permeability assay (PAMPA) shows the results of an incubation with 2μM Mn on one side of the artificial membrane for 30 minutes when paired with DMSO (vehicle), 3μM MESM, 3μM Calcimycin (Mn-ionophore; positive control), or 3μM VU0026921 (another "Mn-increaser" capable of binding Mn). Fura-2 quenching is measured on the receiver side (opposite end) of the artificial membrane, showing that Mn can cross this lipid layer only in the presence of a known ionophore (calcimycin) and purported ionophore (MESM). Statistical significance was determined by a One-Way ANOVA (N=3) and is denoted by (**, $p < 0.01$; or n.s., not significant). N=3 independent plates performed on different days.

Regarding a mechanism of action, we sought to distinguish the possibility between MESM modulating cell-surface ion transport proteins to become Mn-permeable, from MESM itself

forming a Mn-permeable pore or directly facilitating the passage of Mn across cell membranes. To test whether MESM needs cell-surface proteins to transport Mn, we used an artificial membrane to see if Mn transport across it was possible with MESM. We found that while the artificial membrane was impermeable to Mn, co-incubation with MESM facilitates Mn transport (**Figure 5-8B**). This is similar behavior to known Mn-ionophore calcimycin, but in contrast to a second small molecule increaser of net Mn uptake known to bind Mn, VU0026921, which is unable to transport Mn across the artificial membrane (**Figure 5-8B**). Finally, we tested whether MESM requires co-exposure with Mn to promote subsequent Mn transport across membranes. When STHdh cells were pre-treated with MESM, and then washed off prior to a Mn exposure, the cells accumulated more Mn compared to a vehicle pre-treatment (**Figure 5-5S**). This suggests that MESM may partially permeate the cell during the pre-exposure (and Mn is not required to be present for this action). However, pre-treatment alone to MESM led to lower overall Mn accumulation than co-treatment of MESM with Mn exposure. This suggested that the presence of Mn promotes the process by which MESM alters membranes to be Mn permeable. This links MESM with Mn, implying a physical interaction between them.

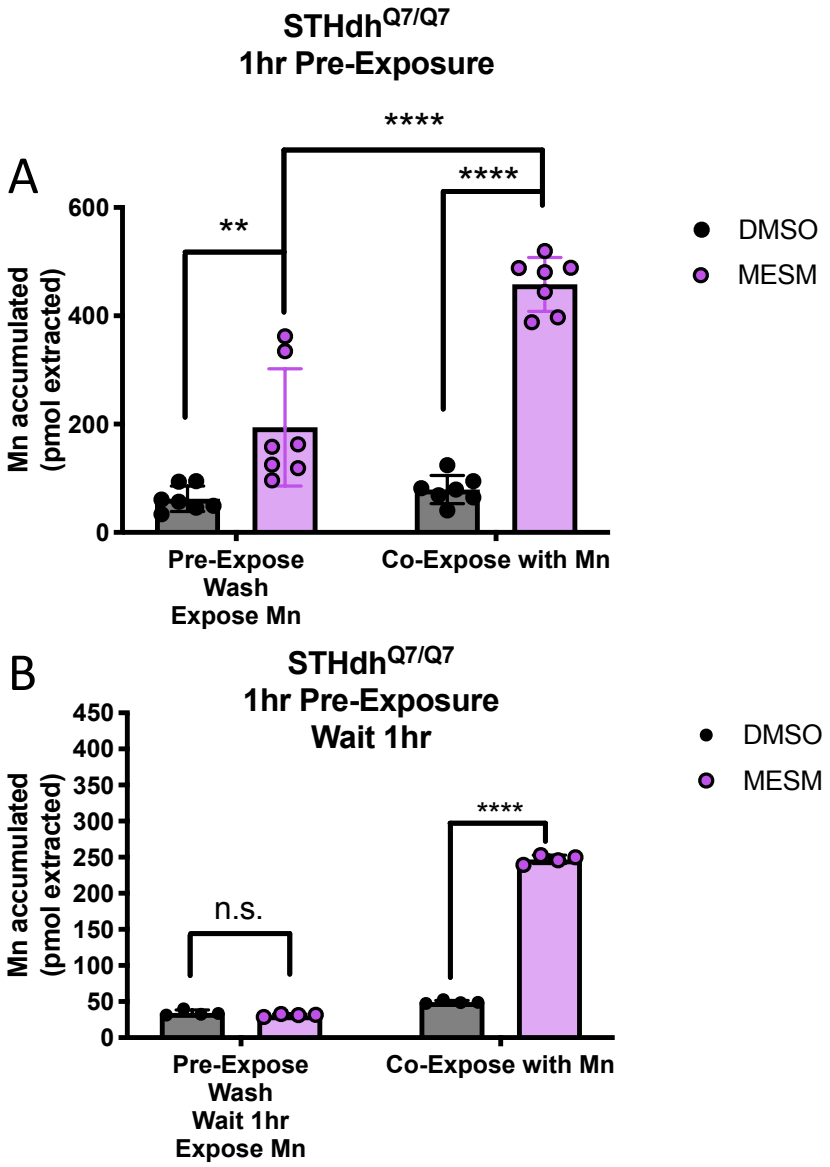

Figure 5-5S. Cells pre-exposed to MESM, but washed prior to Mn exposure, show a similar trend to cells co-exposed with MESM and Mn.
(**A**) STHdh cells were pre-exposed to 10μM MESM or Vehicle equivalent for one hour before washing off with HBSS and adding 125μM Mn for one hour. These cells were compared to cells co-exposed with 125μM Mn and 10μM MESM or equivalent Vehicle for one hour. Mn accumulation was measured by CFMEA. N=7. A Two Way ANOVA showed a main effect for MESM/DMSO ($p < 0.0001$), a main effect for pre-exposure/co-exposure ($p < 0.0001$), and a significant interaction ($p < 0.0001$). In Sidak's multiple comparisons test, significance is denoted by **($p < 0.01$) or **** ($p < 0.0001$)**.** DMSO controls for each exposure paradigm (black bars) were not statistically significant from each other in Sidak's multiple comparisons test. If a similar experiment is run but the cells are incubated an extra hour in between MESM pre-exposure and Mn exposure (**B**), the effect of MESM on Mn accumulation is lost (n.s.).

MESM does not transport calcium across the plasma membrane

While considering that other Mn ionophores such as ionomycin and calcimycin have a significant affinity for Ca^{2+}, we tested the hypothesis that MESM could transport Ca^{2+} across the cellular membrane as well as Mn. HEK293 cells were loaded with the Ca-sensitive fluorescent dye, Fluo-4 (46), prior to adding varying concentrations of calcimycin, ionomycin, Mi2, and MESM. Cells were imaged in real time upon adding the ionophores. As expected, the fluorescence of the cells (indicating increased calcium) following 30μM ionomycin or calcimycin began to spike after just 15 seconds, and peaked around 40 seconds. In contrast, a change in fluorescence was not detected following 30μM MESM or Mi2 even after five minutes, indicating that both MESM and Mi2 do not alter intracellular Ca^{2+} concentrations (**Figure 5-9**).

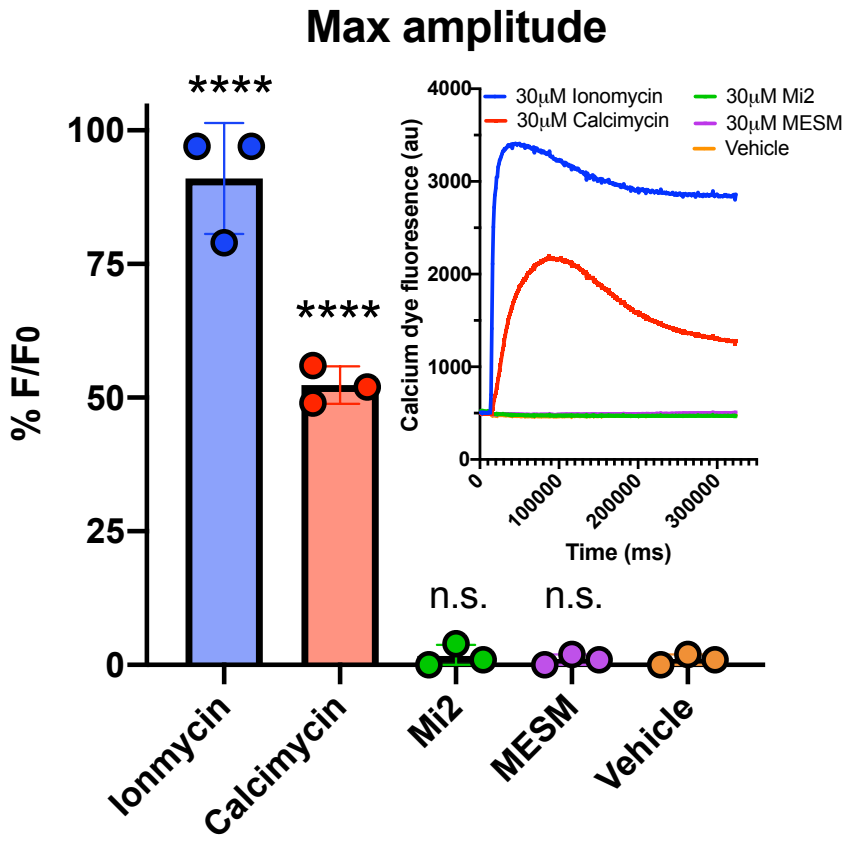

Figure 5-9. MESM does not influence intracellular calcium. HEK293 cells (N=3, each experiment performed in triplicate wells) were plated the day before experiment at 15,000 cells per well and grown until 100% confluency. Cells were soaked with Fluo-4 dye 1 hour at room temperature prior to adding varying concentrations of MESM, ionomycin, calcimycin, and Manganese Ionophore II (Mi2) ranging from 3nM to 30μM. Shown here is the maximum concentration (30μM). Using the PanOptic to measure fluorescence every second for 5 minutes, ionophore from a donor plate was added to the acceptor plate containing cells. Fluorescence was measured at 482 ± 16 nm excitation and 536 ± 20 nm emission. Inset shows a representative trace of each ionophore at maximum concentration (30μM). The maximum amplitude was calculated after normalizing for light variations with a static ratio and subtracting background. Percent fluorescence was normalized to the maximum fluoresced wells in each plate (30μM Ionomycin). An Ordinary One Way ANOVA was performed with Dunnett's multiple comparisons test. Statistical significance from Vehicle is indicated as n.s. (not significant) or **** ($p < 0.0001$).

A novel longitudinal Mn exposure assay to determine if Mn transport is altered by prior Mn exposures in cultured cells

It is currently unknown if cells alter Mn transport properties after prior exposure to elevated levels of extracellular Mn. With a validated MESMER assay capable of longitudinal studies, we

set out to test the effect of continuous Mn exposures in cell cultures over the course of eight days. We designed a parallel experiment in which individual wells are assayed by MESMER without prior Mn exposures, matched for the duration in culture.

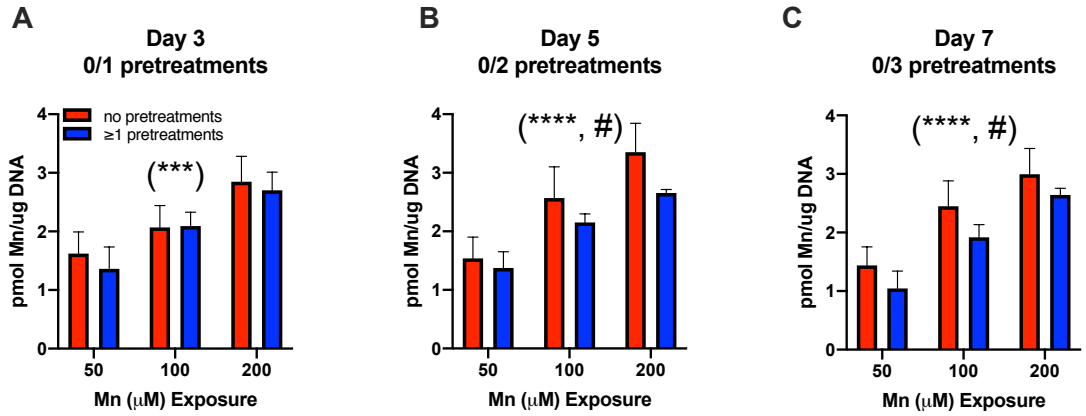

Figure 5-10. First attempt at a repeated, MESMER longitudinal study. By Two-Way ANOVA: there is a main effect for Mn concentration in all days tested. In the same Two-Way ANOVAs, there is a main effect for pre-treatment when tested on day 5 (B) and on day 7 (C), but not day 3 (A).Those that were pre-exposed (in blue) are lower than those not pre-exposed (in red) in Figure 9B and 9C- corresponding to 2 and 3 pre-exposures, respectively. This was the statistically significant main effect of pre-treatment. Post hoc tests following the Two-Way ANOVA were not significant .N=3.

We expected that post-hoc tests would be significant, with more experiments. This was only an N=3. For this reason, we did another 3 experiments to increase our power, however not only did we not achieve post-hoc significance but also we lost significance of the main effect of pre-treatment type (**Figure 5-11**).

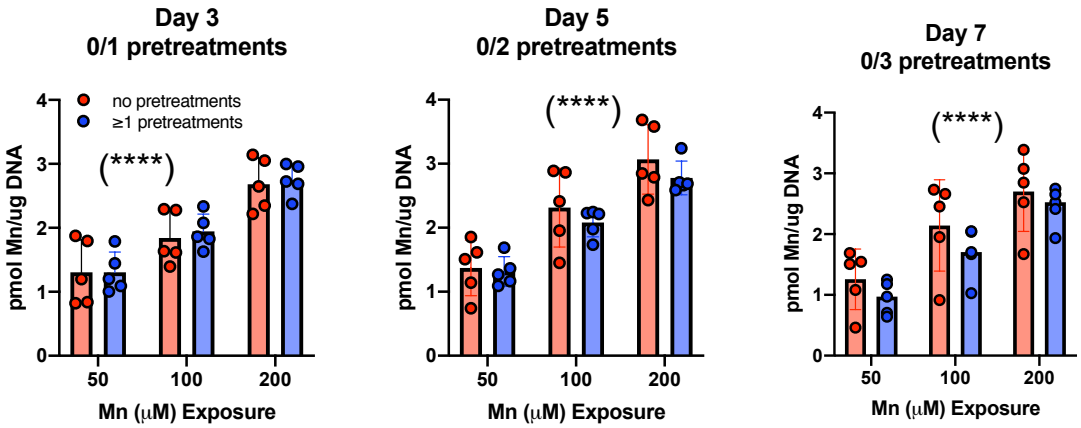

Figure 5-11. The results of an N=6 study, based on the N=3 in Figure 10 and three more biological replicates.

This indicated that we perhaps were on the cusp of an effect, where some cells responded with a homeostatic response but others did not. We hypothesized that 48 hours was too long to later detect clear changes made in cellular uptake/efflux, and we would see a greater effect if we shortened it. Therefore, we shortened the gap time from 48hrs in between exposures to 24 hours. We performed 2 independent trials with 12 wells each per condition:

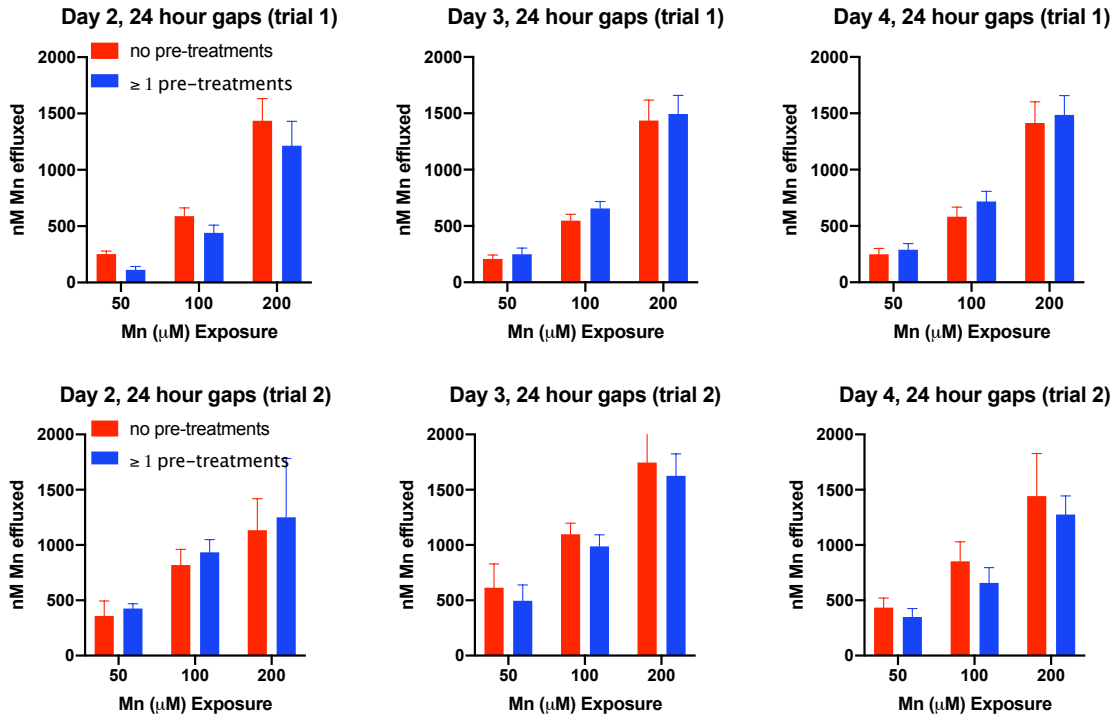

Figure 5-12. Two more independent trials of experiments outlined in Figure 11, but using a 24 hour gap period between measurements instead of 48 hours.

We still did not see a consistent effect of pre-treatment even after shortening our 2-hour long exposures to every 24 hours. Therefore, we decided to remove the gap period entirely and do continuous Mn exposures, and then measure Mn accumulation with MESMER every 24 hours. We had to lower the concentration of the Mn exposures since 100mM and above would be toxic long term, so we exposed cells to 1, 10, or 50 micromolar Mn. We did 2 independent trials with 6 independent wells in each condition. Due to the lack of change that we see between pre-treatment groups in acute exposures previously, and the clear effects that we see with continuous Mn exposure at 50 micromolar, we have replaced **Figure 5-10** in the JBC publication.

Cells were continuously exposed to 1, 10, or 50μM Mn concentrations over the course of eight days and compared to control cells that received Mn only for the first time, for 24 hours, matched for days in culture post-plating. These were controlled for with multiple wells seeded the same day (Day -1), so the plate being MESMER-ized on any day has control wells for comparison

that is the same age and is receiving Mn for the first time. In addition, we had previously verified that multiple MESM exposures did not affect Mn uptake (**Fig. 5-6S**). To minimize cell growth over time, the cells were kept at 37°C degrees starting at Day 0. These cells are conditionally immortal at 33°C, as higher temperatures lead to the destabilization of the temperature sensitive SV40 large T antigen and the cells substantially reduce proliferation.

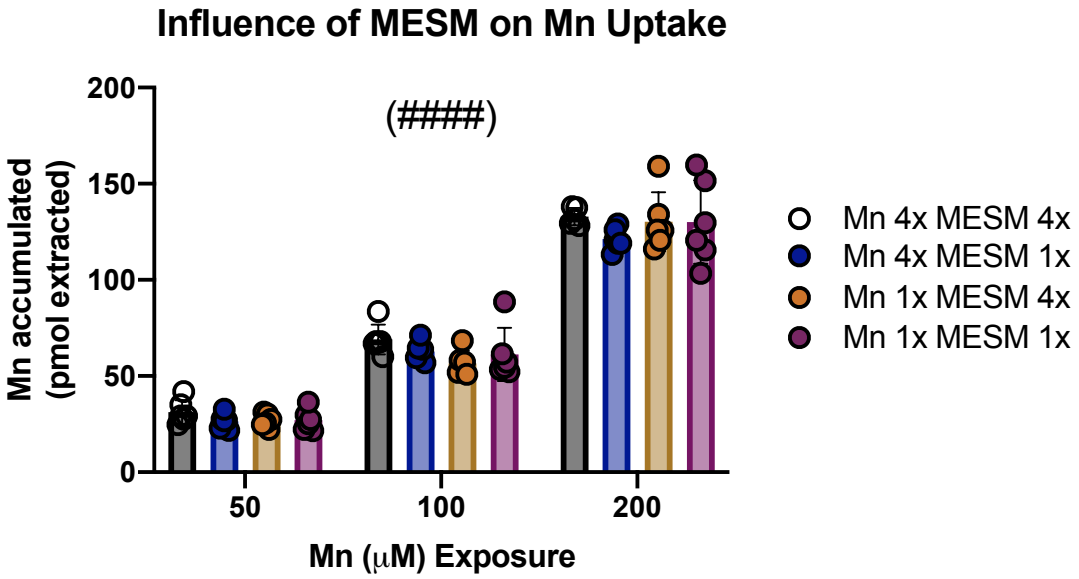

Figure 5-6S. MESM pre-exposures do not impact future Mn accumulation.
STHdh cells were exposed to Mn (50, 100, or 200μM) once per day for 2 hours in HBSS before being extracted with MESMER, or left without extracting. Afterwards the cells were washed in PBS and returned to media at 37°C. Each day, new cells that were plated at the same time but previously unexposed received Mn. This process occurred up to four times, until at last all cells were extracted by MESMER. A Two-Way ANOVA revealed a significant main effect (####, $p < 0.0001$) for Mn concentration, though no significant main effect for exposure paradigm.

Since MESMER allows for repeated Mn assessment of the same cells, we were able to measure the net uptake of Mn after each exposure in the same cell cultures. To our knowledge, this is the first report of longitudinal quantification of Mn in the same cell cultures. We hypothesized that cells that were continuously exposed to elevated Mn would accumulate less Mn over a 24-hour period than cells receiving Mn for the first time. We reasoned that this would occur

due to compensatory homeostatic responses to decrease net Mn uptake (perhaps via down-regulation of uptake transporters), though this might depend on the concentration of Mn exposed.

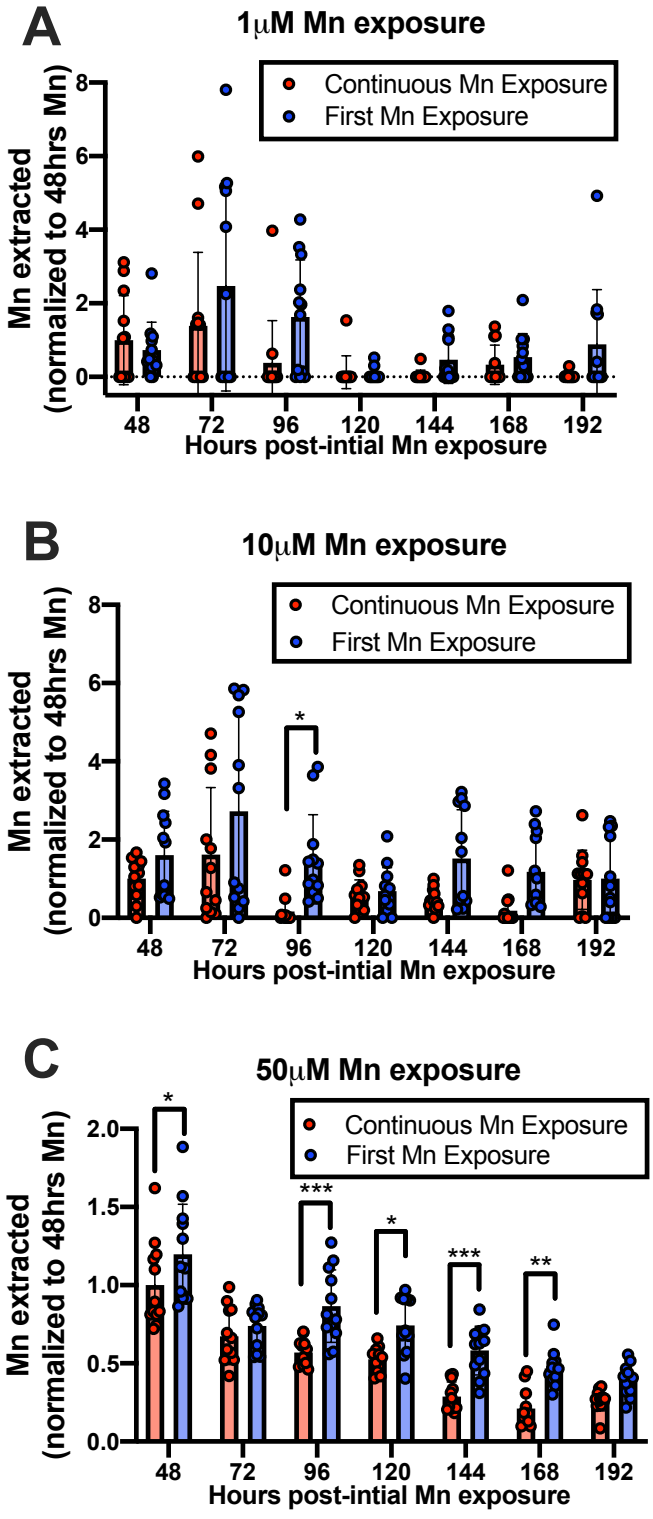

Figure 5-13. Continuous Mn exposure to neuronal cultures leads to decreased Mn accumulation relative to cells exposed to Mn for the first time. STHdh Q7 cells were exposed to 1, 10, or 50μM $MnCl_2$ in cell medium at 37°C. Every 24 hours, control cells (Continuous Mn Exposure) were washed with PBS and assayed with MESMER so that intracellular Mn could be quantified, and then returned to media with Mn (in red). Every 24 hours, new cells that were previously unexposed to Mn, but the same age as the control, were exposed to Mn for the first time and MESMER-ized 24 hours later (in blue). N=12 for each group, across two independent trials. Each point represents one well of cells. A Repeated-Measures Two-Way ANOVA analysis showed significant main effects for number of hours at all Mn concentrations ($p<0.0001$; panels **A-C**). There was also a main effect of treatment type (panels **A-B**, $p<0.01$; panel **C**, $p<0.0001$) but no significant interaction between the two at any concentration exposed. Sidak's multiple comparisons confirmed significant differences in Mn extracted from cells between treatment groups (*, $p<0.05$; **, $p<0.01$; *** $p < 0.001$).

STHdh cells were plated on Day -1, brought to 37°C on Day 0, and treated with 1, 10, or 50μM Mn began on Day 1. Every 24 hours, cells were assayed by MESMER, and then returned to media containing the same Mn concentration as before. Every 24 hours new cells received Mn for the first time, and MESMER would assay their uptake 24 hours later. The first direct comparison between treatment type (Continuous or First Exposure) occurred at 48 hours post-initial Mn exposure of the controls. The results were analyzed by a Repeated Measures Two-Way ANOVA for each exposure concentration. There was a significant main effect of day (hours post-initial Mn) seen at each concentration (####; $p<0.0001$; **Figure 5-10 A, B, C**). There was also a main effect of treatment type (Continuous or First Exposure), (&&, $p<0.01$; &&&& $p<0.0001$) in all three concentrations exposed (**Figure 5-9 A, B, C**). Furthermore, Sidak's multiple comparisons noted significant differences between treatment type groups at specific days (*, $p<0.05$; **, $p<0.01$; *** $p < 0.001$).

It is noteworthy that by using MESMER to perform this experiment, compared to multiple CFMEA plates for each time-point, the experiment took (one) 96-well plates x (three) biological replicates = (three) 96-well plates total. In contrast, multiple CFMEAs would require (four) 96-

well plates just for one replicate, and twelve plates total for three replicates. This MESMER experiment was four times smaller, saving the cost of 864 wells worth of cells and reagents.

DISCUSSION

Here we report on the identification of a small molecule in an efflux screen of Mn influencers, and demonstrate it shows functional properties consistent with being a selective ionophore for Mn (47). We have adapted this small molecule as a tool and modified an assay around it to assess intracellular Mn accumulation. We then used this assay to examine a basic scientific question about cellular Mn homeostasis and compensatory changes due to prior exposures. Advancements in technology and innovation drive research science discoveries. Thus, in this case, we were lacking the ability to quantitatively measure Mn concentrations in living cells without killing them, a "necessity" for data concerning biological Mn research. Altered Mn biology has been implicated in neurodevelopment and multiple neurological motor disorders, such as Huntington's Disease, and a Parkinsonian-like condition known as manganism (1). Patients with genetic mutations encoding proteins implicated in Mn-homeostasis can suffer from manganese toxicity with symptoms ranging from motor impairment to liver cirrhosis (8–18, 41, 42).

Current assays of intracellular Mn measurements (except using Fura-2 AM- which is responsive to cytosolic (50) Mn specifically as the dye does not typically penetrate intracellular organelles and provides relative quantification or semi-quantitative measures only (27, 46)) require lysis of the cells being studied, which restricts longitudinal experiments and multiplexed outcome measures. This includes the CFMEA, which has been previously validated by AAS (38). In addition to this limitation, it's a time and financial burden to kill cells that may have required

substantial funds and time to grow. For example, the differentiation of hiPSCs down the floorplate lineage to make mature (150 day) dopamine neurons currently costs approximately $1,000 per multi-titer plate (calculations not shown). For this reason, it is notable that we are able to quantify concentration and time dependent effects by MESMER in NPCs (**Fig. S3**). This opens the door for any future experiments with hiPSC-derived cultures- and fully takes advantage of repeatability/non-toxicity of the assay that would normally be a financial and time burden in lethal assays.

We postulate that MESM is acting as an ionophore at the cell surface, so that Mn ions may move in either direction; whether there is net efflux or accumulation would depend on the relative concentration of Mn in the cytosol versus extracellular space. Thus under different contexts (e.g. high extracellular Mn, or previous Mn exposure followed by low extracellular Mn) it may induce a net increase or decrease in cellular Mn levels following the direction of the Mn concentration gradient. The differences between the net Mn efflux and net Mn accumulation experiments (e.g. **Fig. 5-1 C** vs **D**) are due to differences in the direction of the Mn concentration gradient. For the efflux experiments, cells are first exposed to high extracellular Mn to "load" more Mn into the cells. Then the extracellular Mn concentration is brought back to low again as the extracellular Mn is washed away. This creates a concentration gradient of Mn to move outside (efflux) from the cell, and this is greatly facilitated when MESM is then added. In contrast, if MESM is instead simply co-exposed with micromolar Mn, and extracellular Mn is kept high, Mn will accumulate more with MESM than vehicle alone. This data suggest that cytosolic levels of Mn are lower than the extracellular concentrations we are exposing to - thus leading to a net influx of Mn.

MESMER allows total intracellular Mn to be quantified by equilibrating total cellular Mn with the extracellular buffer where it is quantified by Fura-2 quenching. Given the small total intracellular volume of the cultured cells in one well (approximately 100-1000 nL), compared to the 100 µL extracellular volume Mn is extracted in; the dilution of intracellular to extracellular Mn is at least 1:100. Thus, provided MESM enables a Mn equilibrium where intracellular and extracellular Mn concentrations are the same, the majority of total Mn (>99%) would be extracellular and quantifiable by Fura-2 quenching. This is supported by the ICP-MS data (**Fig 5-5A**), where the Mn remaining after MESMER, as measured by ICP-MS is not zero, but approximately 1% of the total Mn effluxed by MESMER.

The results of the ICP-MS analysis (**Fig 5-5**) independently confirm that MESMER is accurately and precisely measuring Mn content. Indeed, the ionophore appears to be Mn specific; other divalent metals are not depleted from the cell by MESM exposure, whether extracellular Mn is added or not. Notably, there is a small but statistically significant increase of Ca^{2+} and Cu^{2+} from vehicle to MESM treated, as measured by ICP-MS, however several aspects make this statistic misleading. First, is that the cells are washed with PBS prior to extraction with MESM, and this efflux buffer contains no added Ca^{2+} or Cu^{2+}. In other words, there aren't any extracellular sources that Ca^{2+} or Cu^{2+} could be coming from to increase Ca^{2+} or Cu^{2+} in the cell. Second, under these conditions, the concentration gradient is facing outwards, so an ionophore would only move Ca^{2+} or Cu^{2+} out of the cell, rather than in. Thus we postulate that Ca^{2+} and Cu^{2+} are normally lost from the cell during the wash process, but MESM is decreasing this loss only in cells which had previously been exposed to Mn. Third, calcium transport experiments following ionophore

exposures (**Fig. 5-9**) previously confirmed the null affinity MESM has for Ca^{2+}.

Lastly, we point out that the Ca^{2+} measured by ICP-MS is ^{44}Ca, rather than ^{40}Ca, which makes up only 2.9% of all Ca (^{40}Ca is not readable as it coincides with argon which is an important component used in the ICP-MS methodology). The amount of ^{44}Ca may not necessarily representative of all cellular Ca^{2+}, as isotope fractionation variability exists biologically (51, 52).

Regarding the efflux screen, one could hypothesize that the small molecules that increase net Mn uptake when co-incubated with Mn might do so by blocking efflux, or those that decrease net Mn levels do so by facilitating efflux. Combined with the data shown in **Figure 5-1S**, it is clear that whether a molecule was identified to increase or decrease net Mn levels did not predict an increase or decrease in efflux rates. However, the only molecule that was seen, based upon the N=2 screen, to substantially slow Mn efflux was in fact a "Mn decreaser"; VU00243195 (**Figure 5-1A; 5-1S**). This was the only one of six decreasers screened that had a significant impact with an altered $t_{1/2}$ value. Out of the 22 total, nine classified "increasers" had significantly different $t_{1/2}$ values than vehicle.

The two cell lines primarily used in this study were chosen because the STHdh cells are neuronally-derived from the striatum - an area of the brain that is particularly affected by Mn accumulation and toxicity. Furthermore, this cell line is amongst the most sensitive cell lines to Mn cytotoxicity with an LC50 value of ~1mM after 24 hours (31). These wild-type cells also have a HD model counterpart that demonstrates a clear deficit in Mn accumulation. HEK293 cells were chosen as they are a common human cell line used, and are quite dissimilar from a mouse neuronal

lineage, with an LC50 value of 2.1mM after 16 hours (53). As MESMER also was able to replicate concentration and time dependent effects of Mn on hiPSC-derived human striatal precursors- we would suspect that MESMER would work on most mammalian cell types (**Figure 5-3S**). This is further supported by our data showing that MESM does not appear to require energy or cellular transporters for its actions (**Figure 5-8A**)- so cell type differences in Mn transporters should not influence the ability of the assay to work. Of course, this does not mean MESMER will be effective in all types of cells. Of particular interest: specialized polarized cells such as enterocytes or hepatocytes may not be quantifiable with MESMER. This remains to be unseen. We should also note that due to the Ca/Mg –free conditions required for MESMER to detect Mn, this technique could not be used in animal tissue. MESM cannot influence intracellular Mn while in the presence of media (**Fig. 5-7S**), presumably due to the majority of the molecule being bound by protein in the serum.

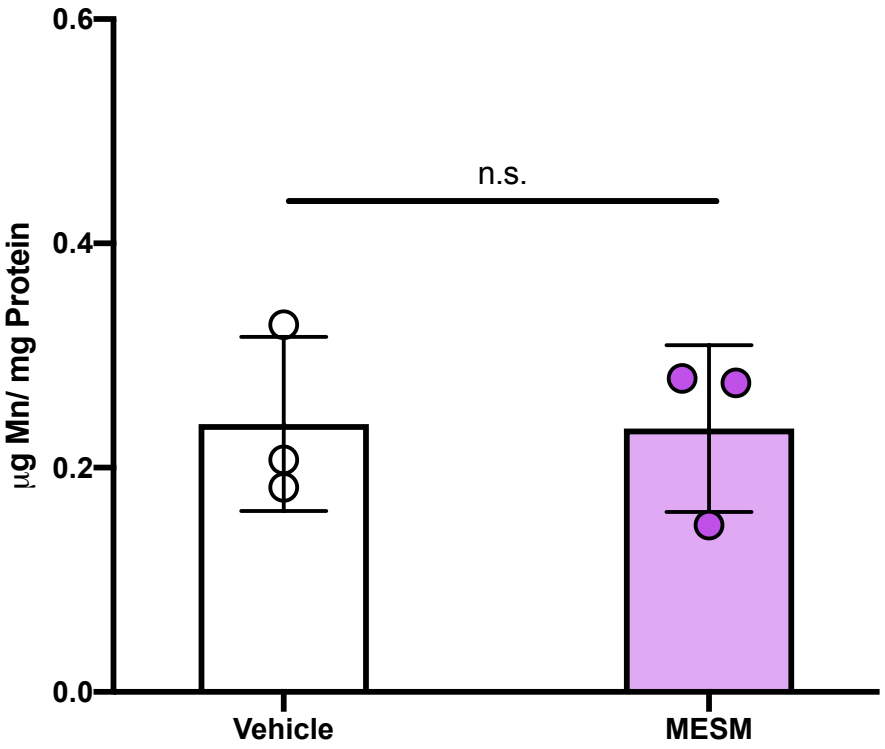

Figure 5-7S. MESM loses the ability to extract Mn when exposed in DMEM. STHdh cells were exposed to 50µM Mn for 2 hours prior to washing and the Mn-extraction step by 3µM MESM or Vehicle (DMSO). Samples were then prepared for ICP-MS. If MESM was active as an ionophore, one would expect to see a decline from Vehicle to MESM in µg Mn/mg protein, as intracellular Mn would have been extracted from the MESM-treated cells. The two conditions were compared using a two-tailed Student's t-test (not significant; n.s).

There are two broadly defined types of ionophores, namely channel forming and carrier-mediated (54). Our data suggests that MESM is the latter. The observation that co-treatment is significantly more effective than sequential treatment of MESM and Mn (**Fig 5-5S**), is more consistent with a mechanism of a carrier-mediated ionophore than one that forms a pore. Channel formers also tend to have a longer effect than carrier-mediated ionophores (54). When STHdh cells are pre-exposed to MESM for one hour, washed, and then incubated an additional hour before Mn exposure, no effect of MESM is seen (**Figure 5-5S**). This relatively fast degradation time is consistent with MESM not being a channel-former. Future studies can confirm this using planar lipid bilayers and measuring the rate of ion flux across the membrane. Ion channels are characterized by high transport rates and low temperature coefficients (47). One picoamp of current for a divalent ion is estimated to travel through a single channel at a flux of 3 million ions per second. In contrast, the fastest non-channel transporter has an exchange rate of 10,000 ions/s; carrier-mediated transporters are several orders of magnitude slower than channel-formers (47). From a thermodynamics perspective, carrier-mediated ionophores also have higher enthalpies of activation, corresponding to higher temperature coefficients, as defined by the change in rate of a reaction when the temperature is changed. Given that our data is consistent with MESM as a carrier-mediated ionophore, we would expect the temperature coefficient for MESM currents to be higher than reported values of channel-forming ionophores (47).

Future experiments should also explore the structure-activity relationship of MESM and Mn by testing similarly structured small molecules. It is noteworthy that MESM lacks a poly-ether motif common among ionophores, thus how it binds Mn is currently unknown. We suspect that at

concentrations above 10μM, MESM competes with Fura-2 for Mn-binding, and that is why Figure 5 is parabolic. This is not seen in Figure 2 since it does not go above 3μM, but this idea is supported in **Figure 5-2S**. Two structural analogs have already been tested in the screen: VU0028040 and VU0027832. They demonstrate a clear increase in the rate of efflux compared to vehicle, with $t_{1/2}$ values of 22.3 and 22.6 minutes, respectively (compared to vehicle of 79.1 minutes). However they still require an hour to release nearly 100% of Mn compared to MESM's 15 minutes **Figure 5-1SP; Figure 5-1SQ**; (39). Radiolabeled or fluorescent analogs could help tighten the kinetics of the molecule and help identify its localization within the cell, as it is currently uncertain where MESM is located at a subcellular level, though evidence supporting Mn uptake into the nucleus, mitochondria and Golgi apparatus have been reported (55–59). The use of a selective and cell permeable Mn sensor in combination with MESM would identify where MESM affects Mn within the cell (55,60). Considering how much Mn is accumulated within the cell during Mn/MESM co-exposure, (an amount much higher than predicted if only equilibrium is being reached), we hypothesize that MESM is only impacting transport of Mn across the plasma membrane or an extracellular-cytosol transporter- but not where Mn is being stored in a subcellular compartment. Most literature suggests that the majority of subcellular Mn is stored in the mitochondria (56–58,61). In this model, MESM would bring Mn from the extracellular space across the plasma membrane to the cytosol, where Mn is then taken up by a compartment not accessible to MESM-selective Mn permeabilization. MESM is thus able to promote an increase in total cellular Mn levels over time, while only maintaining equilibrium between the cytosol and extracellular space. Since the location of where MESM is binding at a subcellular level is unknown, likewise we do not know which proteins might be "de-metalled" following MESMER. This may have metabolic or homeostatic consequences not detected by our studies.

The experiments in **Figure 5-10** are the first longitudinal studies of cellular Mn levels performed in cultured cells of the same wells following continued Mn exposures. The results provide evidence of a compensatory homeostatic response to continuous elevated Mn exposures. While the overall decline in Mn uptake over time seen in **Figure 5-10C** is unprecedented, the magnitude in effect of treatment does not appear to change across time ranges between 48-168 hours. This effect (main effect of treatment type) can be detected with just a 1μM addition of Mn, well below the physiological concentration range of Mn in humans (20-55 μM). The effect size varies at the 1μM and 10μM levels up to 8-fold, which is at least in part due to the fact that the amount of Mn quantified was hovering around the detection threshold of the assay (approximately 100nM or 10 picomoles Mn), and the average amount of Mn detected in cells exposed to 1μM Mn is at or close to zero. It is noteworthy that when using higher concentrations of Mn (50μM), the max fold-change is only approximately 1.5 fold. In conditions where extracellular Mn is elevated above physiological intracellular levels (e.g. >100μM), no differences in Mn uptake were detected with prior Mn exposure (**Figure 5-11**). This suggests that cells are incapable of adjusting to extracellular Mn concentrations above their total intracellular concentration levels. Unfortunately, detection limits by the assay prevent us from investigating sub-physiological Mn homeostasis, though the importance of staying within physiological levels of Mn while studying Mn homeostasis should inform future experiments.

Physiological intracellular concentrations of Mn are in the low micromolar range; and 50μM represents the high end of that range (2). However, pathophysiological levels could be threefold higher, bringing us to around 150μM. We used exposure levels comparable to what is utilized in the literature to examine the biological effects of Mn toxicity in the absence of cell

death. These concentrations though are total tissue or cellular levels, with the majority believed to be intracellular. Extracellular levels of Mn are typically in the low 10-100nM range in serum and CSF. When we use MESM to equilibrate Mn between intracellular and extracellular, the high extracellular volume substantially dilutes the intracellular concentration, thus making detection of normal physiological levels not possible by Fura-2, which has a limit of detection near 100nM. The dynamic range for the assay is 10 picomoles to 3 nanomoles per sample in 100uL efflux buffer (96-well format).

MATERIALS AND METHODS

Cell Culture

STHdh$^{Q7/Q7}$ wild-type immortalized murine striatal derived cells (STHdh) were obtained from Coriell Cell Repository (Camden, NJ). They were plated at a density of 10,000 cells per well of a 96-well plate and incubated at 33°C with 5% CO_2 in Dulbecco's Modified Eagles Medium (DMEM; high glucose Sigma-Aldrich; D6546; St. Louis, MO) with 10% Fetal Bovine Serum (FBS; Atlanta Biologicals; Flowery Branch, GA), 1% Penicillin/Streptomycin (15140-122; Life Technologies; Carlsbad, CA), 2mM GlutaMAX (Life Technologies), 0.5 mg/mL G418 Sulfate, (Life Technologies) 1X Non-essential Amino Acids Solution (Life Technologies), 14mM HEPES (Life Technologies) for 24 hours prior to the assay. Cells were dissociated using 0.05% Trypsin-EDTA solution (Life Technologies).

HEK293 (human embryonic kidney cell line; ATCC) cells were plated at a density of 60,000 cells per well of a 96-well plate and incubated at 37°C with 5% CO_2 in Dulbecco's Modified Eagles

Medium (Corning; 15-013-CV) with 10% FBS and 1% Penicillin/Streptomycin for 24 hours prior to the assay. Cells were dissociated using 0.05% Trypsin-EDTA solution (Life Technologies, Carlsbad, CA).

hiPSCs Cell Culture

hiPSCs line was derived from a healthy male control subject, CD12, at the age of 53 with no family history of neurodegenerative disease (62). hiPSCs were maintained in mTeSR1 medium (StemCell Technologies, Vancouver, BC) on Matrigel (BD Biosciences, San Jose, CA) coated plates. hiPSCs were dissociated by incubating for 10 minutes in Accutase at 37°C (Innovative Cell Technologies, San Diego, CA), then centrifuged and resuspended in mTeSR1 with 10 μM ROCK inhibitor Y-27632 (Tocris) and replated at 100,000 cells/ml. Striatal neural differentiation was started after the hiPSCs cultures reached 100% confluency. Islet1 striatal differentiation was conducted for 10 days via dual SMAD neural induction protocol using LDN (4 μM) (Stemgent Cat. N. 04-0074) and SB431542 (10 μM) (Stemgent Cat. N.04-0010), but, in addition purmorphamine (0.65 μM) (Stemgent, Cambridge, MA) was added to pattern striatal NPCs. NPCs were replated at 300,000cells/mL. Additional details and validation of this differentiation method have been previously reported (29,31,63).

Mn efflux with small molecules

Cells (excluding NPCs) were washed twice with Hank's-Buffered Balanced Salt Solution (HBSS; with Ca^{2+} and Mg^{2+}; Gibco; 14025-092)) and exposed to varying $MnCl_2$ (AC205891000; Thermo Fisher Scientific; Waltham, MA) concentrations for 2 hours in HBSS and incubated at 37 degrees unless otherwise indicated. After incubation the cells were washed three times with Phosphate

Buffered Solution (PBS; lacking Ca^{2+} and Mg^{2+}) to remove the extracellular Mn. The cells were then incubated in *efflux buffer* (PBS containing 500nM Fura-2; Enzo Life Sciences) to allow for intracellular Mn to efflux into the extracellular space. Small molecules (or corresponding vehicle 0.1% dimethyl sulfoxide; DMSO; D8418; Sigma-Aldrich; St. Louis, MO) were often included in this efflux buffer to assess their impact on Mn efflux rates, as in Figure 1A. VU0026921 and VU0028386 (MESM) were synthesized at the Vanderbilt Synthesis Core. All other small molecules were obtained from the ChemBridge Library. The fluorescence of the Fura-2 in the efflux buffer was then measured at 360nm/535nm (Ex/Em) so that Mn concentrations could be quantified (Synergy H1 Plate Reader; Biotek). Mn was quantified based on standard curves previously described (38) and explained in brief below.

Cellular Mn level assay and extraction with triton/ Cellular Fura-2 Manganese Extraction Assay (CFMEA)

STHdh cells were exposed to varying Mn concentrations, at 37 degrees or on ice, in HBSS for 2 hours. Often other small molecules were co-incubated with the Mn in the HBSS to assess their impact on Mn levels, as in Fig. 1d. After incubation, the cells were washed three times with PBS (without Ca^{2+} and Mg^{2+}) to remove the extracellular Mn. *Extraction buffer* (PBS containing 0.1% TritonX100; Sigma-Aldrich; T8787; St. Louis, MO and 500nM Fura-2) was added to lyse the cells. The fluorescence of the Fura-2 in the extraction buffer was then measured at 360nm/535nm (Ex/Em) so that Mn could be quantified.

Manganese Quantification by Fura-2

A percent max of Fura-2 fluorescence 360nm/535nm (Ex/Em) was calculated for each condition as the corresponding zero Mn condition was defined as 100%. Background fluorescence was subtracted from all values. The concentration of Mn (nM) was calculated with the equation: $[Mn] = 1138 \times ((1 / \%max) - 1)^{0.9682}$, which was generated based on a standard curve of Mn quenching Fura-2 signal (40). The absolute values were calculated by multiplying by the concentration by volume.

Calcium Influx Quantification

HEK293 cells were plated the day before experiment at 15,000 cells per well and grown until 100% confluency. Cells were incubated with Fluo-4 AM (2 □M final concentration; ION Biosciences, San Marcos, TX) dissolved first in DMSO and then diluted in Hanks Balanced Salt Solution plus 20 mM HEPES pH 7.3 and 0.03% Pluronic F-127 (Sigma-Aldrich) for 1 hour at room temperature prior to adding varying concentrations of MESM, ionomycin (Sigma-Aldrich; I0634), calcimycin (Enzo Life Sciences; BML-CA100-0010), and Manganese (II) Ionophore II (Sigma-A1drich; 43359), ranging from 3nM to 30µM. Using the Panoptic kinetic imaging plate reader (WaveFront Biosciences, Franklin, TN) to measure fluorescence every second for 5 minutes, 20µL of ionophore from a donor plate was added to 20µL/well buffer (HBSS + HEPES; (Hanks Balanced Salt Solution + 20 mM HEPES pH 7.3; Thermo Fisher) in the acceptor plate containing cells. Fluorescence was measured at 482 ± 16 nm excitation and 536 ± 20 nm emission. The maximum amplitude was calculated after normalizing for light variations with a static ratio and subtracting background. Percent fluorescence was normalized to the maximum fluoresced wells in each plate (30µM Ionomycin).

Manganese-Extracting Small Molecule Estimation Route (MESMER)

Cells were exposed to Mn and washed in the same conditions as the CFMEA procedure. The difference was that after washing, *efflux buffer* was added containing MESM (3µM unless otherwise indicated) and incubated at 37°C for 15 minutes before reading fluorescence at 360nm/535nm (Ex/Em).

Continuous Mn treatments with MESMER

STHdh cells were seeded in DMEM on day -1 (10,000 cells/well) and incubated at 33 degrees until day 0. On day 0, cells were brought to 37 degrees. On day 1, the initial Mn exposure began on the control cells at 1, 10 or 50µM Mn in DMEM. From this point, every 24 hours these cells were washed three times in PBS (without Ca^{2+} and Mg^{2+}) and then MESMER-ized with 3µM MESM in *efflux buffer*. After 15 minutes the *efflux buffer* was transferred to a separate microplate that would have its fluorescence read at 360nm/535nm (Ex/Em). The cells were returned to media containing the same concentration of Mn exposed prior. Every 24 hours, for the next 7 days, new cells that were also plated on day -1 but previously unexposed were exposed to Mn in media. The new cells were MESMER-ized after 24 hours, and their *efflux buffer* fluorescence was read.

Multiple Mn pretreatments

STHdh cells were seeded in DMEM on day 0 (10,000 cells/well) and incubated at 33 degrees until day 1. Cells were washed twice with Hank's-Buffered Balanced Salt Solution (HBSS) and exposed to 0, 50, 100 or 200 µM Mn for 2 hours at 37 degrees. Afterwards, the extracellular Mn was washed off with three PBS washes and had *extraction buffer* added for CFMEA, *efflux buffer* with 3µM

MESM added for MESMER. After 15 minutes, the cells that were MESMER-ized had their fluorescence read and the efflux buffer was then carefully pipetted off and replaced with DMEM before returning to the incubator for 48 hours. For the cells lysed open by the CFMEA assay, a sample was kept of each well to have their DNA content measured. This process was repeated on Day 3, 5 and 7- corresponding to pre-exposures 1, 2, and 3, respectively. Cells that received multiple Mn pretreatments received it every 48 hrs until lysed by CFMEA.

Cell Viability and Membrane Integrity

Cells were washed twice with Hank's-Buffered Balanced Salt Solution (HBSS) and exposed to varying concentrations (1-30 μM) of MESM and other ionophores or DMSO vehicle in HBSS. After incubating for 2 hours at 37°C, the cells were placed back in DMEM (100μL per well) with 20μL Cell-Titer Blue (CTB) reagent added (Promega; G8081) for 3 hrs at 37°C. The CTB assay relies on viable cells to reduce the reagent reazurin to a fluorescent product. After incubation, the fluorescence of each well was recorded at $560_{Ex}/590_{Em}$. Percent fluorescence was normalized to the vehicle as 100%.

In separate experiments, STHdh cells were exposed to ionophore (3μM) or DMSO (0.03%) for two hours in HBSS and incubated at 37°C before adding CytoTox Green reagent (Promega; G8742) at a 1:2000 dilution. The CellTox Green Cytotoxicity Assay is based on the high fluorescence of a reagent when bound to DNA. The reagent will have higher access to DNA in cells with impaired membrane integrity and will fluoresce more. A positive control of 0.1% detergent was used. After 15 minutes the fluorescence was recorded at $495_{Ex}/525_{Em}$.

Parallel Artificial Membrane Assay (PAMPA)

The 96 trans-well assay plates (Corning Gentest; 353015) were kept packaged and frozen at -20 degrees until one hour prior to the assay. After warming up at room temperature, the membranes were soaked in PBS for another 90 minutes. Mn was added on the donor side of the sandwich membrane at 2μM in PBS, with 500nM Fura-2 in PBS on the opposite side of the sandwich (acceptor side). MESM, calcimycin, VU0026921, or DMSO were added with the Mn on the donor side at 3μM final so that there were equal volumes of buffer (300μL) on each side. The trans-wells were added together and incubated for 30 minutes before 100uL of the acceptor side was removed and placed in a new 96-well plate and read to assess Fura-2 quenching at $360_{Ex}/535_{Em}$.

Inductively-Coupled Plasma Mass Spectrometry (ICP-MS)

Samples were prepared from STHdh cells plated at 100,000 cells/mL and grown until confluency in 6-well plates. Cells were exposed to 50μM $MnCl_2$ in DMEM for two hours before washing three times with PBS. Cells were co-incubated with 3μM MESM or vehicle for 15 minutes. The cells were scraped, collected and spun at 200G for 5 minutes, then the supernatant was aspirated off the pellet. Cell pellets were collected for metal analysis by ICP-MS were resuspended in 100 μL RIPA buffer containing protease inhibitor (Sigma-Aldrich, St. Louis, MO) and phosphatase inhibitor cocktails 2 & 3 (Sigma, Sigma-Aldrich, St. Louis, MO). Cell lysates were centrifuged at 4°C for 10 minutes at 20,000 *g*. 20 μL of the lysates was used for quantifying protein concentration using the BCA assay (Pierce Technologies). Remaining 80 μL of the lysate was diluted (1:10) with 720 μL of concentrated nitric acid (70%) and incubated at 95° C for 40 minutes. All the samples were diluted with 2% nitric acid concentration with ultrapure water. To avoid potentially high results all the samples were further diluted 10-fold. Overall the dilution factor for these samples is 3150. Measurements were made on Thermo Fisher Element 2 ICP-MS instrument at the Purdue

University Analytical Mass Spectrometry Facility. The samples were analyzed for manganese (Mn) alone followed by the other metals including magnesium (Mg), calcium (Ca), iron (Fe), copper (Cu), cobalt (Co), zinc (Zn), molybdenum (Mo). Fresh samples were prepared for both analyses. Standards of 0.1 PPB was prepared for Mn by diluting 1000 µg/mL Mn in 2% nitric acid (Exaxol Corporation, Clearwater, FL). Standard of 0.1 PPB, 1 PPB and 10 PPB were prepared for all other by diluting a 68-element standard in 2% nitric acid (Exaxol Corporation, Clearwater, FL). All the samples were calculated as µg of metal per mg protein based on the protein concentration quantified.

DNA Quantification

Cells were lysed with 0.1% triton and 5µL from each well was added to 95µL Tris-EDTA buffer (Corning; 46-009-CM) with 1:800 PicoGreen Reagent (final; Quant-iT PicoGreen dsDNA Assay Kit; Invitrogen; P7589). Fluorescence of each sample well was measured at $490_{Ex}/525_{Em.}$ DNA content for each well was quantified based on an equation of linear regression generated by the fluorescence of a DNA standard curve containing equal amounts of PicoGreen reagent and 0.1% triton.

MESM Molecule Synthesis

Mass spectra (MS) were obtained on an Agilent series 1200 single quad ChemStation autosampler System using electrospray ionization (ESI) in positive mode. The HPLC was run with Accucore C18 column (2.6 µm, 2.1 mm × 30 mm column) at 40 °C; an acetonitrile/water with 0.1% trifloroacetic acid; gradient 40-90 % ACN for 1.5 min; flow rate of 1.5 mL/min. (**Figure 5-8S**).

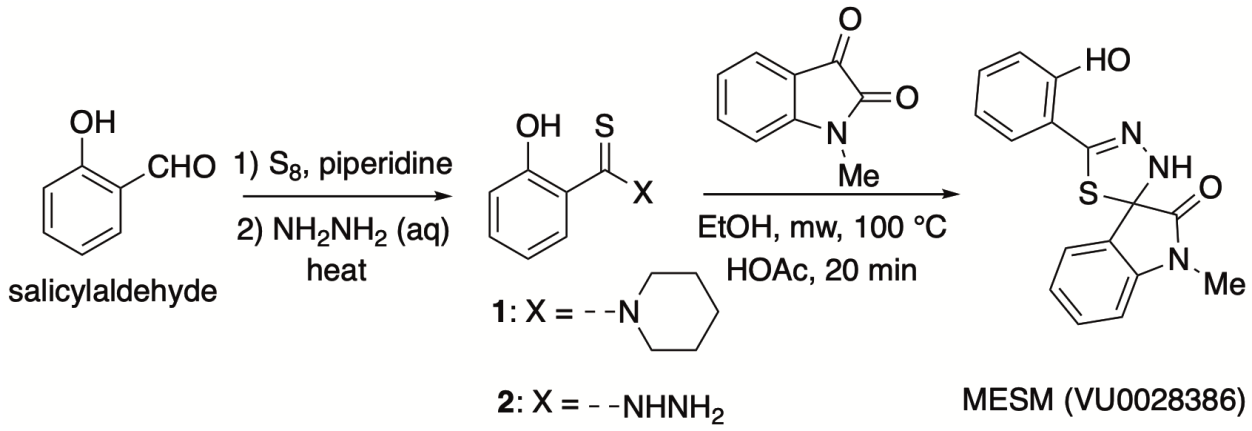

Figure 5-8S. Schematic of MESM molecule synthesis.

Synthesis of (2-hydroxyphenyl) (piperidin-1-yl)methanethione (1). 2-Hydroxybenzaldehyde (1 mL, 0.0094 mol), sulfur (315 mg, 0.0097 mol, 1.05 eq) and piperidine (926 µL, 0.0094 mol, 1eq) were added to a flamed-dried microwave vial (20 mL) equipped with magnetic stir bar. The vial was irradiated at 100 ºC for 2 h, cooled down to room temperature and methanol (1 mL) was added. The mixture was heated at 80 ºC to dissolve the solid and cooled down to room temperature. The resulting solid was filtered and washed with methanol. Obtained 0.89 g (43%). ^{1}H-NMR (DMSO) δ 9.69 (s, 1H), 7.15-7.11 (m, 1H), 7.07 (dd, 1H, J_1 = 8 Hz, J_2= 4 Hz), 6.82-6.78 (m, 2H), 4.46-4.42 (m, 1H), 4.10-4.06 (m, 1H), 1.64 (m, 6H); MS (ESI): mass calculated for $C_{12}H_{15}NOS$, 211.3; m/z found, 212.3 $[M + H]^+$

Synthesis of 2-hydroxybenzothiohydrazide (2).

(2-hydroxyphenyl)(piperidin-1-yl)methanethione (0.89 g, 0.004 mol) and hydrazine hydrate (50 % in water, 5 mL) were added to a round bottom flask and heated under argon at 50 ºC for 2 h. The reaction mixture was cooled down, water added (5 mL) and the solution was carefully

acidified to pH 6 by addition of acetic acid. The mixture was filtered and the filtrate was extracted with ethyl acetate (3 x 20 mL). The combined extracts were washed with water (30 mL) and concentrated in vacuo to half volume. Dry ethanol was added and solvent was removed to half volume. This step was repeated twice more. The crude hydrazide was used as an ethanol solution (5 mL) for the next step. MS (ESI): mass calculated for $C_7H_8N_2OS$, 168.2; m/z found, 168.2 [M + H]+, Rf = 0.34.

Synthesis of 5'-(2-hydroxyphenyl)-1-methyl-3'H-spiro[indoline-3,2'-[1,3,4]thiadiazol]-2-one (VU0028386, MESM). 2-Hydroxybenzo-thiohydrazide (ethanol solution, 5mL) and 1-methylindoline-2,3-dione (220 mg, 1 eq.) were placed in a flamed dried microwave vial (20 mL). Dry ethanol (12 mL) and glacial acetic acid (3 drops) were sequentially added. The vial was capped and irradiated at 100 ºC for 20 min. The resulting solid was filtered off and washed with ethyl acetate to afford 0.36 g (30%) of VU0028386 (MESM). ^{1}H-NMR (DMSO) δ 10.27 (s, 1H), 8.76 (s, 1H), 7.73 (s, 1H), 7.58 (d, 1H, *J* = 8 Hz), 7.42 (m, 2H), 7.29 (tr, 1H, *J* = 8 Hz), 7.14 (tr, 1H, *J* = 8 Hz), 7.06 (d, 1H, *J* = 8 Hz), 6.96-6.92 (m, 2H), MS (ESI): mass calculated for C16H13N3O2S, 311.3; m/z found, 312.2 [M + H]+, Rf = 1.03.

MESM Molecule Availability

The molecule is commercially available from ChemBridge (SC-5679472) in small quantities so interested parties can avoid the cost of synthesis.

Statistical Analysis

All data was analyzed statistically by GraphPad Prism 8. The results of the ICP-MS were analyzed using a two-tailed Student's unpaired t-test. Statistical significance was determined by paired t-tests, Ordinary One-Way ANOVAs, Two-Way ANOVAs with Sidak's multiple comparisons, or Tukey's multiple comparisons where noted. Impact on efflux rates in Fig 1 and Fig S1 were determined by an extra sum of squares F-test to compare if one curve could adequately fit both data sets in a one-phase exponential decay model of nonlinear regression.

Acknowledgments: This work has been partially supported by NIEHS RO1 ES010563 (ABB and MA), and RO1 ES016931 (ABB), as well as T32 ES007028 (KJH and ABB) and T15 LM007450 (KJH and ABB). The Panoptic plate reader was purchase from funds obtain through 1S10OD025281-01. The Panoptic is housed and managed in the Vanderbilt Institute of Chemical Biology's High-throughput Screen Facility.

Conflict of interest: CDW is an owner of WaveFront Biosciences and ION Biosciences, maker of the Panoptic plate reader and Fluo-4 AM, respectively. The remaining authors declare that they have no conflicts of interest with the contents of this article.

REFERENCES

1. Horning KJ, Caito SW, Tipps KG, Bowman AB, Aschner M. Manganese Is Essential for Neuronal Health. Annu Rev Nutr [Internet]. 2015;35(1):71–108. Available from: http://www.annualreviews.org/doi/10.1146/annurev-nutr-071714-034419
2. Bowman AB, Aschner M. Considerations on manganese (Mn) treatments for in vitro studies. Neurotoxicology [Internet]. 2014 Mar [cited 2014 Nov 8];41:141–2. Available from: http://www.ncbi.nlm.nih.gov/pubmed/24509086
3. Madejczyk MS, Ballatori N. Biochimica et Biophysica Acta The iron transporter ferroportin can also function as a manganese exporter. BBA - Biomembr [Internet]. 2012;1818(3):651–7. Available from: http://dx.doi.org/10.1016/j.bbamem.2011.12.002
4. Li X, Xie J, Lu L, Zhang L, Zhang L, Zou Y, et al. Kinetics of manganese transport and

gene expressions of manganese transport carriers in Caco-2 cell monolayers. BioMetals. 2013;26(6):941–53.

5. Yin Z, Jiang H, Lee E-SY, Ni M, Erikson KM, Milatovic D, et al. Ferroportin is a manganese-responsive protein that decreases manganese cytotoxicity and accumulation. J Neurochem [Internet]. 2010 Mar [cited 2014 Nov 20];112(5):1190–8. Available from: http://www.pubmedcentral.nih.gov/articlerender.fcgi?artid=2819584&tool=pmcentrez&rendertype=abstract

6. Jin L, Frazer DM, Lu Y, Wilkins SJ, Ayton S, Bush A, et al. Mice overexpressing hepcidin suggest ferroportin does not play a major role in Mn homeostasis. Metallomics [Internet]. 2019; Available from: http://xlink.rsc.org/?DOI=C8MT00370J

7. Williams BB, Kwakye GF, Wegrzynowicz M, Li D, Aschner M, Erikson KM, et al. Altered manganese homeostasis and manganese toxicity in a Huntington's disease striatal cell model are not explained by defects in the iron transport system. Toxicol Sci [Internet]. 2010 Sep [cited 2014 Oct 28];117(1):169–79. Available from: http://www.pubmedcentral.nih.gov/articlerender.fcgi?artid=2923282&tool=pmcentrez&rendertype=abstract

8. Leyva-Illades D, Chen P, Zogzas CE, Hutchens S, Mercado JM, Swaim CD, et al. SLC30A10 Is a Cell Surface-Localized Manganese Efflux Transporter, and Parkinsonism-Causing Mutations Block Its Intracellular Trafficking and Efflux Activity. J Neurosci [Internet]. 2014 Oct 15 [cited 2014 Nov 20];34(42):14079–95. Available from: http://www.ncbi.nlm.nih.gov/pubmed/25319704

9. Quadri M, Federico A, Zhao T, Breedveld GJ, Battisti C, Delnooz C, et al. Mutations in SLC30A10 Cause Parkinsonism and Dystonia with Hypermanganesemia, Polycythemia,

and Chronic Liver Disease. Am J Hum Genet [Internet]. 2012 Mar;90(3):467–77. Available from: https://linkinghub.elsevier.com/retrieve/pii/S0002929712000511

10. Tuschl K, Clayton PT, Gospe SM, Gulab S, Ibrahim S, Singhi P, et al. Erratum: Syndrome of Hepatic Cirrhosis, Dystonia, Polycythemia, and Hypermanganesemia Caused by Mutations in SLC30A10, a Manganese Transporter in Man (American Journal of Human Genetics (2012) 90 (457–466) (S0002929712000523) (10.1016/j.ajhg.2012.01.018)). Am J Hum Genet [Internet]. 2016;99(2):521. Available from: http://dx.doi.org/10.1016/j.ajhg.2012.01.018
11. Lechpammer M, Clegg MS, Muzar Z, Huebner P a, Jin L-W, Gospe SM. Pathology of inherited manganese transporter deficiency. Ann Neurol [Internet]. 2014 Apr [cited 2014 Nov 20];75(4):608–12. Available from: http://www.ncbi.nlm.nih.gov/pubmed/24599576
12. He L. ZIP8, member of the solute-carrier-39 (SLC39) metal-transporter family: characterization of transporter properties. Mol Pharmacol [Internet]. 2006;70(1):171–80. Available from: http://molpharm.aspetjournals.org/cgi/doi/10.1124/mol.106.024521
13. Koike A, Sou J, Ohishi A, Nishida K, Nagasawa K. Inhibitory effect of divalent metal cations on zinc uptake via mouse Zrt-/Irt-like protein 8 (ZIP8). Life Sci. 2017;173:80–5.
14. Lin W, Vann DR, Doulias PT, Wang T, Landesberg G, Li X, et al. Hepatic metal ion transporter ZIP8 regulates manganese homeostasis and manganese-dependent enzyme activity. J Clin Invest. 2017;127(6):2407–17.
15. Choi EK, Nguyen TT, Gupta N, Iwase S, Seo YA. Functional analysis of SLC39A8 mutations and their implications for manganese deficiency and mitochondrial disorders. Sci Rep [Internet]. 2018;8(1):1–17. Available from: http://dx.doi.org/10.1038/s41598-018-21464-0

16. Park JH, Hogrebe M, Fobker M, Brackmann R, Fiedler B, Reunert J, et al. SLC39A8 deficiency: Biochemical correction and major clinical improvement by manganese therapy. Genet Med [Internet]. 2018;20(2):259–68. Available from: http://dx.doi.org/10.1038/gim.2017.106

17. Aydemir TB, Cousins RJ. The multiple faces of the metal transporter ZIP14 (SLC39A14). J Nutr. 2018;148(2):174–84.

18. Zhao N, Zhang AS, Wortham AM, Jue S, Knutson MD, Enns CA. The tumor suppressor, P53, decreases the metal transporter, ZIP14. Nutrients. 2017;9(12).

19. Aydemir TB, Kim M-H, Kim J, Colon-Perez LM, Banan G, Mareci TH, et al. Metal Transporter *Zip14* (*Slc39a14*) Deletion in Mice Increases Manganese Deposition and Produces Neurotoxic Signatures and Diminished Motor Activity. J Neurosci [Internet]. 2017;37(25):5996–6006. Available from: http://www.jneurosci.org/lookup/doi/10.1523/JNEUROSCI.0285-17.2017

20. Xin Y, Gao H, Wang J, Qiang Y, Imam MU, Li Y, et al. Manganese transporter Slc39a14 deficiency revealed its key role in maintaining manganese homeostasis in mice. Cell Discov [Internet]. 2017;3:17025. Available from: http://www.nature.com/articles/celldisc201725

21. Zogzas CE, Mukhopadhyay S. Inherited Disorders of Manganese Metabolism. In: Handbook of Clinical Neurology [Internet]. 2017. p. 35–49. Available from: http://link.springer.com/10.1007/978-3-319-60189-2_3

22. Taylor CA, Hutchens S, Liu C, Jursa T, Shawlot W, Aschner XM, et al. cro SLC30A10 transporter in the digestive system regulates brain manganese under basal conditions while brain SLC30A10 protects against neurotoxicity. 2019;294(23):1860–76.

23. Jenkitkasemwong S, Akinyode A, Paulus E, Weiskirchen R, Hojyo S, Fukada T, et al. SLC39A14 deficiency alters manganese homeostasis and excretion resulting in brain manganese accumulation and motor deficits in mice. Proc Natl Acad Sci [Internet]. 2018;115(8):E1769–78. Available from: http://www.pnas.org/lookup/doi/10.1073/pnas.1720739115

24. Vollet K, Haynes EN, Dietrich KN. Manganese Exposure and Cognition Across the Lifespan: Contemporary Review and Argument for Biphasic Dose–Response Health Effects. Curr Environ Heal Reports [Internet]. 2016;3(4):392–404. Available from: http://dx.doi.org/10.1007/s40572-016-0108-x

25. Torres-Agustín R, Rodríguez-Agudelo Y, Schilmann A, Solís-Vivanco R, Montes S, Riojas-Rodríguez H, et al. Effect of environmental manganese exposure on verbal learning and memory in Mexican children. Environ Res. 2013;121:39–44.

26. Haynes EN, Sucharew H, Kuhnell P, Alden J, Barnas M, Wright RO, et al. Manganese exposure and neurocognitive outcomes in rural school-age children: The communities actively researching exposure study (Ohio, USA). Environ Health Perspect. 2015;123(10):1066–71.

27. Roth J, Ponzoni S, Aschner M. Manganese Homeostasis and Transport. In: Banci L, editor. Dordrecht: Springer Netherlands; 2013 [cited 2014 May 1]. (Metal Ions in Life Sciences; vol. 12). Available from: http://link.springer.com/10.1007/978-94-007-5561-1

28. Herrero E, Discalzi G, Valentini C, Carmellino C, Rossi L, Venturi F, et al. Follow-up of patients affected by manganese-induced Parkinsonism after treatment with CaNa 2 EDTA §. 2006;27:333–9.

29. Bryan MR, Uhouse MA, Nordham KD, Joshi P, Rose DIR, O'Brien MT, et al.

Phosphatidylinositol 3 kinase (PI3K) modulates manganese homeostasis and manganese-induced cell signaling in a murine striatal cell line. Neurotoxicology [Internet]. 2018;64:185–94. Available from: https://doi.org/10.1016/j.neuro.2017.07.026

30. Bichell TJ V., Wegrzynowicz M, Tipps KG, Bradley EM, Uhouse MA, Bryan M, et al. Reduced bioavailable manganese causes striatal urea cycle pathology in Huntington's disease mouse model. Biochim Biophys Acta - Mol Basis Dis [Internet]. 2017;1863(6):1596–604. Available from: http://dx.doi.org/10.1016/j.bbadis.2017.02.013

31. Tidball AM, Bryan MR, Uhouse MA, Kumar KK, Aboud AA, Feist JE, et al. A novel manganese-dependent ATM-p53 signaling pathway is selectively impaired in patient-based neuroprogenitor and murine striatal models of Huntington's disease. Hum Mol Genet. 2014;24(7):1929–44.

32. Pan Z, Choi S, Luo Y. Mn2+ Quenching Assay for Store-Operated Calcium Entry. In: Penna A, Constantin B, editors. New York, NY: Springer New York; 2018. p. 55–62. (Methods in Molecular Biology; vol. 1843). Available from: http://link.springer.com/10.1007/978-1-4939-8704-7

33. Forbes JR, Gros P. Iron , manganese , and cobalt transport by Nramp1 (Slc11a1) and Nramp2 (Slc11a2) expressed at the plasma membrane. 2003;102(5):1884–92.

34. Lockwich T, Mertz LM, Ambudkar IS. Involvement of carboxyl groups in the divalent cation permeability of rat parotid gland basolateral plasma membrane. Mol Cell Biochem. 1993;126(2):143–50.

35. Lukács GL, Kapus A. Measurement of the matrix free Ca 2+ concentration in heart mitochondria by entrapped fura-2 and quin2. Biochem J. 1987;248(2):609–13.

36. Denny MF, Hare MF, Atchison WD. Methylmercury alters intrasynaptosomal

concentrations of endogenous polyvalent cations. Vol. 122, Toxicology and Applied Pharmacology. 1993. p. 222–32.

37. Komagiri Y, Nakamura K, Kubokawa M. A nicardipine-sensitive Ca2+ entry contributes to the hypotonicity-induced increase in [Ca2+]i of principal cells in rat cortical collecting duct. Cell Calcium [Internet]. 2011;49(1):35–42. Available from: http://dx.doi.org/10.1016/j.ceca.2010.11.006

38. Kwakye GF, Li D, Kabobel OA, Bowman AB. Cellular fura-2 Manganese Extraction Assay (CFMEA). Curr Protoc Toxicol. 2011;2651(SUPPL.48):1–26.

39. Kumar KK, Lowe EW, Aboud A a, Neely MD, Redha R, Bauer J a, et al. Cellular manganese content is developmentally regulated in human dopaminergic neurons. Sci Rep [Internet]. 2014 Jan [cited 2014 Nov 2];4:6801. Available from: http://www.ncbi.nlm.nih.gov/pubmed/25348053

40. Kumar KK, Aboud AA, Patel DK, Aschner M, Bowman AB. Optimization of Fluorescence Assay of Cellular Manganese Status for High Throughput Screening. J Biochem Mol Toxicol [Internet]. 2013 Jan;27(1):42–9. Available from: http://doi.wiley.com/10.1002/jbt.21457

41. Kumar KK, Aboud AA, Bowman AB. The potential of induced pluripotent stem cells as a translational model for neurotoxicological risk. Neurotoxicology. 2012;33(3):518–29.

42. Reed PW, Lardy H a. A23187 : A Divalent Ionophore. J Biol Chem. 1972;247:6970–7.

43. Pfeiffer DR, Reed PW, Lardy HA. Ultraviolet and fluorescent spectral properties of the divalent cation ionophore A23187 and its metal ion complexes. Biochemistry. 1974;13(19):4007–14.

44. Pfeiffer DR, Deber CM. Isosteric metal complexes of ionophore A23187. A basis for

cation selectivity. FEBS Lett. 1979;105(2):360–4.

45. Kauffman RF, Taylor W, Pfeiffer DR. Cation Transport and Specificity of Ionomycin. J Biol Chem. 1980;255(7):2735–9.

46. Gee KR, Brown KA, Chen WNU, Bishop-Stewart J, Gray D, Johnson I. Chemical and physiological characterization of fluo-4 Ca2+-indicator dyes. Cell Calcium. 2000;27(2):97–106.

47. Freedman JC. Ionophores in Planar Lipid Bilayers. Cell Physiol Source B. 2012;61–6.

48. Delnooz CCS, Wevers R a, Quadri M, Clayton PT, Mills PB, Tuschl K, et al. Phenotypic variability in a dystonia family with mutations in the manganese transporter gene. Mov Disord [Internet]. 2013 May [cited 2014 Nov 20];28(5):685–6. Available from: http://www.ncbi.nlm.nih.gov/pubmed/23592301

49. Park JH, Hogrebe M, Grüneberg M, Duchesne I, Von Der Heiden AL, Reunert J, et al. SLC39A8 Deficiency: A Disorder of Manganese Transport and Glycosylation. Am J Hum Genet. 2015;97(6):894–903.

50. Oakes SG, Martin WJ, Lisek CA, Powis G. Incomplete hydrolysis of the calcium indicator precursor fura-2 pentaacetoxymethyl ester (fura-2 AM) by cells. Anal Biochem. 1988;169(1):159–66.

51. Moynier F, Fujii T. Calcium isotope fractionation between aqueous compounds relevant to low-temperature geochemistry, biology and medicine. Sci Rep. 2017;7(February):1–7.

52. Skulan J, DePaolo DJ. Calcium isotope fractionation between soft and mineralized tissues as a monitor of calcium use in vertebrates. Proc Natl Acad Sci U S A. 1999;96(24):13709–13.

53. Zogzas CE, Mukhopadhyay S. Putative metal binding site in the transmembrane domain

of the manganese transporter SLC30A10 is different from that of related zinc transporters. Metallomics. 2018;10(8):1053–64.

54. Stillwell W. Membrane Transport. In: An Introduction to Biological Membranes [Internet]. Elsevier; 2016. p. 423–51. Available from: https://linkinghub.elsevier.com/retrieve/pii/B9780444637727000191

55. Das S, Carmona A, Khatua K, Porcaro F, Somogyi A, Ortega R, et al. Manganese Mapping Using a Fluorescent Mn2+ Sensor and Nanosynchrotron X-ray Fluorescence Reveals the Role of the Golgi Apparatus as a Manganese Storage Site. Inorg Chem. 2019;58(20):13724–32.

56. Gavin CE, Gunter KK, Gunter TE. Manganese and calcium efflux kinetics in brain mitochondria. Relevance to manganese toxicity. Biochem J [Internet]. 1990 Mar 1;266(2):329–34. Available from: http://www.biochemj.org/cgi/doi/10.1042/bj2660329

57. Liccione JJ, Maines MD. Selective vulnerability of glutathione metabolism and cellular defense mechanisms in rat striatum to manganese. J Pharmacol Exp Ther. 1988;247(1):156–61.

58. Morello M, Canini a, Mattioli P, Sorge RP, Alimonti a, Bocca B, et al. Sub-cellular localization of manganese in the basal ganglia of normal and manganese-treated rats An electron spectroscopy imaging and electron energy-loss spectroscopy study. Neurotoxicology [Internet]. 2008 Jan [cited 2014 Nov 8];29(1):60–72. Available from: http://www.ncbi.nlm.nih.gov/pubmed/17936361

59. Kalia K, Jiang W, Zheng W. Manganese accumulates primarily in nuclei of cultured brain cells. Neurotoxicology [Internet]. 2008 May;29(3):466–70. Available from: https://linkinghub.elsevier.com/retrieve/pii/S0161813X08000363

60. Bakthavatsalam S, Sarkar A, Rakshit A, Jain S, Kumar A, Datta A. Tuning macrocycles to design “turn-on” fluorescence probes for manganese(ii) sensing in live cells. Chem Commun. 2015;51(13):2605–8.

61. Kalia K, Jiang W, Zheng W. Manganese accumulates primarily in nuclei of cultured brain cells. Neurotoxicology. 2008;29(3):466–70.

62. Tidball AM, Neely MD, Chamberlin R, Aboud AA, Kumar KK, Han B, et al. Genomic instability associated with p53 knockdown in the generation of Huntington’s disease human induced pluripotent stem cells. PLoS One. 2016;11(3):1–16.

63. Joshi P, Bodnya C, Ilieva I, Neely MD, Aschner M. Huntington ’ s disease associated resistance to Mn neurotoxicity is neurodevelopmental stage and neuronal lineage dependent. Neurotoxicology. 2019;75(March):148–57.

CHAPTER VI

OVERALL DISCUSSION AND FUTURE DIRECTIONS

The overall findings of these studies demonstrate that (1) Mn is an essential metal whose regulation should be studied based on the consequences of disturbances in Mn homeostasis such as chronic exposures, SLC30A10 mutations, and an apparent Mn-handling deficiency in Huntington's disease, (2) characterization of the Mn toolbox can be used to delineate functional pathways, cell-specific activities, and screen against specific functions of mechanism, (3) a chemical biology approach to Mn homeostasis may identify modulators that impact the biological molecules and macromolecules responsible for the Mn deficit in Huntington's disease, (4) the Mn toolbox an be used to screen against specific transporters such as SLC30A10, and (5) the Mn toolbox contains small molecules that can be used as tools to dissect and measure Mn homeostasis, such as VU0028386 (MESM) which acts as a Mn-selective ionophore.

Manganese Is Essential For Neuronal Health

The primary source of Mn intake is dietary, and proper levels are maintained in healthy adults via hepatic/biliary excretion, regulation at the blood-brain barrier, and, at least in a small part, mechanisms of cellular homeostasis. The major cause of concern regarding Mn toxicity occurs in occupational and environmental exposures, where the central nervous system is the primary target. Mn is deposited in the brain with age and exposure, specifically the basal ganglia: a primary motor-control area of the brain. Mn is involved in many commercial and industrial processes, including welding, where airborne Mn can become a risk factor. Chronic exposure to intranasal Mn can lead to a Parkinsonian-like condition called manganism, characterized by motor

symptoms, and emotional/cognitive deficits. Recent studies have noted that increased environmental exposures (example: Mn content in water or soil) inversely correlate with cognitive scores and in-school performance in adolescents.

While toxic in excess, Mn is required for numerous biological actions as a cofactor for about half of all kinases and enzymes particularly relevant to brain function, including glutamine synthetase, arginase, and Mn superoxide dismutase. The metal is also incorporated into metalloproteins, ranging from ligases to oxidoreductases. For this reason, Mn is truly essential for life, and though cases of Mn-deficiency are virtually non-existent, the Institute of Medicine has set a Dietary Reference Intake value of 2 mg/day. Considering that Mn is both essential and toxic in excess, it is clear that the mechanisms that control Mn homeostasis need to be studied in order to have the best chance in combatting instances of Mn dysregulation. The controversy surrounding the role (or lack thereof) of DMT1, and the still-unknown cause of the Mn deficiency in HD, demonstrates just how understudied Mn transport and homeostasis is in its current state.

Besides targeting Mn-permeable transporters, an alternate approach to combatting Mn dysregulation would be to better understand mechanisms of Mn-toxicity, so if the root cause of excess/deficient Mn is still unknown, at least symptoms could be treated. A recent publication demonstrated that mitochondrial and metabolic dysfunction was not the cause of toxicity in the neuronal Q7/Q111 models and in primary striatal neurons; mitochondrial dysfunction as measured by metabolic balance, mitochondrial respiration, and substrate dependence occurred only at or above cytotoxic concentrations of Mn (17). This argues against the idea that Mn induces mitochondrial dysfunction leading to cytotoxicity. While there are several reasons to explain this discrepancy towards previous findings regarding mitochondrial dysfunction, other hypotheses surrounding Mn-induced toxicity should be explored. For example, Mn activates p53 at non-

cytotoxic concentrations, which can induce apoptosis (16). Mn also inhibits the nuclear localization of the transcription factor TFEB, which regulates autophagy and could lead to an accumulation of unhealthy mitochondria (20). Interestingly, a recent study from our lab provided evidence that an acute Mn treatment could restore the impaired cargo-loading phenotype in Huntington's disease (1), further implicating autophagy as mechanism of toxicity targeted by Mn.

Regarding Mn-permeable and Mn-specific transporters in the brain, especially in the context of HD, it is surprising that there has not been any follow-up on HIP14 (Huntingtin-interacting protein 14) and HIP14L (HIP14-like protein). A literature search yields only eight results in from the search terms over the last five years. Only one of these, a review paper, appears to acknowledge HIP14 for its potential role in metal ion transport (specifically magnesium; Mg) transport (13). The rest of these address HIP14's other role as a palmitoyltransferase, and how this relates to habituation behavior (11) in zebrafish, or how manipulation of its expression affect outcomes in HD models (6, 12, 15). The HIP14 and HIP14L connection to HD is intriguing; a putative Mn transporter that has an important role in huntingtin-trafficking and whose function is disrupted in HD should gain the attention to anyone aware of the Mn deficit in HD. To name a few studies: Huang et al. first demonstrated in 2004 that HIP14 was a palmitoyl transferase with substrate specificity for neuronal proteins including SNAP-25, PSD-95, GAD65, synaptotagmin I, and importantly, huntingtin (5), though Singaraja (2002) was the first to show that HIP14 interacted with huntingtin (14). It appears that Yanai (2006) demonstrated first that the palmitoylation of HIP14 was reduced in mutant huntingtin, and this led to inclusion formations which (presumably) led to increased neuronal toxicity (19). These factors have seemed to supersede the findings in 2008 by Goytain et al. that HIP14 and HIP14L had dual functions: palmitoylation and Mg^{2+} transport (4). Using a permeability ratio with Mg normalized to 1, Mn

falls in third only to strontium and nickel at around 0.5 (4). The 2018 review paper on novel Mg^{2+} transporters (13) cites that HIP14 and HIP14L:

"were initially suggested to mediate Mg^2 currents at the Golgi membrane …Subsequently, it was shown that they mainly function as palmitoyl acyltransferase (3)*, specifically involved in the palmitoylation in Huntington disease. Mg^2 transporter activity can therefore be excluded."*

The authors of the 2008 paper (Goytain et al.) likely disagree. Considering the dual function of HIP14 and HIP14L, what should be next in terms of HIP14 and HIP14L research for Mn transport? HIP14 conditional KO mice already exist (12), which die due to paralysis in adulthood. However, primary cultures of striatal neurons could be taken from these mice, and Mn uptake can be assayed by CFMEA, and compared to WT mice. Experiments showing that HIP14 and HIP14L are permeable to Mn have only used Xenopus oocytes as a model (4); neuronal models of HIP14 and HIP14L function have yet to be observed. A former graduate student, Gunnar Kwakye, already has shown that HIP14 protein expression is significantly reduced in the HD-model Q111 cells compared to WT Q7 cells (7). However, mouse models of HD (YAC128) could also be used to show a decrease in function/expression of HIP14 by western blot/CFMEA. Differential activity of the Mn toolbox would indicate which small molecules, if any, target HIP14 and/or HIP14L.

Characterization of the Mn Toolbox

Characterization of the Mn toolbox occurred over the course of a several dozen experiments, and the data was collected in hopes to classify each small molecule into functional groups. Small molecules overall did not fall into clean groups by eye (i.e. all the Zn influencers decreased Mn, or that X groups of small molecules could explain the variation in Mn efflux),

however that did not stop from using predictive modeling to visualize relatedness between populations. A spreadsheet of each characterization readout for all small molecules was compiled, and it is available here at this link:

https://drive.google.com/file/d/1mN2RuSbf1bNTrDIJ8See4zpcOTixm2Ri/view?usp=sharing

Using free software called "Past", we can compile all the factors together and form a hierarchical cluster (**Figure 6-1**).

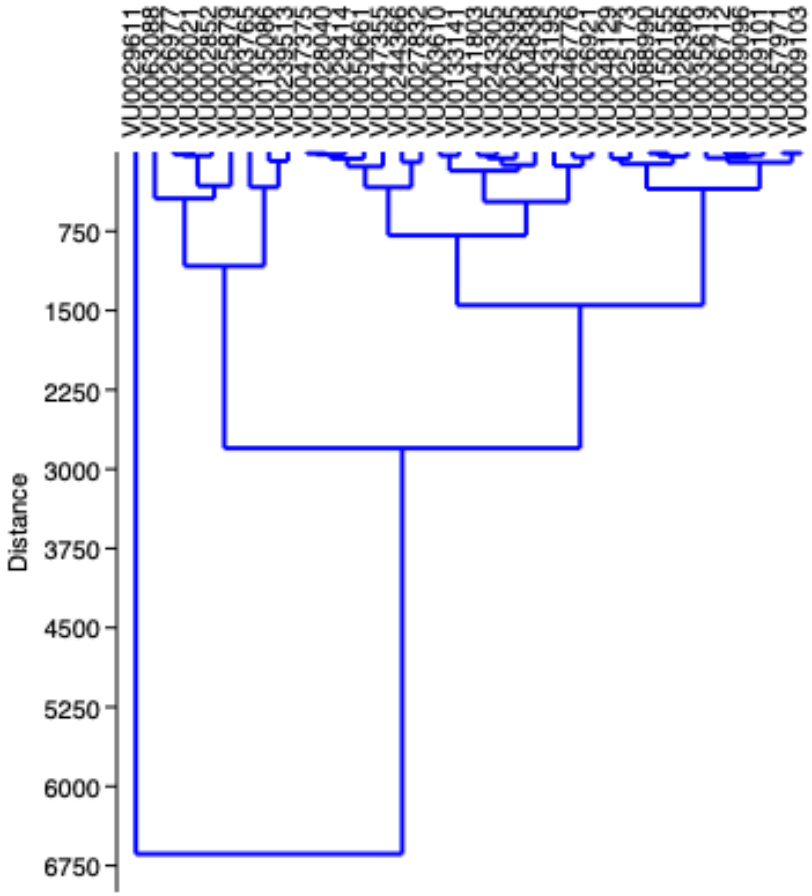

Figure 6-1. Hierarchical cluster using the paired group algorithm (UPGMA) and a Euclidean similarity index. Figure is based on all the variables generated in the toolbox.

To look at the data differently, and investigate which factors contributed the most to these pairings, continuous variables were fed into a principal component analysis while an MCA (multiple correspondence analysis) was used for categorical values (**Figure 6-2**).

A

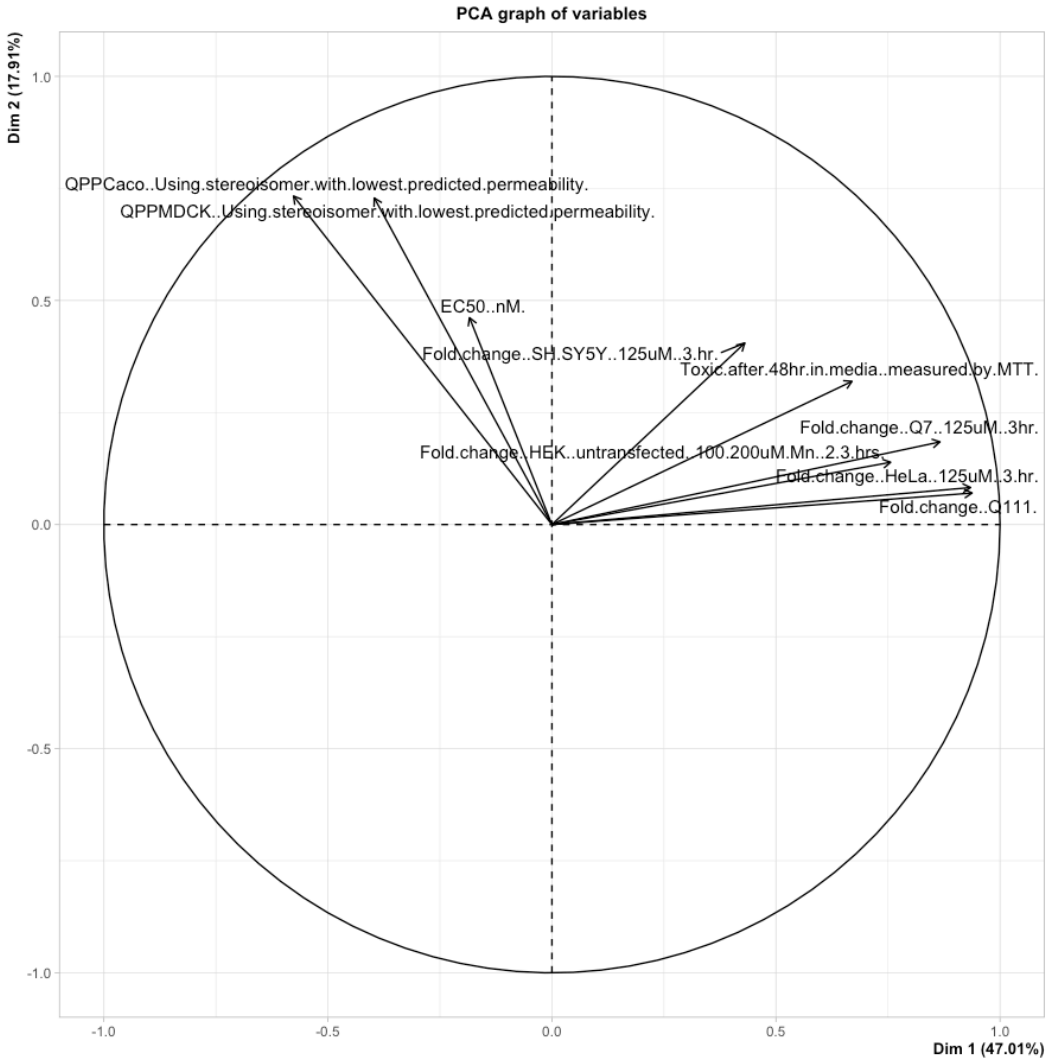

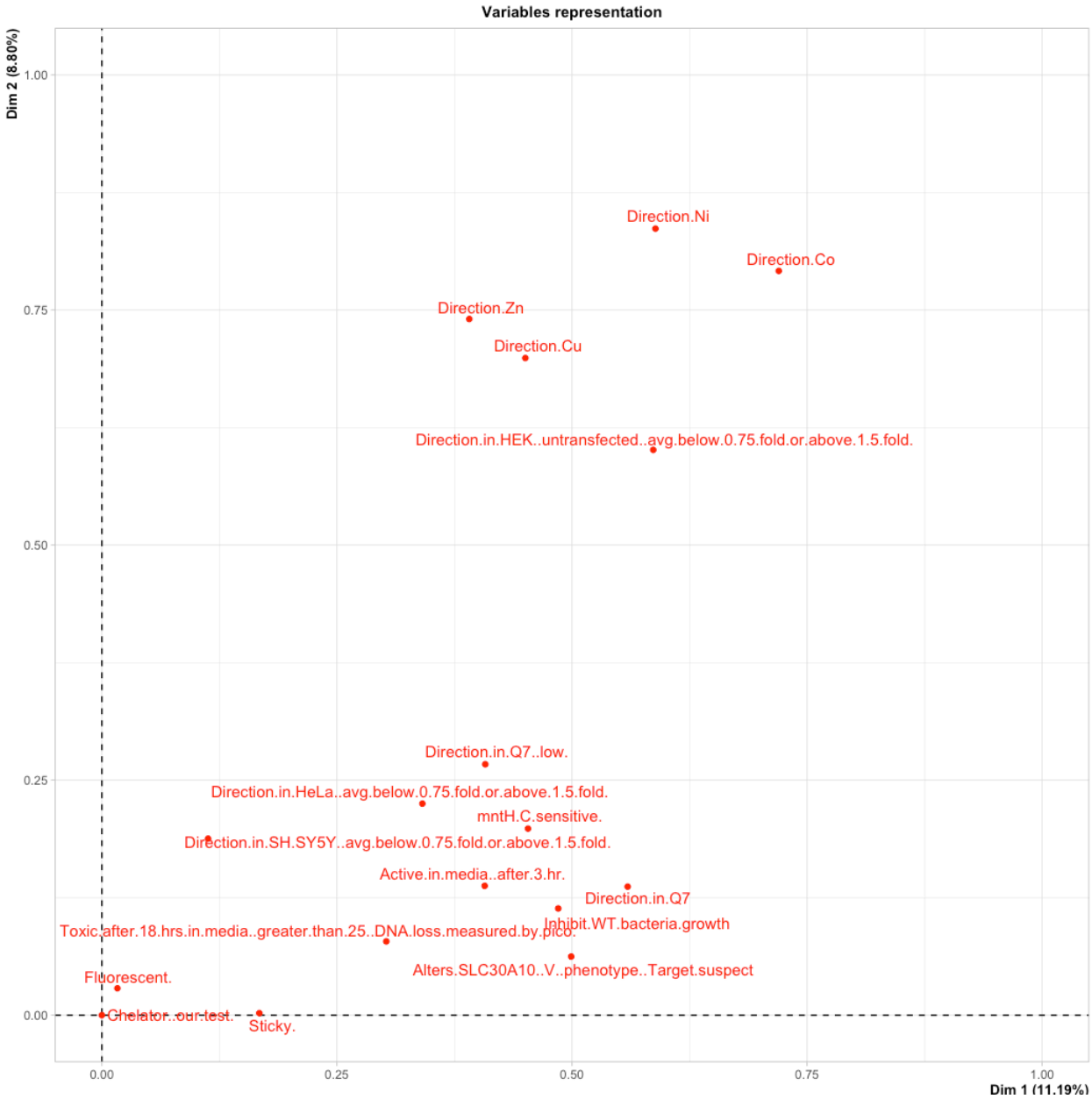

Figure 6-2. All continuous variables for each small molecule were plotted in a Principal Component Analysis (PCA) in (**A**). All categorical values were plotted in a Multiple Correspondence Analysis in (**B**). Analysis performed in RStudio with the "FactoMineR" package.

Based on the percentages on each axis in the PCA and MCA, the continuous variables explain more variation in the molecules than the categorical variables. However, since there are such few continuous variables to begin with, it looks like they all contribute to the PCA highly. In hindsight, it is not surprising that certain categories like "fluorescent at 365/535 nm" are not playing a large part in defining the molecules. Of note, of all the categorical values, it appears that the "direction of the other divalent molecules" plays the largest role. This makes sense, as metal ion selectivity (specifically Mn-selectivity) would likely dictate the actions or the behavior of each small molecule on Mn itself. For this reason, the molecules that appear to be Mn-selective should be placed in higher priority over the rest of the toolbox, if high-throughput methods are not available to include the entire Mn toolbox.

As there is more work that can be and should be done with the Mn toolbox, (not just in terms of classifying the small molecules, but continuing to use the small molecules as tools to understand Mn homeostasis and find potential targets), it will be interesting to see if future data alters the hierarchical clustering, or if they continue to maintain their pairings. Future experiments using the toolbox should take a similar approach as the SLC30A10 phenotype experiments, as this is the best targeted approach in the techniques used to classify the small molecules so far. For example, the role that SPCA1 in Mn transport is still understudied, and it is possible that members of the toolbox can be targeting SPCA1. Knock-out cell lines of SPCA1 already exist in Hap1 and HeLa cells (8), so a collaboration would skip the step of generating these cell lines. In addition, we have HEK293 cells overexpressing WT and mutant ZIP14 (thanks to a collaboration with the Steve Wilson lab), which could be screened against the toolbox as well. As far as known (putative) Mn-selective transporters, this only leaves out ZIP8. ZIP8 is a metal ion-bicarbonate symporter (9), so its function is dependent on bicarbonate being present in the cell medium. Using media

without containing sodium bicarbonate, we can test the activities of the Mn toolbox, and compare them to their activity in the standard DMEM that we use containing sodium bicarbonate and see if there are any changes. If a small molecule loses its ability to influence Mn in the bicarbonate-free media, that would be evidence that the small molecule relies on bicarbonate for its mechanism and links the possibility of a ZIP8-mediated mechanism.

Future studies could also employ a new tool: the fluorescent Mn^{2+} sensor M1 (2). Especially to be used with the small molecules of special interest (MESM, the Mn-specific/different in HD molecules, etc.) the M1 sensor can be used to confirm the mechanism of action of some of these small molecules by showing the location of Mn storage within cells. A small molecule that changes Mn localization in the Golgi on its own would give clues to what the target of the small molecule is. However, the M1 sensor is an exciting tool even without the Mn toolbox; considering that free Mn storage and localization within the cell is still up for debate under physiological and pathophysiological conditions. This could be applied to HD research and also basic science Mn-homeostasis to see under what conditions Mn localization is altered.

Identification of Three Small Molecules Which Can Selectively Influence Cellular Manganese Levels in a Mouse Striatal Cell Model and their Relationship to the Huntington's Disease Mn Phenotype

We sought to test the hypothesis that Mn-selective molecules in the Mn toolbox would be more likely to act on the Mn-specific deficit in the HD model. After using a modified version of the CFMEA to detect changes in other metals when exposed in high exogenous concentrations, we identified three that did not seem to influence other divalent metals like Zn, Ni, Cu, or Co in a significant way. Astonishingly consistent with our hypothesis, two of the three small molecules

identified had differential activity in the HD Q111 model compared to the WT Q7 model striatal cells. This indicates that the target(s) of these two small molecules are the very mechanisms of Mn transport that are deficient in HD. It cannot be overstated that this is the closest we have been to discovering the culprits of the Mn-deficiency in HD, thus finding the targets to these small molecules should be our first priority, above all other follow-up studies described in this manuscript.

It is well known in the field that "target deconvolution" strategies are tedious, time-consuming, and are constrained by technical issues. Finding the targets of small molecules is not an easy task, but there are several approaches one could take. It has previously been mentioned that conjugating a small molecule to biotin or another group to be pulled down and isolated for mass spectrometry is the most direct method but determining where to link the antibody-targeted group without ablating that small molecule's function takes considerable time and money. In fact, there are commercial services available that use techniques such as two-hybrid screening for those looking to find the targets of their drug or small molecule. "Omics" type experiments could be performed alternatively, which would certainly provide leads but would need to be confirmed with knockout studies at the very least. To find direct protein targets, drug affinity responsive target stability (DARTS) allows for identification of targets without chemically modifying the compound/ small molecule of interest. Rather than using positive selection to identify targets like in affinity chromatography, DARTS uses negative selection to degrade all other proteins except the target protein, which should be stabilized being bound to the small molecule, also known as drug-induced protease resistance (10). This would simply require digestion of protein lysates treated with the small molecule of interest, separation and staining of an SDS-PAGE gel, and comparison to a control sample for which band is enriched in the small molecule-treated set. The

band then could be cut out and identified via mass spectrometry. While this process may not be ideal for a set of 41 molecules, focusing on the one or two (specifically 619 and 173) should be more manageable.

Identification of Small Molecules That Alter a SLC30A10 Phenotype

This study marks an example of how future experiments could screen the Mn toolbox against other putative targets/ transporters. In addition, the "activation" of SLC30A10 seen by Mn suggests there is a Mn sensor that detects intracellular Mn concentrations, and sets in motion a mechanism of activation. Future studies could start to see if this "activation" is reflected in changes of RNA expression or cell surface expression of SLC30A10 in response to an average Mn-increasing small molecule. Next, one could test what some specific inhibitor molecules, like VU0482585, have on SLC30A10 expression. Considering the role that SLC30A10 has for systemic Mn homeostasis, one may be interested in using other cell models (i.e. hepatocytes or enterocytes), which naturally express substantial SLC30A10. Knowing what we know regarding the role of SLC30A10, ZIP8, and ZIP14, based on clinical data of patients with rare mutations in the respective genes, and other studies, it is possible to form a rough model of systemic Mn homeostasis.

Beginning in the gut, dietary Mn is shuttled from the apical membrane of enterocytes into the cell, by a mechanism not yet understood. However, we know that SLC30A10 is able to mediate Mn back out at the apical membrane. On the other side (basolateral), ZIP14 is able to transport Mn from the blood back to the enterocyte. In the liver, it is believed that ZIP14 imports Mn from the basolateral membrane into the hepatocytes (18). At the apical canalicular membrane, SLC30A10

exports Mn into bile. To maintain suitable Mn concentrations, Mn can be reclaimed from the bile at the apical membrane via ZIP8 (18).

Identification of a Selective Manganese Ionophore that Enables Nonlethal Quantification of Cellular Manganese

Finally, regarding repeated Mn exposures, other exposure paradigms might yield stronger effects than seen in these studies. We expect future studies to pursue these instances, so that subsequent experiments can identify protein and expression level changes of putative transporters or accompanying players. One may expect to see changes in the activation of Mn-responsive proteins such as AKT, p53 and GLT-1 if Mn homeostasis is altered. If there are decreases in Mn accumulation, this might be correlated to changes in expression of Mn transporters like ZIP8, ZIP14, and SLC30A10. Most importantly, we would want to know if these changes in Mn accumulation/ protein expression are meaningful. Are there changes in Mn-dependent enzyme activity, such as arginase or glutamine synthetase? Do these changes have pathological consequences? Now that we are able to monitor Mn accumulation longitudinally with MESMER, if we can induce a model of altered Mn homeostasis, then we can ask questions about what it really means to have altered Mn homeostasis on a cellular level.

REFERENCES

1. Bryan MR, Brien MTO, Nordham KD, Rose DIR, Foshage AM, et al. 2019. Acute manganese treatment restores defective autophagic cargo loading in Huntington ' s disease cell lines. . 28(22):3825–41
2. Das S, Carmona A, Khatua K, Porcaro F, Somogyi A, et al. 2019. Manganese Mapping

Using a Fluorescent Mn2+ Sensor and Nanosynchrotron X-ray Fluorescence Reveals the Role of the Golgi Apparatus as a Manganese Storage Site. *Inorg. Chem.* 58(20):13724–32

3. Ducker CE, Stettler EM, French KJ, Upson JJ, Smith CD. 2004. Huntingtin interacting protein 14 is an oncogenic human protein: Palmitoyl acyltransferase. *Oncogene*. 23(57):9230–37
4. Goytain A, Hines RM, Quamme GA. 2008. Huntingtin-interacting proteins, HIP14 and HIP14L, mediate dual functions, palmitoyl acyltransferase and Mg2+ transport. *J. Biol. Chem.* 283(48):33365–74
5. Huang K, Yanai A, Kang R, Arstikaitis P, Singaraja RR, et al. 2004. Huntingtin-interacting protein HIP14 is a palmitoyl transferase involved in palmitoylation and trafficking of multiple neuronal proteins. *Neuron*. 44(6):977–86
6. Kang R, Wang L, Sanders SS, Zuo K, Hayden MR, Raymond LA. 2019. Altered regulation of striatal neuronal N-methyl-D-aspartate receptor trafficking by palmitoylation in Huntington disease mouse model. *Front. Synaptic Neurosci.* 11(February):1–22
7. Kwakye GF. 2011. *DEVELOPMENT OF A NOVEL HIGH THROUGHPUT ASSAY: IMPAIRED MANGANESE TRANSPORT KINETICS AND HOMEOSTASIS IN HUNTINGTON'S DISEASE*. Vanderbilt University
8. Lebredonchel E, Houdou M, Hoffmann HH, Kondratska K, Krzewinski MA, et al. 2019. Investigating the functional link between TMEM165 and SPCA1. *Biochem. J.* 476(21):3281–93
9. Liu Z, Li H, Soleimani M, Girijashanker K, Reed JM, et al. 2008. Cd2+ versus Zn2+ uptake by the ZIP8 HCO3--dependent symporter: kinetics, electrogenicity and trafficking. *Biochem. Biophys. Res. Commun.* 365(4):814–20

10. Lomenick B, Olsen RW, Huang J. 2011. Identification of direct protein targets of small molecules. *ACS Chem. Biol.* 6(1):34–46

11. Nelson JC, Witze E, Ma Z, Ciocco F, Frerotte A, et al. 2020. Acute Regulation of Habituation Learning via Posttranslational Palmitoylation. *Curr. Biol.* 30(14):2729-2738.e4

12. Sanders SS, Parsons MP, Mui KKN, Southwell AL, Franciosi S, et al. 2016. Sudden death due to paralysis and synaptic and behavioral deficits when Hip14/Zdhhc17 is deleted in adult mice. *BMC Biol.* 14(1):1–13

13. Schäffers OJM, Hoenderop JGJ, Bindels RJM, de Baaij JHF. 2018. The rise and fall of novel renal magnesium transporters. *Am. J. Physiol. - Ren. Physiol.* 314(6):F1027–33

14. Singaraja RR. 2002. HIP14, a novel ankyrin domain-containing protein, links huntingtin to intracellular trafficking and endocytosis. *Hum. Mol. Genet.* 11(23):2815–28

15. Skotte NH, Sanders SS, Singaraja RR, Ehrnhoefer DE, Vaid K, et al. 2017. Palmitoylation of caspase-6 by HIP14 regulates its activation. *Cell Death Differ.* 24(3):433–44

16. Tidball AM, Bryan MR, Uhouse MA, Kumar KK, Aboud AA, et al. 2014. A novel manganese-dependent ATM-p53 signaling pathway is selectively impaired in patient-based neuroprogenitor and murine striatal models of Huntington's disease. *Hum. Mol. Genet.* 24(7):1929–44

17. Warren EB, Bryan MR, Morcillo P, Hardeman KN, Aschner M, Bowman AB. 2020. Manganese-induced mitochondrial dysfunction is not detectable at exposures below the acute cytotoxic threshold in neuronal cell types. *Toxicol. Sci.*, pp. 1–14

18. Winslow JWW, Limesand KH, Zhao N. 2020. The functions of ZIP8, ZIP14, and ZnT10 in the regulation of systemic manganese homeostasis. *Int. J. Mol. Sci.* 21(9):

19. Yanai A, Huang K, Kang R, Singaraja RR, Arstikaitis P, et al. 2006. Palmitoylation of huntingtin by HIP14 is essential for its trafficking and function. . 9(6):824–31

20. Zhang Z, Yan J, Bowman AB, Bryan MR, Singh R, Aschner M. 2019. Dysregulation of TFEB contributes to manganese-induced autophagic failure and mitochondrial dysfunction in astrocytes. *Autophagy*, pp. 1–18

APPENDIX A

INTRODUCTION

The following is a grant proposal written to receive VICTR (Vanderbilt Institute for Clinical and Translational Research) funding for labor costs and resources to perform a high-throughput enrichment screen for the molecule VU0026921, which showed promising Mn-dependent antimicrobial activity. It sufficiently provides background information, reasoning for why we were interested in the small molecule, and exactly what we planned to do. **All of the experiments done with *S. aureus* (Figure 2 and 3 in the proposal) were performed by Lillian Juttukonda from Dr. Eric Skaar's lab. Figure 1 in the proposal is taken from the previously published "Cellular manganese content is developmentally regulated in human dopaminergic neurons" by Kumar et al (2014). Scientific reports. 2014;4:6801. doi: 10.1038/srep06801. PubMed PMID: 25348053; PMCID: 4210885.**

The grant was funded and a summary of the results of the experiments follows the grant proposal. In addition, I provide data that I gathered from STHdh Q7 cells in an attempt to determine the mechanism of action of small molecule VU0026921 in mammalian cells.

SPECIFIC AIMS – Manganese (Mn) is an essential biological metal and cofactor involved in many organic processes. Mn is required as a redox-active factor for several mechanisms mediating oxidative stress defense. Mn is particularly important for pathways that promote bacterial pathogenesis. Notably, mammalian defense strategies that deplete extracellular Mn from the invading pathogen have been identified. Conversely, bacteria have evolved specialized, high-

affinity importers for Mn that provide them with sufficient Mn levels when in low concentration environments(1). As widespread antibiotic resistance lowers the efficacy of the current antibiotic arsenal, therapeutic agents targeting host-pathogen metal homeostasis have profound potential as next-generation antibiotics. **We have serendipitously identified an anti-microbial compound that appears to target bacterial Mn-dependent biology. This VICTR proposal seeks to develop chemical resources to allow pre-clinical studies against clinical isolates of *Staphylococcus aureus*.** Mn is an essential cofactor for all life. In an effort to further understand mammalian Mn regulatory processes, our laboratory performed a high-throughput screen of over 40,000 small molecules for intracellular-Mn modulators in an immortalized neuronal cell line (STHdh). This led to the identification of a set of 41 small molecules with significant cellular Mn-altering abilities. To further characterize the properties of these small molecules, we utilized a *S. aureus*-based growth assay in collaboration with Dr. Eric Skaar's lab to evaluate whether any of the small molecules showed Mn-chelation properties. Unexpectedly, we found that one of these molecules (VU0026921) exhibited bacteriostatic activity in both wild-type and mutant strains lacking *mntH* and *mntC*, the major Mn importers of the bacterium(2). These antibacterial properties were rescued by Mn supplementation, strongly suggestive of a Mn-specific antibacterial effect. Furthermore, this rescue from bactericidal effect could not be achieved with other metals with the exception of high concentrations of iron (Fe; 1mM), which can substitute for Mn for many bacterial enzymes. To define the mechanism of action of VU0026921, we conducted a suppressor screen to generate VU0026921-resistant *S. aureus* mutants. This screen failed to generate any VU0026921 resistant mutants; suggesting the targeted mechanism may be difficult for bacterial to gain resistance against. However, this feature also makes mechanistic research and translational

studies more difficult. Identification of small molecules with similar activity will enable such work.

We hypothesize that small molecules with similar structural and chemical features to VU0026921 may have target the same Mn-dependent biological processes. This hypothesis is based on the reasonably probability that the Mn-altering properties of VU0026921 across divergent biological domains (prokaryote and eukaryote) is due to highly conserved structure-activity relationships. In eukaryotes, the mechanistic target may be mitochondria-related, given the endosymbiotic theory of mitochondrial origin, the known sequestration of intracellular Mn into the mitochondria, and the ability of VU0026921 to alter mitochondrial permeability. Thus as our most sensitive and established assay for this activity is eukaryotic based, we have designed a structure-activity based screen for antibiotic compounds targeting Mn-dependent biology.

Aim 1: Perform a high-throughput enrichment screen to identify small molecules similar to VU0026921 with greater activity and lower EC_{50} in murine striatal cells. The goal of this aim is to identify additional small molecules that act on the same target as VU0026921. Given that Cellular Fura-2 Manganese Extraction Assay (CFMEA) is optimized and validated for high throughput screening in our murine striatal cells, the screen can start without further validation (3). Further argument in favor of this indirect strategy for finding additional antimicrobial compounds is that prior screens by the Skaar lab using bacteria have failed to identify validated Mn-dependent antimicrobial leads. We have selected 18,880 candidate compounds for screening, 3,505 of which are “virtual hits”; small molecules with predicted activity based on structure-based computational models.

Aim 2: Validate primary hits by confirmatory screen and concentration dependent curve (CRC) generation. Following the primary screen at 2μM, a confirmatory screen of the functional

hits will be completed. Finally, concentration dependent curves (CRCs) will be generated for validated hits to identify those acting through a direct pharmacological mechanism.

Post-VICTR Aim 3: Test validated compounds to allow for structure-function refinement analysis and confirmation of antibacterial activity in *S. aureus* and *S. aureus* clinical isolates. Following the success of Aims 1 and 2, we will then be able to validate modifiers of intracellular Mn in collaboration with our team (the labs of Drs. Aaron Bowman, Eric Skaar and Jens Meiler). With these, the Meiler lab can improve their computational model of small molecule morphology with a specific Mn-altering activity in mammalian cells. In addition, this will also permit the Skaar lab to test these validated compounds for increased antibacterial efficacy, and directly test clinical applicability in human tissues infected with *S. aureus* and clinical isolates.

BACKGROUND AND SIGNIFICANCE

One of the most pressing challenges in modern medicine is the rising burden of antibiotic resistance. Since the early 1960s, only four new classes of antibiotics have been developed, none of which have made a major public health impact (4). As a result, most research has been focused on generation of derivatives of established antibiotic classes: penicillins, cephalosporins, quinolones, macrolides, and tetracyclines, rather than development of novel classes entirely. One major threat to public health is the emergence of methicillin-resistant *Staphylococcus aureus* (MRSA), a major source of hospitalization and mortality (5). As a result, there is active interest in exploring different classes of antibiotics. In particular, modulation of metal biology for antibiotic purposes has not been extensively explored. There has been some evidence implicating chelation of zinc (Zn) as an antibiotic strategy given that these molecules inhibit Zn-dependent hydrolases

(6, 7). Similarly, *S. aureus* is known to use manganese (Mn) to activate mechanisms needed to survive the oxidative burst present in the nasopharynx, however these have not been directly targeted in a clinical setting (2, 8, 9).

In addition to their role in bacterial pathogenesis, essential trace metals are required to support the structure and function in multitudes of enzymes and other proteins. Given their importance in cellular physiology, these metals are regulated by an intricate network of metallochaperone proteins, metal transporters, signaling pathways, and organelles. Homeostatic measures exist to prevent toxicity of these metals when excess concentrations are present. Considering the scarce knowledge of Mn homeostatic mechanisms, we sought to identify compounds with Mn-altering ability in a high throughput screen. A total of 41 small molecules were identified as capable of significantly increasing or decreasing intracellular Mn content in a concentration dependent manner (**Figure 1**; (10)).

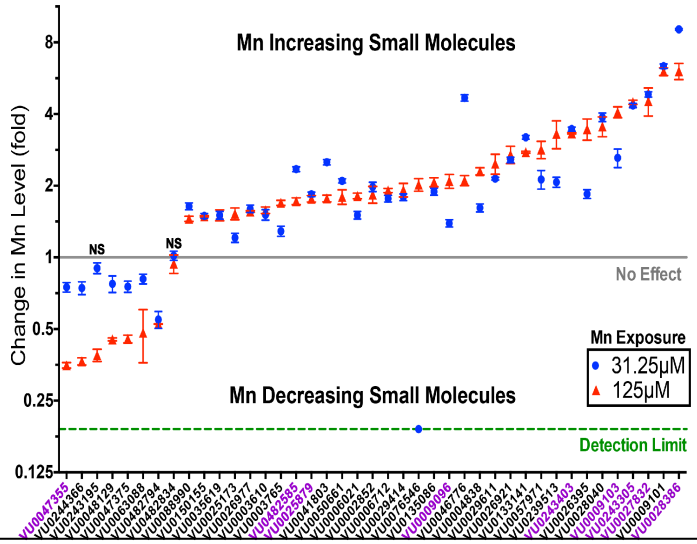

Figure 1: **FROM** Kumar KK, Lowe EW, Jr., Aboud AA, Neely MD, Redha R, Bauer JA, Odak M, Weaver CD, Meiler J, Aschner M, Bowman AB. Cellular manganese content is developmentally regulated in human dopaminergic neurons. Scientific reports. 2014;4:6801. doi: 10.1038/srep06801. PubMed PMID: 25348053; PMCID: 4210885.

Activity of Mn 'toolbox' at both physiological and pathophysiological Mn exposures. Mn 'toolbox' molecules tested in hiPSC-derived mesencephalic dopaminergic precursors are marked in (purple). Statistical significance was determined comparing small molecule treatment versus vehicle by one-way ANOVA, $p<0.05$.

One member of our "Mn toolbox", VU0026921, a Mn level increasing small molecule, has been identified in several other screens but has not been directly linked to Mn. However, the majority of known putative targets have known interactions with Mn biology. For example, three independent studies have found VU0026921 acts as an inhibitor of HSP90 in *Candida albicans*, *plasmodium falciparum*, and humans (11-13). Furthermore, the chelator deferoxamine has been reported to influence mitochondrial chaperone and HSP90 member TRAP1. *TRAP1* functions to attenuate reactive oxidative species through Mn-SOD (14). In addition, exposure to Mn in *Drosophila melanogaster* has been shown to increase mRNA expression of *HSP83* (of which the mammalian homolog is HSP90) (15). Notably, heat shock proteins (HSPs) are conserved across kingdoms, which fit with the observed activity of VU0026921 in both bacteria and mammals. Many HSPs are mitochondrial chaperone proteins, such as HSP60, which is required for the proper

folding and function of manganese superoxide dismutase (Mn-SOD) (16). Interestingly, VU0026921 was noted to enhance mitochondrial function in a screen using yeast model of Friedreich's ataxia, a disorder caused by mutations in *frataxin*, a known iron chelator (17). Other screens have confirmed VU0026921 as an inhibitor of the mitochondrial permeability transition pore (mtPTP) which is an efflux route of Ca^{2+} (18). Importantly, VU0026921 was identified in a screen for inhibitors of streptokinase A, a mechanism to inhibit growth of *Streptococcus pyogenes* (19).

These previous studies suggest possible mechanisms by which VU0026921 is acting to influence intracellular Mn. However, there are potential off-target effects that VU0026921 may have *in vivo*. Thus, future studies in this area require a small molecule with similar activity but with a higher affinity, potency and stability. To facilitate this, we have collaborated with Drs. Jens Meiler, Jonathan Sheehan and Jarrod Smith to identify morphologically similar compounds to VU0026921 that can be screened by our established screening method. Specifically, the virtual hits were identified through property analysis of VU0025921 followed by in-silico screening of the Vanderbilt Discovery Collection of 100,000 compounds using Topomer and Surflex-Sim queries. Both of these methods are capable of identifying binders with novel structures (scaffold hopping). The results of these queries were subsequently merged and ranked by consensus scores, generating a final list of 3,505 small molecules with predicted activity. We predict that these morphologically similar molecules may provide insight into structure-function relationships, lead to the identification of compounds with improved clinical/pharmacological characteristics, and empower mechanistic and translational studies.

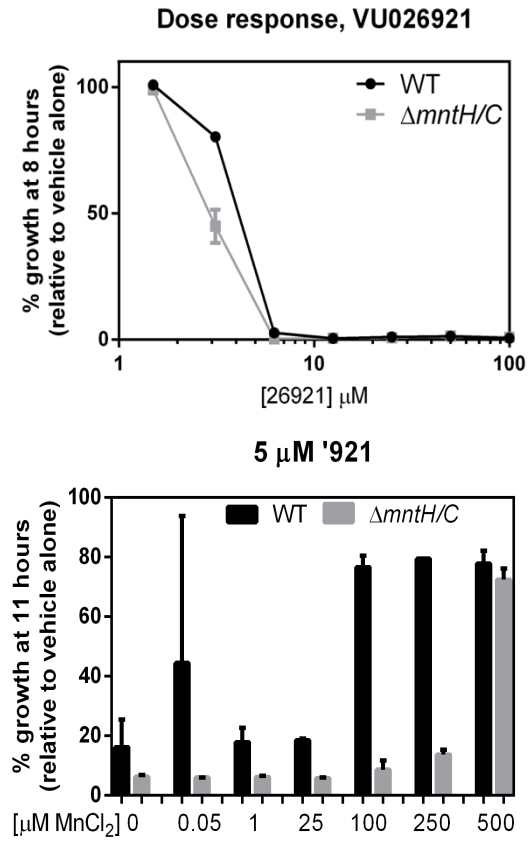

Figure 2: **Performed by Lillian Juttuonda** VU0026921 inhibits the growth of *S. aureus*. Wild-type *S. aureus* and *S. aureus* Δ*mntH*/Δ*mntC* are inhibited by VU0026921 in a dose-dependent manner. *S. aureus* growth inhibition by 5 μM VU0026921 is rescued by the addition of exogenous Mn to the growth medium. All data are graphed as growth in compound relative to growth in vehicle alone.

The identification of an active small molecule with similar structure-function relationship to VU0026921 provides meaningful insight toward the development of a novel antibiotic class against MRSA. Firstly, the primary screen and subsequent validation of hits allows a direct evaluation of the hit-rate enrichment of the virtual screening model of 3,505 compounds compared to the other 15,375 that will also be screened. In collaboration with the laboratory of Dr. Jens Meiler at Vanderbilt, findings from these studies would allow refinement of the computational model in an iterative fashion, directly informing future characterization of structure-function relationships with their target. In addition, we plan to test molecules from the screen within the

context of an established collaboration of Dr. Eric Skaar at Vanderbilt. The Skaar laboratory has established protocols to test identified hits for bacteriostatic/bactericidal activity in *S. aureus*. The goal of these studies is to exclude compounds identified in Aims 1-2 that do not exhibit antibacterial activity in *S. aureus*. Human neutrophils or whole blood will be harvested and *S. aureus* killing assays performed with and without compounds of interest. Alternatively, MIC curves will be generated using human *S. aureus* isolates collected from clinical microbiology labs here at Vanderbilt. The remaining molecules would permit selection of the most promising lead molecule in which to repeat the suppressor screen in *S. aureus*. Generation of stable mutations will permit direct examination of the mechanism of the antibacterial resistance. Upon identification of putative targets, knockout or knockdown studies can be actively pursued in mammalian model systems.

PRELIMINARY STUDIES

To evaluate the activity of small molecule VU026921 in the human pathogen *S. aureus*, an *in vitro* growth assay was developed. Wild-type *S. aureus* strain Newman was used as wild-type control (WT) and a strain inactivated for the Mn importers MntH and MntABC (Δ*mntH/C*) was used to determine Mn-dependence, as Δ*mntH/C* is Mn-starved(2). Single bacterial colonies were isolated from freezer stocks on tryptic soy agar (TSA) and grown overnight in tryptic soy broth (TSB). Overnight cultures were then diluted 1:100 into fresh TSB containing serial dilutions of VU026921 dissolved in vehicle DMSO. Growth of bacteria was then monitored for 24 hours using optical density at 600 nm. Intriguingly, VU026921 inhibits *S. aureus* growth in a dose-dependent fashion (**Figure 1**). Furthermore, Δ*mntH/C* is more sensitive to VU026921 than WT, with significant inhibition at 2.5 μM compound, a concentration that has little effect on WT growth. This finding

indicates that growth inhibition by VU026921 is partially relieved by the Mn import systems MntH and MntABC. The fact that Δ*mntH/C* is still sensitive to VU026921 indicates that MntH and MntABC are not the direct target of VU026921 antimicrobial activity. We hypothesized that VU026921 inhibits *S. aureus* growth in a manner dependent on cellular Mn. To determine whether increased Mn availability to the bacterium can rescue VU26921 inhibition, a range of $MnCl_2$ was added to the TSB growth medium (**Figure 2**). VU26921 was added at 5 μM, a concentration that inhibits the growth of both WT and Δ*mntH/C*, and $MnCl_2$ was then added at concentrations ranging from 50 nm to 500 μM. 100 μM Mn rescues the growth of WT *S. aureus* in the presence of 5 μM VU26921, suggesting that VU26921 disrupts metal homeostasis in *S. aureus.* Importantly, 500 μM Mn is required to rescue Δ*mntH/C,* suggesting that Mn must be imported to rescue growth and that VU26921 effects are mediated intracellularly. Growth assays were also carried out in the presence of other divalent cations iron, zinc, copper, and magnesium to address the metal specificity of VU026921 rescue (**Figure 3**). Intriguingly, none of these metals rescue *S. aureus* growth to the same degree as Mn. Iron rescues but only at 1 mM, and magnesium has no impact on VU026921 inhibition. Copper and zinc enhance VU026921 antimicrobial activity. This suggests that VU026921 dysregulates metal homeostasis in *S. aureus.*

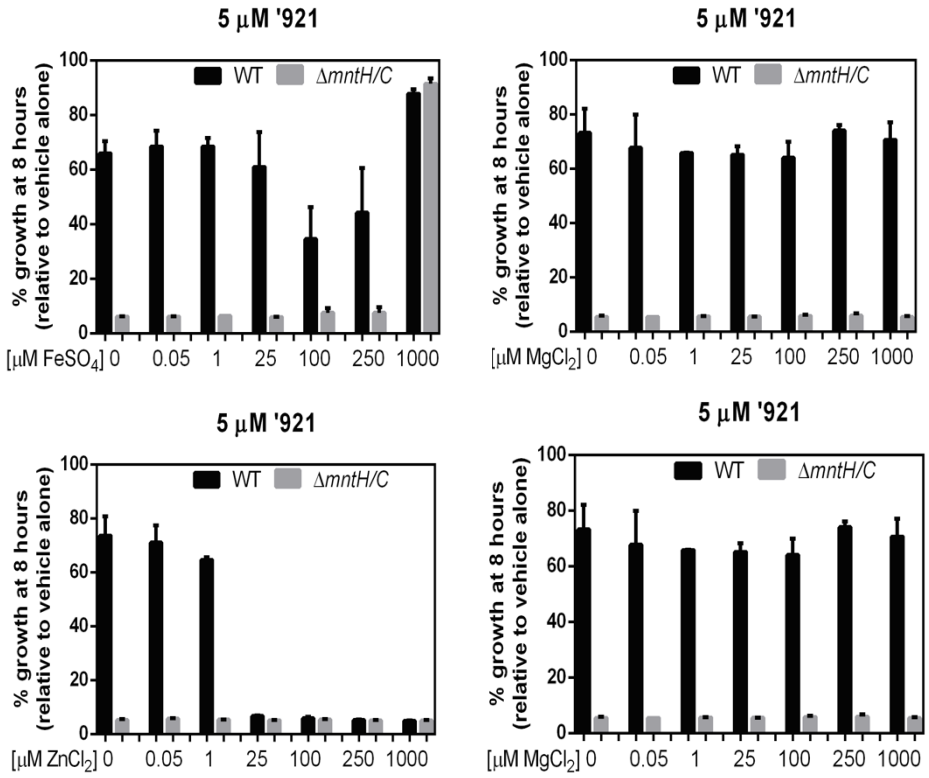

Figure 3: Performed by Lillian Juttuonda. VU0026921 is not rescued by other divalent cations. Iron rescues VU0026921 toxicity at high concentrations only. Copper and zinc unexpectedly increase toxicity of VU0026921. Magnesium has no effect on '921 toxicity. All results are graphed as *S. aureus* growth in the presence of 5 µM VU0026921 relative to vehicle alone.

RESEARCH DESIGN AND METHODS

Fluorescent-based assays are well established and several large screening operations based on this approach have been performed in the Vanderbilt HTS facility which have produced validated hits, several of which have confirmed activity in native systems and in animal models (3, 20). The high-throughput screening portion of this proposal will consist of several stages from validation to confirmation. The experiments are designed taking into consideration 1) quality control of a multiple plate-based assay and 2) appropriate data analysis for the biological phenomenon we are measuring. We have previously optimized (Z'>0.5) and conducted a high throughput screen for

modulators of neuronal Mn status using the Cellular Fura-2 Mn Extraction Assay (CFMEA; (3 10). Using this exact same technique, we will screen a set of 18,880 candidate compounds for screening including 3,505 computationally predicted small molecules.

AIM 1: The primary screening phase seeks to identify compounds that change the response of the EC_{80} concentration of agonist (Mn) within this assay. More specifically, small molecules that increase the readout of intracellular Mn will be identified as measured by the CFMEA assay. These compounds will be moved through the secondary screening process for validation of the desired effect using counter-screening, concentration response, and orthogonal assay approaches. In this initial phase, we want to minimize the number of false negatives that are "lost" in the screening process; we can tolerate the level of false positives we obtained in the first iteration of the primary screen, as the secondary screening process identifies these compounds. Although there will be some rate of false negatives being lost in the primary screening process, the HTS approach is constructed such that the trade-off of screening a larger number of compounds to discover a novel chemotype is chosen over screening with a number of replicates allowing robust statistical comparison with fewer unique compounds. The first addition consists of the small molecules and vehicle controls. The second addition is the Mn exposure (125uM) that will result in the experimental signal. It is the EC_{80} and VHL signals that will be used to calculate the Z' for each plate because it is the reduction in the EC_{80} signal that will be monitored for the detection of hits. The small molecules will be screened at a single concentration (10µM).

AIM 2: Following the primary screen, hits will be validated in duplicate at 2µM to confirm activity. The same quality control parameters and plate layouts will be in place for confirmation as were in

primary screening. However, the effect of the compounds in this set of experiments will be determined in comparison to the EC80 control. A compound will be considered to have an effect if it falls three standard deviations beyond the average EC_{80} response. A compound is considered to be a confirmed hit if both replicates show this degree of effect. Because the number of compounds are greatly reduced at this stage, greater than two replicates may be run. Also, this is the stage where counter-screening may occur to identify false positives. Depending on the number of compounds and replicates being run, counter-screening may also occur after this stage on confirmed hits. These counter screens would test for inherently fluorescent small molecules that would interfere with the Mn-dependent fura-2 fluorescence signal, and molecules that merely adhere Mn to the 384-well plate surface, rather than having a biological and cellular effect. After validation, a concentration response of agonist will be performed to determine the EC_{80} concentration under the automated conditions of the HTS facility. This will consist of ten concentrations plus a vehicle control in triplicate in a single 384-well plate and will be performed on three separate days to establish reproducibility of the concentration response curve. The design will mimic the HTS experiment in that there will be a DMSO vehicle addition before the agonist addition to take into account of any effect of the solvent on the response to agonist.

Post-VICTR AIM 3: We will perform follow-up studies to test the antibiotic activity on human clinical isolates and examine structure-activity relationships of the newly validated compounds – as in Figures 2 and 3 and preliminary studies. Whereas the experiments from Figure 2 and 3 were performed on cultured WT *S. aureus,* the antibiotic activity of the small molecules confirmed in Aim 2 can be tested directly in human *S. aureus* isolates collected from Vanderbilt clinical microbiology labs. In addition, the potency of these molecules can then be compared to their

structure, allowing structure-activity relationships to be pursued further. This information can generate promising leads to repeat the suppressor screen in *S. aureus,* now with enhanced likelihood of success. Following this, the mechanism of the antibacterial resistance and the mechanism through which these antibiotic compounds act can then be revealed in genomic sequencing. **This proposal aims to provide proof of principle/preliminary data for subsequent applications of support from NIH towards developing this new class of antibiotics – evidence of our capacity to identify new agents with similar activity will be advantageous for success of future grants.**

SAMPLE SIZE JUSTIFICATION AND STATISITICAL ANALYSIS PLAN

First and foremost, the sample size and analysis is based on our proven strategy in the original screen. The proposed new screen will utilize the same statistical approach (3, 10). We have achieved a Z-factor of 0.53 and 0.50 for Mn decreasers and increases respectively (10). The original screen of 40,167 small molecules yielded a initial hit rate of 2.2%, with replication and CRC taking this down to 0.33%. We expect an enrichment of this rate in the 3,505 computationally identified chemicals (>11 hits); but a similar rate in the others being screened.

The data reduction practices discussed above and the application of plate acceptance criteria (Z'>0.5 and EC_{80} falling between 70–90% of EC_{max}) are used to ensure that experimental error is minimized allowing for a more sensitive and reliable detection of outliers in each plate. Primary hit selection will be based on Z score and B-score approaches, the latter of which is nonparametric and minimizes positional effects that may occur within the plate reading. Hits will be identified on

a per-plate basis and flagged in the database for follow-up confirmation of effect. This value will be plotted against log[agonist] and fit to a four-parameter logistical equation. From this, the concentration resulting in an 80% maximally effective response (EC_{80}) will be determined as well as a concentration that gives a maximal response (EC_{max}). The latter concentration will be used in experiments to normalize the calculations to "percent maximum response" to help account for plate-to-plate variability and to provide a means to ensure the EC_{80} response is within an acceptable range. Each experimental day will begin with an agonist CRC to determine the best concentrations to use for EC_{80} and EC_{max}. Within each plate, the average EC_{80} magnitude should be between 70% and 90% of the EC_{max} signal magnitude to ensure that the response being acted on by the test compounds is consistent between plates. Plates not meeting this requirement will be discarded and the compounds from that plate rerun.

RESULTS AND DISCUSSION

A primary screen of 19,200 compounds was completed. Of these, 3,505 of these were virtually predicted hits based on structure. Source plates were chosen with the highest frequency of virtual hits, and the entire plates (60 total) were screened. Primary hits were based on "Mn-increasers" with a z-score over 3.0, and "Mn-decreasers" with a z-score over 2.0. There was an exception of one plate that had clear positional effects, and hits were instead based on a B-score analysis. In total, 603 primary hits (~3% hit rate) were run in duplicate in a confirmation test.

Figure 4. Representative plot of normalized Fura-2 Values of one experimental plate.

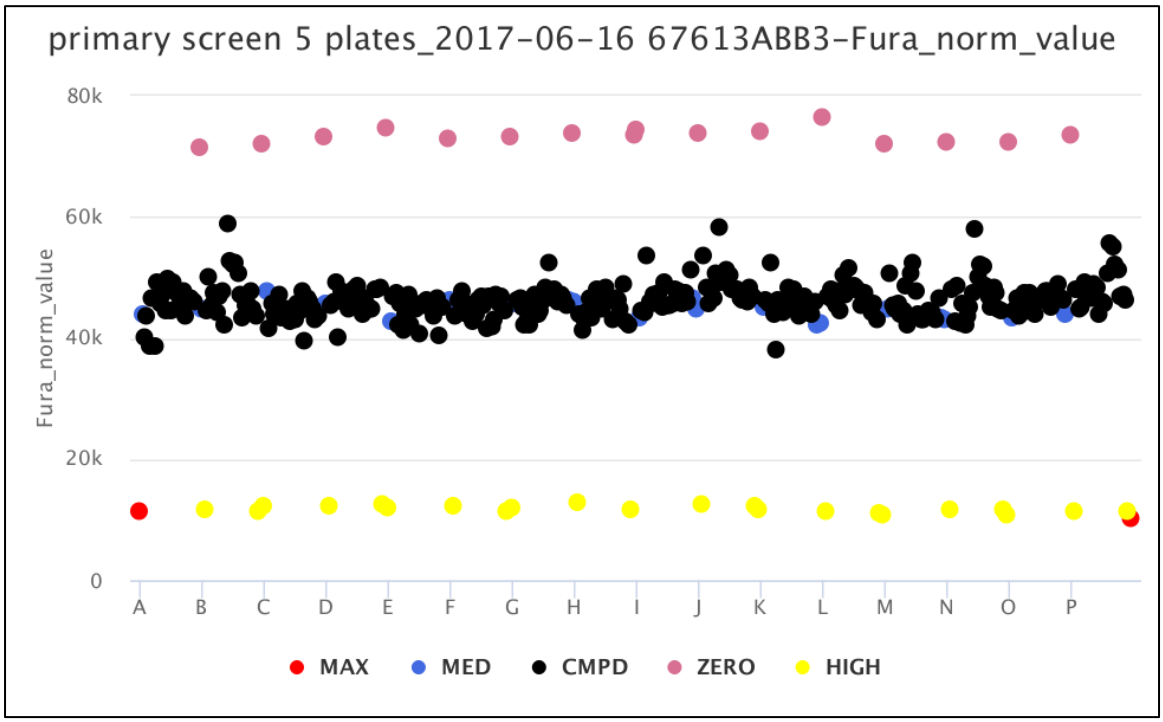

Of the 603 that entered confirmation screening, there were only 9 hits.

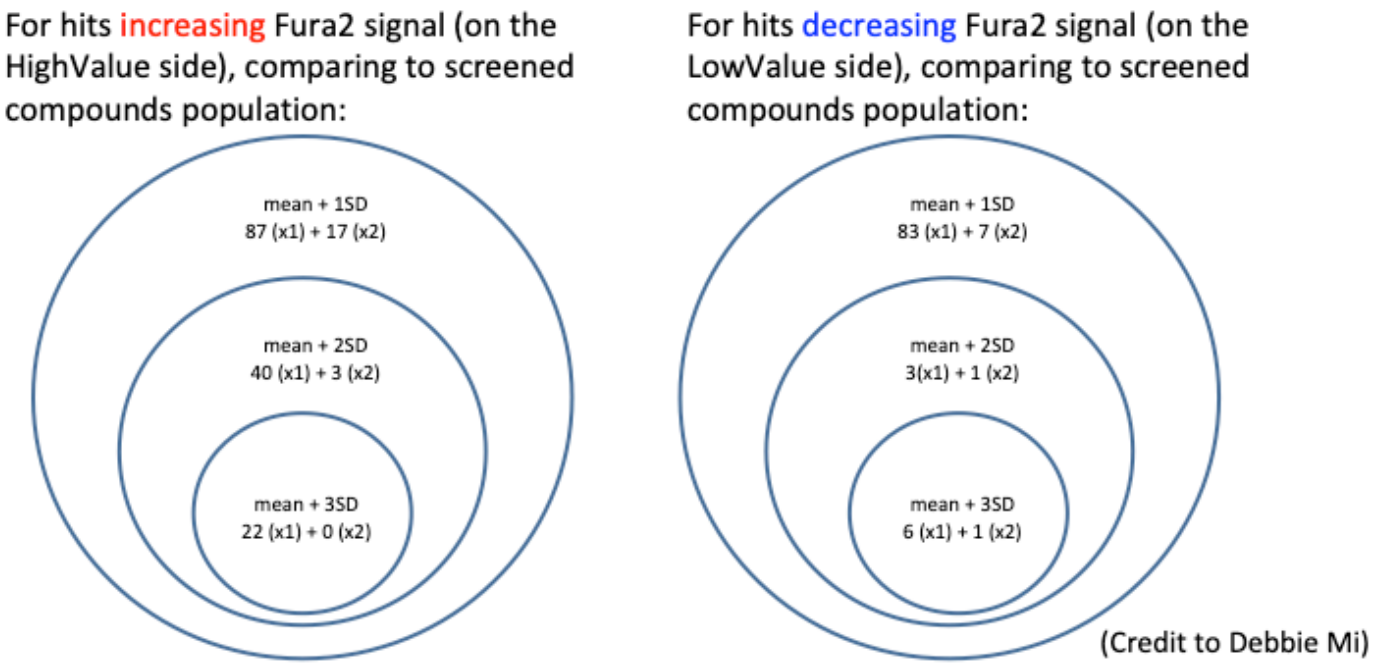

Figure 5. Breakdown of hits in confirmation screen. Data shown here is compared to other screened compounds- other analysis was done compared to bscore correction, or compared to negative controls. Here we see 4 hits total at 2SD and above. The other 5 were from the other unique hits from the other analyses.

Note the concentration tested was 2 micromolar, which was quite low, though we were searching for more potent small molecules than "921". In the previous screen from Kumar et al (2014), there were many hits with high EC_{50}s, and we were hoping to avoid that situation again. Confirmed hits were those that hit twice and fall into the category of two standard deviations or above the mean. Because of the low confirmation hit rate (nine), another six were added going into concentration response curves (CRCs) which were strong primary hits but did not make it through confirmation. The hit list generated with and without B-score correction are quite similar, highly overlapped, which means the data quality was good. The hit list that was generated by comparing to either the screened compound population or to the negative controls is also quite similar, which in another angle showed that confirmation rate was really low.

There were two rounds of CRCs. Of the 15 compounds that went into CRCs, the first round yielded four curves.

- VU0634501 yielded an EC50 = 1.21E-6 M, (Mn increaser)
- VU0498874 yielded an EC50 = 6.59E-9 M, (very shallow curve)
- VU0610509 yielded an EC50 = 1.39E-6 M, (Mn decreaser, shallow curve)
- VU0500009 gave EC50 = 3.13E-6 M, (Mn increaser, shallow curve)

On the second round, there was only one that converged; VU0634501 gave EC50 = 1.49E-6 M, 1.64E-6 M. This was not a predicted hit, but VU0500009 was virtually predicted. To rescue possibly missed hits, a 0.8 similarity search in ChemCart was performed for the one confirmed hit, '501. Of 129 results, 7 had been already tested in primary screen, another 125 hadn't. These 125 were tested in a second screen and generated 35 confirmed hits. These 35 were run in CRC, yielding 29 curves.

Regarding future directions, we should consider adding '501 into the Mn toolbox, if it appears to be Mn-specific (it can be screened against other divalents). In addition, structure-activity relationships can be pursued for the 125 homologs that did or did not hit.

REFERENCES:

1. Juttukonda LJ, Skaar EP. Manganese homeostasis and utilization in pathogenic bacteria. Mol Microbiol. 2015;97(2):216-28. doi: 10.1111/mmi.13034. PubMed PMID: 25898914; PMCID: PMC4631260.

2. Kehl-Fie TEZ, Y.; Moore, J.L.; Farrand, A.J.; Hood, M.I.; Rathi, S.; Chazin, W.J.; Caprioli, R.M.; Skaar, E.P. MntABC and MntH Contribute to Systemic Staphylococcus aureus Infection by Competing with Calprotectin for Nutrient Manganese. Infection and Immunity. 2013;81(9):3395-405.
3. Kumar KK, Aboud AA, Patel DK, Aschner M, Bowman AB. Optimization of fluorescence assay of cellular manganese status for high throughput screening. J Biochem Mol Toxicol. 2013;27(1):42-9. doi: 10.1002/jbt.21457. PubMed PMID: 23169769; PMCID: PMC3774111.
4. Fischbach MAW, C.T. Antibiotics for Emerging Pathogens. Science. 2009;325:1089-93.
5. Klein EY, Sun L, Smith DL, Laxminarayan R. The changing epidemiology of methicillin-resistant Staphylococcus aureus in the United States: a national observational study. Am J Epidemiol. 2013;177(7):666-74. doi: 10.1093/aje/kws273. PubMed PMID: 23449778.
6. Noskin GAR, R.J.; Schentag, J.J.; Kluytmans, J.; Hedblom, E.C.; Smulders, M.; Lapetina, E.; Gemmen, E. The Burden of Staphylococcus aureus Infections on Hospitals in the United States. Arch Intern Med. 2005;165:1756-61.
7. King AM, Reid-Yu SA, Wang W, King DT, De Pascale G, Strynadka NC, Walsh TR, Coombes BK, Wright GD. Aspergillomarasmine A overcomes metallo-beta-lactamase antibiotic resistance. Nature. 2014;510(7506):503-6. doi: 10.1038/nature13445. PubMed PMID: 24965651.
8. Salazar N, Castiblanco-Valencia MM, da Silva LB, de Castro I, Monaris D, Masuda HP, Barbosa AS, Areas AP. Staphylococcus aureus manganese transport protein C (MntC) is

an extracellular matrix- and plasminogen-binding protein. PloS one. 2014;9(11):e112730. doi: 10.1371/journal.pone.0112730. PubMed PMID: 25409527; PMCID: PMC4237344.

9. Kehl-Fie TE, Chitayat S, Hood MI, Damo S, Restrepo N, Garcia C, Munro KA, Chazin WJ, Skaar EP. Nutrient metal sequestration by calprotectin inhibits bacterial superoxide defense, enhancing neutrophil killing of Staphylococcus aureus. Cell Host Microbe. 2011;10(2):158-64. doi: 10.1016/j.chom.2011.07.004. PubMed PMID: 21843872; PMCID: PMC3157011.

10. Kumar KK, Lowe EW, Jr., Aboud AA, Neely MD, Redha R, Bauer JA, Odak M, Weaver CD, Meiler J, Aschner M, Bowman AB. Cellular manganese content is developmentally regulated in human dopaminergic neurons. Scientific reports. 2014;4:6801. doi: 10.1038/srep06801. PubMed PMID: 25348053; PMCID: 4210885.

11. Fluorescence Cell-Based Retest of C. albicans Growth in the Presence of Fluconazole [Internet] [cited Mar. 6, 2016]. Available from: https://pubchem.ncbi.nlm.nih.gov/bioassay/2467.

12. Anti-Malarial Hsp90 Inhibitors Measured in Microorganism System Using Plate Reader - 2121-01_Inhibitor_Dose_CherryPick_Activity [Internet] [cited Mar. 6, 2016]. Available from: https://pubchem.ncbi.nlm.nih.gov/bioassay/540268.

13. HsHsp90 Counterscreen Measured in Microorganism System Using Plate Reader - 2121-02_Inhibitor_Dose_CherryPick_Activity [Internet] [cited Mar. 6, 2016]. Available from: https://pubchem.ncbi.nlm.nih.gov/bioassay/540270

14. Im CN, Lee JS, Zheng Y, Seo JS. Iron chelation study in a normal human hepatocyte cell line suggests that tumor necrosis factor receptor-associated protein 1 (TRAP1) regulates

production of reactive oxygen species. J Cell Biochem. 2007;100(2):474-86. doi: 10.1002/jcb.21064. PubMed PMID: 16927372.

15. Ternes APLZ, A.P.; Cezar da Cruz, L.; Felipe da Silva, G.; Saidelles, A.P.F.; Trindade de Paula, M.; Wagner, C.; Golombieski, R.M.; Marlon de Moraes Flores, E.; Picoloto, R.S.; Pereira, A.B.; Franco, J.L.; Posser, T. Drosophila Melanogaster- An embryonic model for studying behavioral and biochemical effects of manganese exposure. EXCLI. 2014;13:1239-53.

16. Magnoni R, Palmfeldt J, Hansen J, Christensen JH, Corydon TJ, Bross P. The Hsp60 folding machinery is crucial for manganese superoxide dismutase folding and function. Free Radic Res. 2014;48(2):168-79. doi: 10.3109/10715762.2013.858147. PubMed PMID: 24151936.

17. Screen For Small Molecule Probes Relevant To Friedreich's Ataxia, Single Dose And Dose Response [Internet] [cited Mar. 6, 2016]. Available from: https://pubchem.ncbi.nlm.nih.gov/bioassay/1465

18. Summary Assay For Small Molecule Inhibitors Of The Mitochondrial Permeability Transition Pore [Internet] [cited Mar. 6, 2016]. Available from: https://pubchem.ncbi.nlm.nih.gov/bioassay/602491.

19. Luminescence Microorganism-Based Dose Confirmation HTS to Identify Inhibitors of Streptokinase Promotor Activity [Internet] [cited Apr. 12, 2016]. Available from: https://pubchem.ncbi.nlm.nih.gov/bioassay/1902.

20. Kwakye GF, Li D, Bowman AB. Novel high-throughput assay to assess cellular manganese levels in a striatal cell line model of Huntington's disease confirms a deficit in

manganese accumulation. Neurotoxicology. 2011;32(5):630-9. doi:

10.1016/j.neuro.2011.01.002. PubMed PMID: 21238486; PMCID: PMC3135664.

APPENDIX B

Regarding the mechanism of VU0026921 in mammalian cells, we have two hypotheses. First, ‘921 is acting on a conserved, biological target or mechanism between mammals and bacteria, dependent on Mn. We know that ‘921 increases intracellular Mn in mammalian cells. So, ‘921 works by binding intracellular Mn itself or binding Mn and a target. We can disregard the hypothesis that ‘921 shuttles Mn across the cellular membrane as an ionophore, because it failed to permeate the PAMPA plates (see Chapter V). Originally data that prompted the hypothesis that Mn binds and possibly activates 921 at a 2:1 ratio, but this could not be replicated.

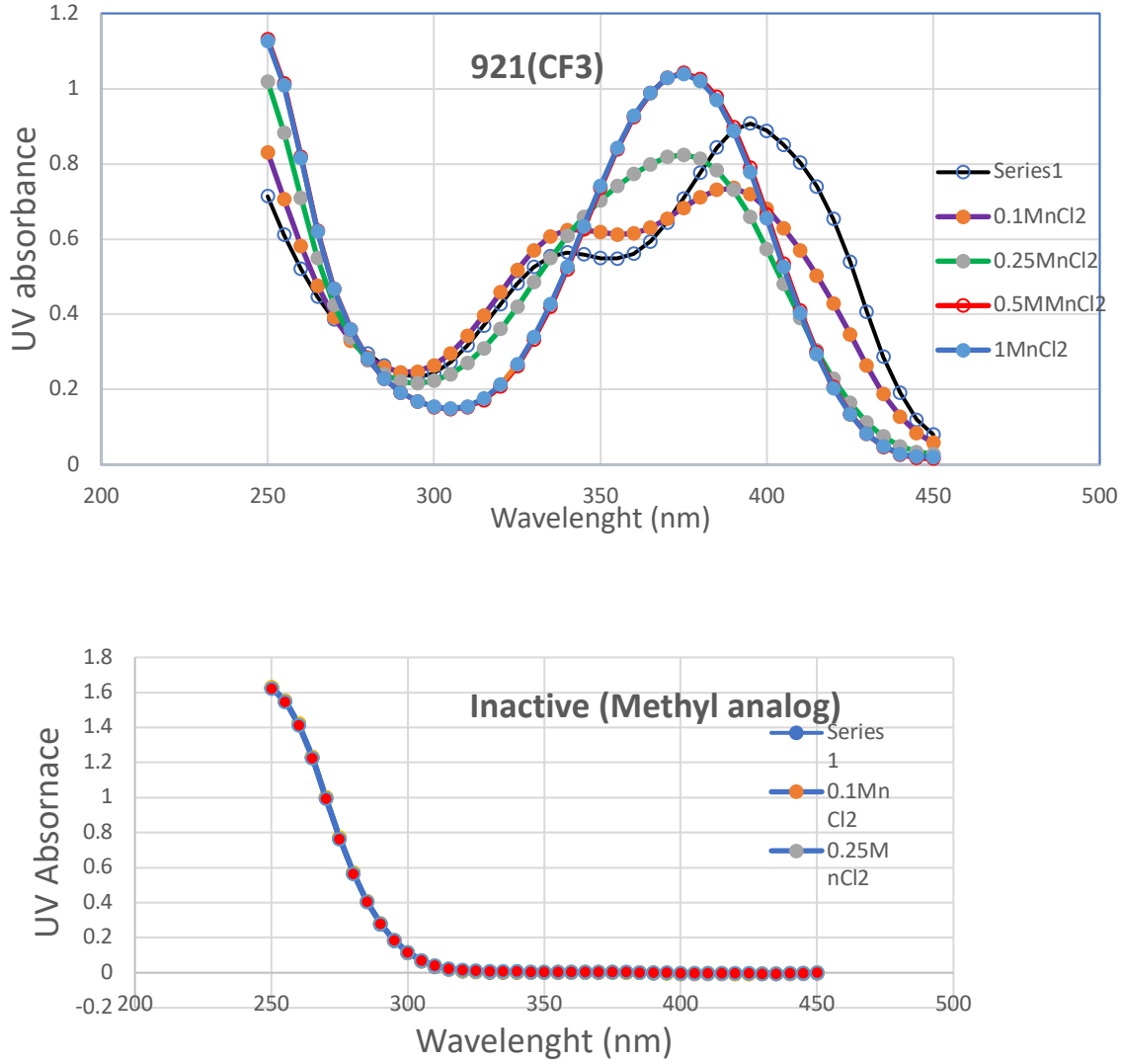

Figure 6. UV spectrum of '921 in the presence of varying Mn.

(My data)

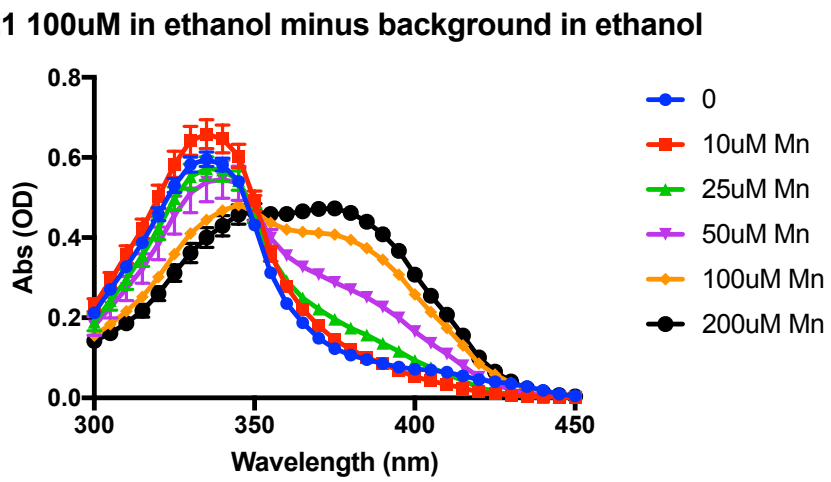

(Data from Plamen)

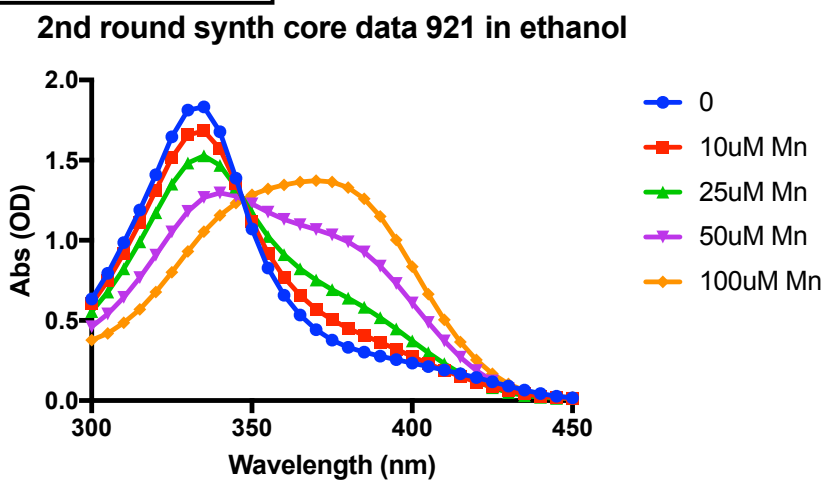

Figure 6. UV spectrum of '921 in the presence of varying Mn in ethanol.

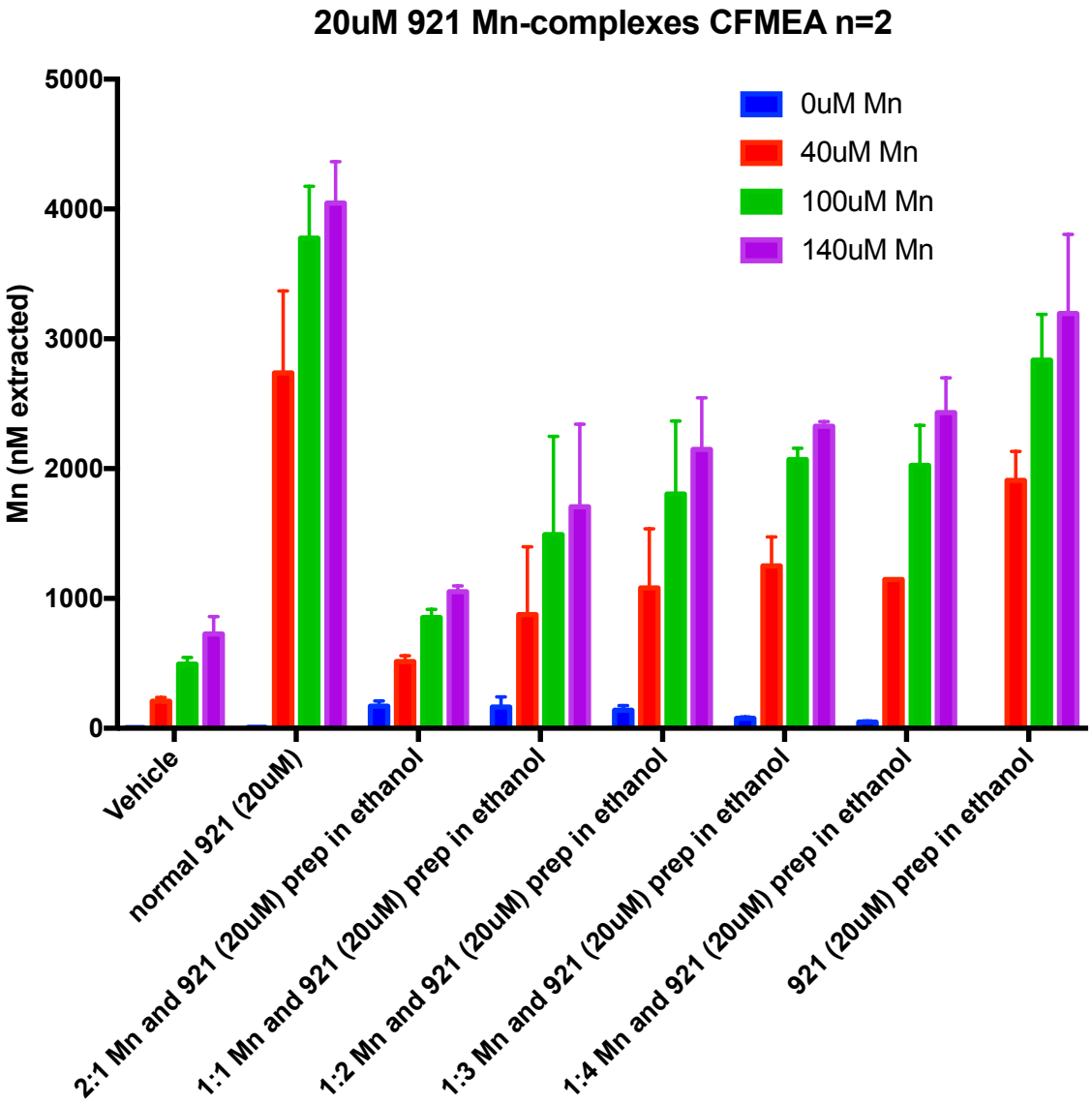

Figure 7. Mn complexed to 921 INHIBITS '921.

We originally thought that the degrades/disables scenario was unreasonable, so this was proof that 921 had to get in the cell unbound to Mn. However, 921 being disabled by Mn or other divalents, in a specific environment or pH, does make sense. The bacteriostatic/ antibiotic effect of 921 was rescued by Mn- perhaps because Mn simply disabled 921. In mammalian cells, pretreating with Cu or Zn prevents 921's effect. This is consistent; that divalents, more specifically Mn, deactivate

921. Whether chemical or structural change to prevent membrane transport, 921 is essentially deactivated. But this doesn't get at 921 action- it is still acting on an unknown target- the only thing we have identified is that 921 is the off switch- 921 is deactivated by the same process it sets in motion, as a negative feedback loop. This, however, doesn't get us anywhere about its target or Mn biology. The only remaining hypothesis is that once 921 and Mn are both inside the cell, 921 and Mn act on a target, though this seems unlikely.